Synthesis and Investigation of Light Responsive Molecules Containing Cyclopropenium Ions

Richard Le Sueur, B. Sc. (Honours)

A thesis submitted in partial fulfillment of the requirements for the degree of

Masters in Science

Faculty of Mathematics and Science, Brock University

St. Catharines, Ontario

Abstract:

The present thesis describes recent advances in the pursuit of novel light-responsive molecules containing cyclopropenium ions. In an effort to understand the underlying factors regarding the photophysical properties of cyclopropenium ions, emphasis was placed on the previously reported "Janus sponge", where systematic structural modifications to four individual components of the molecule led to measurable and predictable changes in molar extinction coefficients, quantum yields, and Stokes shifts. Using time-dependent density functional theory calculations, the origin of these trends were traced to internal charge transfer. Additionally, modulating hydrogen bonding between intermolecular, bifurcated, and intramolecular interactions by choice of counterion was used to alter the quantum yield of cyclopropenium ion-containing fluorophores. The basis of this switchability was examined using X-ray diffraction analysis, ^{1}H NMR spectroscopy, density functional theory calculations, and fluorescence spectroscopy. Notably, this work led to the development of the first cyclopropenium ion containing "true" proton sponge. As an extension, light responsive molecules are not isolated to fluorescence. This thesis also outlines the development of the first cyclopropenium ion containing an azo group. Key findings include the fact that cyclopropenium ion containing azo compounds are stable and cyclopropenium ions red-shift the absorbance wavelength in comparison to azobenzene by 75 nm. The synthetic, structural, electronic, and photophysical properties of these compounds are discussed.

Acknowledgements:

First and foremost, I would like to thank my supervisor, Dr. Travis Dudding. I have had the pleasure of getting to know Dr. Dudding as both a professor and a mentor, thoroughly enjoying the time I spent working under his supervision. It is clearly visible that Dr. Dudding is enthusiastic about the success of his students through his daily visits to the lab. In these past two years, I have grown tremendously as an individual. I would also like to extend my gratitude to my committee members, Dr. Martin Lemaire and Dr. Paul Zelisko. Collectively, they offered guidance during committee meetings, and contributed to my academic growth as I had the pleasure of taking a number of classes under their supervision.

I would also like to thank my co-workers, Matt Guest, Ivor Smajlagic, Hayden Foy and Brenden Carlson. Over the past years, it was really enjoyable spending the days building friendships that hopefully will last a lifetime. I would also like to thank my fellow "Cairns" graduate students who I also got to know very well, especially Sean Mason and Frank Betancourt, my fellow gym partners.

Of course, I would not be here today without the loving support of my family, both financially and emotionally. My Mother and Father have always been there when I needed them, without hesitation. A very special thank you to Jessica Salvagna and her family for being a part of this journey, and my life.

Table of Contents

Abstract ii

Acknowledgements: iii

Table of Contents iv

List of Figures vi

List of Tables ix

List of Schemes x

List of Abbreviations xii

Chapter 1: Introduction 1

1.1 Organobases 1

1.2 Proton Sponges 4

1.2.1 The Prototypical Proton Sponge 4

1.2.2 Guidelines for Proton Sponge 6

1.2.3 Cyclopropenium Functionalized Sponge Derivatives 7

1.3 Cyclopropenium Ions and Amino-Substituted Cyclopropenium Ions 9

1.3.1 Stability of the Cyclopropenium Ion 9

1.3.2 Cyclopropenimines as Strong Brønsted Bases 10

1.3.3 Synthesis of Cyclopropenium Ion Derivatives 12

1.4 Photochemistry 15

1.4.1 Fluorescence Fundamentals 15

1.4.2 Fluorescence Scaffolds 18

1.4.3 Azo compounds 22

1.4.4 Synthetic Procedures for Symmetric and Non-Symmetric Azobenzenes 24

1.5 Summary and Thesis Objectives 26

Chapter 2: Fluorescence of Cyclopropenium Ion Derivatives 28

2.1 Introduction 28

2.2 Results and Discussion 30

2.2.1 Modifications to the Cyclopropenium Ion Group: Derivatives 48, 49, and 58 31

2.2.2 Modifications to the NMe_2 Group: Derivatives 50, 51, 52, and 53 33

2.2.3 Modifications to the Naphthalene Backbone: Derivatives 54, 55, 56, and 57 34
2.2.4 Computational Studies 35
2.2.5 Conclusion 41

Chapter 3: Competitive Hydrogen Bonding of Cyclopropenium Ions: Implications of an Anion Switch 42
3.1 Introduction 42
3.2 Results and Discussion 44
3.2.1 Crystal Structure Analysis 45
3.2.2 Computational and NMR Experiments 46
3.2.3 Fluorescence Investigation 48
3.2.4 Conclusions 50

Chapter 4: Guanidine – Cyclopropenium Ion Superbase 52
4.1 Introduction 52
4.2 GCSB Synthetic Pathway 53
4.3 Conclusion 61

Chapter 5: Cyclopropenium Ion Functionalized Azo Compounds 62
5.1 Introduction: Next Generation Applications of Azo Compounds 62
5.2 Cyclopropenium Ion Containing Azo Compound Synthetic Pathway 64
5.3 Conclusion 68

Chapter 6: Summary 69

Chapter 7: Experimental Details 71
7.1 Experimental Procedures 73

Appendix A: Spectral Data 96

Appendix B: DFT Calculated Geometries, Thermochemical and Crystal Structure Data, and Calculated Molecular Orbitals 145

Chapter 8: References 173

List of Figures

Figure 1: *Derivatives of amines and their respective pK_a values of the conjugate acids in H_2O.*. 2

Figure 2: *Resonance forms of acetamidine upon protonation.* 2

Figure 3: *Example of P_1 and P_4 phosphazene bases.* 3

Figure 4: *Subsequent methylation of 1,8-diaminonaphthalene, and their respective pK_a.* 5

Figure 5: *1,8-Bis(tetramethylguanidino)naphthalene (TMGN) and 1,8-bis(hexamethyltriaminophosphozenyl)naphthalene (HMPN).* 6

Figure 6: *Alder's original sponge DMAN, and the newly synthesized derivative DACN.*[7] 7

Figure 7: *The Janus sponge containing remnants of original sponge (DMAN), and cyclopropenimine functionality.*[14] 8

Figure 8: *Cyclopropenimines and protonated conjugate acids, cyclopropenium ions.* 11

Figure 9: *Visual representation of fluorescence mechanism.* 16

Figure 10: *Select examples of fluorophores with widely used coumarin (**28**), fluorescein (**29**), BODIPY (**30**), naphthalene (**31**), and rhodamine scaffolds (**32**).* 18

Figure 11: *Typical description of an ICT style fluorophore.* 20

Figure 12: *Light driven molecular motor cycle developed by Feringa and colleagues. In the presence of light, the coloured portion of the molecule makes full circular rotations, flipping from **33** to **33a** and vice versa.* 21

Figure 13: *Prototypical azo compound, azobenzene, and its structural isomers.* 23

Figure 14: *Polymer initiator azobisisobutyronitrile.* 23

Figure 15: *Selected naphthalene containing fluorescent organic molecule: Janus Sponge (**12**), dansyl amide (**44**), 4-aminonaphthalimide (**45**), 1,2-benzo-3,4-dihydrocarbazole-9-ethyl chloroformate (BCEOC) (**46**),[7] 6-Propionyl-2-(dimethylamino) naphthalene (PRODAN) (**46**).* . 30

Figure 16: *Prepared derivatives to probe the structural implications on the photophysical properties.* 31

Figure 17: *Compound **12** alongside derivatives **48**, **49**, and **58** accompanied by photophysical properties calculated in ethanol.* 31

Figure 18: *Derivatives **50**, **51**, **52,** and **53** accompanied by photophysical properties calculated in ethanol.* 33

Figure 19: *Derivatives* ***54****,* ***55****,* ***56,*** *and* ***57*** *accompanied by photophysical properties calculated in ethanol.* 34

Figure 20: *Enlarged Two-dimensional representation of (****12****).* 36

Figure 21: *A) DFT computed geometry, HOMO, and LUMO of* $\mathbf{12_{In}}$*, as well as its TD-DFT optimized singlet excited state geometry. B) DFT computed geometry, HOMO, and LUMO of* $\mathbf{12_{out}}$*, as well as its TD-DFT optimized singlet excited state geometry. Level of theory: M062X-D3/6-31+g(d,p) scrf=(dichloromethane). Selected hydrogen atoms were removed for clarity.*.. 38

Figure 22: *(A) Cyclopropenium ions. (B) Cyclopropenium ion functionalized systems (****12*** *and* ***58****), and respective anions used in this work.* 43

Figure 23: *(A) 2D schematic for compound* ***12*** *with appropriate labeling scheme (the largest numbers are referred to in text) and ORTEP plots of the molecular structures of derivatives* $\mathbf{12a}_{Cl}$*,* $\mathbf{12b}_{BF4}$*,* $\mathbf{12c}_{PF6}$*, and* $\mathbf{12d}_{BPh4}$*. Thermal ellipsoids are plotted at 50%. (B) 2D schematic of the inter- and intramolecular hydrogen bonding, the computed strength of the intramolecular hydrogen bond (IMHB), and the quantum yield (*ϕ*). (C) Experimentally determined N(3)—H(3) hydrogen shifts of* $\mathbf{12a}_{Cl}$*,* $\mathbf{12b}_{BF4}$*,* $\mathbf{12c}_{PF6}$*, and* $\mathbf{12d}_{BPh4}$ *in* $CDCl_3$*.* 44

Figure 24: *(A) Non-covalent interaction (NCI) plots displaying favourable van der Waals interactions (green isosurfaces) in* $\mathbf{12b}_{BF4}$ *and* $\mathbf{12c}_{PF6}$*.. The surfaces are coloured on a rainbow scale based on values of sign(*λ_2*) between −0.04 to 0.04 au. Bifurcated hydrogen bonding between the anion and dialkylamine depicted by green lines. (B) Bifurcated hydrogen bonds between dialkylamine* NMe_2 *group and external hydrogen bond donors* BF_4^- *and* PF_6^-*.* 47

Figure 25: *Enlarged version of Figure 23C denoting chemical shifts of H(3) with respective derivatives.* 48

Figure 26: *Computationally derived HOMO, LUMO, LUMO+1 of* $12d_{\mathbf{BPh4}}$*.* 50

Figure 27: *Visual representation of anion interactions resulting in diminished fluorescence efficiency.* 51

Figure 28: *Protonated Janus sponge (****12****) along with new targets* ***59*** *and* ***59a****.* 52

Figure 29: *Derivative* ***64****, analogues to known BODIPY dyes* ***60****,* ***61****,* ***62****, and* ***63****.* 53

Figure 30: *X-ray crystal structure of* ***59.*** *Thermal ellipsoids plotted at 50%.* 58

Figure 31: *X-ray crystal structure of* ***64****.* 61

Figure 32: A) *The cyclopropenium motif with modifiable R and* X^- *groups. B) Lipophilic and hydrophobic areas outlined in the cyclopropenium ion motif. C) Target azo molecule* ***73****, incorporating cyclopropenium ion functionality.* 64

Figure 33: *X-ray structure of* ***73****. Thermal ellipsoids plotted at 50%*..... 67

Figure 34: *Absorption profile of* ***73*** *with absorption maximum recorded at 395 nm.* 68

List of Tables

Table 1: *Key metrics associated with* ***12***a_{Cl}, ***12***b_{BF4}, ***12***c_{PF6}, *and* ***12***d_{BPh4}, *where intramolecular hydrogen bond is denoted as IMHB.* X^- *denotes the respective anion.* 45

Table 2: *Select photophysical properties of derivatives* ***12***a_{Cl} – ***12***d_{BPh4}. *IMHB denotes intramolecular hydrogen bond* 49

Table 3: *Selected photophysical properties of* ***59***..... 59

List of Schemes

Scheme 1: *Synthesis of the triphenylcyclopropenyl cation by Breslow.* 10

Scheme 2: *A) protonation of a general cyclopropenimine. B) Depiction of the movement of electrons that share the positive charge among the entire cyclopropenyl cation core.* 11

Scheme 3: *Synthesis of pentachlorocyclopropane by Tobey and West.* 12

Scheme 4: *Formation of tetrachlorocyclopropene.* 13

Scheme 5: *Synthesis of tris(dialkylamino)cyclopropenium ions (top). Examples of tris substituted cyclopropenium ions (below).* 14

Scheme 6: *Synthesis of chlorobis(dialkylamino)cyclopropenium ion derivatives (top). Examples of chlorobis(dialkylamino)cyclopropenium ions,* ***27*** *and* ***28****.* 14

Scheme 7: *Diazotization of a primary amine.* 24

Scheme 8: *Azo coupling reaction.* 24

Scheme 9: *Electrolytic oxidation of amine (****39****) to azobenzene (****40****).* 25

Scheme 10: *Dehydrogenation reaction to afford azobenzene derivatives* ***(42)*** *from diphenylhydrazine derivatives (****41****).* 26

Scheme 11: *Jablonski-type diagram, representing the general electronic transitions associated with the photoexcitation and emission of* $\mathbf{12}_{out}$***.*** 37

Scheme 12: *Synthetises of* ***59*** *– step one: mono BOC protection of* ***65*** *to afford* ***66****.* 53

Scheme 13: *A) Synthesis of necessary precursor 2-chloro-1,3-dimethylimidazolium chloride, 68. B) Guanidine functionalization of* ***66*** *to afford* ***69****.* 54

Scheme 14: *Attempt to deprotect the carbamate group of 69 using TFA as the acid.* 55

Scheme 15: *Successful deprotection affording* ***70.*** 56

Scheme 16: *Attempt at cyclopropenium ion functionalization using the same procedure for the Janus sponge.* 56

Scheme 17: *Successful synthesis of* ***59.*** 57

Scheme 18: *Optimized reaction conditions for the cyclopropenium functionalization of* ***70.*** 58

Scheme 19: *Deprotonation of* ***59*** *using KHMDS.* 59

Scheme 20: *Failed attempt at synthesizing BOPS.* 60

Scheme 21: *Successful synthesis of BOPS (**64**).* 60

Scheme 22: *Synthesis of isolatable compound **73**.* 64

Scheme 23: *Synthesis of already reported compounds **75** and **76** necessary for diazonium coupling reaction.* 65

Scheme 24: *Attempt 1: diazonium coupling reaction. Both **75** and **76** were attempted, X^- denoting BF_4^- and Cl^- anions respectively.* 65

Scheme 25: *Reaction to form hydrazine **79**.* 66

Scheme 26: *Final synthesis of the first cyclopropenium ion containing azo compound **73**.* 66

List of Abbreviations

B3LYP	Becke's three parameter hybrid density functional using Lee, Yang, and Parr's correlation
Bu	Butyl
DCM	Dichloromethane
DFT	Density functional theory
h	Hour(s)
ICT	Internal charge transfer
IEFPCM	Integral equation formalism polarized continuum model
IMHB	Intramolecular hydrogen bond
LED	Light emitting diode
LCAO	Linear combination of atomic orbitals
Me	Methyl
min	Minute(s)
NBO	Natural bond orbital
NMR	Nuclear magnetic resonance spectroscopy
Ph	Phenyl
Pr	Propyl
rt	Room temperature
TFA	Trifluoroacetic acid
TLC	Thing layered chromatography
THF	Tetrahydrofuran

Chapter 1: Introduction

1.1 Organobases

Throughout history, the definition of acids and bases slowly developed into what seems to be common knowledge today. In the 1890s, Svante August Arrhenius delivered the first actual theory for defining acids and bases.[1] He defined acids as "substances delivering hydrogen cations to the solution", while bases were "substances that deliver hydroxyl anions to the solution". This theory had one underlying flaw. It meant that, as an example, nitric acid would technically not be an acid in its purest form and could only be classified as an acid in solution where it could deliver its hydrogen cation to water. This definition posed many problems until finally, in 1923, a Danish chemist by the name of Johannes Brønsted and an English chemist Thomas Lowry proposed a modification to Arrhenius's theory.[2] Their extended theory of acids and bases depicted an acid as a molecule, whether neutral or electrically charged, that has a tendency to lose a hydrogen nucleus. Inversely, this theory defined a base as a molecule, whether neutral or charged, that has a tendency to unite with a hydrogen nucleus.

Bases play an integral role in organic chemistry, as many reactions cannot proceed without the removal of a proton to facilitate a particular reaction process. Organic bases (organobases) are extremely useful, due to the fact that they can be easily manipulated, making them quite versatile. Normally, organobases consist of amines, which are relatively weak bases, given Brønsted and Lowry's definition.[3]

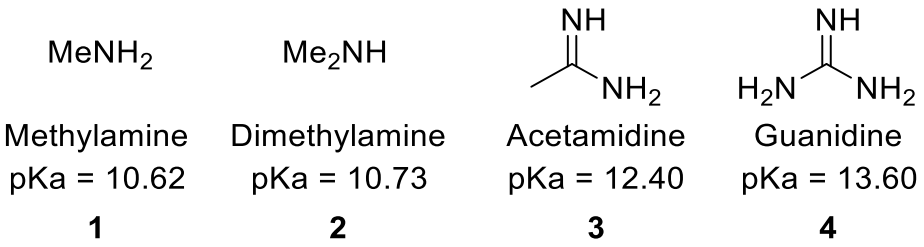

Figure 1: Derivatives of amines and their respective pK_a values of the conjugate acids in H_2O.[4]

The strength of a neutral base can be associated with the capacity of the conjugate acid to stabilize the positive charge formed upon protonation. Based on this theory, organobases can be strengthened by the addition of electron donating groups, demonstrated by the increased pK_a of dimethylamine (**1**) compared with methylamine (**2**) (**Figure 1**). The addition of another methyl group to the nitrogen atom results in additional electron donation to the amine, effectively increasing the electron density at the nitrogen atom making positive charge accumulation and conjugate acid formation more feasible.[4] In the case of acetamidine (**3**), the addition of an imine (=NH) to the α-carbon affords a more basic species, because it introduces the added benefit of resonance stabilization upon protonation (**Figure 2**).

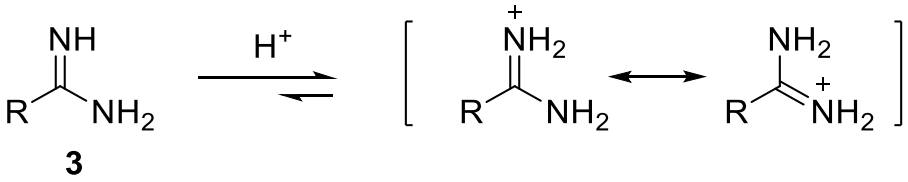

Figure 2: Resonance forms of acetamidine upon protonation.

The movement of electrons allows for the positive charge to be shared among the two nitrogen atoms, inherently making the conjugate acid more stable. This effect is also observed with guanidine compounds (**4**), and is even greater owing to the presence of an additional amine group resulting in increased resonance stabilization. The resonance of the molecule allows for the

conjugate acid's positive charge to be shared among three nitrogen atoms, rather than just two, causing the basicity of the guanidine moiety to be comparable to that of the hydroxyl ion.[4]

In 1985, further development on basicity was completed by Schwesinger by introducing phosphazenes containing a phosphorus atom bonded to four nitrogen functions additionally housing three amine groups, and one imine component (**Figure 3**). These types of phosphorus containing organobases are classified as P_n bases, where "n" is the number of phosphorus atoms contained within the molecule.[4]

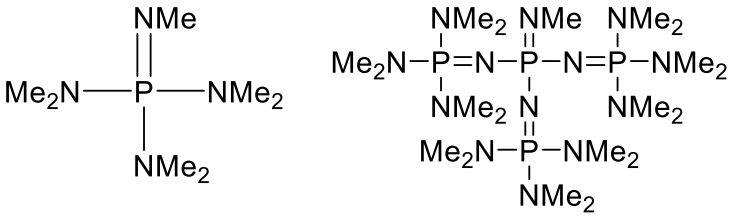

P1 base
5

P4 base
6

Figure 3: Example of P_1 and P_4 phosphazene bases.[4]

These phosphazene bases are readily soluble in common organic solvents and are not susceptible to nucleophilic attack, as a result of their steric bulk, all while exhibiting very high basicities.[4]

Compounds **5** and **6** have high pK_a values and are well known *superbases*. The first definition of a superbase was proposed by Caubère in a 1993 in order to clarify the difference between the ambiguous terms "strong" and "super". His definition implied that the term 'super base' should only be applied to bases resulting from a mixing of multiple bases leading to a new basic species possessing new properties. Caubère proposed that the term super base does not mean a base is thermodynamically and/or kinetically stronger than another but is instead defined as a basic reagent being created by combining the characteristics of several different base.[5]

Before Caubère's proposed definition, there was no defined term or explanation as to what separated ordinary organobases from a superbase. It was not until 1998 that Raczyńska added a qualitative component to the definition of a superbase. This addition states that the term superbase is defined as any base having an absolute proton affinity (APA) larger than 245.3 kcal/mol and gas phase basicity (GB) over 239 kcal/mol.[6] Newly synthesized base pK_a values can be either experimentally determined, or computationally predicted, and given these two definitions, the superbase concept can be further extended to species that involve the combination of multiple superbases to form "higher-order superbases". A recent report by Lambert focused on higher order superbases that incorporated a cyclopropenimine functionality in order to achieve remarkably high basicity.[7] The report indicates that cyclopropenimines are as basic as the P_1 phosphazene outlined above in **Figure 3**, but have dramatically improved stability in non-inert atmospheres. The extreme basicity of cyclopropenimines is associated with the formation of an aromatic structure upon protonation, but this will be discussed in greater detail in Section 1.2.3. Strong Brønsted bases play an important role in the sense that as the basicity increases, the number of substrates amenable to activation increases and therefore broadening the scope of available reagents. Superbases permit the recycling of the proton between the base and the acid counterpart, so that the reagent may be reused in subsequent reactions.

1.2 Proton Sponges

1.2.1 The Prototypical Proton Sponge

In regards to Raczyńska's criteria, the value (245.3 kcal/mol) that defined the cutoff for superbases stems from Alder's prototypical proton sponge that was synthesized in 1968.[8] Alder was methylating 1,8-diaminonaphthalene in increments while studying the interactions of the lone pairs, and tested the effect steric bulk had on the pK_a of the newly generated compounds. Alder

reported steady increases in the pK_a for every subsequent methyl group added to the molecule, until there was a spike upon the addition of the final methyl group (**Figure 4**).

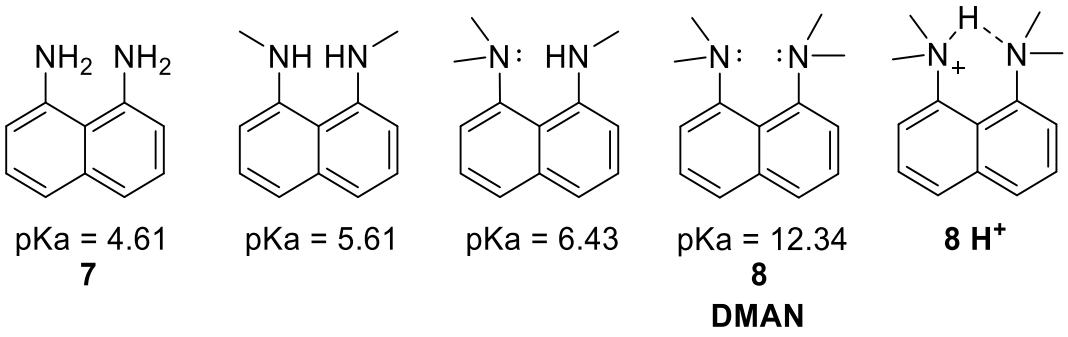

Figure 4: Subsequent methylation of 1,8-diaminonaphthalene, and their respective pK_a.[8]

The dramatic increase in pK_a is associated with the steric strain of the methyl groups causing the lone pairs to face inwards toward each other. The lone pair repulsion causes the lone pairs to elevate out of plane by roughly 35˚ resulting in relief of lone pair strain. The same strain is further reduced by the intramolecular hydrogen bond (IMHB) formation upon protonation (**8 H**$^+$), and the combination of these factors is what gives rise to the basicity of **8**. In addition to their high thermodynamic basicities, these molecules are known for their slow intermolecular proton transfer kinetics, and it is for this reason the term "sponge" is used. In most cases, the proton is surrounded by a hydrophobic shell hindering the approach of other basic species. This feature, together with the strong intramolecular hydrogen bond, is the cause of the slow kinetic activity in relation to intermolecular proton transfer.[9] All the factors and attributes of proton sponges were the primary driving force for research into increasing the basicity of this class of compound by adding iminophosphorane and guanidine functional groups (**Figure 5**). It was shown that by modifying the *N*-substituents with more basic species, one can impart greater changes to the pK_a of the system.[10]

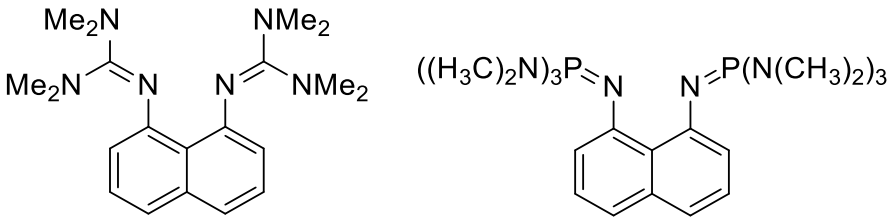

TMGN
9

HMPN
10

Figure 5: 1,8-Bis(tetramethylguanidino)naphthalene (TMGN) and 1,8-bis(hexamethyltriaminophosphozenyl)naphthalene (HMPN).[10]

1.2.2 Guidelines for a Proton Sponge

As briefly stated above, there are three main factors that contribute to the high basicities of proton sponges and have henceforth become a guideline for compounds being described as such. These three factors are as follows: 1) destabilization of the base as a consequence of the strong electron lone pair repulsion associated with the *peri*-amines; 2) relief from steric strain upon protonation, that being the uptake of a single hydrogen atom; and 3) the formation of an intramolecular hydrogen bond (IMHB). In 2016, an additional criterion was proposed by Pazharskii *et al*.[11] He mentioned that many proton sponges are lacking, or have largely distorted IMHB angles and therefore are not adhering criterion 3, the formation of a full IMHB. This observation is due to the coordination of the counterion to the acidic proton, making the distance of the individual counterions in the protonated molecules an important component. That being said, a quotation from the 2016 paper summarizes it nicely:

> *"One can see that for DMAN cation 1H*$^+$ (compound **8 H**$^+$ in this thesis), *the shortest distances between the NH proton and a counterion are those for F*$^-$ *and BF*$_4^-$ *(2.75 and 2.91 Å, respectively). This means that all bases for which these values are nearly the same or larger can be considered as proton sponges. In*

contrast, superbases with lesser NH···anion distances should be classified as pseudo-proton sponges."[11]

It is important to note that the counterion distances with respect to the intramolecularly bound hydrogen atoms are derived from the crystal structures of the molecules of interest. This is an important factor that will be revisited later in **Chapter 3**.

Alder's prototypical proton sponge not only provided the structural basis for proton sponges with ever increasing proton affinities (PA), but also furthered our understanding of superbases and hydrogen bonding. Up until the development of the proton sponge, hydrogen bonding studies were isolated to intermolecular hydrogen bonding between molecules in X-ray crystal structure lattices.[12] The fixed interatomic distances allowed chemists to study, for the first time, the nature of the IMHB.

1.2.3 Cyclopropenium Functionalized Sponge Derivatives

The Dudding group, through their interest in cyclopropenimines and hydrogen bonding, functionalized 1,8-diaminonaphthalene with bis(dialkylamino)cyclopropenimines to create 1,8-bis(bis(diisopropylamino)cyclopropeniminyl)-naphthalene (DACN, **Figure 6**).[13]

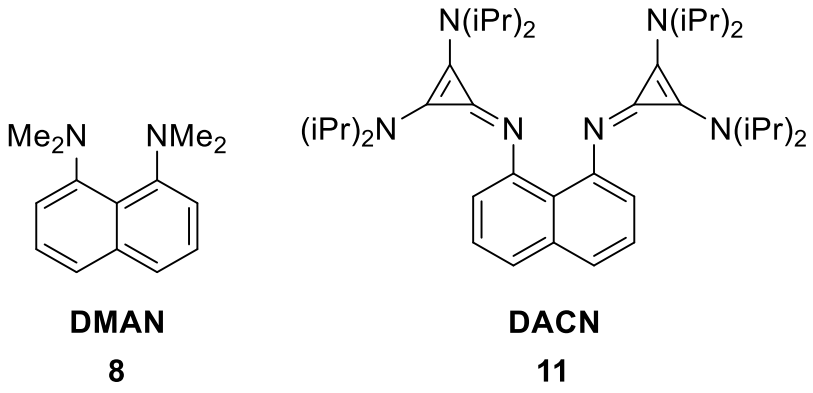

Figure 6: Alder's original sponge DMAN, and the newly synthesized derivative DACN.[8,13]

The proton affinity of DACN calculated at the B3LYP/6-311G++(d,p)//B3LYP/6-31G(d,p) level, taking into account thermal corrections estimated by the B3LYP/6-31G(d,p) method, was 282.3 kcal/mol, a dramatic increase from the original sponge DMAN (245.4 kcal/mol). This large increase in the PA is directly associated with the formation of the cyclopropenyl cation upon protonation, and the calculated pK_a of DACN was estimated to be 27.0, comparable to extraordinarily strong bases. As a result of the basicity of DACN, the mono-protonated form of the sponge could not be isolated, and therefore the pK_a value could not be experimentally determined.

Building upon this work, in 2015, the Dudding group synthesized a new, non-symmetrical proton sponge that included the functionality of both DMAN, and the cyclopropenimine derivative DACN. Being a non-symmetrical sponge, and making use of "two faces", the sponge was deemed the "Janus Sponge" derived from the Roman god of beginnings and endings, Janus (**12a**) **Figure 7.**[14]

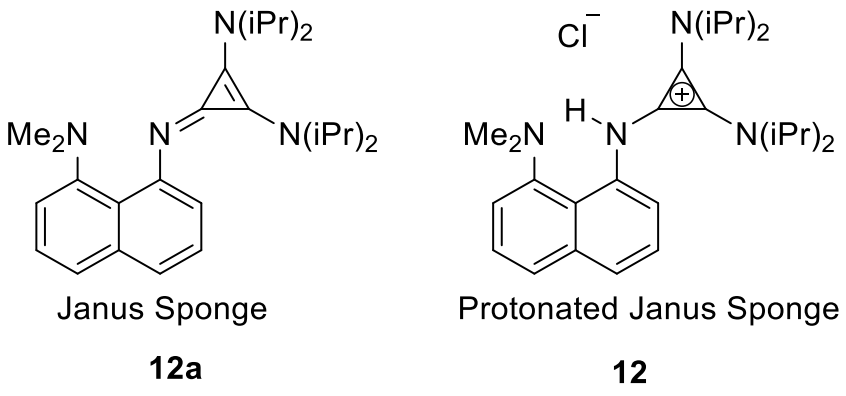

Figure 7: The Janus sponge containing remnants of original sponge (DMAN), and cyclopropenimine functionality.[14]

The experimental pK_a of the Janus sponge was determined to be 23.8, in good agreement with the calculated pK_a value of 23.9, while the proton affinity was 266.8 kcal/mol. The protonated form of Janus sponge (**12)** was also found to exhibit fluorescent properties, notably representing the first

ever cyclopropenimine-based fluorescent molecule. Compound **12** absorbs light at a λ_{max} of 333 nm and has emission λ_{em} at 472 nm corresponding to a large stokes shift of 139 nm in DCM. In the original paper, the quantum yield was determined to be 0.37 in ethanol. Interestingly, the molecule also fluoresces in the solid state, yet no measurements or investigations have been made on this front to date.

1.3 Cyclopropenium Ions and Amino-Substituted Cyclopropenium Ions

1.3.1 Stability of the Cyclopropenium Ion

One of the substantial successes of the simple molecular orbital theory developed by Hückel is that out of the completely conjugated, planar, monocyclic polyolefins such as benzene, etc., possessing (4n+2) π-electrons will be more stable because they posses fully filled molecular orbitals with substantial resonance energies.[15] Much of the interest in non-benzanoid aromatic compounds centers around verifying the theoretical prediction that, in addition to well-known stable aromatic molecules containing six electrons or more, a three membered ring with only two electrons, the cyclopropenyl cation, should also be aromatic. Further studies on the cyclopropenyl cation applying Hückel's Linear Combination of Atomic Orbitals (LCAO) to calculate delocalization energy revealed that the cyclopropenyl cation contains high delocalization energy, supporting the theory of stability due to the generation of aromaticity. The first derivative developed in 1957 by Ronald Breslow involved the reaction of diphenylacetylene with phenyldiazoacetonitrile yielding 1,2,3-triphenyl-2-cyclopropene carboxylic acid nitrile. The triphenylcyclopropenyl cation (**16**) was then generated through a reaction with boron trifluoride etherate and a trace amount of water (**Scheme 1**).[16]

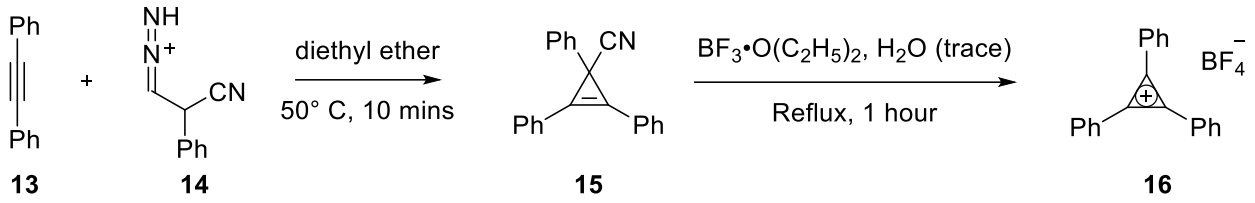

Scheme 1: Synthesis of the triphenylcyclopropenyl cation by Breslow.[16]

The newly synthesized derivative further strengthened the hypothesis that the stability of the cyclopropyl cation arises from the generation of aromaticity. Before the synthesis of **16** it was thought that the ring strain inherent in the cyclopropyl cations with two π-electrons delocalized over three 2p orbitals would supersede aromatic stability. However, as described above, Hückel aromaticity results in significant thermodynamic stability.

1.3.2 Cyclopropenimines as Strong Brønsted Bases

Hückel's prediction of cyclopropenium ion stability and Breslow's synthetic achievement laid the foundations for nitrogen containing cyclopropenimines (**Figure 8**) having utility as Brønsted bases. As mentioned previously, as a result of the prevalence of chemical reactions involving proton transfer as a key mechanistic event, Brønsted bases are indispensable tools for organic chemistry. Bases such as tetramethylguanidine and diazabicycloundecene have proven to be highly useful as reagents. However, the amidine and guanidine functionalities associated with these molecules have inherent limitations associated with increasing their basicity.[17] There exists the need to develop bases that provide exceptional and tunable basicity, while being straightforward to synthesize. Lambert and Bandar in 2012, further explored the basicity of cyclopropenimine bases through the the cyclopropenyl cation. Their findings showed that the basicity of their cyclopropenimine representative was comparable to the P_1 phosphazene base.[18]

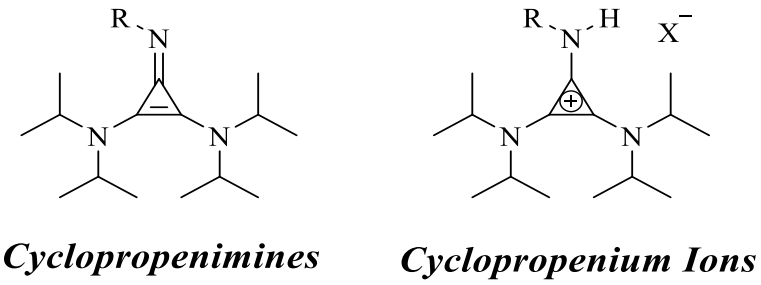

Figure 8: Cyclopropenimines and protonated conjugate acids, cyclopropenium ions.

A cyclopropenimine molecule consists of a three-nitrogen bearing system, with the three-membered ring as its core. Two of the three nitrogen groups are amine functionalities, while the third, and the most basic site for this class of molecule, is an imine. The two main components for the strong basicity are the fact that the conjugate acid is stabilized by the three-nitrogen atom lone pairs (**Scheme 2A**), and as previously mentioned, the generation of aromaticity making the cyclopropenium ion the smallest carbon based aromatic ring system (**Scheme 2B)**.

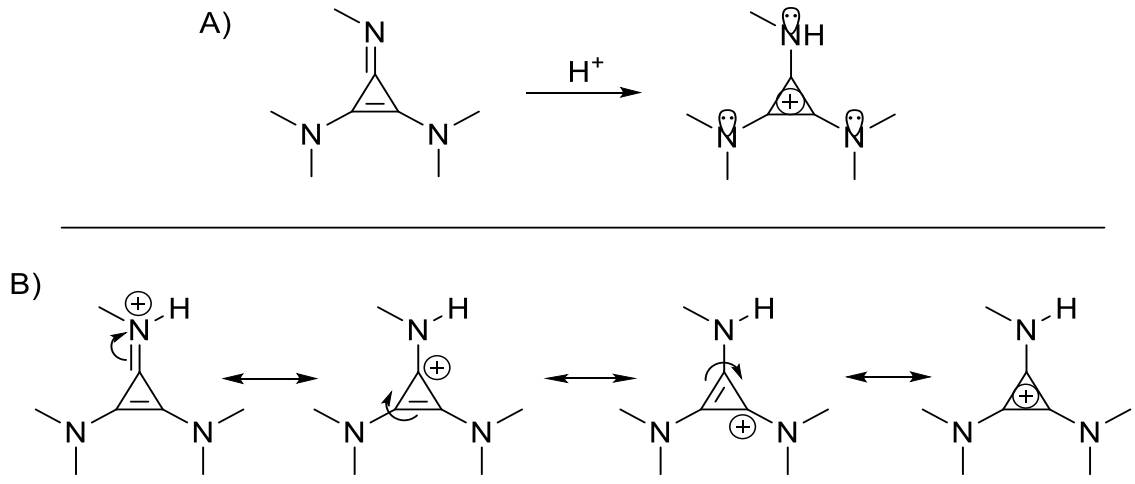

Scheme 2: A) protonation of a general cyclopropenimine. B) Depiction of the movement of electrons that share the positive charge among the entire cyclopropenyl cation core.

The capacity of these molecules to have tunable basicity stems from the types of groups that are attached to the nitrogen atoms. Groups that donate electron density to the nitrogen atoms will inherently be more basic than withdrawing components. This is due to the stability of the conjugate

acid, stemming from the sharing of the charge that is generated. If electron density is removed from the ring scaffold, the stability of the conjugate acid will decrease, thereby hindering the overall basicity of the molecule. Given this concept, cyclopropenimines are popular as they are useful precursors for building superbases with a wide range of basicities, for a broad range of applications.

1.3.3 Synthesis of Cyclopropenium Ion Derivatives

Commonly, the synthesis of cyclopropenium ion derivatives (especially for all of the cyclopropenium ions reported in this thesis) begins with tetrachlorocyclopropene (**22**). Although this reagent is commercially available today, Stephen Tobey and Robert West developed a two-step synthetic protocol for this compound. The first step, the formation of pentachlorocyclopropane (**21**), was achieved in 1963 by reacting trichloroethylene with sodium trichloroacetate in the presence of 1,2-dimethoxyethane (1,2-DME).[19] 1,2-DME facilitates the formation of dichlorocarbene leading to the addition of the carbene to the chlorinated olefin (**Scheme 3**). The final product is isolated by a rigorous vacuum distillation. It is important to note that the reaction is highly dependent on the temperature, and excessive heating leads to decomposition of the final product.

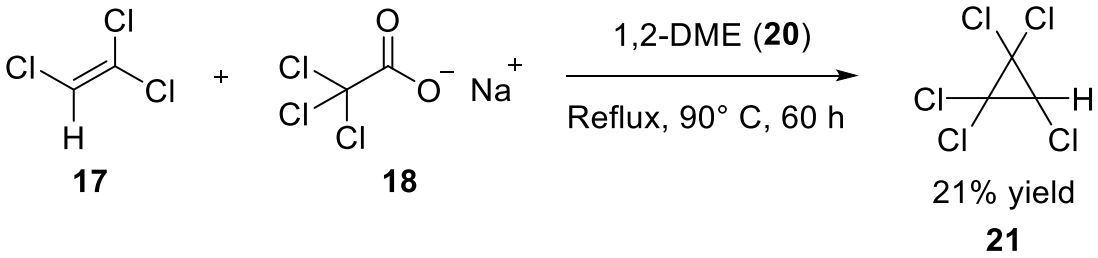

Scheme 3: Synthesis of pentachlorocyclopropane by Tobey and West.[19]

The synthesis of **21** was truly ground breaking work, allowing the three membered cyclopropane ring to become largely accessible by many others. Tobey and West then afforded **22** under extremely basic conditions depicted below in **Scheme 4**.[20]

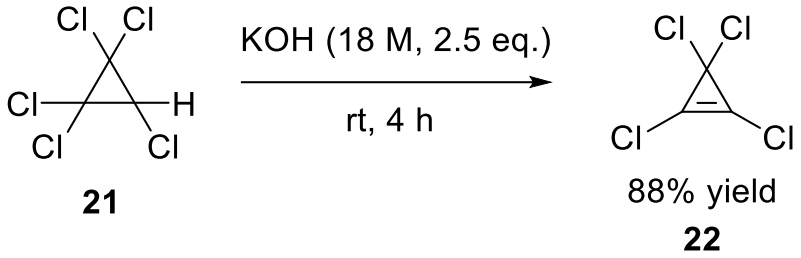

21 **22**

Scheme 4: Formation of tetrachlorocyclopropene.[20]

The final product was isolated by distillation under an inert atmosphere. Tobey and West indicated that the title compound was highly reactive and susceptible to ring opening reactions in the presence of water and ammonium hydroxide.

To prepare cyclopropenium ion derivatives, the original method described by Yoshida is widely used for its simplicity and efficiency,[21] which involves reacting compound **22** with an excess of dialkylamine resulting in the rapid formation of the corresponding product. It is important to note that the steric congestion of the dialkylamine plays an important role, where small steric contributions lead to tris(dialkylamino)cyclopropenium ion derivatives (**Scheme 5**). This can be seen with alkylamines such as, but not limited to, dimethylamine, piperidine, and morpholine.

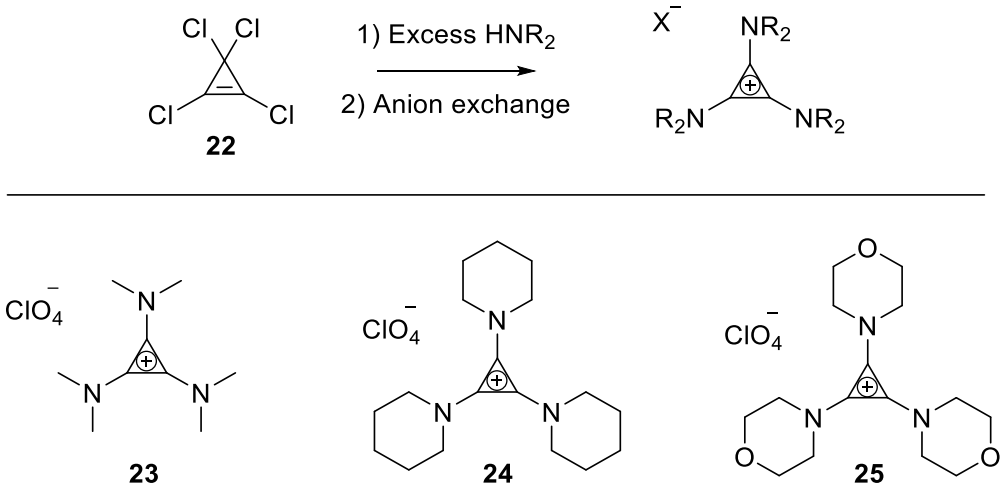

Scheme 5: Synthesis of tris(dialkylamino)cyclopropenium ions (top). Examples of tris substituted cyclopropenium ions (below).[21]

However, the substitution with more hindered alkylamines leads to chlorobis(alkylamino)cyclopropenium ions (**Scheme 6**). Examples of bulky alkylamines leading to bis substitution are diisopropylamine and dicyclohexylamine.

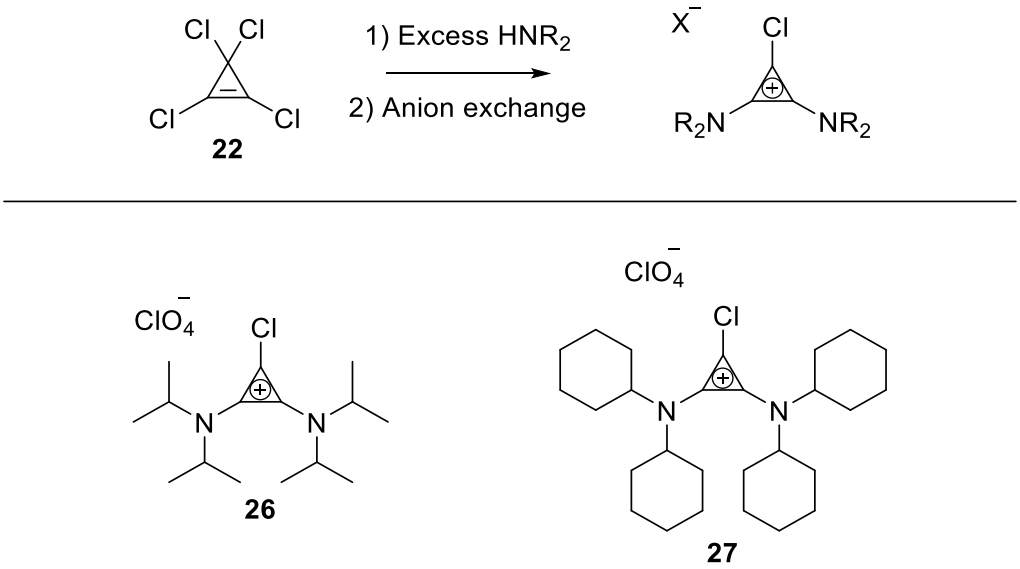

Scheme 6: Synthesis of chlorobis(dialkylamino)cyclopropenium ion derivatives (top). Examples of chlorobis(dialkylamino)cyclopropenium ions**, 27** and **28.**[21]

The resonance donating capacity of alkylamines assists in providing high cation stability and a low oxidation potential. Alkylamine-substituted cyclopropenium ions have been under

investigation since the 1970s but have only recently found use in applications. Through the research performed by the Dudding group, the addition of cyclopropenium ions can not only add superbasic properties to molecules, but these compounds have also found use as phase transfer catalysts. A publication by Dudding and Mir, showed the use of cyclopropenium ions as phase transfer catalysts in *O*-silyl ether deprotection.[22] The origin of this reactivity was explored through LFER analysis and density functional theory (DFT) calculations and it was discovered that cyclopropenium ions have the capacity to act as catalytic platforms for shuttling fluoride into solution. This activity is not limited to deprotection, but also extends to benzylation and benzylic fluorination.[23] The potential application of cyclopropenimines is still a main research focus for the Dudding group today, including the recent development of charged enhanced thioureas,[24] and further investigations of light responsive cyclopropenium ion containing compounds that will be discussed in greater detail further in this thesis (**Chapters 2-5**).

1.4 Photochemistry

1.4.1 Fluorescence Fundamentals

Fluorescence is a major component in many research fields, making small organic fluorophores important in both materials and biological sciences. The breadth of applications drives researchers to develop new molecules, or even modes of fluorescence. The majority of fluorescent molecules contain conjugated π systems that absorb UV or visible light at some λ_{max}, the maximum absorbance wavelength. A very small amount of conjugated systems emit the absorbed energy as fluorescence, and the highest intensity in the fluorescence curve is denoted as λ_{em}.[25] Specifically, absorbance of light by these conjugated systems is the result of incoming UV and/or visible light matching the energy gap for π to π* transitions. This generates an excited state of the molecule (S_n), but given the fact that the excited state is higher in energy than the ground

state (S_0), a thermodynamic driving force is present for returning to the lower energy ground state (**Figure 9**).[26]

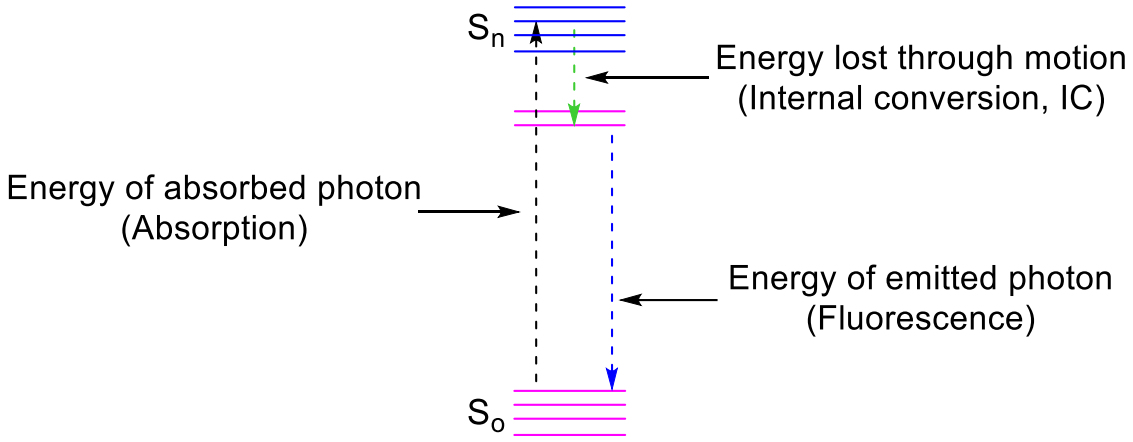

Figure 9: Visual representation of fluorescence mechanism.[26]

There are three primary mechanisms of which an excited molecule can revert back to the ground state: internal conversion (IC), which refers to the mechanical (motion) dissipation of energy; intersystem crossing (ISC), which involves inverting the spin of one of the electrons; and fluorescence, being the emission of a photon of exact energy separating the excited state at a given configuration and allowing for direct relaxation to the ground state.[26] It is important to note that intersystem crossing is absent in **Figure 9** because it is a process in which a singlet excited state transitions to a triplet excited state at the point where the two potential energy curves cross. A triplet formed in this way, being in an excited state, loses energy through collisions with other molecules. Both transitions from excited singlet to excited triplet, and the reversion of excited triplet to excited singlet are forbidden processes in the absence of spin-orbit coupling giving rise to the slow emission of electromagnetic radiation, commonly known as phosphorescence.[26] This present thesis focuses on the investigation of fluorescent molecules, therefore intersystem crossing is not observed and henceforth will not be discussed further.

The absorbance and emission of a particular fluorophore are important for its use in applications, and the difference between the absorbed and emitted light gives rise to "Stokes shifts". This wavelength depends on factors related to the lowest energy structure of the excited state, and the lowest energy structure of the ground state.[27] Excitation occurs on a timescale much faster than structural relaxation, therefore the resulting structure of the initial excited state is the same as the structure of the ground state that absorbed the photon, and is not the optimal structure for the excited state. Excited state molecules persist long enough to undergo structural reorganization or internal conversion. Subsequent emission leads to a ground state configuration that is optimal for the excited state, but not the ground state. It is the combination of these effects that narrow the energetic separation of the ground and excited states, and the energetic loss is what leads to the difference between absorbed and emitted wavelengths. The internal conversion process is much faster than that of fluorescence, which is why the majority of organic molecules do not fluoresce.[28] Two additional parameters of importance in fluorescence applications are the molar extinction coefficient ε, being the efficiency at which light is absorbed by a molecule, and the quantum yield ϕ, a dimensionless ratio between 0.0 and 1.0 representing (emitted photons)/(absorbed photons), also referred to as the quantum efficiency. The multiplicity of ε and ϕ subsequently divided by 1000 represents the "brightness" and is used to compare fluorophores, although scarcely used in the literature. These parameters described are key traits specific to individual fluorophores and numerous fluorophore scaffolds have been utilized to optimize these properties.[29]

1.4.2 Fluorescence Scaffolds

Among the vast number of fluorophores, the most widely utilized make use of coumarin, naphthalene, BODIPY (4,4-difluoro-4-bora-3a,4a-diaza-s-indacene), fluorescein, or rhodamine scaffolds (**Figure 10**).

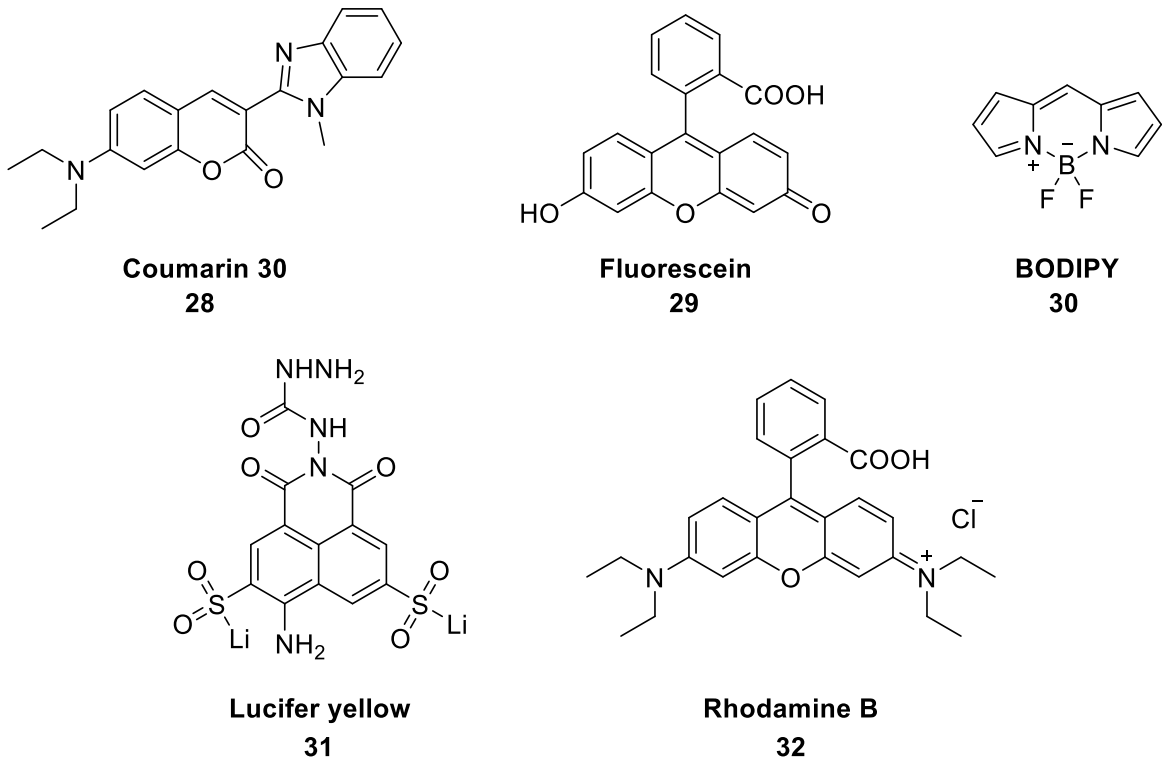

Figure 10: Select examples of fluorophores with widely used coumarin (**28**), fluorescein (**29**), BODIPY (**30**), naphthalene (**31**), and rhodamine scaffolds (**32**).

Coumarins are among the most easily synthesized,[30] but typically have excitation wavelengths in the UV region (short excitation wavelengths) hindering their use in sensitive biological studies such as cellular assays or imaging. High energy wavelengths are detrimental to studies performed *in vivo*. They also contain relatively low brightness (generally low ε values) but have large Stokes shifts and are very photostable molecules. Photostability refers to the fact that multiple instances of light exposure, as well as extended periods of exposure can occur with minimal degradation of the fluorophore.

Rhodamines and fluoresceins, however, being the most widely recognized,[31] remain among the brightest fluorophores available for common use. The synthesis of these molecules dates back to the 1800s, and new derivatives have shifted emission wavelengths into the red region of the spectrum. These fluorophores are consistently used in chemical, biochemical, biological, and medical applications. Although there are many established synthetic protocols for fluorescein and rhodamine compounds, the syntheses are often low yielding reactions with tedious/laborious purifications. Contrary to coumarins, fluorescein and rhodamine compounds suffer from limited photostability leading to significant photobleaching via oxidative degradation in the excited state.[32]

In 1968, Treibs and Kreuzer achieved the first synthesis of a BODIPY dye.[33] This class of dyes has henceforth been utilized as active media in dye lasers due to their high molar extinction coefficients, high quantum yields, and high photostability.[34] Additionally, the absorption and emission bands are very sharp owing to the rigidity of the core structure, which limits internal conversion leading to line broadening and diminishing the quantum efficiency. While they are very bright, a consequence of such structural rigidity comes in the form of extremely small Stokes shifts. The small Stokes shifts can make resolving excitation and emission wavelengths problematic because of the inevitable excitation scattering that overlaps with the emission. This issue does not occur with fluorophores containing large Stokes shifts, as the scattering lies outside of the detection window. Another distinctive feature of this class of dye is that they are "self-contained", meaning that the polarity of the environment does not heavily influence their photophysical properties (limited solvatofluorochromism).[34,35] There are many available BODIPY dyes on the market, yet research is constantly being conducted in order to broaden the Stokes shifts, and improve the synthetic protocols because many of the dyes result in low yields accompanied by laborious purification requirements.[35]

Among the scaffolds discussed in this thesis, naphthalene-based fluorescent compounds are of great interest as this is the class of fluorophore that the Janus sponge belongs to. Naphthalene-based fluorophores contain the highly conjugated naphthalene ring system at the core of the molecule. Researchers heavily employ naphthalene-based fluorophores because they have a number of desirable and tunable properties.[36] Usually considered short wavelength fluorophores, there are now derivatives with excitation and emission in the red or near IR region of the electromagnetic spectrum. These compounds usually exhibit fluorescence efficiencies and brightness greater than those derived from coumarins. Their synthesis is usually predictable and relatively versatile, but their most influential properties consist of large Stokes shifts (like coumarins) and very high resistivity to photobleaching. Naphthalene-based fluorophores are similar to coumarins in the sense that they operate by internal charge transfer mechanisms (ICT).

Figure 11: Typical description of an ICT style fluorophore.

Molecules that operate via ICT mechanisms have an electron donor site, along with an acceptor region (**Figure 11**). This is also known as a "push – pull" mechanism where upon photoexcitation, the donor site donates electron density to the acceptor region.[37] Excited states of ICT molecules often have larger dipole moments than the ground state leading to an odd scenario. The newly excited state is placed in a solvation "shell" that is optimal for the ground state, but not the excited state. The persistence of the excited state gives enough time for the solvation "shell" to rearrange to a more optimized scenario, essentially lowering the energy of the excited state. At the point of fluorescence, the solvent shell does not have enough time to reorganize itself upon returning to the

ground state before the fluorescence process occurs.[34] The ground state now has sub-optimal solvation, raising the relative energy of the initially formed ground state, further reducing the energy gap of the π to π* transition. As a result, ICT fluorophores have longer wavelength emissions, inevitably linked to desirable properties such as larger Stokes shifts and red shifted emissions. For this reason, current research efforts have focused on altering the different donor and acceptor groups to allow more efficient ICT to occur, offering strategies for tuning the photophysical properties of naphthalene fluorophores.[38,39]

Light responsive molecules are a major theme in this thesis, but light responsive compounds do not necessarily have to fluoresce. In 2016, the Nobel Prize in chemistry was awarded to Jean Pierre Sauvage, Sir James Fraser Stoddart, and Bernard Feringa for their contributions to the design and synthesis of molecular machines.[40]

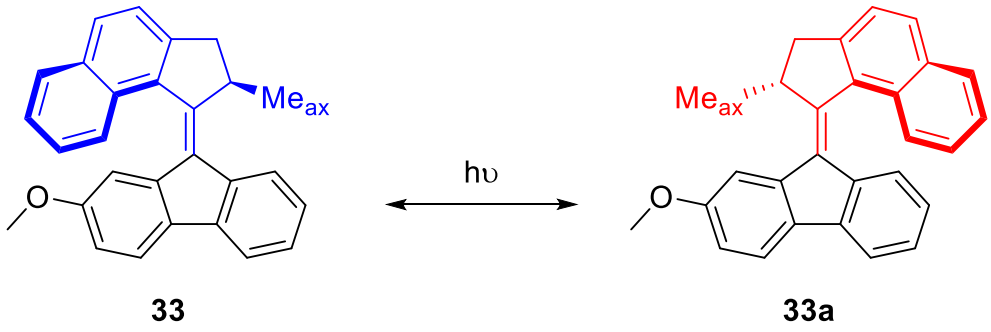

Figure 12: Light driven molecular motor cycle developed by Feringa and colleagues. In the presence of light, the coloured portion of the molecule makes full circular rotations, flipping from **33** to **33a** and vice versa.[41]

Molecular machines, very generally, are defined as compounds undergoing structural changes (rotations, extensions, contractions, etc.) in the presence of an external stimulus. A molecular motor synthesized by Feringa and colleagues (**Figure 12**) fully rotates about a carbon-carbon double bond in the presence of light.[41] There are an abundance of molecular machines in the

literature,[42] yet a simple, widely used method to install this type of motion utilizes the azo functional group.[42]

1.4.3 Azo compounds

The term "azo" refers to compounds bearing the R-N=N-R' functionality, where the nitrogen atoms are sp^2 hybridized and the R and R' groups can be of any organic class. The name azo stems from the French name for nitrogen, "azote", derived from the Greek ἀ (a-"not"), and ζωή, (zoe-"life").[43] The prototypical azo compound is azobenzene, where both R groups represent a phenyl ring (**34**). A massive library of aryl azo compounds has been synthesized due to the stabilizing resonance factor imparted by the aromatic nature of the molecules.[44] Evidence for this comes from the bond shortening of the carbon-nitrogen bond from its usual 1.47 Å to 1.41 Å, as a result of conjugation. The nitrogen-nitrogen double bond acts as a bridge for the free-flowing movement of electrons, inherently increasing the stability of the molecule by resonance. One of the key properties of azo compounds comes from the fact that two isomeric forms, *cis* and *trans*, exist (**Figure 13**).[45] In 1937, Hartley, during a spectroscopic study of the solubility properties of *trans*-azobenzene noted that the solutions changed colour when exposed to light, a phenomenon that could be reversed through long exposure to darkness. By using a tedious solvent distribution technique, Hartley was able to isolate the *cis* conformation responsible for these changes.[46] Given that azobenzene and its derivatives are thermally active, it is possible to obtain the all-*trans* isomer state through thermal equilibration in the dark. However, light irradiation produces a photostationary state as an enriched mixture of *cis* and *trans* isomers. With that being said, it is noteworthy to mention that the all-*cis* state has never been isolated.[47] The *trans* (**34**) form of azobenzene is known to be considerably more stable than the *cis* (**34a**) form due to the almost

coplanar structure of the *trans* form. The *cis* isomer's phenyl rings are rotated out of plane containing the nitrogen atoms by about 50˚.

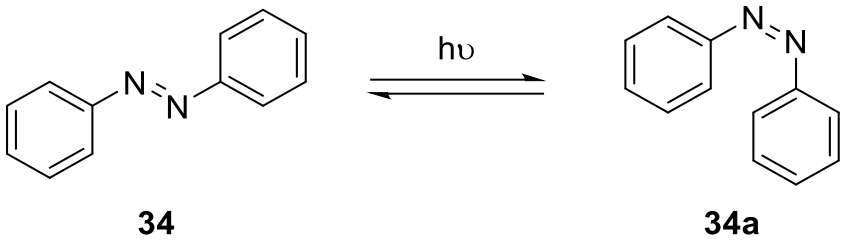

Figure 13: Prototypical azo compound, azobenzene, and its structural isomers.[47]

Throughout history, the main application of azo compounds was in the manufacturing of dyes. As a consequence of π-delocalization, the azo dyes are by far the most important class of dyes, constituting over 50% of all commercial dyes with colours generally in the vibrant reds, yellows, and oranges.[43] These dyes are not limited to just colour as methyl orange, a classic azo compound, can be used as an acid-base indicator due to the change in colour in acidic/basic environments.[43] Aliphatic azo compounds, such as azobisisobutyronitrile (**35**), are far less stable and therefore are used in applications such as polymer initiators (**Figure 14**).[43]

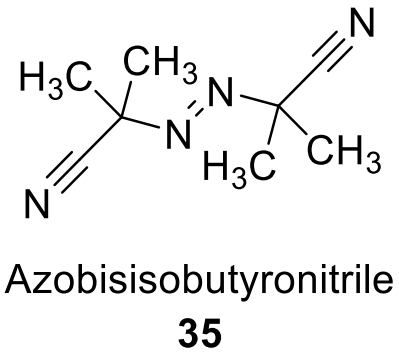

Figure 14: Polymer initiator azobisisobutyronitrile.[43]

1.4.4 Synthetic Procedures for Symmetric and Non-Symmetric Azobenzenes

A multitude of synthetic routes exist for the formation of azo compounds, including coupling reactions, reductions, oxidations, decompositions, and metal catalyzed reactions,[48] but only a selection will be discussed in detail here. To begin, the azo coupling reaction is by far the most widely used synthetic route and is referred to as a classic method to achieving a variety of substituted azobenzenes.[49] This methodology begins with the diazotization of an aromatic primary amine at low temperature (**Scheme 7**).

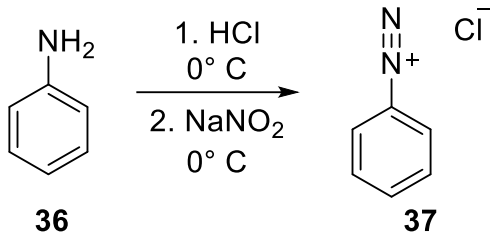

Scheme 7: Diazotization of a primary amine.[49]

The resulting diazonium salt (**37**) is rather unstable and must be used immediately to avoid decomposition leading to nitrogen gas expulsion and forming, in this case, phenol.[50] The coupling reaction is then performed with an electron rich aromatic nucleophile. Reaction times are short and high yielding, for example, the reaction depicted below yields the corresponding azobenzene in 92% yield using potassium carbonate as the base (**Scheme 8**).[51]

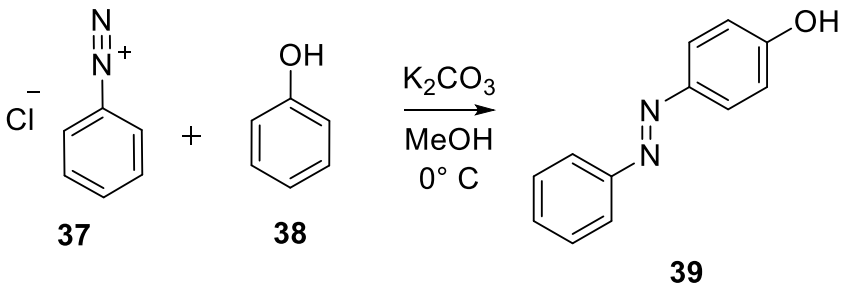

Scheme 8: Azo coupling reaction.[51]

Phenols must be converted to their ionized form because the neutral species is not sufficiently nucleophilic. Moderately alkaline conditions are essential due to the possibility of the diazonium salt forming diazohydroxide in the presence of a stronger base, and thereby inhibiting the azo coupling reaction. Several mechanisms have been proposed for the reaction, but the most widely accepted is the electrophilic aromatic substitution of the phenol with the electrophilic nitrogen atom of the diazonium salt.[52] Unfortunately, the diazonium coupling reaction is limited to the formation of non-symmetrical azobenzenes, and the relatively harsh conditions inhibit the use of sensitive starting materials.

The electrolytic oxidation of aromatic amines using platinum electrodes in dimethylformamide and in the presence of pyridine was first presented in 1972 as a new method for obtaining azobenzenes.[53] However, as depicted below, the reaction led to the corresponding azobenzene in low yields (**Scheme 9**).

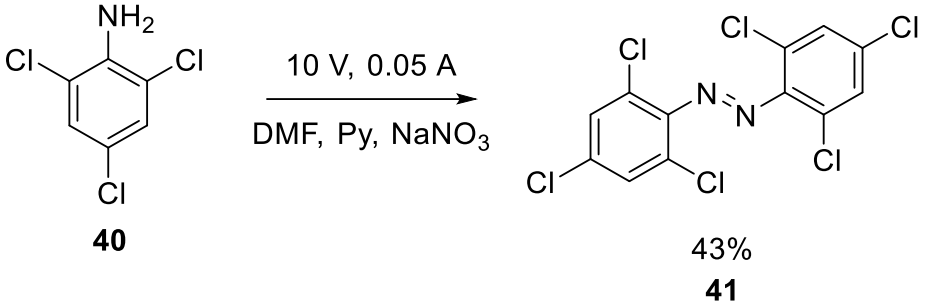

Scheme 9: Electrolytic oxidation of amine (**39**) to azobenzene (**40**).[53]

These low yields led to different oxidizing agents being investigated in the synthesis of azo compounds from aromatic amines, like sodium perborate/acetic acid, copper (II) sulfate pentahydrate, Cr_2O_7, and HgO/I_2.[54, 55] The drawbacks of such oxidations involve the use of metal salts in stoichiometric amounts that are often not environmentally friendly.

There are several oxidation methods that do not require the use of metals, such as the dehydration of arylhydrazines using *N*-bromosuccinimide as depicted in **Scheme 10**.[56,57] The yields from the dehydrogenation are excellent and have short reaction times.

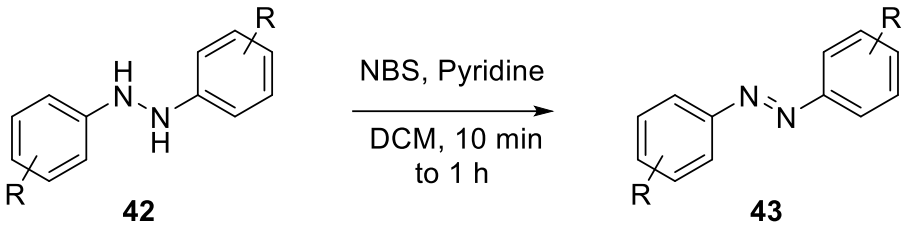

Scheme 10: Dehydrogenation reaction to afford azobenzene derivatives **(42)** from diphenylhydrazine derivatives **(41).**[56,57]

The reaction begins with the homolytic cleavage of NBS to yield the succinimidyl radical and bromine in the presence of light. The final products are the newly formed azo derivatives (**43**) and succinimide molecules. Of course, the preparation of the associated phenylhydrazine (**42**) is necessary. A variety of substituted compounds tolerate these mild reaction conditions.

The utility and interest in azo compounds has led to a variety of techniques and methods to synthesize these molecules.[48] Only a few synthetic pathways were briefly discussed along with present advantages and disadvantages alike. The azo coupling reaction makes use of explosive diazonium salts and the requirement for precise temperature control, while the oxidations lead to symmetrical azobenzenes.

1.5 Summary and Thesis Objectives

Fluorophores are capable of being used in a variety of applications. The fluorescence findings and interesting hydrogen bonding properties concerning the Janus sponge are by far the most intriguing properties of the molecule. The objective of this thesis is to further develop, introduce, and understand new light responsive molecules containing cyclopropenium ions.

Chapter 2, 3 and **4** will focus on structural modifications to the Janus sponge in an effort to understanding the relationship between structure, and the associated photophysical properties. This understanding allows for the preparation of a multitude of fluorophores containing cyclopropenium ions with inherent new properties. Additionally, incorporating cyclopropenium ions on azo functionality has never been reported, therefore **Chapter 5** in this thesis is focused on synthesizing the first ever photo-switch incorporating cyclopropenium ion functionality and comparing the absorbance to azobenzene. The aromatic and easily modified nature of this positively charged three-membered ring allows for engineering photo-responsive compounds with the potential to showcase different properties, all while adding to the rich class that is cyclopropenium ions.

Chapter 2: Fluorescence of Cyclopropenium Ion Derivatives

Majority of the following chapter was taken from the author's article published in *Journal of Organic Chemistry* with minor changes.[*,98] The chapter deals with the implications of structural changes to individual components of the Janus molecule. Richard Le Sueur contributed by synthesizing compounds **12**, **50**, **53**, and **58**, forming protected precursors of **49**, **51** and **52**, performing absorption measurements and generating HOMO and LUMO images of all compounds, as well as contributing to the preparation of the manuscript. The time dependant density functional theory calculations however, were solely performed by Dr. Travis Dudding and Dr. Lee Belding.

2.1 Introduction

Small molecule-based fluorophores play an integral part in day-to-day research, as light emitting diodes,[58,59,60] chemical sensors,[61,62,63] biological probes,[64] cellular imaging agents,[65] and light harvesting agents.[66] Their utility is broadened by their many mechanisms of action, such as Förster resonance energy transfer[67], photo-induced electron transfer,[68] aggregation and disaggregation-induced emission,[69,70] internal charge transfer,[71] and recently, motion-induced changes in emission.[72] Furthermore, their rapid photoactive response times, minimal disruption of local environments, and high sensitivity and visibility, makes them well-suited for monitoring real-time events with excellent spatial and temporal resolution.[73,74]

Currently, several classes of small organic fluorophores are commercially available. These fluorophores and their derivatives, however, often do not meet the desired photophysical and/or

chemical properties needed for a given application[1]. For this reason, new classes of small organic fluorophores are highly desirable, especially, if they expand the range of properties sought by consumers.

The Janus sponge (**12**), which falls under the category of fluorophores containing a conjugated naphthalene π–system, such as dansyl amide (**44**), 4-aminonaphthaliamide (**45**), 1,2-benzo-3,4-dihydrocarbazole-9-ethyl chloroformate (**46**), and 6-propionyl-2-(dimethylamino) naphthalene (**47**) (**Figure 15**). These naphthyl-based fluorophores (i.e., **44 - 47**) are known to derive their fluorescence from a donor-acceptor (D-A) charge transfer mechanism, wherein photoexcitation involves a transfer of charge from the nitrogen donor substituent to the naphthalene-based acceptor.[75,76]

Regardless of their classification, certain characteristics of organic fluorophores are universally useful: *i*) high molar attenuation coefficients, *ii*) good photo and chemical stability, *iii*) high quantum yields, and *iv*) large Stokes shifts. The Janus sponge possesses these characteristics to varying degrees. For instance, **12** has a quantum yield (ϕ) of 0.37, a molar attenuation coefficient (ε) of 4.70 x 10^3 M^{-1} cm^{-1}, and a Stokes shift of 138 nm. Furthermore, **12** is stable, soluble, and fluorescent with both aqueous and organic solvents. Given these attributes, and its unique electronic and structural qualities outlined in our previous work, we envisioned that **12** could provide a scaffold for developing new, useful fluorescent organic molecules. Thus, we report herein the synthesis and photophysical analysis of systematically modified derivatives of this

[*]Belding, L.; Guest, M.; **Le Sueur, R**.; Dudding, T. Fluorescence of Cyclopropenium Ion Derivatives. *J. Org. Chem.* **2018**, *83*, 6489.

cyclopropenium ion-containing fluorophore, in conjunction with TD-DFT calculations, to provide mechanistic insight that will guide the future development of this new class of fluorophores.

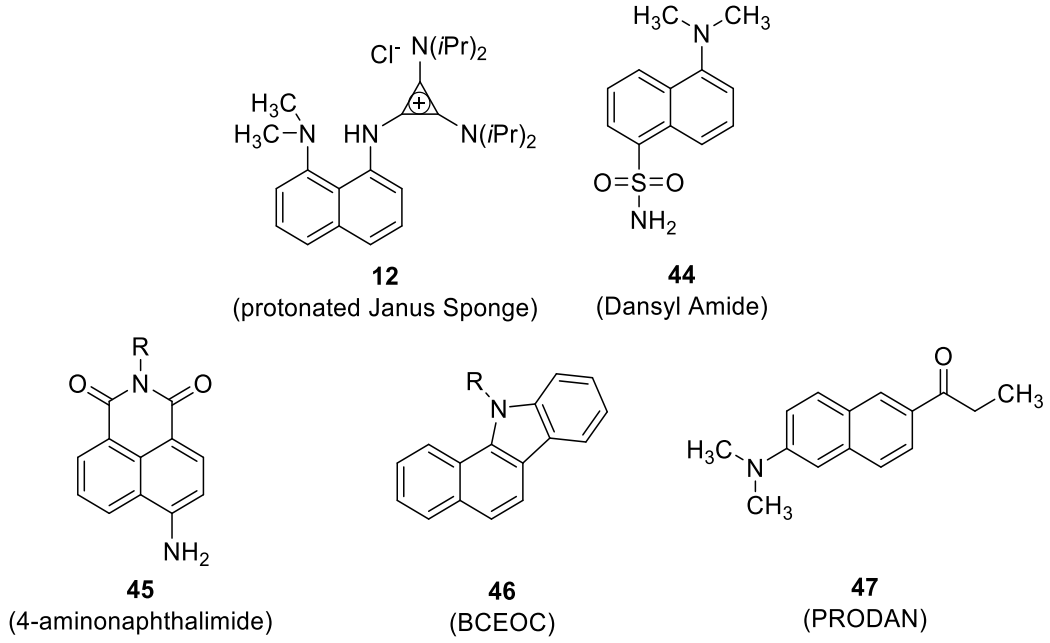

Figure 15: Selected naphthalene containing fluorescent organic molecule: Janus Sponge (**12**), dansyl amide (**44**),[77] 4-aminonaphthalimide (**45**),[78] 1,2-benzo-3,4-dihydrocarbazole-9-ethyl chloroformate (BCEOC) (**46**),[79,80] 6-Propionyl-2-(dimethylamino) naphthalene (PRODAN) (**46**).[81]

2.2 Results and Discussion

At the outset of this work, it was reasoned that the photophysical properties of compound **12** originated from the collective interactions of three defining structural components: namely, the cyclopropenium ion group, the (dimethyl)amine group, and the naphthalene backbone. Following this logic, each of these components were systematically modified, *via* the synthesis of **48 - 58**, and the impact on quantum yield, molar attenuation coefficient, absorbance maximum, emission maximum, and Stokes shift were recorded (**Figure 16**).

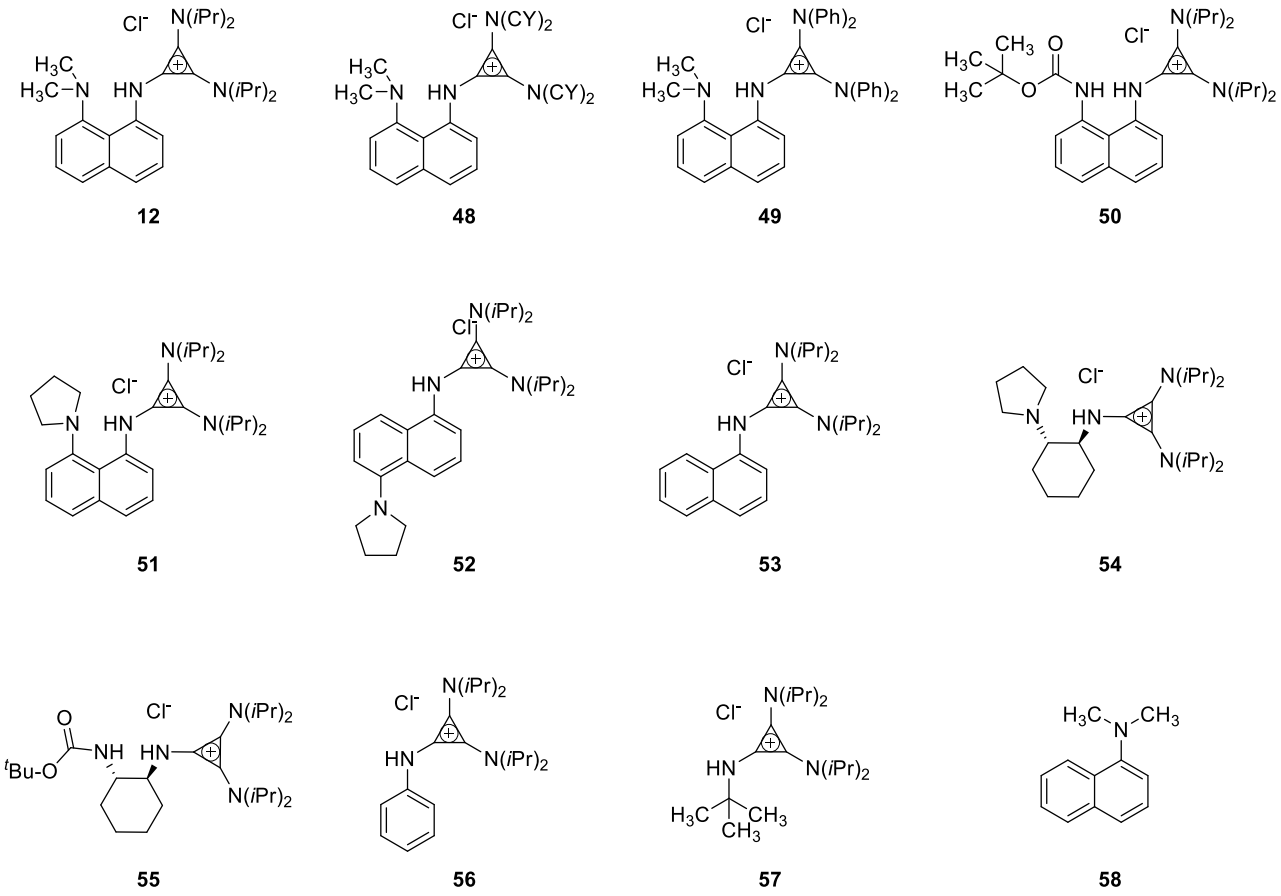

Figure 16: Prepared derivatives to probe the structural implications on the photophysical properties.

2.2.1 Modifications to the Cyclopropenium Ion Group: Derivatives 48, 49, and 58

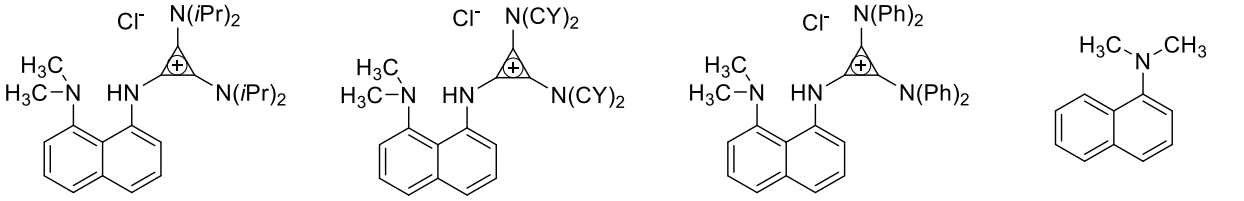

12	**48**	**49**	**58**
ϕ = 0.37	ϕ = 0.26	ϕ = 0.18	ϕ = 0.13
ε = 4.70 x 10^3 $M^{-1}cm^{-1}$	ε = 9.10 x 10^3 $M^{-1}cm^{-1}$	ε = 1.66 x 10^4 $M^{-1}cm^{-1}$	ε = 9.13 x 10^3 $M^{-1}cm^{-1}$
λ_{max}= 334 nm	λ_{max}= 335 nm	λ_{max}= 345 nm	λ_{max}= 305 nm
λ_{em}= 472 nm	λ_{em}= 476 nm	λ_{em}= 487 nm	λ_{em}= 416 nm
Stokes Shift = 138 nm	Stokes Shift = 141 nm	Stokes Shift = 142 nm	Stokes Shift = 111 nm

Figure 17: Compound **12** alongside derivatives **48**, **49**, and **58** accompanied by photophysical properties calculated in ethanol.

Turning first to the dependency of the cyclopropenium ion group showcased in **Figure 17**, compound **48** was used to gauge the impact of resonant lone pair donation from the nitrogen alkyl-substituents. Exchanging the *N*-diisopropyl substituents of **12** for *N*-dicyclohexyl groups resulted in a lower quantum yield (ϕ = 0.26) and molar absorptivity, and a small bathochromic (red) shift in the absorption and emission maxima. The source of these changes was, in part, thought to derive from less effective nitrogen lone pair (LP) donation to the cyclopropenium π-system, owing to the greater flexibility of the *N*-dicyclohexyl substituents. This greater flexibility obstructs ideal alignment for η_{LP}-to-π_{aryl} orbital overlap, thus reducing the electron density of the cyclopropenium ion ring π-system, and with it, attenuating its donor capacity. Analog **49**, features a π-rich cyclopropenium ion substituent (*N*-diphenyl), and had a quantum yield of ϕ = 0.18, a larger molar attenuation coefficient, and bathochromically shifted absorption ($\Delta\lambda$ = 9 nm) and emission ($\Delta\lambda$ = 11 nm) maxima. These trends are accounted for by competing nitrogen lone pair donation to the appended phenyl groups, rendering the cyclopropenyl-ring less electron rich, and/or localized donor-acceptor self-quenching. Meanwhile, removing the cyclopropenium ion unit altogether afforded compound **58**, which had a dramatically reduced quantum yield (ϕ = 0.13), hypsochromic (blue) shifted absorption ($\Delta\lambda$ = 29 nm) and emission ($\Delta\lambda$ = 56 nm) maxima, and a substantially smaller Stokes shift (111 nm), relative to **12**.

Taken together, these modifications to the cyclopropenium ion moiety demonstrate its role in luminescence. Decreasing the electron donating ability of the cyclopropenyl-amino groups, or increasing their electron withdrawing abilities, improves the photon absorption, while simultaneously impeding the fluorescence decay process (or facilitating the non-radiative decay processes). Furthermore, the difference between **12** and **58** shows that the cyclopropenium ion group drastically changes the quantum yield and Stokes shift of the aminonaphthalene core.

2.2.2 Modifications to the NMe_2 Group: Derivatives 50, 51, 52, and 53

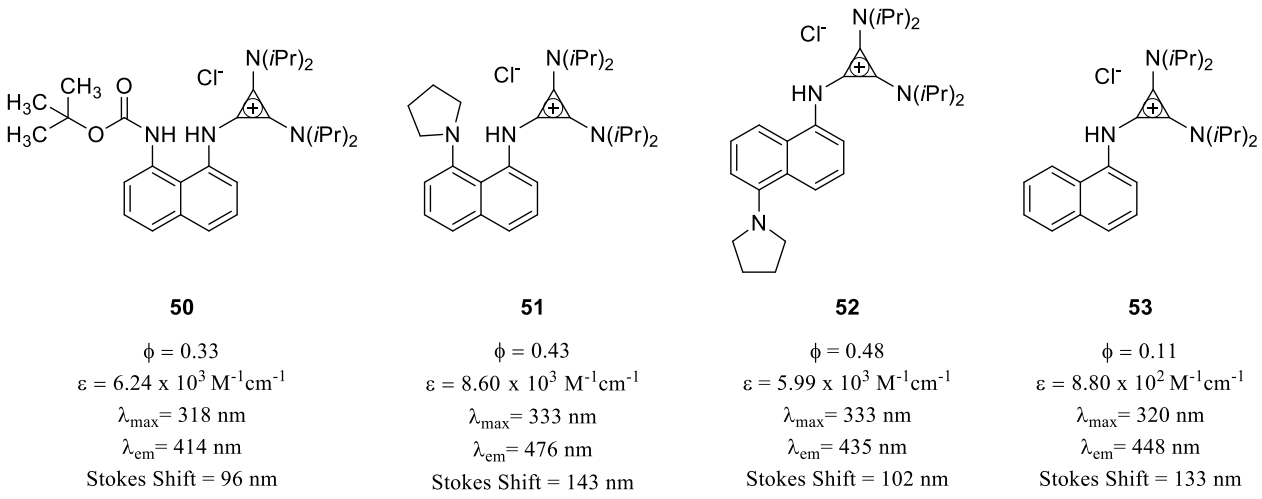

Figure 18: Derivatives **50**, **51**, **52,** and **53** accompanied by photophysical properties calculated in ethanol.

Modifications to the NMe_2 group as shown in **Figure 18** included fundamental electronic changes, tethering of the alkyl groups, positional isomerization, and removal of the amine altogether. To this end, exchange of the NMe_2 substituent for a *N*-*tert*-butyloxycarbonyl (*N*-Boc) group resulted in derivative **50** having a broad absorption band centered at 318 nm, with a shoulder displaying a maximum at 370 nm. Excitation at either 308 nm or 334 nm resulted in emission at 414 nm, while excitation at 361 nm resulted in an emission maximum at 448 nm, indicating the presence of two different fluorescence transitions. Nonetheless, derivative **50** showed a similar quantum yield (ϕ = 0.33), relative to **12**, but a 42 nm lower Stokes shift.

Incorporation of a pyrrolidine ring in substituted compound **51** had an increased quantum yield (ϕ = 0.43) of nearly 10 % and a slight bathochromically shifted emission maxima ($\Delta\lambda$ = 4 nm), which in turn gave a marginally higher Stokes shift ($\Delta\lambda$ = 5 nm). The spatial influence of the amine group, relative to the cyclopropenium ion group, was probed by preparing the 1,5-positional isomer compound **52**. This modification resulted in a larger quantum yield (ϕ = 0.48) and a 37 nm lower emission maximum, resulting in a 36 nm decrease in Stokes shift. Removal of the amine

group altogether as in compound **53** substantially reduced the quantum yield (ϕ = 0.11), resulting in a hypsochromic shift in the absorption ($\Delta\lambda$ = 14 nm) and emission ($\Delta\lambda$ = 24 nm) values, and thus a smaller Stokes shift ($\Delta\lambda$ = 10 nm).

These modifications to the NMe_2 group of **12** clearly showed its importance for luminescence. The increased quantum yield observed by modifying the NMe_2 group likely stems from non-radiative decay processes associated with rotational and vibrational degrees of freedom (such as those found in twisted intramolecular charge transfer (TICT) states).[82, 83, 84] Supporting this premise were the enhanced quantum yields and other emissive properties of compounds **51** and **52**, in which the motion of the nitrogen was restricted by incorporation into a pyrrolidine ring. Moreover, the spatial relationship between the NMe_2 (or pyrrolidine) group and the cyclopropenium ion had a definitive influence on luminescence, undoubtedly owing to some combination of steric congestion (and thus restricted rotation) and direct non-covalent bonding interactions, such as an intramolecular hydrogen bond (IMHB).

2.2.3 Modifications to the Naphthalene Backbone: Derivatives 54, 55, 56, and 57

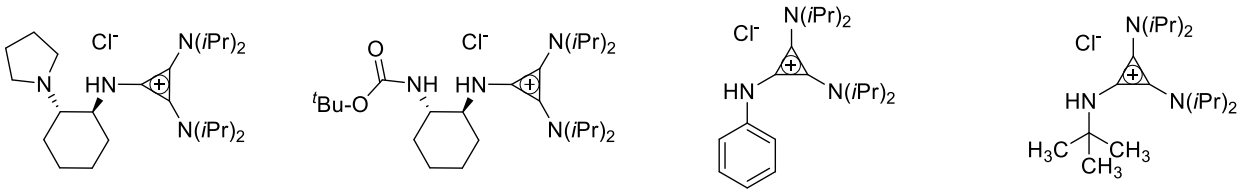

54
ϕ = 0.05
$\varepsilon = 5.00 \times 10^2\ M^{-1}cm^{-1}$
λ_{max}= 325 nm
λ_{em}= 468 nm
Stokes Shift = 133 nm

55
ϕ = 0.08
$\varepsilon = 1.80 \times 10^2\ M^{-1}cm^{-1}$
λ_{max}= 323 nm
λ_{em}= 463 nm
Stokes Shift = 137 nm

56
ϕ = 0.11
$\varepsilon = 2.70 \times 10^2\ M^{-1}cm^{-1}$
λ_{max}= 322 nm
λ_{em}= 468 nm
Stokes Shift = 146 nm

57
ϕ = 0.09
$\varepsilon = 2.00 \times 10^2\ M^{-1}cm^{-1}$
λ_{max}= 322 nm
λ_{em}= 468 nm
Stokes Shift = 146 nm

Figure 19: Derivatives **54**, **55**, **56,** and **57** accompanied by photophysical properties calculated in ethanol.

The importance of the naphthalene backbone was investigated by substitution for surrogates seen in **Figure 19**, which still maintained the close spatial relationship between the

amine and cyclopropenium ion groups. To this end, pyrrolidine and *N*-Boc cyclohexyl functionalized compounds **54** and **55** revealed that removing the naphthalene backbone manifested in drastically reduced molar attenuation coefficients ($5.0 \times 10^2\ M^{-1}cm^{-1}$ and $1.8 \times 10^2\ M^{-1}cm^{-1}$) and quantum yields ($\phi = 0.05$, $\phi = 0.08$). Despite this reduced luminescence character, there were only slight shifts in the absorbance and emission maxima of **54** and **55**, which retained large Stokes shifts of 143 nm and 137 nm. Similarly, the derivatives without the NMe_2 or naphthalene groups (*i.e.*, **56** and **57)** had low quantum yields ($\phi = 0.09$, $\phi = 0.11$) and low molar absorptivity, but exhibited only small blue shifts in absorbance and emission maxima, thus retaining large Stokes shift of 146 nm.

It is obvious from derivatives **54** – **57** that the conjugated naphthalene backbone is important for high molar attenuation coefficients and high quantum yields. What is perhaps the most surprising result, however, is that while the amino-naphthyl group has beneficial photophysical effects, the fundamental transitions are still present in, and likely inherent to, the cyclopropenium ion core itself.

2.2.4 Computational Studies

To gain insight into the electronic transitions of this class of fluorophores we performed time-dependent density functional theory (TD-DFT) calculations using compound **12** as a representative example (See **Figure 20** for atom labels).

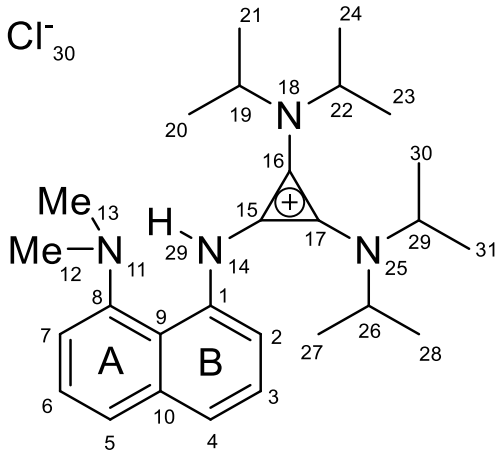

Figure 20: Enlarged Two-dimensional representation of (**12**).

To this end, initial conformational searches provided several low-energy geometries that could be grouped into two categories, depending on if the N(14)-lone pair was facing inwards (**12$_{In}$**) or outwards (**12$_{out}$**), with the former being ~1.90 kcal mol^{-1} more stable (**Figure 21**). This energetic difference was influenced by an intramolecular N(11)···H(29) H-bond (*d* = 1.85 Å) present in **12$_{In}$**, which was not present in **12$_{Out}$**, where instead there was an intermolecular N(14)–H(29)···Cl(30) (*d* = 2.10 Å) H-bond. The energetic preference for **12$_{In}$** deserves mention as it is a structural homolog of **12$_{Out}$**, which was the previously reported ground state structure of **12**. This discrepancy, most likely, derives from differences in computational methodology, as the use of Grimme's D3 dispersion correction and Truhlar's M06-2X global hybrid functional used in this work provides a more accurate description of non-covalent interactions than B3LYP. Irrespective, given the small energetic difference between **12$_{In}$** and **12$_{Out}$**, and the likelihood of their rapid interconversion, both conformers are considered.

The photophysical process of interest is generalized for conformer **12$_{out}$** in **Scheme 11**. Photon absorption from ground state (GS) **12$_{out}^{GS}$** affords the Frank-Condon (FC) state **12$_{out}^{FC}$**, *via* an electronic reorganization. A nuclear and electronic relaxation process (*i.e.*, internal conversion

(IC)), then yields the lower energy singlet excited (S_1) state $\mathbf{12_{out}^{S1}}$. Relaxation of the S_1 state back to the GS proceeds through a radiative or non-radiative decay process. Thus, the wavelength of the observed radiative decay (fluorescence) correlates with the free energy difference between the S_1 state and the GS. We discuss these transitions (shown in **Figure 21**), first for $\mathbf{12_{in}^{S1}}$, and then for $\mathbf{12_{out}^{S1}}$, below.

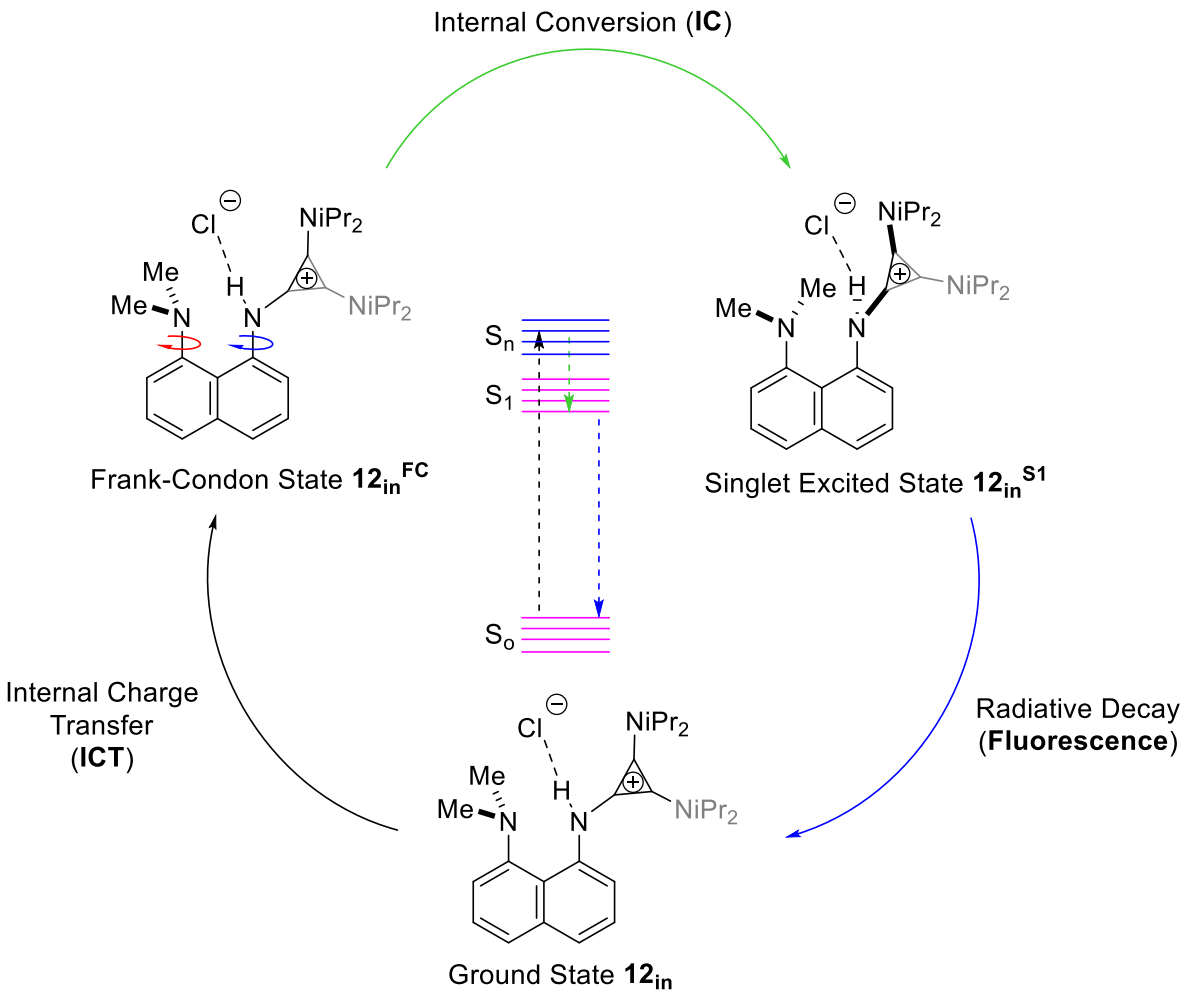

Scheme 11: Jablonski-type diagram, representing the general electronic transitions associated with the photoexcitation and emission of $\mathbf{12_{out}}$.

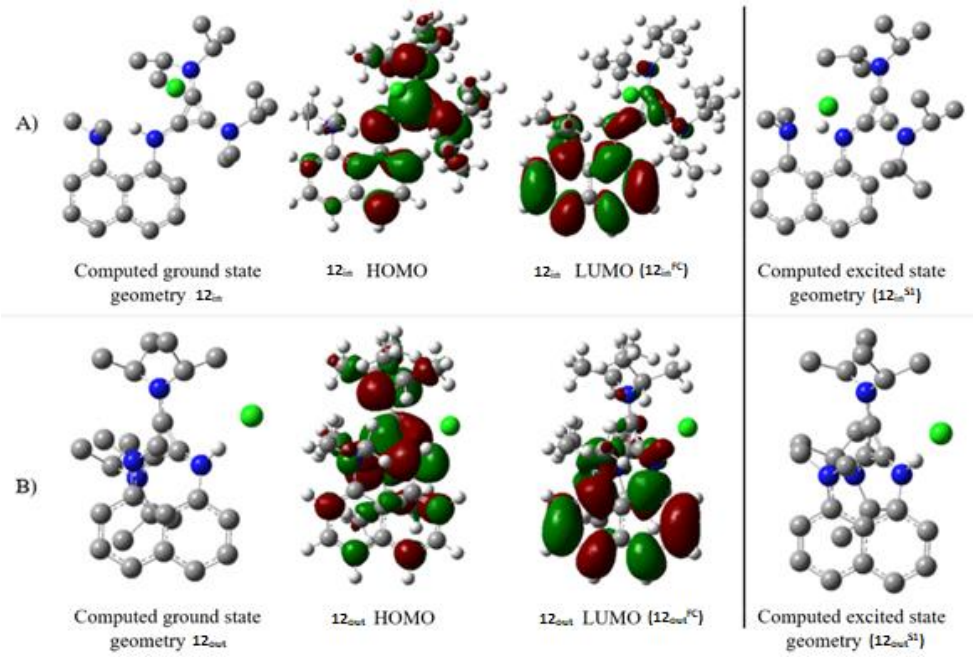

Figure 21: A) DFT computed geometry, HOMO, and LUMO of **12In**, as well as its TD-DFT optimized singlet excited state geometry. B) DFT computed geometry, HOMO, and LUMO of **12out**, as well as its TD-DFT optimized singlet excited state geometry. Level of theory: M062X-D3/6-31+g(d,p) scrf=(dichloromethane). Selected hydrogen atoms were removed for clarity.

We first computed the ultraviolet−visible (UV−vis) spectrum of **12In**, which had an absorbance maximum ($\lambda_{max,abs}$) at 312 nm (experimental $\lambda_{max,abs}$ = 334 nm) with an oscillator strength (*f*) of 0.4292, and a large dipole moment (δ = 12.48 Debye). A photoexcitation process involving a transition from the π_{HOMO}, where the electron density is largely located on the cyclopropenium ion ring, to the π_{LUMO}, which was located mainly on the naphthalene ring (**Figure 21**). Thus, in this internal charge transfer (ICT) process, the cyclopropenium ion, as opposed to the dimethylamine, acts as the primary donor group, while the naphthalene acts as the acceptor group.

The conformation of **12in^{S1}** was dominated by two features (**Figure 21**): i) an inward gearing of the cyclopropenium ion and naphthalene rings towards co-planarity, and ii) a strengthened intramolecular H-bond (IMHB). The increased co-planarity was apparent from the dihedral angle between the two aromatic rings ($\Theta_{C(15)\text{-}N(14)\text{-}C(1)\text{-}C(9)}$ = 161.9 ° to 164.3 °), and likely

originates from a preference for better π,π-orbital overlap leading to increased conjugation in the excited state. The increased strength of the IMHB in $\mathbf{12_{in}^{S1}}$ was apparent from a contracted N(14)−H(29)···N(11) H-bond distance (Δd = ~0.24 Å) and a slightly elongated N(14)−H(29) H-bonded distance (Δd = ~0.05 Å). Furthermore, the redistribution of electron density from nitrogen N(14) (Mulliken charges (q) = -0.206 eV to -0.088 eV) to the adjacent carbon atoms of the cyclopropenium ion (C(15) q = -0.396 eV to -0.567 eV) and naphthalene (C(1) q = 0.441 eV to 0.229 eV) rings, as well as increased electron density on N(11) (q = -0.604 eV to -0.775 eV), also supported a stronger IMHB. Quantum Theory of Atoms in Molecules (QTAIM) analysis of this N(14)−H(29)···N(11) H-bond revealed substantial increase in electron density (ρ) at the bond critical point (BCP) (Appendix B).

Associated with the formation of this IMHB and increased π-conjugation was a large observed Stokes shift. The TD-DFT computed structures show the emission as 384 nm (experimental = 472 nm), giving a computed Stokes shift of 72 nm (experimental = 132 nm). We ascribe these differences in computed and experimental Stokes shift values to limitations in explicitly accounting for solvent reorganization and other intermolecular vibrational energy redistribution pathways.

The computed UV−vis spectrum of $\mathbf{12_{Out}}$ had a $\lambda_{max,abs}$ of 319.2 nm and an oscillator strength (f) of 0.2535, which was noticeably smaller in magnitude than that of $\mathbf{12_{in}}$. Nevertheless, the photoexcitation was again dominated by a π_{HOMO}−π_{LUMO} based ICT processes (**Scheme 11**), wherein electron density is transferred largely from the cyclopropenium ion ring, to the naphthalene ring. The relaxation from $\mathbf{12_{out}^{FC}}$ to $\mathbf{12_{out}^{S1}}$ also involved increased co-planarity between the cyclopropenium ion and naphthalene rings ($\Theta_{C(9)\text{-}C(1)\text{-}N(14)\text{-}C(15)}$ = -53.21 ° to -39.79 °). Because there is no IMHB in $\mathbf{12_{out}}$, this inward gearing of the cyclopropenium ion ring was coupled

with twisting of the *peri*-NMe_2 group ($\Theta_{C(9)\text{-}C(8)\text{-}N(11)\text{-}C(12)}$ = -66.96 ° to -43.37 °) into conjugation with the naphthalene ring, resulting in nitrogen rehybridization to a $sp^{2.2}$-geometry and increased lone pair donation into the naphthalene ring π-system ($N_{11\ (LP)} \rightarrow C_7\text{-}C_{8\ (BD^*)}$, ΔE_{NBO} = 20.0 kcal mol^{-1}). This concerted motion led to a distortion of the aromatic naphthalene backbone from planarity ($\Theta_{C(5)\text{-}C(10)\text{-}C(9)\text{-}C(1)}$= -172.4 °) and a 0.1 Å elongation of the N(11)···N(14) interatomic distance to 2.91 Å. In the absence of the IMHB, it appears that a larger increase in π-conjugation provided the stability associated with the large observed Stokes shift, which was computed to be 92 nm for $\mathbf{12_{out}^{S1}}$.

From these computed results, we can make several comparisons with the experimental data. From the compounds that share the same general structure as **12** (**48**, **49**, **50**, **51**, **52** and **53**), we note that **50**, **52**, and **53** have significantly lower Stokes shifts, and that these compounds are all likely candidates to have greater co-planarity between the cyclopropenium ion and naphthalene rings in their ground states. This aligns qualitatively with the TD-DFT results, which indicate that the Stokes shift is, in part, a consequence of a change in this co-planarity during IC. It thus follows that pre-existing co-planarity would decrease the Stokes shift. Furthermore, the larger cyclopropenium ion-based π-system associated with **49** (due to the Ph-groups) is likely to be affected more strongly upon increased π-conjugation during IC, thus accounting for a higher Stokes shift. Lastly, we note the contribution of the cyclopropenium ion nitrogen groups in the HOMO and cyclopropenyl π-system in the LUMO, suggest that it can play the role of both the donor and the acceptor, in agreement with the experimental observation that the fluorescent transitions are inherent to the cyclopropenium ion core itself.

2.2.5 Conclusion

We have demonstrated, using systematic modifications, how the three key structural components of compound **12** (the cyclopropenium ion group, the (dimethyl)amine group, and the naphthalene backbone), influence its photophysical properties. By doing so, we found that cyclopropenium ions are inherently fluorescent, with large Stokes shifts. The understanding gained from this systematic study, together with the computational insight, provides us with the ability to rationally design new derivatives with targeted photophysical properties. More obvious modifications, such as extending the π-conjugation of the naphthalene acceptor group can increase the quantum yields, molar attenuation coefficients, Stokes shifts as well as red-shifting absorbance and emission wavelengths.[85, 86]

We expect that this new class of fluorescent cyclopropenium ions will find utility in niche applications. The freebase of **12** is, in addition to being highly basic, poorly fluorescent, suggesting that it can be applied as a pH-responsive fluorescent probe at high pH-values (a range unavailable to most pH-dependent fluorescent probes). This class of cyclopropenium ion-functionalized amino containing derivatives[87,88] and cyclopropenium ions in general[89] are also good metal-chelating ligands, and we thus expect **12** and its derivatives to have metal ion-dependent fluorescence properties. Given the high sensitivity of **12** to even subtle electronic perturbations, we expect that replacing H^+ with M^+ will have a drastic influence on fluorescence, which can lead to highly sensitive and metal-ion selective fluorescent probes.

Chapter 3: Competitive Hydrogen Bonding of Cyclopropenium Ions: Implications of an Anion Switch

Majority of the following chapter was taken from the author's article published in *Tetrahedron Letters* with minor changes.[*,90] The chapter deals with the implications of anion exchange on the hydrogen bonding style and photophysical properties of cyclopropenium ion containing fluorophores (**12a**$_{Cl}$, **12b**$_{BF4}$, **12c**$_{PF6}$, and **12d**$_{BPh4}$) synthesized, characterized, and computationally modelled by Richard Le Sueur. Various techniques are discussed such as X-ray crystallography (Dr. Melanie Pilkington), fluorescence spectroscopy (Matt Guest), and nuclear magnetic resonance spectroscopy. Richard Le Sueur largely contributed to the preparation of the manuscript.

3.1 Introduction

Hydrogen bonding plays countless roles in chemical processes, such as those regulating the vast network of reactions controlling life. In studying this through-space, non-covalent interaction, chemists have refined the hydrogen bond into a precision tool widely used in materials science, analytical chemistry, and synthesis. In this context, *N*-protonated cyclopropenium ions are an increasingly relevant class of hydrogen bond donors with unique electronic properties (**Figure 22A**).[91,92] For instance, cyclopropenium ions are charged and aromatic with the rare characteristic of being electron rich cations known to weakly associate with counterions. This distinct feature, in part, has led to their growing use as organocatalysts,[93,94,95] phase-transfer catalysts,[96,97] fluorescent probes,[98] transfection agents,[99] and polyelectrolytes,[100] yet the influence of the associated cyclopropenium ion counterions in these applications remains largely elusive. This flaw represents a systemic lack of understanding of the competition[2] in hydrogen bonding between

[*] **Le Sueur, R**.; Guest, M.; Belding. L.; Pilkington, M.; Dudding, T. Competitive hydrogen bonding of cyclopropenium ions: Implications of an anion switch. *Tetrahedron Letters*. **2019**, *60*, 150928.

cyclopropenium ions and their counterions (e.g., by N-H hydrogen bonding). This understanding has ramifications such as how counterion hydrogen bonding influences organocatalytic cyclopropenium ion reactivity or alters the photophysical profile of a cyclopropenium ion fluorophore. Answering these questions is vital for understanding existing and advancing future applications of cyclopropenium ions in catalysis, biological sciences, and materials, etc.

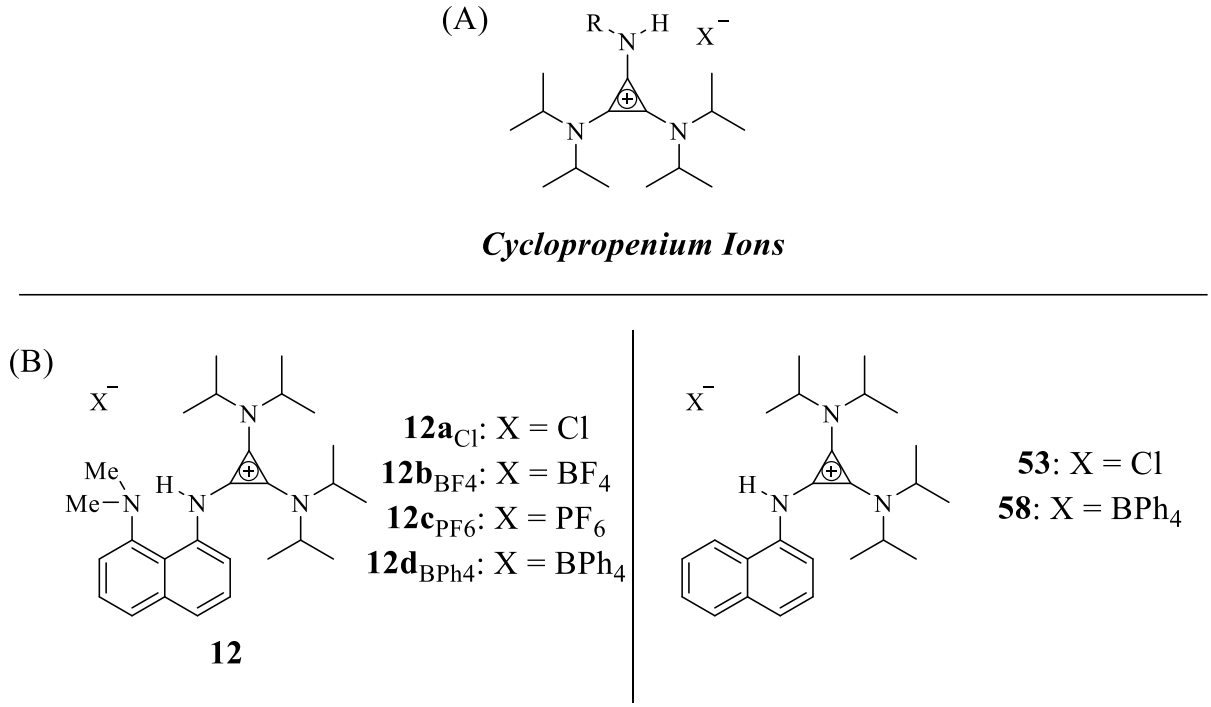

Figure 22: (A) Cyclopropenium ions. (B) Cyclopropenium ion functionalized systems (**12** and **58**), and respective anions used in this work.

Accordingly, this work shows for the first time counterion specificity in modulating the reactivity of cyclopropenium ions as hydrogen bond donors. We offer a basis for tuning cyclopropenium ion fluorescence through competitive hydrogen bonding and in doing so add to the rich class of fluorophores known as naphthalene-based dyes. Thus, building upon our interest in small-molecule fluorophores and their applications in new technologies such as cellular imaging agents,[101] multi-responsive probes,[102] light emitting diodes,[103,104,105] and components of light harvesting systems.[106,107,108,109,110,111]

3.2 Results and Discussion

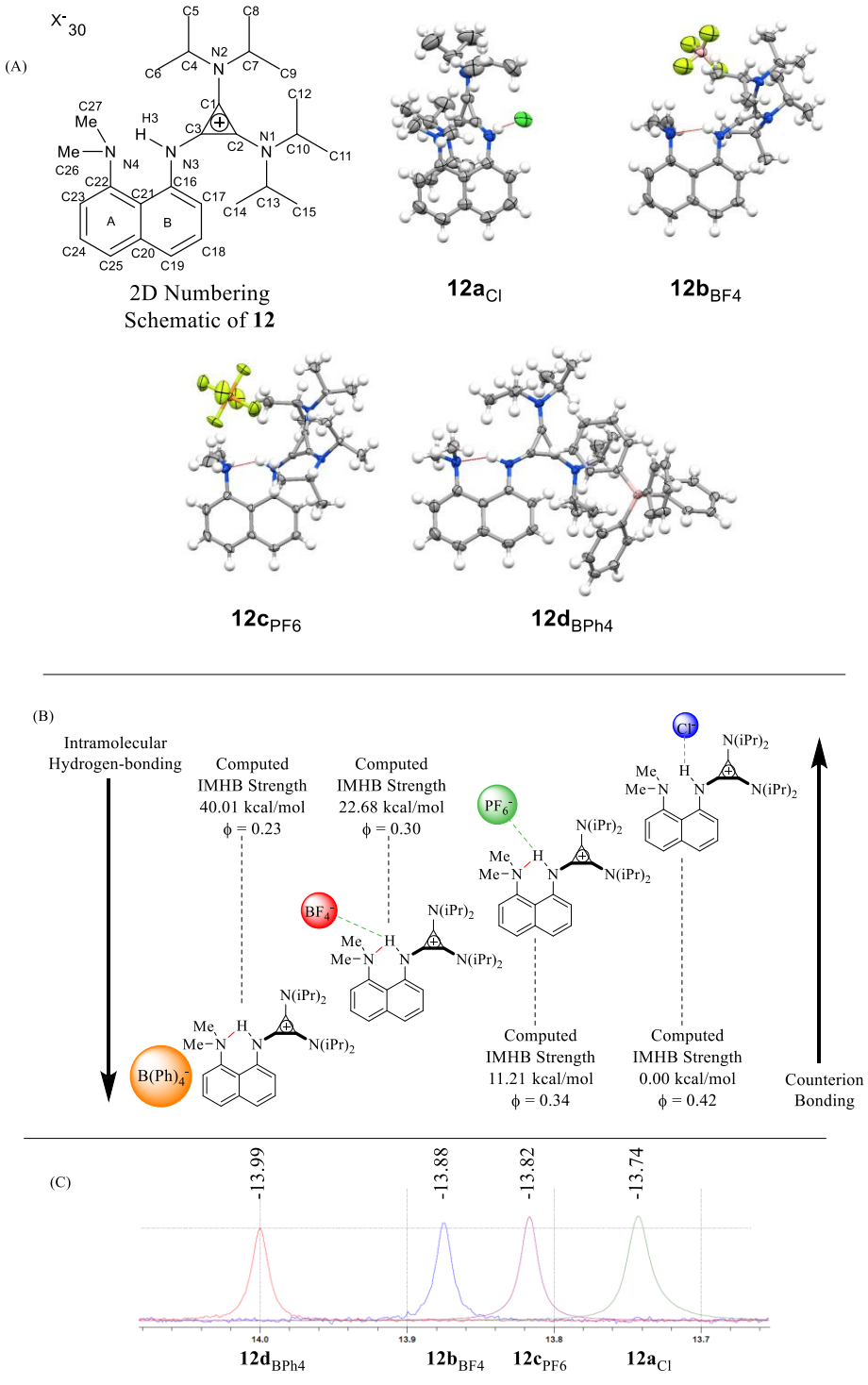

Figure 23: (A) 2D schematic for compound **12** with appropriate labeling scheme (the largest numbers are referred to in text) and ORTEP plots of the molecular structures of derivatives **12a**$_{Cl}$, **12b**$_{BF4}$, **12c**$_{PF6}$, and **12d**$_{BPh4}$. Thermal ellipsoids are plotted at 50%. (B) 2D schematic of the inter- and intramolecular hydrogen bonding, the computed strength of the intramolecular hydrogen bond (IMHB), and the quantum yield (ϕ). (C) Experimentally determined N(3)—H(3) hydrogen shifts of **12a**$_{Cl}$, **12b**$_{BF4}$, **12c**$_{PF6}$, and **12d**$_{BPh4}$ in $CDCl_3$.

Table 1: Key metrics associated with **12a$_{Cl}$, 12b$_{BF4}$, 12c$_{PF6}$,** and **12d$_{BPh4}$,** where intramolecular hydrogen bond is denoted as IMHB. X^- denotes the respective anion.

Derivative	Crystal Structure IMHB Distance (Å)	Computational Solution Phase IMHB distance (Å)	Crystal structure X^- distance to N(3)—H(3) bond (Å)	Computational X^- distance to N(3)—H(3) bond (Å)	Crystal Structure N(3)—H(3)···N(4) Angle
12a$_{Cl}$	N/A	N/A	2.28(7)	2.07	N/A
12b$_{BF4}$	1.99(5)	1.77	3.59(4)	2.24	128.1(4) º
12c$_{PF6}$	1.86(6)	1.95	5.27(2)	2.35	136.8(1) º
12d$_{BPh4}$	1.82(7)	1.75	3.93(1)	3.75	143.8(9) º

At the outset of this study with the aim of probing counterion effects on cyclopropenium ion hydrogen bonding, we employed naphthalene-based proton sponge derivative **12** as a model system (**Figure 22B**). Guiding this selection was the prospect that this scaffold would provide a structurally simple, yet useful platform for studying competitive intramolecular hydrogen bonding vs. intermolecular hydrogen bonding with different hydrogen bond acceptors by (i) solid state X-ray analyses, (ii) solution-phase ^{1}H NMR, UV-vis and fluorescence spectroscopy, and (iii) density functional theory (DFT) calculations.

3.2.1 Crystal Structure Analysis

In turning first to the solid state, several insightful findings emerged from the X-ray crystal structures of **12a**$_{Cl}$, **12b**$_{BF4}$, **12c**$_{PF6}$, and **12d**$_{BPh4}$ (see **Figure 23A** and **Table 1**). Clear from a comparison of the X-ray crystal structures of these derivatives was intermolecular hydrogen bonding to the electronegative chloride anion in **12a**$_{Cl}$, while superseding intermolecular hydrogen bonding to the tetraphenylborate anion in **12d**$_{BPh4}$ was an intramolecular hydrogen bond between

the peri-NMe_2 group and the cyclopropenium N-H bond. Notably, this extreme switch in hydrogen bonding from intermolecular to intramolecular hydrogen bonding in **12d**$_{BPh4}$ provides the first example of a cyclopropenium ion proton sponge according to the criteria of Pozharskii et al.[11] Meanwhile, an intramolecular N-H···NMe_2 hydrogen bond was present in **12b**$_{BF4}$ and **12c**$_{PF6}$ that slightly deviated further from linearity owing to crystal packing forces.

3.2.2 Computational and NMR Experiments

Computational modelling was next undertaken to gauge the influence of solvation effects on these hydrogen bond interactions and to unveil underlying electronic facets. DFT calculations (B3LYP-D3//6-31+G(d,p)/IEFPCM(DCM)) using the X-ray coordinates of **12a**$_{Cl}$ **12b**$_{BF4}$, **12c**$_{PF6}$, and **12d**$_{BPh4}$ as input revealed the hydrogen bonding in **12a**$_{Cl}$ and **12d**$_{BPh4}$ were largely unaltered, while a more noticeable perturbation was observed for **12b**$_{BF4}$ and **12c**$_{PF6}$ following *in silico* optimization (see Appendix B). Additionally, migration of the relatively small tetrafluoroborate anion towards one face of the aromatic cyclopropenium ring system concurrent with reinforcement of the intramolecular N(3)-H(3)···N(4) hydrogen bond (distance = 1.8 Å) in **12b**$_{BF4}$. The driving force for this molecular reorganization was traced to increased anion-π interactions between the tetrafluoroborate anion and the aromatic cyclopropenium ring as well as strengthening of a network of B-F···H-C hydrogen bond contacts. Supporting the presence of these favourable interactions was a non-covalent interaction (NCI) plot (**Figure 24A**) displaying stabilizing interactions (green isosurfaces). Associated with the intramolecular N(3)-H(3)···N(4) hydrogen bond of **12b**$_{BF4}$ and contributing to a bifurcated hydrogen bond motif was a N(3)-H(3)···F-B intermolecular hydrogen bond measuring 2.2 Å (**Figure 24A** (green lines) and 3B left). By contrast, fewer non-covalent interactions between the cyclopropenium ring and the comparatively larger hexafluorophosphate anion were visible in **12c**$_{PF6}$. Moreover, the intramolecular N(3)-

H(3)···N(4) hydrogen bond distance of 2.0 Å in this derivative was slightly elongated, resulting in a bifurcated hydrogen bonding scenario associated with an intermolecular N(3)-H(3)···F-PF_5^- hydrogen bond measuring 2.4 Å (**Figure 24A** (green lines) and **Figure 24B** right).

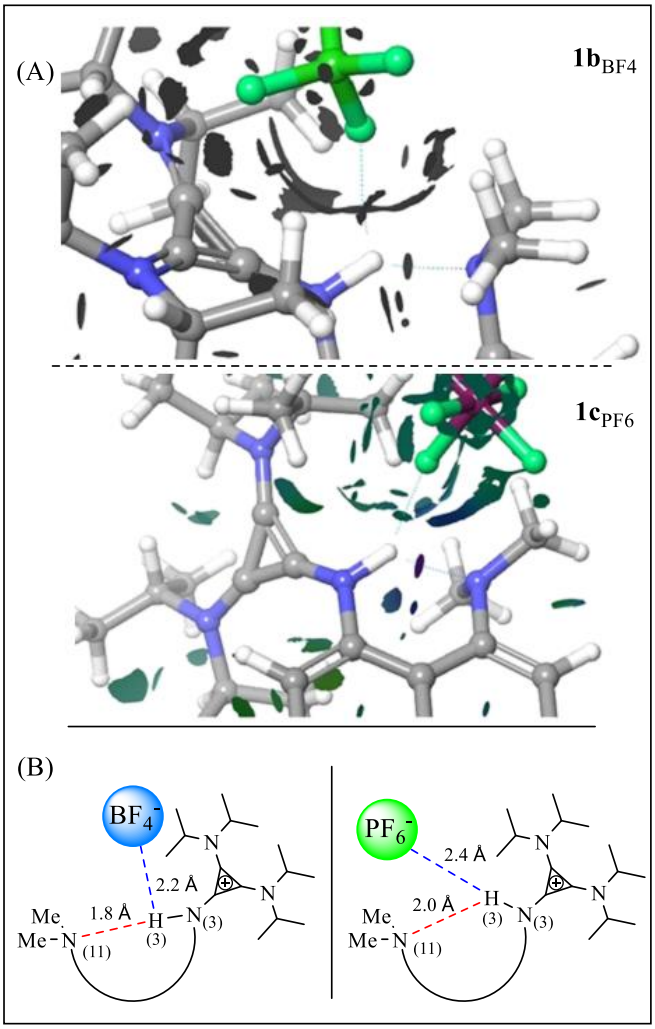

Figure 24: (A) Non-covalent interaction (NCI) plots displaying favourable van der Waals interactions (green isosurfaces) in **12b**$_{BF4}$ and **12c**$_{PF6}$.. The surfaces are coloured on a rainbow scale based on values of sign(λ_2) between −0.04 to 0.04 au. Bifurcated hydrogen bonding between the anion and dialkylamine depicted by green lines. (B) Bifurcated hydrogen bonds between dialkylamine NMe_2 group and external hydrogen bond donors BF_4^- and PF_6^-.

To gain further insight into the solution phase hydrogen bonding of these derivatives ^{1}H NMR studies were performed. Surfacing from the studies was a progressive downfield chemical shift of the cyclopropenium nitrogen H(3) signal in the order **12a**$_{Cl}$ < **12c**$_{PF6}$ < **12b**$_{BF4}$ < **12d**$_{BPh4}$

attributed to an increasing degree of intramolecular N(3)-H(3)···N(4) hydrogen bonding at the expense of intermolecular anion hydrogen bonding (**Figure 25**).

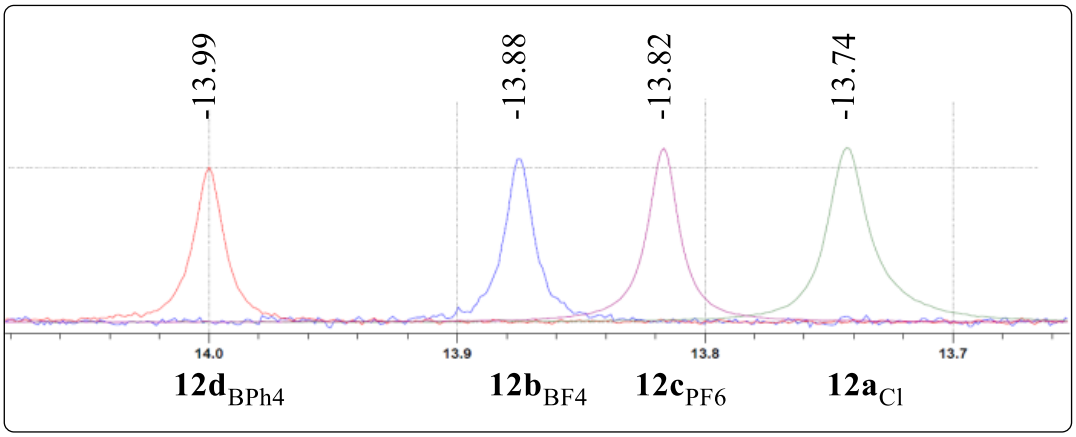

Figure 25: Enlarged version of Figure 23C denoting chemical shifts of H(3) with respective derivatives.

To probe the counterion effect further, compounds **53** and **58** (**Figure 22B**) lacking the capacity to engage in intramolecular hydrogen bonding were investigated, which displayed cyclopropenium nitrogen H(3) signals at 11.58 ppm and 6.25 ppm, respectively. Based on these trends and in extrapolating from the above-mentioned X-ray crystal structure data, the upfield chemical shift of H(3) for **58** is ascribed to no intermolecular anion hydrogen bonding, while the large downfield chemical shift of H(3) for **53** is accredited to significant intermolecular anion hydrogen bonding.

3.2.3 Fluorescence Investigation

Given structural alterations often manifest in electronic changes, we hypothesized that these variations in hydrogen bonding in **12a**$_{Cl}$ **12b**$_{BF4}$, **12c**$_{PF6}$, and **12d**$_{BPh4}$ might influence the luminescent properties of these cyclopropenium ion derivatives. In line with this reasoning, a correlation between the florescence quantum yield in solution and competitive hydrogen bonding was observed (**Table 2**).

Table 2: Select photophysical properties of derivatives **12a**$_{Cl}$ **– 12d**$_{BPh4}$. IMHB denotes intramolecular hydrogen bond

Derivative	λ_{max} (nm)	λ_{em} (nm)	NBO calculated IMHB strength (kcal/mol)	ϕ	$\Delta\lambda$ (nm)
12a$_{Cl}$	334	465	0.00	0.42	131
12b$_{BF4}$	333	467	22.68	0.30	134
12c$_{PF6}$	333	465	11.21	0.34	132
12d$_{BPh4}$	333	467	40.01	0.23	134

The basis for this phenomena is thought to arise from less effective NMe_2 group lone pair electron donation into the naphthalene ring system as a result of increasing intramolecular N(3)-H(3)···N(4) hydrogen bonding and by association reduced internal charge transfer (ICT) rates leading to altered photophysical profiles, e.g., decreased quantum efficiency. Consistent with these trends was NBO analysis, indicating the strength of these intramolecular hydrogen bonds arose in part from N(11) lone pair (LP) donation into the N(3)-H(3) antibonding orbital (BD*. This data reveals that an inverse relationship exists between intramolecular hydrogen bond strength and fluorescence quantum yield.

Meanwhile the absorbance maxima and Stokes shifts were similar for **12a**$_{Cl}$, **12b**$_{BF4}$, **12c**$_{PF6}$, and **12d**$_{BPh4}$ (**Table 2**). We previously showed the electronic nature of cyclopropenium ion groups can alter both of these properties,[8] however, for the case at hand it is likely the change in hydrogen bonding interactions that influences the quantum yield almost entirely through a change in geometry. In turn, this altered geometry predominantly affects the fraction of accessible fluorescent states, and not the energy or nature of the states themselves. This influence, and the similar absorption profiles of the congeners of **12** infer that the primary reason for the lower

quantum yields is a change in non-radiative decay processes likely associated with differing vibronic coupling modes, and not in the efficiency of photon absorption. That being said, the lower quantum yield for **12d**$_{BPh4}$ likely arises from fluorescence quenching by the BPh_4^- counterion (**Figure 26**) offering a competing, non-fluorescent pathway for energetic decay from the excited state.

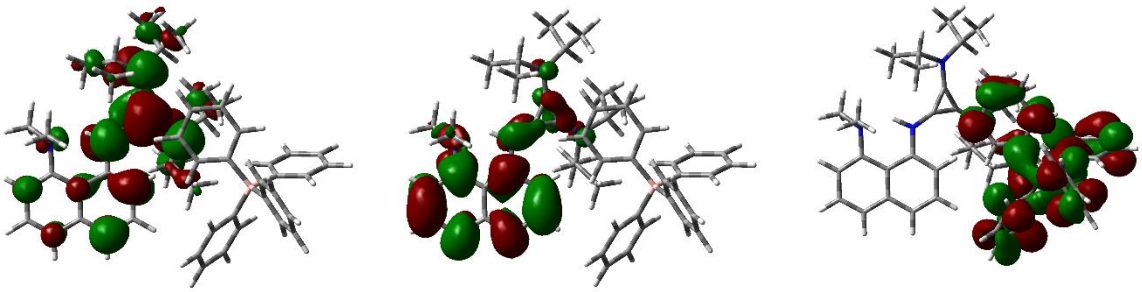

12d$_{BPh4}$ Ground State Geometry (HOMO)

12d$_{BPh4}$ Franck Condon Excited State Geometry (LUMO)

12d$_{BPh4}$ Franck Condon Excited State Geometry (LUMO+1)

Figure 26: Computationally derived HOMO, LUMO, LUMO+1 of 12d$_{BPh4}$.

3.2.4 Conclusions

To summarize from the findings of this study exploring hydrogen bonding in cyclopropenium ions, four main conclusions were reached: (i) cyclopropenium ion hydrogen bonding is influenced by the strength of the hydrogen bond acceptor (i.e., counterion) and interactions of the acceptor with the cyclopropenium ion; (ii) these interactions persist in solution; (iii) the ability to switch between inter- to intramolecular hydrogen bonding led to the first cyclopropenium ion containing proton sponge according to the criteria of Pozharskii *et al.* (refer to introduction, section "defining proton sponges") hydrogen bonding influences the electronics of cyclopropenium ions. In a larger context, the relevance of these conclusions is of importance as cyclopropenium ions are increasingly finding use in catalysis, materials, biochemistry, etc. and

understanding their hydrogen bonding properties is paramount for the development of these applications.

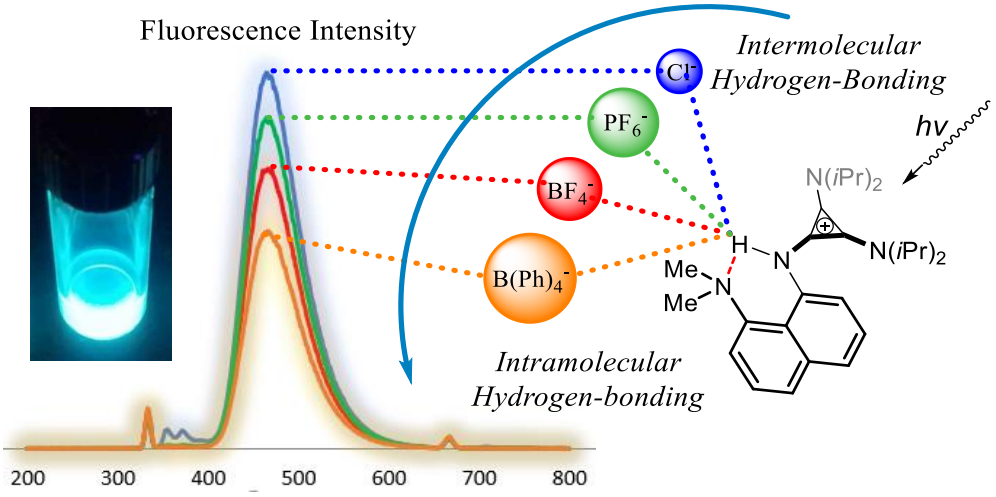

Figure 27: Visual representation of anion interactions resulting in diminished fluorescence efficiency.

Taken together, we have demonstrated cyclopropenium N-H hydrogen bond switchability from intermolecular interactions in the presence of small, strongly donating anions to intramolecular interactions with large, poorly donating anions. Influencing this preference in hydrogen bonding were interactions between the counterion and the cyclopropenium core itself. From this understanding, we can now modulate the quantum yield (**Figure 27**) of cyclopropenium ion-based fluorophores by counterion exchange — in the absence of other external influences — governing its hydrogen bonding state. The relatively large changes in electronic and structural properties arising from these changes serve as a prelude to future applications of cyclopropenium ion-based molecular switches and/or ion sensors.

Chapter 4: Guanidine – Cyclopropenium Ion Superbase

4.1 Introduction

The synthesis of the non-symmetrical Janus sponge introduced a synthetic pathway for the potential development of a variety of non-symmetric proton sponges.[14] Building upon this fact, controlling non-covalent interactions is important for designing catalysts and components for molecular recognition, and for tuning materials properties. Hydrogen bonding in particular, is one of the most important and valuable non-covalent interactions, and our understanding of its physical nature has benefited greatly from the development of proton sponges.[112] Therefore, the development of different proton sponges with inherent new properties remains an important research topic.

As part of continuing efforts to understand hydrogen transfer and proton sponges, an extension in the form of synthesizing a di-functionalized non-symmetric proton sponge (**59a**) with considerably high basicity incorporating guanidine and cyclopropenium ion functionality (abbreviated GCSB, **Figure 28**) was undertaken.

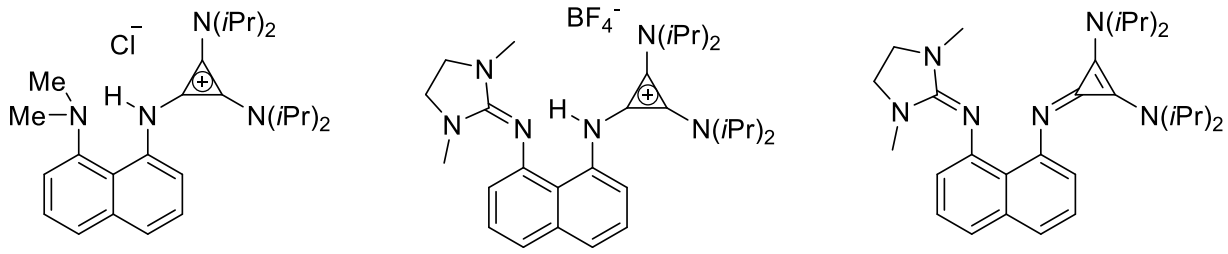

Protonated Janus **12** | Protonated GCSB **59** | GCSB **59a**

Figure 28: Protonated Janus sponge (**12**) along with new targets **59** and **59a**.

Additionally, exploring the effects of boron functionalization on both structural and electronic properties is important, as luminescence is a central focus. A discussion on the incorporation of

BF_2 bound to the nitrogen atoms of **59a** (analogous to BODIPY functionality) is also included (**Figure 29**).

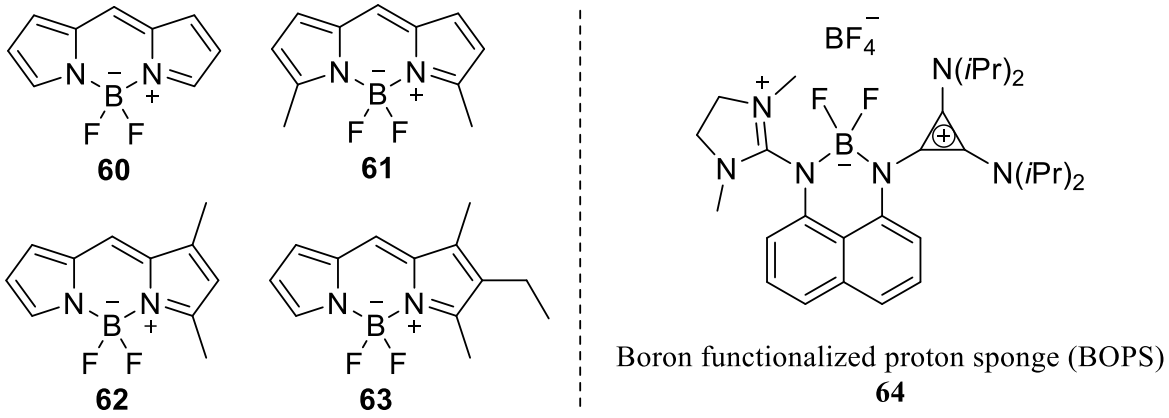

Figure 29: Derivative **64**, analogues to known BODIPY dyes **60**, **61**, **62**, and **63**.[113]

4.2 GCSB Synthetic Pathway

Similar to the Janus sponge, the key step in the synthesis of **59** is the di-*tert*-butyl dicarbonate (Boc_2O) mono amine protection of 1,8-diaminonaphthalene, **Scheme 12**. This procedure is often used in our laboratory and has henceforth been optimized.[14] A necessary step in this reaction involves the dropwise addition of Boc_2O over 2 h via a syringe pump. The reaction is then left to stir for 16 h affording **66** in 88% yield after purification via column chromatography.

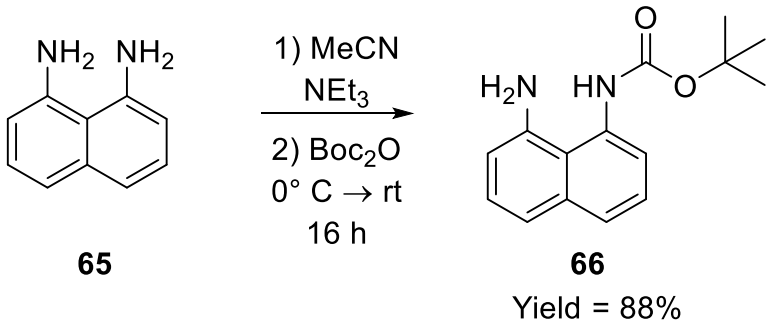

Scheme 12: Synthetises of **59** – step one: mono BOC protection of **65** to afford **66**.

Triethylamine (NEt_3) was added dropwise to a cooled solution of **65** and acetonitrile (MeCN). Di-*tert*-butyl dicarbonate has been found to be an efficient protecting group in basic conditions, all while being an inexpensive reagent.[114] The combination of dropwise addition and the bulk of the added protecting group effectively eliminated the chance of accidentally protecting both amines.

To install the guanidine functionality, **66** was allowed to react with 2-chloro-1,3-dimethlimidazolium chloride (DMC salt, **68**). Compound **68** was prepared by heating 1,3-dimethylimidazolidinone (**67**) in the presence of oxalyl chloride, $(COCl)_2$. Both reactions are depicted in **Scheme 13**.

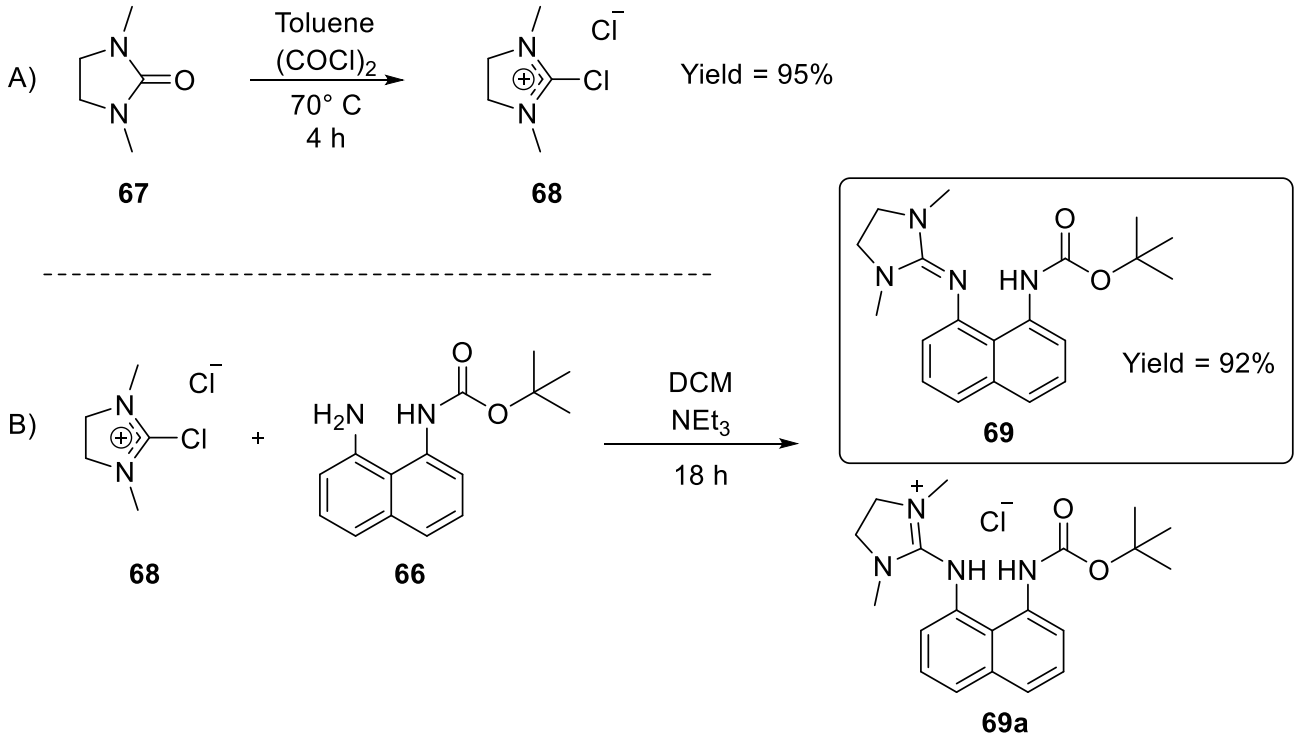

Scheme 13: A) Synthesis of necessary precursor 2-chloro-1,3-dimethylimidazolium chloride, **68**. B) Guanidine functionalization of **66** to afford **69.**

The literature reports heating the DMC salt reaction to reflux,[115] however, keeping a constant temperature of 70˚ C afforded compound **68** in nearly quantitative yield. Additionally, the

hygroscopic nature of the DMC salt was troublesome, and therefore the material was used immediately after being prepared. Efficient cleaning of compound **68** with ether was also necessary, otherwise the subsequent addition to **66** afforded low yields. Guanidine functionalization leading to **69** using pure material afforded a 92% yield. It is important to note that acid workup with 1 M HCl led to the protonation of the newly formed guanidine, **69a**, where the protecting group remained.

The following step in the synthetic route involved the deprotection of the carbamate group. This was achieved by acid-catalyzed hydrolysis, but strong acids such as trifluoroacetic acid (TFA) are required to hydrolyze the N—C bond.[116] The same procedure used for the Janus molecule, using 40 equivalents of TFA, was attempted.

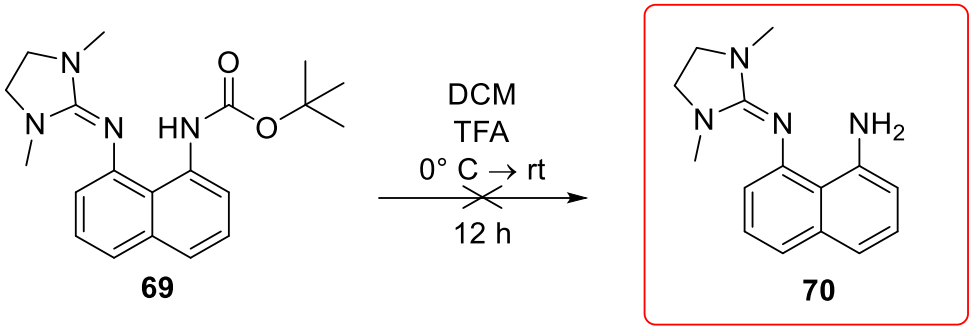

Scheme 14: Attempt to deprotect the carbamate group of **69** using TFA as the acid.

As depicted in **Scheme 14**, no product was observed and no starting material was recovered. Reviewing the literature afforded a new procedure using 3M HCl in ethyl acetate (EtOAc).[117] Using these deprotection conditions product **70** was afforded in 83% yield (**Scheme 15**). The procedure was easy to perform, and the isolation of the final product did not require purification by column chromatography.

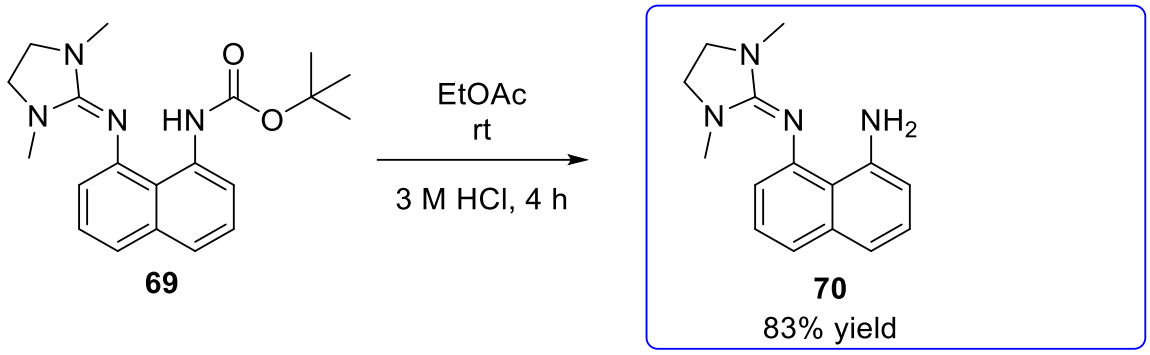

Scheme 15: Successful deprotection affording **70.**

The final step involved cyclopropenium ion functionalization of **70** (**Scheme 16**). A well-known, previously discussed procedure by Tobey and West was used to synthesize **22**. To synthesize **71**, an excess amount of diisopropylamine (HN(*i*Pr)$_2$) was used. The amine added via nucleophilic addition to **22**, generating HCl *in situ* that was subsequently quenched by the excess HN(*i*Pr)$_2$. The reaction was left to stir for 4 h before **70** was added to the solution.

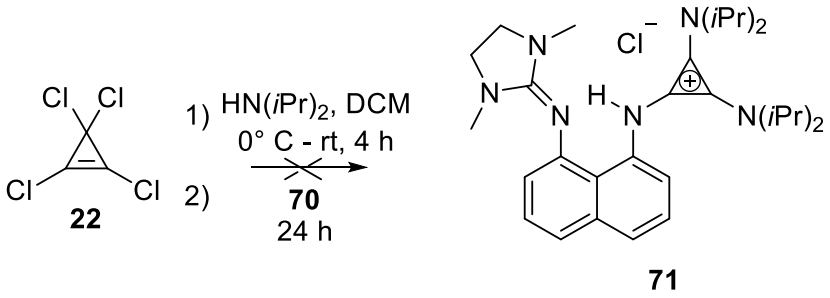

Scheme 16: Attempt at cyclopropenium ion functionalization using the same procedure for the Janus sponge.

Unfortunately, the reaction yielded no product. Given this result, a new synthetic procedure was utilized using an isolated cyclopropenium ion derivative. Amine functionalization of **22** remained the same in this step, but instead of the addition of **70**, sodium tetrafluoroborate ($NaBF_4$) was used for anion exchange. Compound **72** was then isolated through washes with water to remove the amine salt, followed by recrystallization from a DCM/ether solution. Compound **72** was more stable than its chloride anion counterpart, being a benchtop stable solid that was used for

subsequent reactions. Compound **70** was then stirred in the presence of potassium bis(trimethylsilyl)amide (KHMDS) in an ice bath, and the dropwise addition of **72** in DCM was performed (**Scheme 17**). KHMDS was used in this case because it is a very strong (pK_a = 26) and non-nucleophilic base. [118]

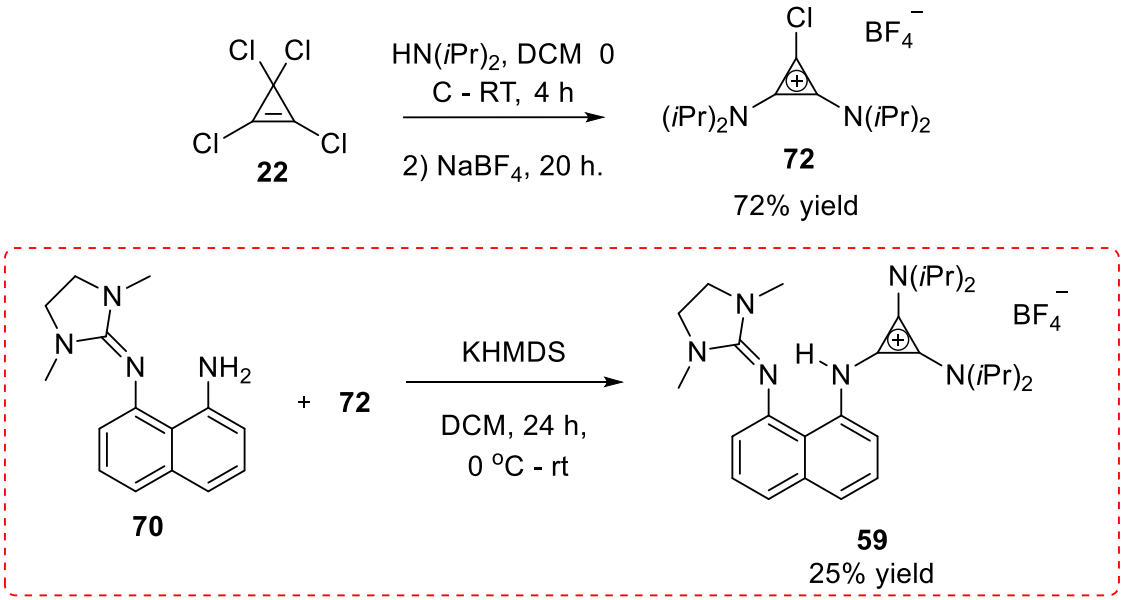

Scheme 17: Successful synthesis of **59**.

Compound **59** was isolated as an off-white solid through trituration in ether and ethyl acetate, followed by silica gel flash column chromatography using 9:1 DCM/methanol as the mobile phase. The low yield was thought to arise from the deprotonation step using KHMDS. Given this reasoning, the reaction was then optimized by switching the base to lithium diisopropyl amide. The switch afforded **59** in 51% yield; the highest yield achieved to date (**Scheme 18**).

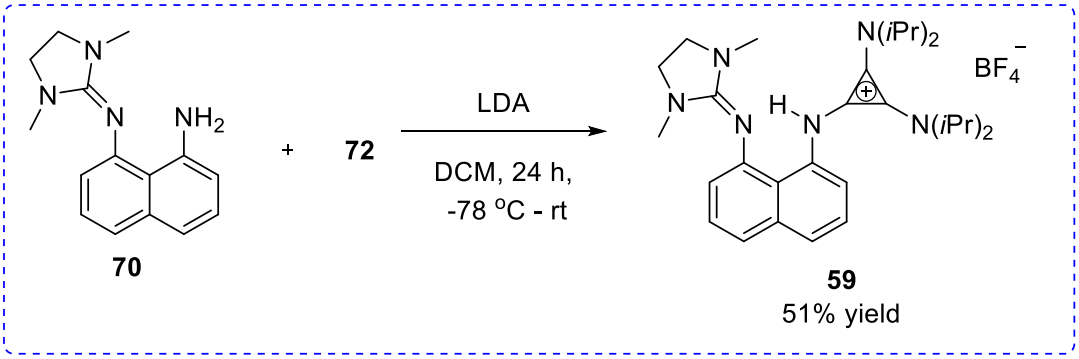

Scheme 18: Optimized reaction conditions for the cyclopropenium functionalization of **70**.

As **59** is a derivative of Janus (**12**), its properties regarding hydrogen bonding and luminescence are of great interest. Single crystals were grown and subject to X-ray crystal analysis (**Figure 30**).

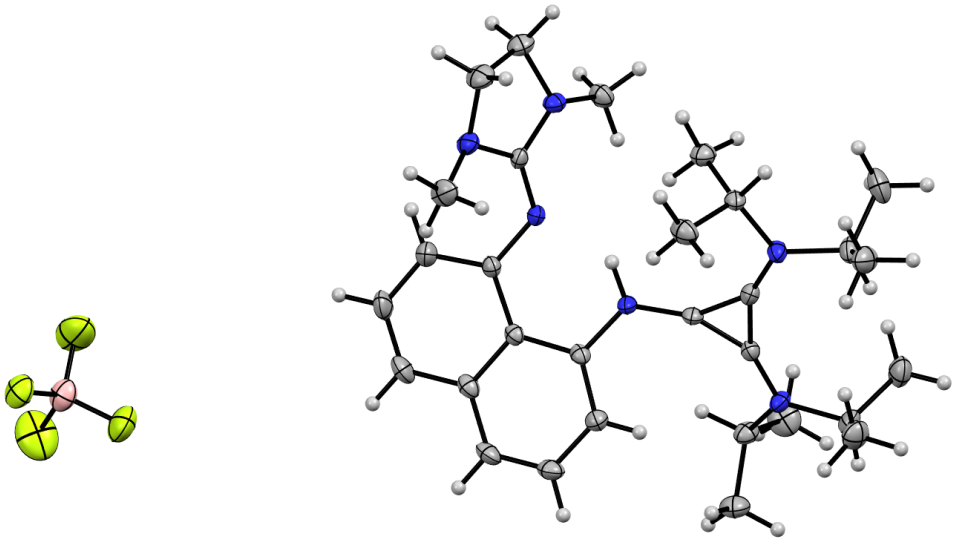

Figure 30: X-ray crystal structure of **59.** Thermal ellipsoids plotted at 50%.

From the X-ray data, a full intramolecular hydrogen bond (1.865(1) Å) was seen in the solid state. No interactions of the BF_4^- anion were observed with the acidic proton, where the anion maintained a distance of 10.473(8) Å. These experimental findings confirm the synthesis of another "true" proton sponge.

Compound **59** was subject to photophysical investigation and displayed two absorption bands at 300 and 350 nm. Excitation at 300 resulted in emission at 597 nm, while excitation at 350 nm manifested in an emission maximum at 700 nm. The molar attenuation coefficient, quantum yields, and Stokes shifts data are summarized in **Table 3**.

Table 3: Selected photophysical properties of **59.**

λ_{max} (nm)	λ_{em} (nm)	Molar Attenuation Coefficient (ε)(M^{-1} cm^{-1})	Quantum Yield (ϕ)	Stokes Shift (nm)
300	597	1.96×10^4	0.013	297
350	700	2.62×10^4	0.004	350

The quantum yield at each excitation point was very small, yet the observed Stokes shifts are very large. The presence of two excitation bands indicates that there are two different fluorescence transitions in the molecule, similar to the carbamate containing Janus derivative **50** previously discussed (**Chapter 2**). The poor quantum efficiency observed initiated the concept of boron incorporated proton sponges, abbreviated BOPS. Functionalizing **59** with a BF_2 group, similar to BODIPY dyes (**Figure 29**), has the potential to increase the fluorescence efficiency effectively switching "on" the compound. The synthesis was initiated with the deprotonation of **59** using KHMDS to afford **59a**, **Scheme 19**.

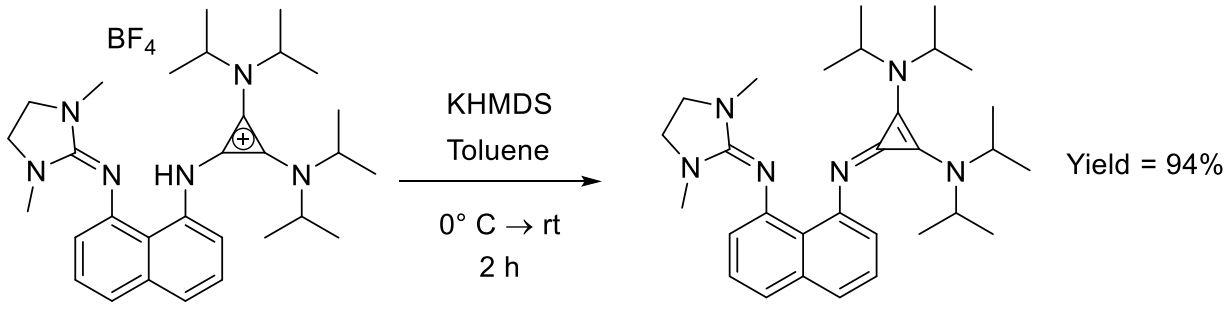

59 **59a**

Scheme 19: Deprotonation of **59** using KHMDS.

The deprotonation occurred smoothly and after extraction with hot hexanes, the final product was isolated in 94% yield as a yellow, needle-like solid.

The deprotonated product was then reacted with boron trifluoride diethyl etherate $BF_3O(C_2H_5)_2$ in an attempt to install the BF_2 group in-between the nitrogen atoms of the molecule, (**Scheme 20**).

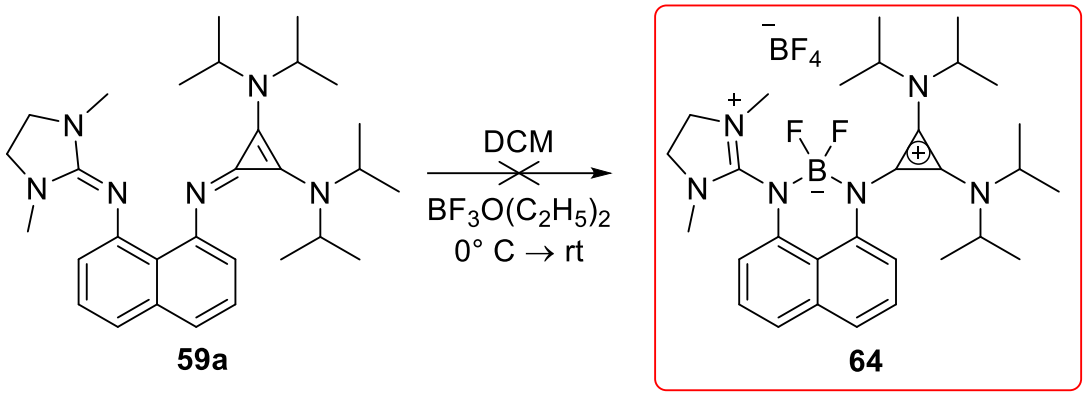

Scheme 20: Failed attempt at synthesizing BOPS.

The reaction was unsuccessful, and **59a** reverted back to the protonated species, **59**. In another attempt, **Scheme 21**, the reaction was cooled in an ice bath, and KHMDS again was used to deprotonate in situ before the addition of $BF_3O(C_2H_5)_2$.

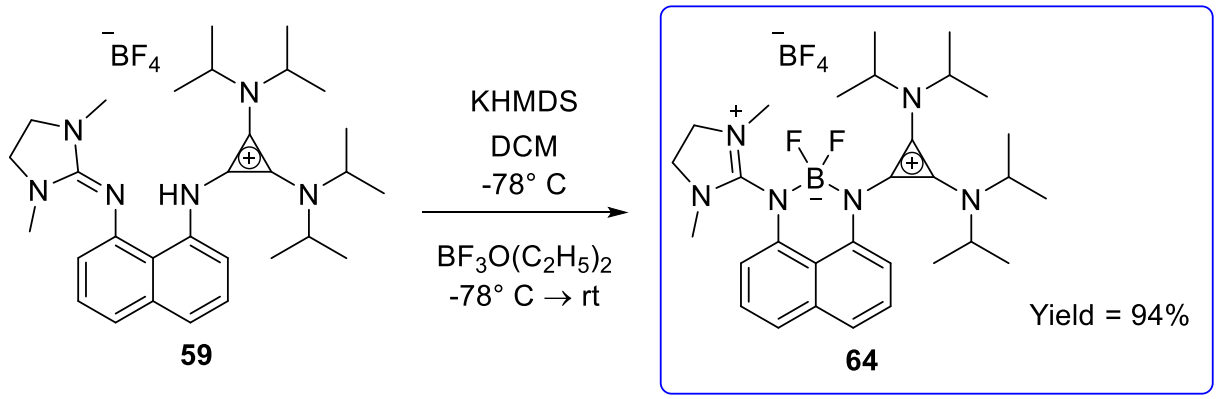

Scheme 21: Successful synthesis of BOPS (**64**).

Given the fact that BODIPY dyes have problematic purification steps resulting in poor yields, the high yielding synthesis of **64** came as a surprise. Purification involved column chromatography using polar solvents (9:1 DCM/methanol), the single crystals were grown using the slow diffusion method (solvents: EtOAc and MeCN) successfully indicating boron incorporation into this new sponge derivative (**Figure 31**).

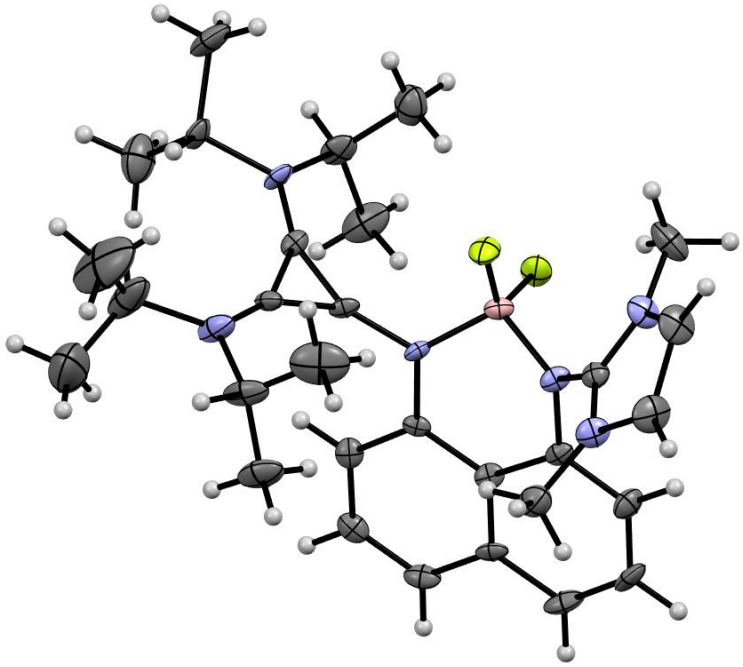

Figure 31: X-ray crystal structure of **64**. Ellipsoids plotted at 50%

4.3 Conclusion

In conclusion, the synthesis protocol used for the Janus sponge effectively extends to other non-symmetric proton sponge derivatives. The successful inclusion of boron in the sponge structure alludes to applications such as potential sensors or ligands. Unfortunately, only the synthesis of **59** and **64**, and brief examination of the photophysical properties of compound **59** were accomplished in the time of writing this document. When completed, the difference in the fluorescence profiles will indicate whether boron inclusion "turns on" the fluorescence.

Chapter 5: Cyclopropenium Ion Functionalized Azo Compounds

5.1 Introduction: Next Generation Applications of Azo Compounds

Selective, non-invasive, external control of function is a long-standing challenge that involves both biology and the material sciences.[119] In terms of biology, there are ways one can try to invoke this type of functionality through small molecules such as enzyme inhibitors, permitting great temporal control, but these approaches may suffer from a lack of target specificity. Light offers amazing solutions for this problem because it can be controlled with high spatial and temporal precision so that if a particular molecule can be made light sensitive, it would achieve precise spatial and temporal control. The most widely used approach in making a biomolecule light sensitive is through the use of a caging strategy. With caging, a key functional group in the biomolecule is protected with a light sensitive protecting group rendering the molecule inactive until it is irradiated with light.[120] These types of molecules are sometimes referred to as photo-triggers, because once the deprotection process is triggered by the light, it is irreversible. In comparison to photo-triggers, a class of molecules known as photoswitches undergo reversible photochemistry leading to multiple instances of inactive and active forms.[121] As a result of their light sensitivity, azobenzenes have become a widely used class of photoswitches.[42] To realize light responsive systems at a molecular level, photoswitchable compounds are utilized that show a distinct change in their properties upon irradiation. Azobenzenes fall directly under such classification because of their large change in geometry, as well as dipole moment upon isomerisation from the *trans* to the *cis* isomer. Applications for photoswitches are seen in protein/peptide control and pharmacology, allowing the control of drug activity in chemotherapy, neurology, and antibiotic treatment.[122,123,124]

Research has been conducted on red shifting the "switching" wavelengths of azobenzenes within the bio-optical window (650-1100nm) because within this window, blood supported tissue is transparent.[125] The advantages of visible light vs. ultraviolet light for photoswitching is the reduced phototoxicity, as well as increased tissue-depth penetration making the development of red shifted azobenzenes key for precise photo control of biological systems with light.[125] The design of red shifted azobenzene derivatives is mainly based on the data produced by Hecht and Woolley. The authors introduced *ortho*-fluoroazobenzenes and *ortho*-methoxyazobenzenes respectively.[126] The downfall of these compounds stems from the laborious synthesis of these sterically encumbered molecules, extensive work up, and the relatively low to moderate yields of the final product. Further research is required in order to achieve photoswitches that are easy to produce, as well as have their "switching wavelength" well into the far-red region of the electromagnetic spectrum.

As mentioned previously, cyclopropenium ions are the smallest carbon-based aromatic ring systems and it is this trait that makes them viable substitutes for azo compounds. The nature of the cyclopropenium ion motif allows for engineering derivatives, by varying the R and X^- components in **Figure 32**, with the potential to showcase different properties (red shifted, fluorescence, alternate ion pairs, etc.). Engineering photo-switches with fluorescent properties coupled with biologically active groups enables synthesis of precise targeting devices for pharmaceutical and biological applications.

5.2 Cyclopropenium Ion Containing Azo Compound Synthetic Pathway

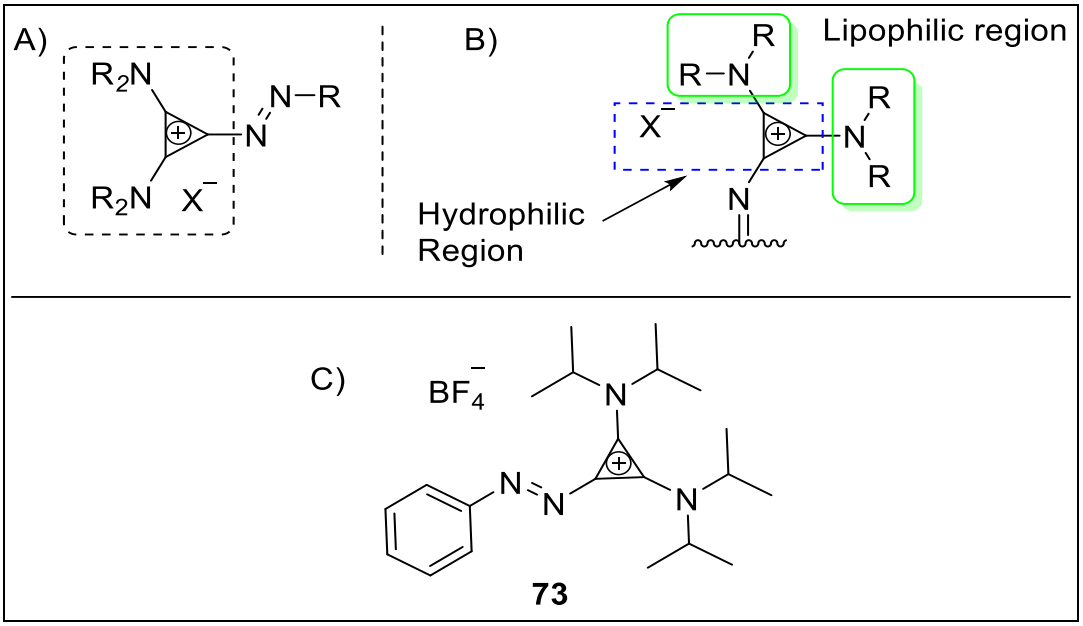

Figure 32: A) The cyclopropenium motif with modifiable R and X^- groups. B) Lipophilic and hydrophobic areas outlined in the cyclopropenium ion motif. C) Target azo molecule **73**, incorporating cyclopropenium ion functionality.

At first, the diazonium coupling reaction was attempted to synthesize **73**.[127] Isolating the diazonium salt was necessary as the subsequent reactions were very moisture- and base-sensitive. Generating a stable and isolatable diazonium salt involved switching the chloride anion to tetrafluoroborate.[127]

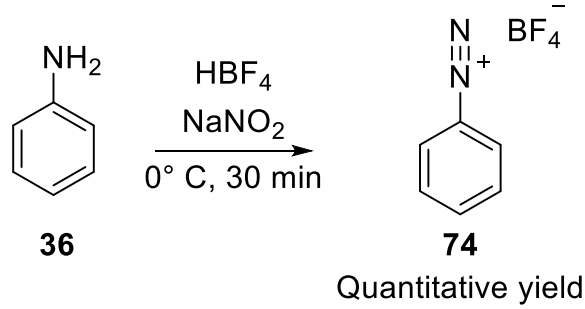

Scheme 22: Synthesis of isolatable compound **74.**

Scheme 22 depicts the synthesis of **74**, which was performed with fluoroboric acid (HBF_4), isolated with vacuum filtration, and purified with diethyl ether trituration. A necessary precursor for the coupling reaction involves material that was previously synthesized by a previous member

of the Dudding research team (Dr. Roya Mir). The synthetic route involves the diisopropylamine functionalization of **22**, counterion exchange to BF_4^-, carbene generation by triphenylphophine (PPh_3), and finally protonation with water affording material **75**.

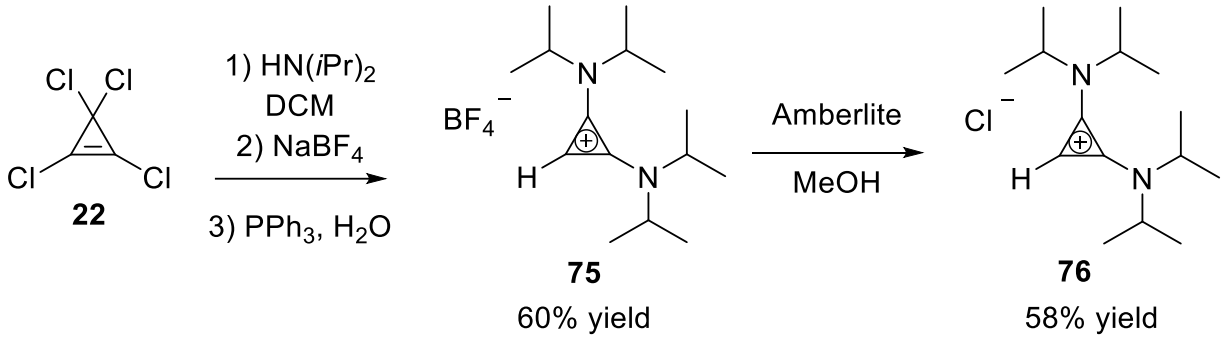

Scheme 23: Synthesis of already reported compounds **75** and **76** necessary for diazonium coupling reaction.

Counterion exchange using a source of chloride trademarked "Amberlite™" in methanol gave **76**, **Scheme 23,** and both **75** and **76** were used in an attempt to form the final desired azo compound **73**. The following procedure (**Scheme 24**) was taken from a recent publication where the synthesis of a series of bis(amino) trifluoroborates were performed.[128]

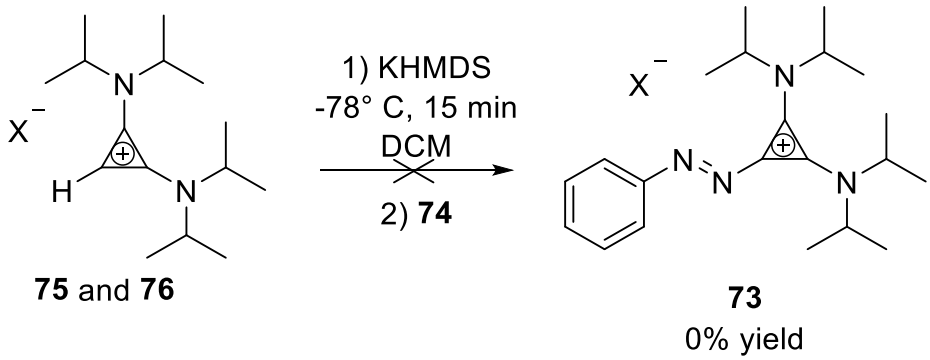

Scheme 24: Attempt 1: diazonium coupling reaction. Both **75** and **76** were attempted, X^- denoting BF_4^- and Cl^- anions respectively.

Both **75** and **76** were subject to deprotonation with KHMDS, allowing to stir for 15 min at -78˚ C. Diazonium salt **74** was then added dropwise as a solution in DCM. The reaction was left to warm up to room temperature and monitored by thin layer chromatography (TLC). Unfortunately, no reaction was observed by TLC.

The next reaction (**Scheme 25**) involved the nucleophilic addition of phenylhydrazine (**78**) to **72**, in an effort to install a hydrazine functionality that could be subsequently oxidized to the azo group.

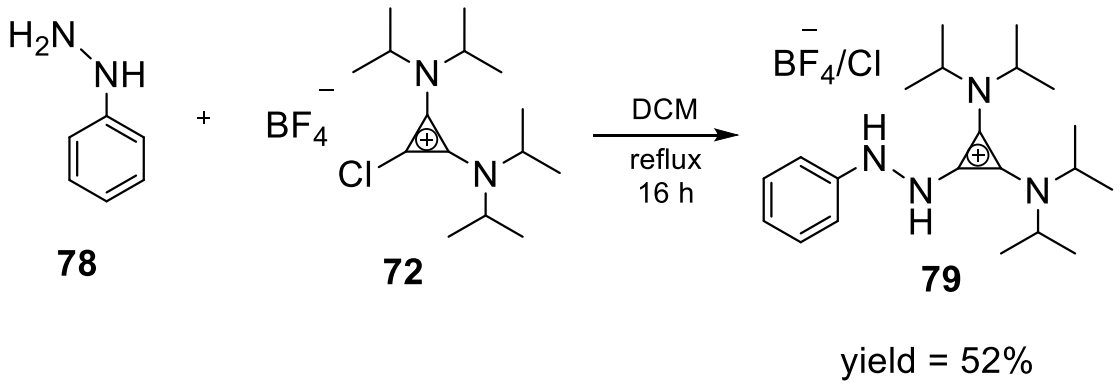

Scheme 25: Reaction to form hydrazine **79**.

Initially, purification of **79** was difficult, where attempts to isolate the material through column chromatography led to decomposition of the final product. This led to attempts to crystallize the material using different concentrations of DCM and ether, eventually leading to the purification of **79** in 52% yield. It is important to note that the reaction contained a mixture of counter anions, arising from the release of chloride from the nucleophilic substitution reaction with phenylhydrazine. Subsequently, the oxidation of **79** was accomplished by procedures previously discussed using *N*-bromosuccinimide and pyridine (**Scheme 26**).[55,56]

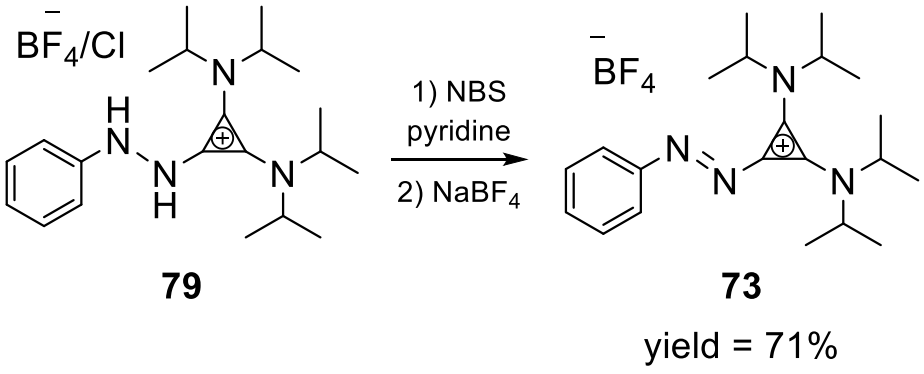

Scheme 26: Final synthesis of the first cyclopropenium ion containing azo compound **73.**[55]

Following the fact that two counterions were present in the starting material, a counterion exchange was performed with $NaBF_4$ in an effort to form one species. The product was isolated through the same crystallization technique mentioned for **79**, affording orange crystals in 71% yield. Single crystals were formed using the slow diffusion method (EtOAc and MeCN) and were subject to X-ray crystallography.

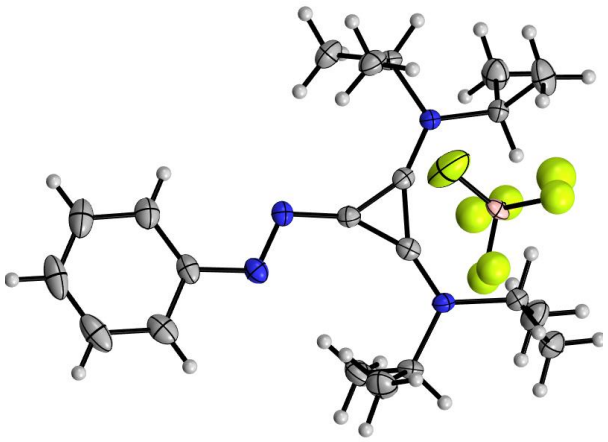

Figure 33: X-ray structure of **73**. Thermal ellipsoids plotted at 50%

The X-ray structure (**Figure 33**) of **73** indicated that the bond distance between the carbon of the phenyl group and the nitrogen atom is 1.41(6) Å due to conjugation, and the azo bond was measured to be 1.27(0), in good agreement with the comparable bonds in azobenzene. X-ray crystallography confirmed the structure of compound **73**, which, to the best of our knowledge, is the first cyclopropenium ion containing an azo derivative.

Apart from the crystal structure, striking features of **73** include its absorption profile and lack of fluorescence. Azobenzene absorbs at 320 nm, with a very small absorption peak at 440 nm. These two peaks represent the *trans* and *cis* isomers respectively, where a solution of azobenzene contains a small amount of *cis* isomer. Compound **73**, however, exhibits a very broad absorption band with a maximum at 395 nm, **Figure 34**.

Notably, the substitution of a phenyl ring by cyclopropenium ion redshifted the absorption wavelength by 75 nm. Unfortunately, in the time of writing this thesis, no further progress has been made in regards to the photophysical properties of **73**.

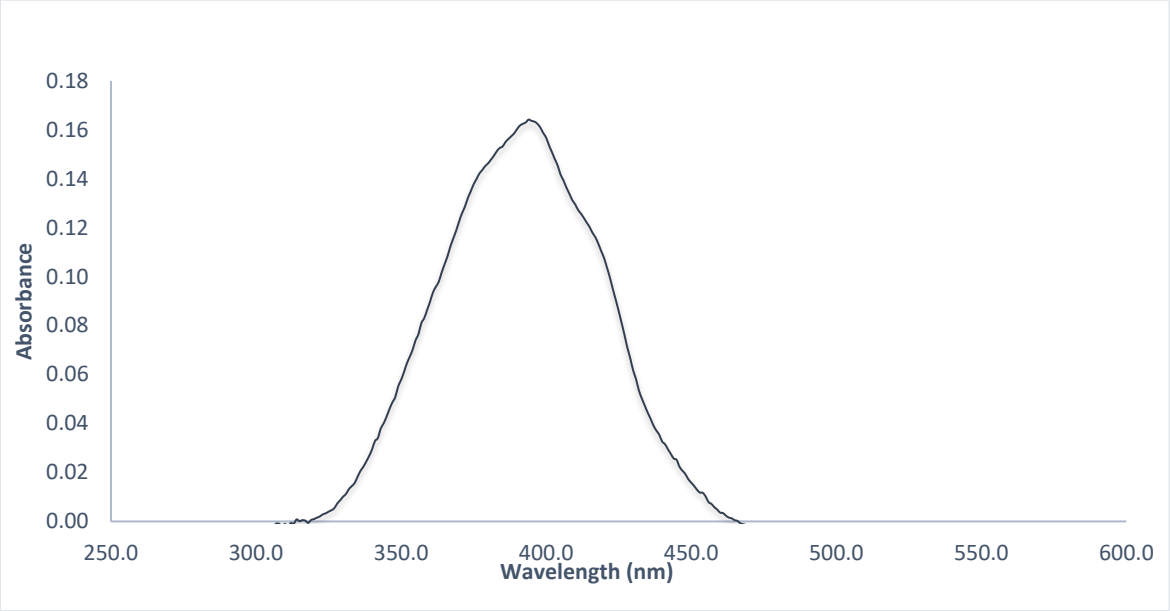

Figure 34: Absorption profile of **73** with absorption maximum recorded at 395 nm.

5.3 Conclusion

This work represents, to the best of our knowledge, the first cyclopropenium ion containing an azo derivative. In an effort to study the properties imparted by cyclopropenium ions, the absorbance profile of **73** (395 nm) was compared to the prototypical azo compound, azobenzene (320 nm). Specifically, the incorporation of the cyclopropenium ion red-shifted the absorption wavelength by 75 nm, a promising result introducing cyclopropenium ions as viable aromatic replacements for azo style compounds. Further developments within photo-physical properties and cyclopropenium ion functionality will be improved upon, all while working to ameliorate the quality of life through selective, non-invasive, external control of function.

Chapter 6: Summary

The work presented herein has described the synthesis of Janus sponge derivatives in order to understand the underlying photochemistry of cyclopropenium based fluorophores. Firstly, **Chapter 2** reports the fluorescence profiles of cyclopropenium ion derivatives. Three major structural components (the naphthalene ring system, cyclopropenium motif, and *peri*-dimethylamino moiety) were altered and found to collectively contribute to the fluorescence profile of the molecules. Key in this study was the discovery that cyclopropenium ions are inherently fluorescent and contain large Stokes shifts. The internal charge transfer mechanism concerning these derivatives provides the ability to rationally design new fluorophores with targeted photophysical properties. Secondly, the data reported in **Chapter 3** involved altering the anion component of Janus (from Cl^- to BF_4^-, PF_6^-, and $B(Ph)_4^-$) to study both the luminescence, and hydrogen bonding properties of the compound. X-ray crystal analyses indicated that all new derivatives contained intramolecular hydrogen bonds in the solid state notably representing the first ever cyclopropenium ion containing "true" proton sponges according to the criteria put forward by Pozharskii *et al*. Moreover, the only photophysical property to be greatly affected by the anion exchange was the quantum yield (ϕ). This fact was traced to compounds with stronger intramolecular hydrogen bonds correlate with weaker fluorescence efficiency. This is due to the fact that the intramolecular hydrogen bond inhibits lone pair donation from the *peri*-dimethylamino group, thereby hindering the ICT mechanism of the molecule. Additionally, focus was also placed on the synthesis of another mono-cyclopropenium ion containing proton sponge, replacing the *peri*-dimethylamino group with a guanidine moiety (**Chapter 4**). Successful synthesis added another cyclopropenium ion "true" proton sponge to the list of cyclopropenium ion containing proton sponge. Incorporation of a boron group to the same molecule was also

successful where the objective was to develop new dyes that are similar to BODIPY functionality, adding to the rich class of naphthalene and BODIPY style fluorophores. Surprisingly, boron incorporation achieved a yield of 94% far surpassing the low yields of conventional BODIPY dyes mentioned in section 1.4.2. Further, the synthesis of the first cyclopropenium ion containing azo derivative (**Chapter 5**) was accomplished. The absorbance profile of the cyclopropenium ion containing azo compound was compared to the prototypical azo compound, azobenzene. Notably, the incorporation of the cyclopropenium ion red-shifted the absorption wavelength by 75 nm, a promising result given previously mentioned desirable properties of azo compounds at the beginning of **Chapter 5**. With further research into this new class of compound, cyclopropenium ions could be viable aromatic replacements for engineering azo compounds with desirable properties.

Chapter 7: Experimental Details

Materials were obtained from commercial suppliers and were used without further purification, unless otherwise specified. Dichloromethane (DCM) was distilled over CaH, tetrahydrofuran (THF) was distilled over Na and a benzophenone indicator, and acetonitrile (MeCN) was distilled over Na_2CO_3. Reactions were monitored by thin layer chromatography (TLC) using TLC silica gel 60 F254. NMR spectra were obtained with a 300 MHz spectrometer (^{1}H 300 MHz, ^{13}C 75.5 MHz or ^{13}C 150.9 MHz, ^{19}F 292.4 MHz, ^{31}P 121.4 MHz and ^{11}B 96.3 MHz) or a 400MHz spectrometer. The chemical shifts are reported as δ values 105 (ppm) relative to tetramethylsilane. All reactions were performed under an inert nitrogen atmosphere. HRMS (high-resolution mass spectrometry) spectra were measured using electron ionization (EI), electrospray ionization (ESI) or fast atom bombardment (FAB) and a time-of-flight (TOF) mass analyzer in positive ionization mode.

The quantum yield (ϕ), was measured relative to that of naphthalene in cyclohexane.[129] Absorption spectra were measured using a UV-Vis-NIR spectrophotometer at ambient temperature. Emission spectra for the quantum yield calculation were acquired using 1cm quartz cuvettes in a fluorescence spectrophotometer with a Xenon flash lamp at ambient temperature. Sample and standards were prepared as $1x10^{-6}$ M solutions in dichloromethane. Entrance and exit slit widths were set to 5 mm, and the excitation wavelength was 334 nm for the samples. Quantum yields were calculated using Equation S1, according to the 2011 IUPAC technical report on standards for photoluminescence quantum yield measurements in solution.[130]

$$\phi_f^x = \frac{F^x f_{st} n_x^2}{F^{st} f_x n_{st}^2} \phi_f^{st}$$

Where ϕ_f^x and ϕ_f^{st} are the quantum yields of the sample and the standard, respectively. $F^x$and $F^{st}$are the integrated fluorescence intensities of sample and standard spectra. f_x and f_{st} are the absorption factors of the sample and standard at the excitation wavelength (where $f = 1 - 10^{-A}$, and A = absorbance). n_x and n_{st} are the refractive indices of the sample and reference solution, respectively, which were assumed to be the same in this experiment.

Calculations were carried out using Kohn-Sham Hybrid-Density Functional Theory (DFT) at the level of theory specified for each individual calculation. Geometry optimization were performed at standard temperature and pressure using Gaussian 09 and 16 programs and the resulting vibrational frequencies and molecular orbitals visualized with GaussView v5.0.8.[131] Natural bond orbital analysis (NBO Version 3.1[132] as implemented in Gaussian 09) was used to quantify the electronic donor-acceptor interactions as second-order perturbation energies (E_{NBO}). To account for solvent effects, the Integrated Equation Formalism Polarized Continuum Solvation Model (IEFPCM)[133] was used throughout the computations with default parameters for the chosen solvent(s). Quantum theory of atoms in molecules (QTAIM) calculations were computed using AIM2000.[134] The noncovalent interactions (NCI) index analysis was performed using the Schrödinger Jaguar program, and the results were visualized with Maestro 11.5.011.[135]

7.1 Experimental Procedures

N1-(2,3-Bis(diisopropylamino)cycloprop-2-en-1-ylidene)-N8,N8-dimethylnaphthalene-1,8-diamine hydrochloride (Janus) (**12**).

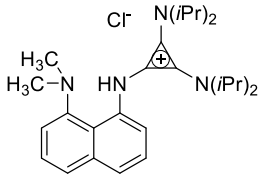

To a solution of tetrachlorocyclopropene (0.03 mL, 0.2 mmol), in dichloromethane (2 mL) was added freshly distilled diisopropylamine (0.11 mL, 0.8 mmol) in a dropwise manner under a inert atmosphere. The reaction was stirred for 4 h at room temperature, after which time N1,N1-dimethylnaphthalene-1,8-diamine (**81**) (16 mg, 0.1 mmol) was added dropwise as a solution in dichloromethane (2 mL) and the reaction was stirred for an additional 8 h. The crude product was diluted with 5 mL of H_2O, quenched with 5 mL of 1 M HCl and extracted three times with 10 mL of DCM. The combined organic extracts were dried over $MgSO_4$ and the solvent was removed under reduced pressure. The crude product was purified by flash chromatography (11% methanol in DCM) to afford **1** as an off-white solid in 90% yield (59 mg, 0.08 mmol). m.p. = 225 °C – 230 °C. ^{1}H NMR (300 MHz, $CDCl_3$): δ = 13.81 (s, 1H), 7.74 – 7.71 (m, 1H), 7.55 – 7.50 (m, 3H), 7.44 – 7.38 (m, 1H), 6.97 (d, J = 7.0 Hz,1H), 4.03 – 3.94 (m, 4H), 2.84 (s, 6H) 1.41 (d, J = 6.75 Hz, 24H) 2.75 (s, 6H), 1.14 (d, J = 6.8 Hz, 24H). ^{13}C {^{1}H} NMR (75.5 MHz, $CDCl_3$): δ = 150.3, 138.2, 136.2, 126.9, 126.7, 125.3, 123.2, 119.9, 119.4, 118.9, 112.3, 110.0, 51.4, 46.4, 22.1. HRMS (ESI): m/z calcd for $C_{27}H_{41}N_4$ (M+): 421.3326, found: 421.3331.

N1-(2,3-Bis(dicyclohexylamino)cycloprop-2-en-1-ylidene)-N8,N8-dimethylnaphthalene-1,8-diamine hydrochloride (**48**).

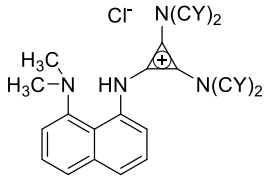

To a solution of tetrachlorocyclopropene (35.6 mg, 0.2 mmol) in dichloromethane (2 mL) under a nitrogen atmosphere was added dicyclohexylamine (0.16 mL, 0.8 mmol). The reaction was stirred for 4 h at room temperature, after which time N1,N1-dimethylnaphthalene-1,8-diamine (**81**) (37.25

mg, 0.2 mmol) was added dropwise as a solution in dichloromethane (2 mL) and the reaction was stirred for an additional 16 h. The crude product was diluted with 5 mL of H_2O, quenched with 5 mL of 1 M HCl and extracted three times with 10 mL of DCM. The combined organic extracts were dried over $MgSO_4$ and the solvent was removed under reduced pressure. The crude product was purified by flash column chromatography (11% methanol in DCM) to afford **6** as a white solid in 82% yield (123.1 mg, 0.18 mmol). m.p. = 125 °C – 129 °C. ^{1}H-NMR (300 MHz, $CDCl_3$): δ = 13.07 (s, 1H), 7.70 – 7.73 (dd, J = 7.17, 2.17 Hz, 1H) (m,3H), 7.58 – 7.60 (d, J = 7.83 Hz, 1H), 7.47 – 7.54 (m, 2H), 7.39 – 7.44 (t, J = 7.83 Hz, 1H), 6.94 – 9.97 (d, J = 7.17, 1H), 3.93 - 3.47 (m, 1H), 2.82 (s, 6H), 1.84 – 1.94 (m, 16H), 1.49 - 1.68 (m, 12H), 1.21 – 1.34 (m, 8H), 1.03 – 1.07 (m, 4H).^{13}C {^{1}H} NMR (75.5 MHz, $CDCl_3$): δ = 150.3, 138.0, 136.3, 126.8, 125.7, 123.6, 121.13, 119.3, 118.9, 114.1, 110,5, 60.2, 46.6, 32.4, 25.6, 24.8. HRMS (EI): m/z calcd for $C_{39}H_{56}N_4$ (M+): 580.4505, found: 580.4487.

N1-(2,3-Bis(diphenylamino)cycloprop-2-en-1-ylidene)-N8,N8-dimethylnaphthalene-1,8-diamine hydrochloride (**49**).

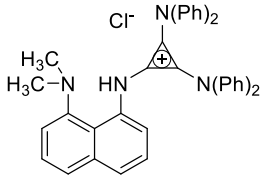

To a solution of tetrachlorocyclopropene (35.6 mg, 0.2 mmol) in dichloromethane (2 mL) under an inert nitrogen atmosphere was added diphenylamine (0.11 mL, 0.8 mmol). The reaction was stirred for 4 h at room temperature, after which time N1,N1-dimethylnaphthalene-1,8-diamine (**81**) (37.3 mg, 0.2 mmol) was added dropwise as a solution in dichloromethane (2 mL) and the reaction was stirred for an additional 16 h. The crude product was diluted with 5 mL of H_2O, quenched with 5 mL of 1 M HCl and extracted three times with 10 mL of DCM. The combined organic extracts were dried over MgSO4 and the solvent was removed under reduced pressure. The crude product was purified by flash column chromatography (11% methanol in DCM) to afford **7** as a white solid in 70% yield (83.5 mg, 0.14 mmol). m.p. = 138 °C – 140 °C. ^{1}H-NMR (300 MHz, $CDCl_3$): δ =15.42 (s, 1H), 6.87–7.95 (m, 26H), 2.95 (s, 6H). ^{13}C {^{1}H} NMR (75.5 MHz, $CDCl_3$): δ =149.6, 142.8, 137.3, 136.8, 130.0, 129.6, 129.1, 127.1, 127.0, 125.8, 124.5, 124.1, 124.0, 119.7, 119.0, 116.8, 110.6, 46.34. HRMS (EI): m/z calcd for $C_{39}H_{32}N_4$ (M+): 556.2627, found: 556.2626.

tert-Butyl (8-((2,3-bis(diisopropylamino)cycloprop-2-en-1 ylidene) amino)naphthalen-1-yl)carbamate hydrochloride (**50**).

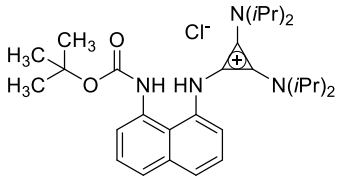

To a solution of tetrachlorocyclopropene, (35.6 mg, 0.2 mmol) in dichloromethane (2 mL) under an inert nitrogen atmosphere was added diisopropylamine (0.11 mL, 0.8 mmol). The reaction was stirred for 4 h at room temperature, after which time *tert*-butyl (8-aminonaphthalen-1-yl)carbamate (**66**) (57.3 mg, 0.2 mmol) was added dropwise as a solution in dichloromethane (2 mL) and the reaction was stirred for an additional 16 h. The crude product was diluted with 5 mL of H_2O, quenched with 5 mL of 1 M HCl and extracted three times with 10 mL of DCM. The combined organic extracts were dried over $MgSO_4$ and the solvent was removed under reduced pressure. The crude product was purified by flash column chromatography (11% methanol in DCM) to afford **50** as a light red solid in 90% yield (95.2 mg, 0.18 mmol). The solid decomposes before reaching its melting point. ^{1}H-NMR (300 MHz, $CDCl_3$): δ = 11.57 (s, 1H), 9.22 (s, 1H), 7.79 – 7.82 (dd, J = 7.82, 1.34 Hz, 1H), 7.71 – 7.73 (d, J = 7.94 Hz, 1H), 7.64 – 7.66 (d, J = 7.26 Hz, 1H), 7.45 – 7.51 (t, J = 7.89 Hz, 1H), 7.33 – 7.42 (m, 2H), 3.52 – 3.65 (m, 4H), 1.48 (s, 9H), 1.23 – 1.25 (d, J = 6.93 Hz, 24H).^{13}C {^{1}H} NMR (75.5 MHz, $CDCl_3$): δ = 155.1, 136.2, 134.9, 133.1, 129.2, 127.6, 127.3, 126.7, 126.6, 126.3, 124.7, 115.6, 114.0, 79.0, 50.7, 28.5, 22.0. HRMS (EI): m/z calcd for $C_{30}H_{44}N_4O_2$ (M+): 492.3464, found: 492.3448.

N1,N1,N2,N2-Tetraisopropyl-3-((8-(pyrrolidin-1-yl) naphthalen-1-yl)imino) cycloprop-1-ene-1,2-diamine hydrochloride (**51**).

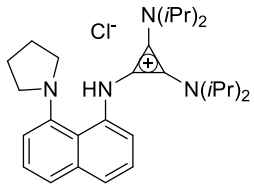

To a solution of tetrachlorocyclopropene, (35.6 mg, 0.2 mmol) in dichloromethane (2 mL) under an inert nitrogen atmosphere was added diisopropylamine (0.11 mL, 0.8 mmol). The reaction was stirred for 4 h at room temperature, after which time 8-(pyrrolidin-1-yl)naphthalen-1-amine (**20**)

(42.5 mg, 0.2 mmol) was added dropwise as a solution in dichloromethane (2 mL) and the reaction was stirred for an additional 16 h. The crude product was diluted with 5 mL of H_2O, quenched with 5 mL of 1 M HCl and extracted three times with 10 mL of DCM. The combined organic extracts were dried over $MgSO_4$ and the solvent removed under reduced pressure. The crude product was purified by flash column chromatography in (11% methanol in DCM) to afford **51** as a white solid in 91% yield (88.5 mg, 0.18 mmol). m.p. = 72 °C – 78 °C. ^{1}H-NMR (300 MHz, $CDCl_3$): δ = 13.42 (s, 1H), 7.66 – 7.69 (dd, J = 7.32, 2.10 Hz, 1H), 7.43 – 7.54 (m, 3H), 7.35 – 7.40 (t, J = 7.51 Hz, 1H), 6.86 – 6.88 (dd, J = 7.35, 1.00 Hz, 1H), 3.86 – 3.99 (m, 4H), 3.38 (bs, 2H), 3.08 (bs, 2H), 2.14 (bs, 2H), 1.97 (bs, 2H), 1.34 – 1.36 (d, J = 6.78 Hz, 24H). ^{13}C {^{1}H} NMR (75.5 MHz, $CDCl_3$): δ =148.5, 137.9, 136.0, 127.1, 125.2, 123.9, 120.4, 120.2, 119.9, 113.4, 110.6, 56.6, 51.5, 25.0, 22.3. HRMS (EI): m/z calcd for $C_{29}H_{43}N_4$ (M+): 447.3482, found: 447.3490.

N-(2,3-Bis(2,4-dimethylpentan-3-yl)cycloprop-2-en-1-ylidene) -5-(pyrrolidin-1-yl)naphthalen-1-aminium chloride (**52**).

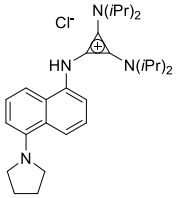

To a solution of tetrachlorocyclopropene (73.8 mg, 0.35 mmol) in dichloromethane (10 mL) under an inert nitrogen atmosphere was added diisopropylamine (0.21 mL, 1.47 mmol). The reaction was stirred for 4 h at room temperature, after which time 5-(pyrrolidin-1-yl)naphthalen-1-amine (**24**) (73.8 mg, 0.35 mmol) was added dropwise as a solution in dichloromethane (4 mL) and the reaction was stirred for an additional 16 h. The crude product was diluted with 5 mL of H_2O, quenched with 5 mL of 1 M HCl and extracted three times with 10 mL of DCM. The combined organic extracts were dried over $MgSO_4$ and the solvent was removed under reduced pressure. The crude product was purified by flash column chromatography (11 % methanol in DCM) to afford **52** as a white solid in 95% yield (160.6 mg, 0.33 mmol). m.p. = 66 °C – 70 °C ^{1}H-NMR (300 MHz, $CDCl_3$): δ = 11.14 (s, 1H), 8.05 (d, J = 8.68 Hz, 1H), 7.53 (d, J = 7.00 Hz, 1H), 7.41 (d, J = 8.68 Hz, 1H), 7.33 – 7.25 (m, 2H), 3.41 (m, 4H), 3.24 (m, 4H), 1.96 (m, 4H), 1.07 (d, J = 7.03 Hz, 24H).^{13}C {^{1}H} NMR (75.5 MHz, $CDCl_3$): δ = 148.2, 135.8, 131.8, 129.1, 126.9, 124.2, 123.8,

116.3, 115.9, 115.0, 112.1, 52.8, 50.7, 24.6, 21.8. HRMS (EI): m/z calcd for $C_{29}H_{43}N_4$ (M+): 447.3471, found: 447.3468.

N1,N1,N2,N2-Tetraisopropyl-3-(naphthalen-1-ylimino)cycloprop-1-ene-1,2-diamine hydrochloride (**53**).

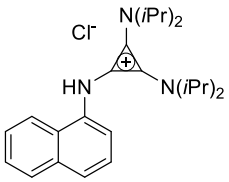

To a solution of tetrachlorocyclopropene, (35.6 mg, 0.2 mmol) in dichloromethane (2 mL) under an inert nitrogen atmosphere was added diisopropylamine (0.11 mL, 0.8 mmol). The reaction was stirred for 4 h at room temperature, after which time 1-naphthylamine (28.6 mg, 0.2 mmol) was added dropwise as a solution in dichloromethane (2 mL) and the reaction was stirred for an additional 16 h. The crude product was diluted with 5 mL of H_2O, quenched with 5 mL of 1 M HCl and extracted three times with 10 mL of DCM. The combined organic extracts were dried over $MgSO_4$ and the solvent removed under reduced pressure. The crude product was purified by flash column chromatography (11% methanol in DCM) to afford **53** as a white solid in 95% yield (21.7 mg, 0.19 mmol). m.p. = 250 °C – 255 °C. ^{1}H-NMR (300 MHz, $CDCl_3$): δ = 11.58 (s, 1H), 7.96 – 7.99 (dd, J = 6.22, 1.08 Hz, 1H), 7.80 – 7.83 (m, 1H), 7.70 – 7.73 (d, 8.32 Hz, 1H), 7.58 – 7.60 (d, J = 7.14 Hz, 1H), 7.37 – 752 (m, 3H) 3.42 – 3.56 (m, 4H), 1.12 – 1.14 (d, J = 6.89 Hz, 24H).^{13}C {^{1}H} NMR (75.5 MHz, $CDCl_3$): δ = 152.8, 134.7, 130.5, 127.3, 125.9, 125.2, 125.1, 124.7, 123.8, 118.6, 116.4, 113.7, 49.4, 22.3. HRMS (EI): m/z calcd for $C_{25}H_{35}N_3$ (M+): 377.2831, found: 377.2822.

N1-(2,3-Bis(diisopropylamino)cycloprop-2-en-1-ylidene)-N2-pyridin-1-ylcyclohexane-1,2-diamine hydrochloride (**54**).

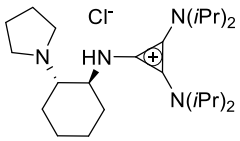

To a solution of tetrachlorocyclopropene, (35.6 mg, 0.2 mmol) in dichloromethane (2 mL) under an inert nitrogen atmosphere was added diisopropylamine (0.11 mL, 0.8 mmol). The reaction was stirred for 4 h at room temperature, after which time (trans)-2-(pyrrolidin-1-yl)cyclohexanamine (**23**) (33.6 mg, 0.2 mmol) was added dropwise as a solution in dichloromethane (2 mL) and the reaction was stirred for an additional 8 h. The crude product was diluted with 5 mL of H_2O, quenched with 5 mL of 1 M HCl and extracted three times with 10 mL of DCM. The combined organic extracts were dried over $MgSO_4$ and the solvent removed under reduced pressure. The crude product was purified by flash column chromatography (11% methanol in DCM) to afford **54** as a orange oil in 90% yield (790.4 mg, 1.8 mmol). ^{1}H-NMR (300 MHz, $CO(CD_3)_2$): δ = 4.04 (m, 4H), 3.50 (m, 1H), 3.30 (m, 1H), 2.80 (m, 4H), 2.09 (m, 4H), 1.58–1.87 (m, 8H), 1.36 (d, J = 6.82, 24H).^{13}C {^{1}H} NMR (75.5 MHz, $CO(CD_3)_2$): δ =117.4, 114.7 62.2, 60.3, 50.6, 48.5, 33.7, 24.7, 24.7, 23.3, 21.5, 21.2. HRMS (EI): m/z calcd for $C_{25}H_{47}N_4$ (M+): 403.3795, found: 403.3795.

tert-Butyl((1S,2S)-2-((2,3-bis(diisopropylamino)cycloprop-2-en-1-ylidene)amino)cyclohexyl)carbamate hydrochloride (**55**).

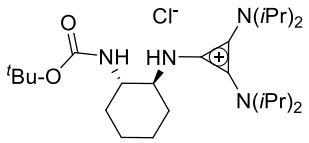

To a solution of tetrachlorocyclopropene, (35.6 mg, 0.2 mmol) in dichloromethane (2 mL) under an inert nitrogen atmosphere was added diisopropylamine (0.11 mL, 0.8 mmol). The reaction was stirred for 4 h at room temperature, after which time tert-butyl ((trans)-2-aminocyclohexyl)carbamate[136] (**21**) (33.6 mg, 0.2 mmol) was added dropwise as a solution in dichloromethane (2 mL) and the reaction was stirred for an additional 8 h. The crude product was diluted with 5 mL of H_2O, quenched with 5 mL of 1 M HCl and extracted three times with 10 mL of DCM. The combined organic extracts were dried over $MgSO_4$ and the solvent removed under reduced pressure. The crude product was purified by flash column chromatography (11% methanol in DCM) to afford **13** as a white solid in 90% yield (790.4 mg, 1.8 mmol). Product decomposes before its melting point, at 80 °C – 84 °C. ^{1}H-NMR (300 MHz, $CDCl_3$): δ = 8.41 (bs, 1H), 6.17 (bs, 1H), 4.06 (m, 1H), 3.88 (m, 4H), 3.74 (m, 1H), 2.08 (m, 1H), 1.93 (m, 2H), 1.73 (m, 5H), 1.39 – 1.35 (m, 33H) .^{13}C {^{1}H} NMR (75.5 MHz, $CDCl_3$): δ = 156.6, 116.4, 113.3, 78.5, 59.7, 53.9,

50.5, 34.7, 30.7, 28.3, 25.1, 24.5, 22.2, 22.1 . HRMS (EI): m/z calcd for $C_{26}H_{49}N_4O_2$ (M+): 484.3544, found: 484.3548.

N-(2,3-Bis(diisopropylamino)cycloprop-2-en-1-ylidene)benzenaminium chloride (**56**).[137]

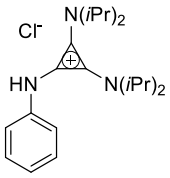

To a solution of tetrachlorocyclopropene, (35.6 mg, 0.2 mmol) in dichloromethane (2 mL) under an inert nitrogen atmosphere was added diisopropylamine (0.11 mL, 0.8 mmol). The reaction was stirred for 4 h at room temperature, after which time aniline (18.6 mg, 0.2 mmol) was added dropwise as a solution in dichloromethane (2 mL) and the reaction was stirred for an additional 8 h. The crude product was diluted with 5 mL of H_2O, quenched with 5 mL of 1 M HCl and extracted three times with 10 mL of DCM. The combined organic extracts were dried over $MgSO_4$ and the solvent removed under reduced pressure. The crude product was purified by crystallization in MeCN/EtOAc (1:1) to afford **14** as a white crystalline solid in 96% yield (69.9 mg, 0.19 mmol). m.p. = 188 °C – 190 °C. ^{1}H-NMR (300 MHz, $CDCl_3$): δ = 11.69 (s, 1H), 7.41 – 7.45 (m, 2H), 7.30 – 7.35 (m, 2H), 7.10 – 7.15 (m, 1H), 3.75 – 3.89 (m, 4H), 1.34 – 1.37 (d, J = 6.83 Hz, 24H).^{13}C {^{1}H} NMR (75.5 MHz, $CDCl_3$): δ = 139.5, 130.0, 126.4, 123.2, 117.1, 112.9, 51.4, 22.2. HRMS (EI): m/z calcd for $C_{21}H_{34}N_3$ (M+): 328.2736, found: 328.2753.

3-(*tert*-Butylimino)-N1,N1,N2,N2-tetraisopropylcycloprop-1-ene-1,2-diamine hydrochloride (**57**).[138]

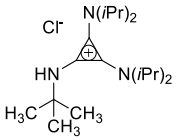

To a solution of tetrachlorocyclopropene, (35.6 mg, 0.2 mmol) in dichloromethane (2 mL) under an inert nitrogen atmosphere was added diisopropylamine (0.11 mL, 0.8 mmol). The reaction was stirred for 4 h at room temperature, after which *tert*-butylamine (14.6 mg, 0.2 mmol) was added dropwise as a solution in dichloromethane (2 mL) and the reaction was stirred for an additional 8 h. The crude product was diluted with 5 mL of H_2O, quenched with 5 mL of 1 M HCl and extracted

three times with 10 mL of DCM. The combined organic extracts were dried over $MgSO_4$ and the solvent removed under reduced pressure. The crude product was purified by crystallization in MeCN/EtOAc (1:1) to afford **15** as a white crystalline solid in 98% yield (67.4 mg, 0.2 mmol). m.p. = 171 °C – 172 °C. ^{1}H-NMR (300 MHz, $CDCl_3$): δ = 3.99 – 4.08 (m, 4H), 1.49 (s, 9H), 1.34 – 1.37 (d, J = 6.82, 24H).^{13}C {^{1}H} NMR (75.5 MHz, $CDCl_3$): δ = 118.0, 116.8, 53.3, 51.0, 30.3, 22.5. HRMS (EI): m/z calcd for $C_{19}H_{38}N_3$ (M+): 308.3049, found: 308.3069.

N,N-Dimethylnaphthalen-1-amine (**58**).[139]

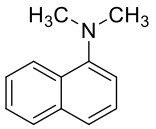

Na_2CO_3 (386 mg, 4.60 mmol) was added to 1-napthylamine (100 mg, 0.70 mmol) in a flame-dried 100 mL round bottom flask fitted with a reflux condenser, and backfilled with $N_{2(g)}$. Acetonitrile (20 mL) was then added, followed by the dropwise addition of freshly distilled Me_2SO_4 (0.46 mL, 4.90 mmol). The reaction solution was heated to reflux, and stirred for 16 h. The solution was then concentrated under reduced pressure, diluted with 20 mL of H_2O, and extracted three times with 10 mL of dichloromethane. The combined organic extracts were dried over $MgSO_4$ and concentrated under reduced pressure. The purified compound was acquired by flash column chromatography (12.5% ethyl acetate in hexanes). The final product was isolated as a light brown liquid in 18% yield (21.2 mg, 0.12 mmol). Spectroscopic data was consistent with the literature.[139] ^{1}H NMR (300 MHz, $CDCl_3$): δ = 8.24 – 8.27 (d, 1H, J = 9.5 Hz), 7.82 – 7.85 (d, 1H, J = 7.5 Hz), 7.39 - 7.55 (m, 3H), 7.44 – 7.47 (t, 1H, J = 7.8 Hz), 7.08 – 7.11 (d, 1H, J = 7.5 Hz), 2.93 (s, 6H).

tert-Butyl (8-aminonaphthalen-1-yl)carbamate (**66**).[140]

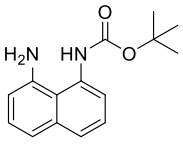

To a flame dried 100 mL round bottom flask backfilled with $N_{2(g)}$ was added 1,8-diaminonaphthalene (2.0 g, 12.6 mmol), followed by the addition of THF (40 mL) and NEt_3 (2 mL, 27.2 mmol). To the resulting solution a solution of di-*tert*-butyl-dicarbonate (3.0 g, 13.9 mmol) in THF (10 mL) was added dropwise over 2 h *via* syringe pump and allowed to stir at room temperature for 18 h. THF was removed under reduced pressure and the crude product mixture

was dissolved in toluene (20 mL), washed sequentially with 1 M NaOH (20 mL), brine (20 mL), and distilled H_2O (20 mL). The organic layer was subsequently dried over $MgSO_4$ and concentrated under reduced pressure. After purification by flash column chromatography (20% ethyl acetate in hexanes), the final product was isolated as red crystals in 84% yield. Spectroscopic data was consistent with the literature.[140] ^1H NMR (300 MHz, $CDCl_3$): δ = 9.79 (s, 1H), 8.08 (d, J = 7.3 Hz, 1H), 7.49 (t, J = 7.7 Hz, 1H), 7.40 (m, 2H), 7.22 (t, J = 7.7, 1H), 6.78 (d, J = 7.2 Hz, 1H).

tert-Butyl(8-(dimethylamino)naphthalene-1-yl)carbamate (**80**).

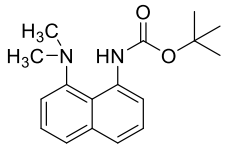

Na_2CO_3 (210 mg, 2.51 mmol) was added to tert-butyl (8-aminonaphthalen-1-yl)carbamate (**66**) (100 mg, 0.38 mmol) in a flame-dried 100 mL round bottom flask fitted with a reflux condenser, and backfilled with $N_{2(g)}$. Acetonitrile (10 mL) was then added, followed by the dropwise addition of freshly distilled Me_2SO_4 (0.26 mL, 2.69 mmol). The reaction solution was heated to reflux, and stirred for 16 h. The crude material was then concentrated under reduced pressure, diluted with 20 mL of H_2O, and extracted three times with 10 mL of dichloromethane. The combined organic extracts were dried over $MgSO_4$ and concentrated under reduced pressure. The purified compound was acquired using flash column chromatography (12.5% ethyl acetate in hexanes). The final product was isolated as a clear oil in 70% yield (3.4 mmol, 0.98 g). ^1H NMR (300 MHz, $CDCl_3$): δ = 12.79 (s, 1H), 8.35-8.32 (dd, J = 7.0, 2.3 Hz, 1H), 7.62 (d, J = 8 Hz, 1H), 7.45-7.27 (m, 4H), 2.81 (s, 6H), 1.58 (s, 9H). ^{13}C {^1H} NMR (75.5 MHz, $CDCl_3$): δ = 153.7, 150.3, 137.0, 136.1, 126.4, 125.3, 122.0, 119.3, 117.6, 114.1, 79.2, 45.9, 28.5. HRMS (ESI): m/z calcd for $C_{17}H_{22}N_2O_2$ (M+H)+: 287.1754, found: 287.1748.

N1,N1-Dimethylnaphthalene-1,8-diamine (**81**).

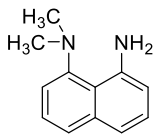

To a 50 mL round bottom flask backfilled with $N_{2(g)}$ and containing tert-butyl (8-(dimethylamino)naphthalen-1-yl)carbamate (**80**) (250 mg, 0.873 mmol) was added DCM (15 mL). To the resulting solution trifluoroacetic acid (0.67 mL, 8.73 mmol) was added in a dropwise

manner and the reaction was allowed to stir for 16 h at room temperature. The crude product was diluted with 10 mL of H_2O, neutralized with 1 M NaOH and extracted three times with 10 mL of dichloromethane. The combined organic extracts were dried over $MgSO_4$ and concentrated under reduced pressure. The purified compound was isolated using flash chromatography (11% ethyl acetate in hexanes). Compound **81** was obtained as a brown oil in a 90% yield (0.830 mmol, 154.5 mg). ^{1}H NMR (300 MHz, $CDCl_3$): δ = 7.80 – 7.70 (d, J = 7.8 Hz, 1H), 7.54 - 7.45 (m, 2H), 7.40 - 7.37 (d, J = 7.6 Hz, 1H), 7.33 - 7.30 (d, J = 7.6 Hz, 1H), 6.80 - 6.78 (d, J = 7.6 Hz, 1H), 6.33 (bs, 2H), 2.93 (s, 6H). ^{13}C {^{1}H} NMR (75.5 MHz, $CDCl_3$): δ = 152.1, 145.5, 137.0, 126.6, 125.4, 125.4, 118.7, 117.0, 115.1, 109.7, 46.2 HRMS (ESI): m/z calcd for $C_{12}H_{15}N_2$ (M+H)+: 187.1230, found: 187.1239.

8-(Pyrrolidin-1-yl)naphthale-1-amine (**82**).

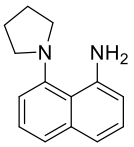

A 50 mL RBF containing Na_2CO_3 (455 mg, 4.2 mmol), fitted with a reflux condenser, was flame-dried and backfilled with N_2(g). A solution of 1,8-diaminonaphthalene (316.2 mg, 2.0 mmol) in DMF (5 mL) was then added under a nitrogen atmosphere, followed by 1,4-dibromobutane (0.24 mL, 2.0 mmol). The reaction was heated to 60 °C for 48 h. The crude reaction mixture was partitioned between H_2O (15 mL) and DCM (15 mL). The organic layer was dried over $MgSO_4$ and concentrated *in vacuo*. The product was purified by flash column chromatography (20% ethyl acetate in hexanes) to afford **20** as a dark brown oil in 24% yield (101.9 mg, 0.48 mmol). ^{1}H-NMR (300 MHz, $CDCl_3$): δ = 7.50 – 7.53 (dd, J = 9.12, 1.10 Hz, 1H), 7.14 – 7.34 (m, 4H), 6.60 – 6.63 (dd, J = 7.37, 1.17 Hz, 1H), 6.15 (bs, 2H), 3.45 – 3.49 (m, 2H), 2.80 – 2.87 (m, 2H), 2.00 – 2.04 (m, 4H). ^{13}C {^{1}H} NMR (75.5 MHz, $CDCl_3$): δ = 148.5, 137.9, 136.0, 127.1, 126.7, 125.2, 123.9, 121.0, 120.4, 120.2, 119.9, 113.4, 110.6, 56.6, 51.5, 25.0, 22.3. HRMS (EI): m/z calcd for C14H16N2 (M+): 212.1314, found: 212.1309.

tert-Butyl ((*trans*)-2-aminocyclohexyl)carbamate (**83**).[136]

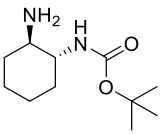

To a 50 mL RBF, flame-dried and backfilled with $N_{2(g)}$, was added 1,2-*trans*-diaminocyclohexane (0.48 mL, 4.0 mmol), and 10 mL of DCM. The reaction was cooled to 0 °C in an ice bath, and a solution of di-*tert*-butyl dicarbonate (Boc_2O, 436.5 mg, 2.0 mmol) in DCM (8 mL) was added over 2 h *via* syringe pump. The reaction was stirred for an additional 3 h at room temperature. The reaction mixture was diluted with H_2O (10 mL) acidified to pH 5 with 1 M HCl and the organic layer extracted with Et_2O (10 mL). The aqueous layer was then basified to pH 10 with 1 M NaOH and extracted three times with 10 mL EtOAc. The combined EtOAc extracts were dried over $MgSO_4$ and concentrated *in vacuo*. The product was obtained in sufficiently pure form as a white solid in 35% yield (300.0 mg, 1.4 mmol). Spectroscopic data agrees with the literature.[37] m.p. = 113 °C - 115 °C. ^{1}H-NMR (300 MHz, $CDCl_3$): δ = 4.67 (bs, 1H), 3.02 – 3.12 (m, 1H), 2.33 – 2.31 (m, 1H), 1.88 – 1.97 (m, 2H), 1.63 – 1.67 (dt, J = 9.63, 2.69 Hz, 2H), 1.40 (s, 9H), 1.04 – 1.31 (m, 6H).^{13}C {^{1}H} NMR (75.5 MHz, $CDCl_3$): δ = 157.4, 78.9, 57.1, 54.4, 33.9, 32.6, 27.9, 25.3, 25.1.

tert-Butyl ((*trans*)-2-(pyrrolidin-1-yl)cyclohexyl)carbamate (**84**).

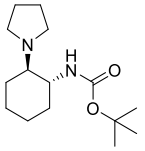

A 50 mL RBF containing Na_2CO_3 (296.8 mg, 2.8 mmol), fitted with a reflux condenser, was flame-dried and backfilled with $N_{2(g)}$. tert-Butyl ((1R,2R)-2-aminocyclohexyl)carbamate (300.0 mg, 1.4 mmol), DMF (5 mL), and 1,4-dibromobutane (0.17 mL, 1.4 mmol) were then added and the reaction was heated to 60 °C for 24 h. The crude reaction mixture was partitioned between H_2O (15 mL) and DCM (15 mL). The organic layer was dried over $MgSO_4$ and concentrated *in vacuo*. The product was purified by flash column chromatography (5% methanol in DCM) to afford **22** as an orange oil in 90% yield (338.14 mg, 1.26 mmol). ^{1}H-NMR (300 MHz, $CDCl_3$): δ = 5.22 (bs, 1H), 3.27 – 2.22 (m, 1H), 2.60 – 2.64 (m, 2H), 2.50 – 2.56 (m, 2H), 2.34 – 2.44 (m, 2H), 1.70 – 1.79 (m, 6H), 1.45 (s, 9H), 1.10 – 1.39 (m, 4H).^{13}C {^{1}H} NMR (75.5 MHz, $CDCl_3$): δ = 156.0, 78.9, 62.3, 52.1, 47.9, 32.2, 28.3, 24.2, 24.0, 23.6, 23.2.HRMS (EI): m/z calcd for $C_{15}H_{28}N_2O_2$ (M+): 268.2151, found: 268.2149.

(*trans*)-2-(Pyrrolidin-1-yl)cyclohexanamine (**85**).

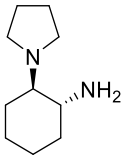

To a 50 mL round bottom flask containing tert-butyl ((trans)-2-(pyrrolidin-1-yl)cyclohexyl)carbamate (**22**) (214.7 mg, 1.12 mmol), backfilled with $N_{2(g)}$, was added was added DCM (15 mL), followed by the dropwise addition of trifluoroacetic acid (0.86 mL, 11.2 mmol). The reaction was stirred at room temperature for 16 h. The crude product was diluted with H_2O (10 mL), basified to pH 10 with 1M NaOH and extracted 3x with 10 mL DCM. The combined organic extracts were dried over $MgSO_4$ an concentrated *in vacuo*. The product was purified by flash column chromatography (11% ethyl acetate in hexanes) to afford **85** as a brown oil in a 90% yield (170.0 mg, 1.01 mmol). ^{1}H-NMR (300 MHz, $CDCl_3$): δ = 2.32–2.66 (m, 4H), 2.26 (m, 1H), 1.95 (m, 1H), 1.69–1.97 (m, 8H), 1.33 (m, 4H).^{13}C {^{1}H} NMR (75.5 MHz, $CDCl_3$): δ = 65.2, 52.8, 47.1, 35.0, 25.5, 25.0, 23.8, 21.5. HRMS (EI): m/z calcd for $C_{10}H_{20}N_2$ (M+): 168.1627, found: 168.1620.

5-(Pyrrolidin-1yl)naphthalen-1-amine (**86**).

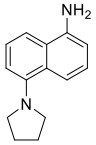

To a solution of 1,5-diaminonaphthalene (200 mg, 1.26 mmol) in dimethylformamide (20 mL) under an inert nitrogen atmosphere was added Na_2CO_3 (265 mg, 2.5 mmol) 1,4-dibromobutane (0.075 mL, 0.63 mmol). The reaction was fitted with a reflux condenser and heated to 60 °C for 16 h. The crude product was diluted with 50 mL of H_2O and extracted three times with 20 mL DCM. The combined organic extracts were dried over $MgSO_4$ and the solvent was removed under reduced pressure. The crude product was purified by flash column chromatography (33.3 % ethyl acetate in hexanes) to afford **86** as a light brown oil in 55% yield (73.8 mg, 0.35 mmol). ^{1}H-NMR (300 MHz, $CDCl_3$): δ = 7.77 (d, J = 8.67 Hz, 1H), 7.49 (d, J = 8.48 Hz, 1H), 7.41 (t, J = 7.88 Hz, 1H), 7.34 – 7.30 (m, 1H), 7.07 (dd, J = 7.46, 1.01 Hz, 1H) 6.80 (dd, J = 7.46, 0.92 Hz, 1H), 4.08 (bs, 2H), 3.40 (m, 4H) 2.07 (m, 4H).^{13}C {^{1}H} NMR (75.5 MHz, $CDCl_3$): δ =148.3, 142.4, 129.3, 125.2, 125.0, 124.8, 115.9, 114.2, 111.0, 109.8, 52.8, 24.8. HRMS (EI): m/z calcd for $C_{14}H_{16}N_2$ (M+): 212.1314, found: 212.1321.

N1-(2,3-Bis(diisopropylamino)cycloprop-2-en-1-ylidene)-N8,N8-dimethylnaphthalene-1,8-diamine hydrochloride (Janus) (**12a$_{Cl}$**).

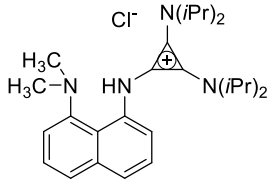

To a solution of tetrachlorocyclopropene (0.025 mL, 0.2 mmol), in dichloromethane (2 mL) was added freshly distilled diisopropylamine (0.11 mL, 0.8 mmol) in a dropwise manner under a nitrogen atmosphere. The reaction was stirred for 4 h at room temperature, after which time N1,N1-dimethylnaphthalene-1,8-diamine (**81**)(16 mg, 0.1 mmol) was added in a dropwise manner as a solution in dichloromethane (2 mL) and the reaction was stirred for an additional 8 h. The crude product was diluted with 5 mL of H_2O, quenched with 5 mL of 1 M HCl and extracted three times with 10 mL of DCM. The combined organic extracts were dried over $MgSO_4$ and the solvent removed under reduced pressure. The crude product was purified by flash column chromatography (11% methanol in DCM) to afford **12a$_{Cl}$** as an off-white solid in 90% yield (59 mg, 0.08 mmol). m.p. = 225 °C – 230 °C. ^{1}H NMR (300 MHz, $CDCl_3$): δ = 13.74 (s, 1H), 7.57–7.54 (m, 1H), 7.41–7.35 (m, 3H), 7.32–7.22 (m, 1H), 6.82-6.80 (d, J = 7.2 Hz, 1H), 3.88 – 3.79 (m, 4H), 2.66 (s, 6H), 1.25-1.23 (d, J = 6.90 Hz, 24H). ^{13}C {^{1}H} NMR (75 MHz, $CDCl_3$): δ = 149.6, 137.3, 136.0, 126.9, 126.8, 125.1, 123.8, 119.5, 118.7, 118.5, 112.7, 110.0, 51.3, 46.3, 22.1. HRMS (ESI): m/z calcd for $C_{27}H_{41}N_4$ (M+): 421.3326, found: 421.3331.

N1-(2,3-Bis(diisopropylamino)cycloprop-2-en-1-ylidene)-N8,N8-dimethylnaphthalene-1,8-diamine tetrafluoroborate (**12b$_{BF4}$**)

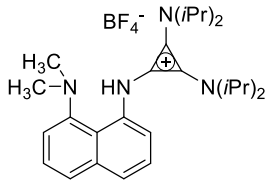

To a 10 mL round-bottom flask backfilled with $N_{2(g)}$ and containing N1-(2,3-bis(diisopropylamino)cycloprop-2-en-1-ylidene)-N8,N8-dimethylnaphthalene-1,8-diamine hydrochloride (Janus) (**12a**$_{Cl}$, 70 mg, 0.15 mmol) was added DCM (3 mL). To the resulting solution was added sodium tetrafluoroborate (33 mg, 0.30 mmol) as a solid in a single portion, and

the reaction was allowed to stir for 24 h at room temperature. The crude product was diluted with 10 mL dH_2O and extracted three times with 10 mL of dichloromethane. The combined organic extracts were dried over $MgSO_4$ and concentrated under reduced pressure. The purified compound was isolated using flash column chromatography (11% methanol in DCM) to afford **12b$_{BF4}$** as an off-white solid in 91% yield (69.5 mg, 0.14 mmol). m.p. = 152 ^oC – 153 ^oC. ^1H NMR (300 MHz, $CDCl_3$): δ = (ppm) 13.875 (s, 1H), 7.72–7.69 (m, 1H), 7.56–7.49 (m, 3H), 7.41–7.36 (m, 1H), 6.96-6.93 (d, J = 7.5 Hz, 1H), 4.00–3.96 (m, 4H), 2.80 (s, 6H), 1.39-1.37 (d, J = 6.90 Hz, 24H). ^{13}C {^1H} NMR (75.5 MHz, $CDCl_3$): δ (ppm) = 150.2, 138.0, 136.2, 126.9, 126.7, 125.3, 123.3, 119.6, 119.4, 118.8, 112.4, 110.0, 51.4, 46.4, 22.1.^{11}B {^1H} NMR (96.3 MHz, $CDCl_3$) δ (ppm) = -0.99 (s). ^{19}F {^1H} NMR (292.4 MHz, $CDCl_3$) δ (ppm) = -153.5 (s).

N1-(2,3-Bis(diisopropylamino)cycloprop-2-en-1-ylidene)-N8,N8-dimethylnaphthalene-1,8-diamine hexafluorophosphate (**12c**$_{PF6}$)

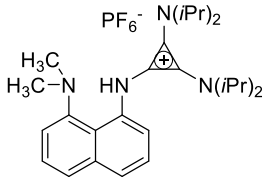

To a 10 mL round-bottom flask backfilled with $N_{2(g)}$ and containing N1-(2,3-bis(diisopropylamino)cycloprop-2-en-1-ylidene)-N8,N8-dimethylnaphthalene-1,8-diamine hydrochloride (Janus) (**12a**$_{Cl}$, 40 mg, 0.09 mmol) was added DCM (3 mL). To the resulting solution was added potassium hexafluoro borate (33 mg, 0.18 mmol) as a solid in a single portion, and the reaction was allowed to stir for 24 h at room temperature. The crude product was diluted with 10 mL dH_2O and extracted three times with 10 mL of dichloromethane. The combined organic extracts were dried over $MgSO_4$ and concentrated under reduced pressure. The purified compound was isolated using flash column chromatography (11% methanol in DCM) to afford **12c$_{PF6}$** as an off-white solid in 90% yield (46.0 mg, 0.08 mmol). m.p. = 174 ^oC – 175 ^oC. ^1H NMR (300 MHz, $CDCl_3$): δ = (ppm) 13.816 (s, 1H), 7.73–7.70 (m, 1H), 7.54–7.50 (m, 3H), 7.43–7.37 (m, 1H), 6.96-6.93 (m, 1H), 4.03–3.94 (m, 4H), 2.84 (s, 6H), 1.42-1.40 (d, J = 6.90 Hz, 24H). ^{13}C {^1H} NMR (75.5 MHz, CDCl3): δ (ppm) = 150.4, 138.3, 136.2, 126.8, 126.7, 125.3, 123.0, 120.0, 119.4, 118.9, 112.1, 109.9, 51.4, 46.4, 22.0. ^{19}F {^1H} NMR (292.4 MHz, $CDCl_3$) δ (ppm) = -71.9 – -

74.43 (d, J = 714 Hz). ^{31}P {^{1}H} NMR (121.4 MHz, $CDCl_3$) δ (ppm) = -126.9 – -162.0 (septet, J = 711 Hz).

N1-(2,3-Bis(diisopropylamino)cycloprop-2-en-1-ylidene)-N8,N8-dimethylnaphthalene-1,8-diamine tetraphenyl borate (**12d**$_{BPh4}$)

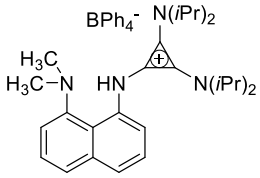

To a 10 mL round-bottom flask backfilled with $N_{2(g)}$ and containing N1-(2,3-bis(diisopropylamino)cycloprop-2-en-1-ylidene)-N8,N8-dimethylnaphthalene-1,8-diamine hydrochloride (Janus) (**12a**$_{Cl}$, 70 mg, 0.15 mmol) was added DCM (3 mL). To the resulting solution was added potassium hexafluoro borate (108 mg, 0.30 mmol) as a solid in a single portion, and the reaction was allowed to stir for 24 h at room temperature. The crude product was diluted with 10 mL dH_2O and extracted three times with 10 mL of dichloromethane. The combined organic extracts were dried over $MgSO_4$ and concentrated under reduced pressure. The purified compound was isolated using flash column chromatography (11% methanol in DCM) to afford **12d**$_{BPh4}$ as an off-white solid in 88% yield (101.2 mg, 0.14 mmol). m.p. = 184 ºC – 189 ºC. ^{1}H NMR (300 MHz, $CDCl_3$): δ = (ppm) 13.998 (s, 1H), 7.76–7.50 (m, 1H), 7.59–7.52 (m, 12H), 7.45–7.44 (m, 8H), 7.06-6.90 (m, 5H), 3.92–3.87 (m, 4H), 2.76 (s, 6H), 1.33-1.31 (d, J = 6.90 Hz, 24H). ^{13}C {^{1}H} NMR (75.5 MHz, $CDCl_3$): δ (ppm) = 149.6, 137.4, 136.3, 136.2, 127.3, 127.1, 125.4, 125.4, 125.3, 125.1, 124.1, 121.5, 119.8, 118.5, 112.5, 110.1, 51.3, 46.4, 22.1. ^{11}B {^{1}H} NMR (96.3 MHz, $CDCl_3$) δ (ppm) = -6.51 (s).

N1,N1,N2,N2-Tetraisopropyl-3-(naphthalen-1-ylimino)cycloprop-1-ene-1,2-diamine hydrochloride (**53**)

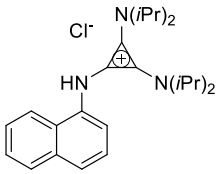

Diisopropylamine (0.11 mL, 0.8 mmol) was added to a solution of tetrachlorocyclopropene, (35.6 mg, 0.2 mmol) in dichloromethane (2 mL) under a nitrogen atmosphere . The reaction was stirred for 4 h at room temperature, after which time 1-naphthylamine (28.6 mg, 0.2 mmol) was added in a dropwise manner as a solution in dichloromethane (2 mL) and the reaction was stirred for an additional 16 h. The crude product was diluted with 5 mL of H_2O, quenched with 5 mL of 1 M HCl and extracted three times with 10 mL of DCM. The combined organic extracts were dried over $MgSO_4$ and the solvent removed under reduced pressure. The crude product was purified by flash column chromatography (11% methanol in DCM) to afford **53** as a white solid in 95% yield (21.7 mg, 0.19 mmol). m.p. = 250 °C – 255 °C. ^{1}H NMR (300 MHz, $CDCl_3$): δ = 11.58 (s, 1H), 7.99 – 7.96 (dd, J = 6.22, 1.08 Hz, 1H), 7.83 – 7.80 (m, 1H), 7.73 – 7.70 (d, 8.32 Hz, 1H), 7.60 – 7.58 (d, J = 7.14 Hz, 1H), 7.50 – 737 (m, 3H) 3.51 – 3.46 (m, 4H), 1.14 – 1.12 (d, J = 6.89 Hz, 24H).^{13}C {^{1}H} NMR (75.5 MHz, $CDCl_3$): δ = 136.0, 134.4, 130.2, 128.3, 127.3, 126.8, 126.4, 125.6, 124.2, 123.1, 116.3, 115.3, 50.8, 21.9. HRMS (EI): m/z calcd for $C_{25}H_{36}N_3$ (M+): 377.2831, found: 377.2822.

N1,N1,N2,N2-Tetraisopropyl-3-(naphthalen-1-ylimino)cycloprop-1-ene-1,2-diamine tetraphenyl borate (**58**)

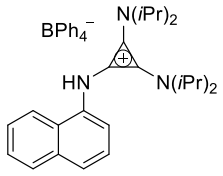

To a 25 mL round-bottom flask backfilled with $N_{2(g)}$ and containing N1,N1,N2,N2-tetraisopropyl-3-(naphthalen-1-ylimino)cycloprop-1-ene-1,2-diamine hydrochloride (**53**, 225 mg, 0.55 mmol) was added DCM (10 mL). To the resulting solution was added potassium tetrafluoro borate (280 mg, 0.71 mmol) as a solid as a single portion, and the reaction was allowed to stir for 24 h at room temperature. The crude product was diluted with 10 mL dH_2O and extracted three times with 10 mL of dichloromethane. The combined organic extracts were dried over $MgSO_4$ and concentrated under reduced pressure. The purified compound was isolated using flash column chromatography (11% methanol in DCM) to afford **58** as an off-white solid in 86% yield (330.1 mg, 0.47 mmol). m.p. = 181 °C – 182 °C. ^{1}H NMR (300 MHz, $CDCl_3$): δ = 7.97–7.94 (m, 1H), 7.89–7.87 (m, 1H), 7.69–7.66 (m, 1H), 7.60 – 7.57 (m, 2H), 7.45 – 7.37 (m, 9H), 7.04 – 7.00 (m, 9H), 6.90-6.85 (m,

4H), 6.25 (s, 1H), 3.46 – 3.37 (m, 4H), 1.06 – 1.03 (d, J = 6.90 Hz, 24H). ^{1}H NMR (300 MHz, $CDCl_3/D_2O$): δ = 7.97–7.94 (m, 1H), 7.90–7.87 (m, 1H), 7.70–7.67 (m, 1H), 7.60 – 7.57 (m, 2H), 7.46 – 7.39 (m, 9H), 7.04 – 6.99 (m, 9H), 6.89-6.84 (m, 4H), 3.47 – 3.38 (m, 4H), 1.07 – 1.05 (d, J = 6.90 Hz, 24H). ^{13}C {^{1}H} NMR (75.5 MHz, $CDCl_3$): δ = 136.3, 134.3, 133.1, 129.9, 129.0, 127.9, 127.2, 125.7, 125.6, 125.5, 125.4, 121.6, 121.3, 115.2, 113.7, 50.9, 21.9. ^{11}B {^{1}H} NMR (96.3 MHz, $CDCl_3$) δ (ppm) = -6.51 (s).

tert-Butyl (8-aminonaphthalen-1-yl)carbamate (**66**)[141]

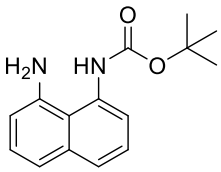

To a flame dried 100 mL round bottom flask backfilled with $N_{2(g)}$ was added 1,8-diaminonaphthalene (2.0 g, 12.6 mmol), followed by THF (40 mL) and NEt_3 (2 mL, 27.2 mmol). To the same RBF was added a solution of di-*tert*-butyl-dicarbonate (3.0 g, 13.9 mmol) in THF (10 mL) in a dropwise manner over 2 h *via* syringe pump and allowed to stir at room temperature for 18 h. THF was removed under reduced pressure and the crude product mixture was dissolved in toluene (20 mL), washed sequentially with 1 M NaOH (20 mL), brine (20 mL), and distilled H_2O (20 mL). The organic layer was subsequently dried over $MgSO_4$ and concentrated under reduced pressure. After purification by flash column chromatography (20% ethyl acetate in hexanes), the final product was isolated as red crystals in 84% yield (2.73 g, 10.6 mmol). Spectroscopic data was in good agreement with the literature.[140141] ^{1}H NMR (300 MHz, $CDCl_3$): δ = 9.79 (s, 1H), 8.09 – 8.07 (d, J = 7.3 Hz, 1H), 7.51 – 7.47 (t, J = 7.7 Hz, 1H), 7.43 – 7.37 (m, 2H), 7.28 – 7.20 (t, J = 7.7, 1H), 6.80 – 6.78 (d, J = 7.2 Hz, 1H), 4.01 (s, 2H), 1.60 (s, 9H).

tert-Butyl(8-(dimethylamino)naphthalene-1-yl)carbamate (**80**)

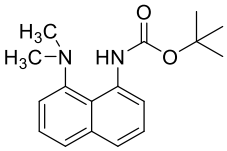

Na_2CO_3 (210 mg, 2.51 mmol) was added to a 100 mL round bottom flask fitted with a reflux condenser, flame-dried, and backfilled with $N_{2(g)}$ and containing tert-butyl (8-aminonaphthalen-1-yl)carbamate (**66**) (100 mg, 0.38 mmol. Acetonitrile (10 mL) was then added, followed by the dropwise addition of freshly distilled Me_2SO_4 (0.26 mL, 2.69 mmol). The reaction mixture was heated to reflux and stirred for 16 h. The mixture was then concentrated under reduced pressure, diluted with 20 mL of H_2O, and extracted three times with 10 mL of dichloromethane. The combined organic extracts were dried over $MgSO_4$ and concentrated under reduced pressure. The purified compound was isolated using flash column chromatography (12.5% ethyl acetate in hexanes). The final product was isolated as a clear oil in 70% yield (98 mg, 3.4 mmol). ^{1}H NMR (300 MHz, $CDCl_3$): δ = 12.79 (s, 1H), 8.36-8.33 (dd, J = 7.0, 2.3 Hz, 1H), 7.64 – 7.61 (d, J = 8 Hz, 1H), 7.48-7.31 (m, 4H), 2.82 (s, 6H), 1.58 (s, 9H). ^{13}C {^{1}H} NMR (75.5 MHz, $CDCl_3$): δ = 153.8, 150.3, 137.0, 136.1, 126.5, 125.3, 122.0, 119.3, 117.6, 114.2, 79.2, 45.9, 28.5. HRMS (ESI): m/z calcd for $C_{17}H_{22}N_2O_2$ (M+H)+: 287.1754, found: 287.1748.

N1,N1-Dimethylnaphthalene-1,8-diamine (**81**)

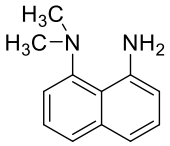

To a 50 mL round bottom flask backfilled with $N_{2(g)}$ and containing tert-butyl (8-(dimethylamino)naphthalen-1-yl)carbamate (**80**) (250 mg, 0.873 mmol) was added DCM (15 mL). Trifluoroacetic acid (0.67 mL, 8.73 mmol) was added to the reaction in a dropwise manner and the reaction was allowed to stir for 16 h at room temperature. The crude product was diluted with 10 mL of H_2O, neutralized with 1 M NaOH and extracted three times with 10 mL of dichloromethane. The combined organic extracts were dried over $MgSO_4$ and concentrated under reduced pressure. The purified compound was isolated using flash chromatography (11% ethyl acetate in hexanes). **81** was obtained as a brown oil in a 90% yield (154.5 mg, 0.830 mmol). ^{1}H NMR (300 MHz, $CDCl_3$): δ = 7.80 – 7.70 (d, J = 7.8 Hz, 1H), 7.54 - 7.45 (m, 2H), 7.40 - 7.38 (d, J = 7.6 Hz, 1H), 7.33 - 7.30 (d, J = 7.6 Hz, 1H), 6.80 - 6.77 (d, J = 7.6 Hz, 1H), 6.33 (bs, 2H), 2.93 (s, 6H). ^{13}C {^{1}H} NMR (75.5 MHz, $CDCl_3$): δ = 152.1, 145.9, 137.4, 126.9, 125.6, 125.6, 118.9,

117.1, 115.2, 109.8, 46.3. HRMS (ESI): m/z calcd for $C_{12}H_{15}N_2$ (M+H)+: 187.1230, found: 187.1239.

2-Chloro-1,3-dimethylimidazolium chloride (**68**)[142]

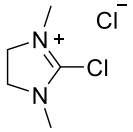

To a flame dried 50 mL round bottom flask backfilled with $N_{2(g)}$ was added 1,3-dimethylimidazolidinone (1.0 g, 8.7 mmol), followed by dry toluene (20 mL). Oxalyl chloride (1.33 g, 10.5 mmol) was then added in a dropwise manner to the stirring solution which was then heated at 70 °C for 4 h. The solvent was decanted and the final product was then washed thoroughly with ether to produce **68** as a light brown solid with 90% yield (1.3 g, 7.9 mmol). Spectroscopic data was in good agreement with the literature.[142] ^{1}H NMR (300 MHz, $CDCl_3$): δ = 4.35 (s, 4H), 3.32 (s, 6H).

tert-Butyl(8-((1,3dimethylimidazolidin-2-ylidene)amino)naphthalene-1-yl)carbamate (**69**)

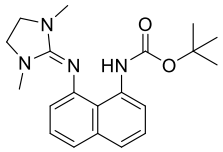

To a flame dried 100 mL round bottom flask backfilled with $N_{2(g)}$ was added **66** (1.3 g, 5.03 mmol), followed by dry DCM (40 mL). Triethylamine (0.9 mL, 6.05 mmol) was added in a dropwise manner. To the resulting mixture, freshly formed DMC salt was added in one batch (1 g, 6.05 mmol) and subsequently left to stir overnight. The solvent was removed under reduced pressure and the crude product mixture was washed thoroughly with ether and dried under vacuum. After purification by flash column chromatography (10% methanol in DCM), the final product was isolated as an off-white solid in 82% yield (3 g, 4.12 mmol). m.p. = 197 - 200 °C. ^{1}H NMR (300 MHz, $CDCl_3$): δ = 12.63 (s, 1H), 8.25 – 8.21 (dd, J = 7.3 Hz, 1H), 7.35 – 7.20 (m, 4H), 6.79 – 6.72 (m, 1H), 3.42 (s, 4H), 2.71 (s, 6H), 1.55 (s, 9H). ^{13}C {^{1}H} NMR (75.5 MHz, $CDCl_3$): δ = 156.8, 155.1, 136.0, 132.3, 130.1, 130.0, 129.4, 127.6, 126.9, 126.0, 124.9, 83.9, 79.2, 49.4, 35.2, 34.9, 28.5, 27.9. HRMS (EI): m/z calcd for $C_{15}H_{18}N_2O_2$ (M+): 258.1308, found: 258.1366.

N^1-(1,3-Dimethylimidazolidin-2-ylidene)naphthalene-1,8-diamine (**70**)

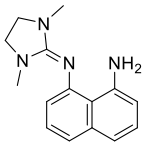

To a 200 mL round bottom flask was added **69** (3.52 g, 9.02 mmol), followed by the addition of a concentration of 3 M HCl made in a solution of ethyl acetate. The solution was stirred for 2 h. The contents of the flask were filtered and thoroughly washed with ethyl acetate giving **70** as a white solid in 98% yield (1.68 g, 9.0 mmol). m.p. = 273 - 275 °C. ^{1}H NMR (300 MHz, D_2O): δ = 7.37—7.28 (m, 4H), 6.79 – 6.77 (d, J = 7.3 Hz, 2H), 3.87 – 3.83 (t, J = 7.7 Hz, 2H), 3.36 – 3.32 (t, J = 7.7 Hz, 2H), 3.19 (s, 3H), 2.74 (s, 3H). ^{13}C {^{1}H} NMR (75.5 MHz, D_2O): δ = 157.6, 136.1, 131.5, 130.2, 128.3, 126.8, 126.5, 121.1, 107.5, 48.9, 46.5, 45.1, 37.3, 33.4, 33.4. HRMS (EI): m/z calcd for $C_{15}H_{18}N_4$ (M+): 254.1526, found: 254.1522.

1-Chloro-2,3-bis(diisopropylamino)cyclopropenium tetrafluoroborate (**72**)

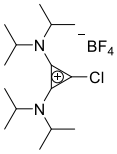

To a flame dried 50 mL round bottom flask backfilled with $N_{2(g)}$ was added tetrachlorocyclopropene (1.0 g, 5.72 mmol), followed by DCM (12 mL). The flask was subsequently cooled to 0 °C. Diisopropylamine (4.7 mL, 34.32 mmol) was added in a dropwise manner and let stir for 4 h. After 4 h sodium tetrafluoroborate (1.25 g, 11.4 mmol) was added in one fraction and the reaction was left to stir overnight. The contents were washed 5 times with 10 mL of water, and purified by recrystallization using DCM and ether. The product was isolated as clear crystals in 72% yield (1.5 g, 4.2 mmol). m.p. = 177 °C - 179 °C. ^{1}H NMR (300 MHz, $CDCl_3$): δ = 4.23—4.09 (m, 2H), 3.92 – 3.80 (m, 2H), 1.44 – 1.42 (dd, J = 6.8 Hz, 24H). ^{13}C {^{1}H} NMR (75.5 MHz, $CDCl_3$): δ = 139.1, 132.2, 93.2, 57.9, 48.2, 22.4, 20.6. ^{11}B {^{1}H} NMR (96.3 MHz, $CDCl_3$) δ (ppm) = -1.14 (s). ^{19}F {^{1}H} NMR (292.4 MHz, $CDCl_3$) δ (ppm) = -153.5 (s). HRMS (EI): m/z calcd for $C_{15}H_{28}N_2Cl$ (M+): 271.1936, found: 271.1940.

N-(2,3-Bis(diisopropylamino)cyclopropylidene)-8-((1,3-dimethylaminoimidazolidin-2-ylidene)amino)naphthalene-1-aminium tetrafluoroborate (**59**)

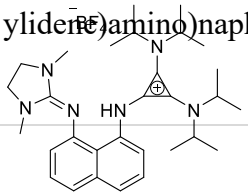

To a flame dried 25 mL round bottom flask backfilled with $N_{2(g)}$ was added **70** (100 mg, 0.34 mmol), followed by DCM (10 mL). The solution was cooled to -78 °C, and the dropwise addition of LDA was performed (0.5 mL, 1.0 mmol). Compound **72** was then added in a dropwise manner as a solution in 3 mL of DCM (122 mg, 0.34 mmol). The mixture was then warmed to room temperature and stirred overnight. The workup involved acidifying the reaction to pH 2 with 1M HCl followed by extraction using 3x10 mL of DCM. The organic layer was dried over $MgSO_4$, filtered, and concentrated under reduced pressure. The crude material was washed with ether prior to flash column chromatography (10% methanol in DCM) to yield the final product as a light brown solid in 51% yield (100 mg, 0.174 mmol). m.p. = 189 °C - 191 °C. ^{1}H NMR (300 MHz, $CDCl_3$): δ = 12.45 (s, 1H), 7.43 – 7.24 (m, 4H), 6.69 – 6.66 (d, J = 7.0 Hz, 2H), 3.97 – 3.88 (m, 4H), 3.62 – 3.47 (m, 4H), 2.74 (s, 6H), 1.38—1.36 (d, J = 6.8 Hz, 24H). ^{13}C {^{1}H} NMR (75.5 MHz, $CDCl_3$): δ = 159.8, 147.4, 139.3, 136.6, 126.9, 124.6, 123.2, 119.8, 119.4, 118.3, 116.6, 111.5, 110.7, 51.4, 48.2, 35.3, 22.1. ^{11}B {^{1}H} NMR (96.3 MHz, $CDCl_3$) δ (ppm) = -1.04 (s). ^{19}F {^{1}H} NMR (292.4 MHz, $CDCl_3$) δ (ppm) = -153.4 (s). HRMS (EI): m/z calcd for $C_{15}H_{18}N_2O_2$ (M+): 489.3706, found: 489.3687.

N1-(2,3-Bis(diisopropylamino)cycloprop-2-en-1-ylidene)-N8-(1,3-dimethylimidazolidin-2-ylidene) naphthalene-1,8-diamine (**59a**)

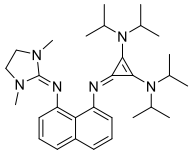

To a suspension of (**59**) (40 mg, 0.070 mmol) in toluene (2 mL) was added potassium bis(trimethylsilyl)amide (KHMDS, 0.5 M in toluene, 0.7 mL, 0.350 mmol) in a dropwise manner under a nitrogen atmosphere at 0 °C. The reaction was stirred for 2 h at room temperature, after which time volatile compounds were removed under reduced pressure. The product was extracted with hot hexanes to afford the product as yellow crystals in 94% yield (32 mg, 0.066 mmol). m.p. = 167 °C – 169 °C. ^{1}H NMR (600 MHz, $CDCl_3$): δ = 7.26–7.24 (d, J = 7.98 Hz, 2H), 7.19–7.16 (t, J = 7.5 Hz, 1H), 7.16–7.14 (t, J = 7.6 Hz, 1H), 6.83-6.82 (d, J = 6.6 Hz, 1H), 6.58-6.57 (d, J = 7.1 Hz, 1H), 3.59 – 3.53 (m, 4H), 3.21 – 3.16 (d, J = 7.9 Hz, 4H), 2.60 (s, 6H), 1.17-1.16 (d, J = 6.8

Hz, 24H). ^{13}C {^{1}H} NMR (150 MHz, $CDCl_3$): δ = 148.4, 136.9, 129.3, 125.9, 125.1, 119.6, 116.5, 50.1, 48.4, 34.9, 22.0. HRMS (EI): m/z calcd for $C_{30}H_{44}N_6$ (M+): 488.3627, found: 488.3630.

1-(2,3-Bis(diisopropylamino)cycloprop-2-en-1-ylidine)-3-(1,3-dimethyl-4,5-dihydro-1Himidazol-3-ium-2-yl)-2,2-difluoro-2,3-dihydro-1H-naphtho(1,8-de)(1,3,2)diazaborinin-1-ium-2-uide tetrafluoroborate (**64**)

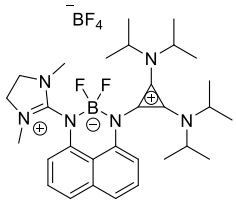

To a flame dried 25 mL round bottom flask backfilled with $N_{2(g)}$ was added **59a** (60 mg, 0.1 mmol), followed by the addition of DCM (10 mL). The reaction was subsequently placed in an ice bath. To the cooled solution was added 0.5 M KHMDS (0.25 mL, 0.12 mmol) in a dropwise manner followed by stirring for 20 min. The ice bath was removed and then boron trifluoride diethyletherate (0.1 mL, 0.20 mmol) was added in a dropwise manner and the reaction was permitted to stir overnight. DCM was removed under reduced pressure and the crude product was purified using flash column chromatography (10% methanol in DCM). The final product was isolated as a light pink solid 94% yield (58.5 mg, 0.094 mmol) mmol). m.p. = 240—241 °C. ^{1}H NMR (300 MHz, $CDCl_3$): δ = 7.47—7.33 (m, 4H), 6.68 – 6.65 (dd, J = 7.1 Hz, 1H), 6.47 – 6.45 (dd, J = 7.2 Hz, 1H), 3.99 – 3.88 (m, 8H), 2.89 (s, 6H), 1.35 — 1.33 (d, J = 6.8 Hz, 24H). ^{13}C {^{1}H} NMR (75.5 MHz, $CDCl_3$): δ = 160.2, 138.3, 137.6, 135.6, 127.2, 126.6, 126.5, 122.2, 121.3, 117.3, 114.2, 113.8, 112.7, 51.9, 48.2, 34.4, 22.0. ^{11}B {^{1}H} NMR (96.3 MHz, $CDCl_3$) δ (ppm) = 0.06 — -0.94 (m). ^{19}F {^{1}H} NMR (292.4 MHz, $CDCl_3$) δ (ppm) = -146.5—-146.9 (m), -15.41 (s). HRMS (EI): m/z calcd for $C_{15}H_{18}N_2O_2$ (M+): 537.3669, found: 537.3681.

2,3-Bis(diisopropylamino)cyclopropenium-1-phenylhydrazine tetraphenylborate salt (**79**)

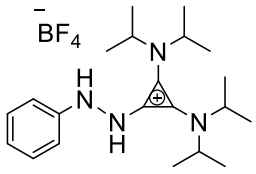

To a dried 50 mL RBF backfilled with nitrogen was added **72** (1 g, 3 mmol) as a solid. The flask was fitted with a reflux condenser, followed by the addition of 20 mL of DCM. Two equivalents

of phenylhydrazine (0.6 mL, 6 mmol) were added in a dropwise manner to the stirring solution, which was then set to reflux overnight. The mixture was removed from the heat source and allowed to cool to room temperature. The contents were gravity filtered into a 100 mL RBF. The contents were layered with 40 mL of ether and placed in the freezer to induce slow diffusion recrystallization. Compound **79** was isolated as golden crystals (0.67 g, 1.56 mmol, 52% yield). m.p. = 156 - 157 °C. ^{1}H NMR (300 MHz, $CDCl_3$): δ = 7.8 (s, 1H), 7.24 – 6.9 (m), 3.9 – 3.8 (m, 4H), 1.34 – 1.32 (d, J = 6.8 Hz, 24H). ^{13}C {^{1}H} NMR (75.5 MHz, $CDCl_3$): δ = 147.6, 129.2, 121.7, 116.3, 114.3, 114.1, 51.5, 51.0, 21.7. ^{11}B {^{1}H} NMR (96.3 MHz, $CDCl_3$) δ (ppm) = -0.95 (s). ^{19}F {^{1}H} NMR (292.4 MHz, $CDCl_3$) δ (ppm) = -152.7 (s). HRMS (EI): m/z calcd for $C_{21}H_{35}N_4BF_4$ (M+): 343.5312, found: 343.5129.

2,3-Bis(diisopropylamino)cyclopropenium-1-azobenzene (**73**)

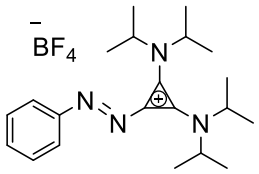

Compound **79** (0.67 g, 1.56 mmol) was added to a dry 50 mL RBF backfilled with nitrogen containing NBS (0.277 g, 1.56 mmol), and the flask was wrapped in foil. DCM (20 mL) was added followed by pyridine (0.13 mL, 1.56 mmol). Contents were stirred overnight. Contents were washed with 15 mL of water, separate the organic layer and dry over $MgSO_4$ and concentrated in vacuo. The product was recrystallized from DCM and ether mixtures affording **73** as a vibrant orange solid (0.474 g, 1.11 mmol, 71% yield). m.p. = 193 - 194 °C. ^{1}H NMR (300 MHz, $CDCl_3$): δ = 7.92—7.89 (m, 2H), 7.65 – 7.54 (m), 4.37 – 4.28 (m, 2H), 4.06 – 3.96 (m, 2H), 1.55 — 1.48 (d, J = 6.8 Hz, 24H). ^{13}C {^{1}H} NMR (75.5 MHz, $CDCl_3$): δ = 153.1, 134.4, 129.6, 127.6, 123.6, 110.1, 58.6, 49.4, 21.3, 20.7. ^{11}B {^{1}H} NMR (96.3 MHz, $CDCl_3$) δ (ppm) = -1.04 (s). ^{19}F {^{1}H} NMR (292.4 MHz, $CDCl_3$) δ (ppm) = -153.6 (s). HRMS (EI): m/z calcd for $C_{21}H_{33}N_4BF_4$ (M+): 341.5141, found: 341.5298.

Appendix A: Spectral Data

Proton NMR

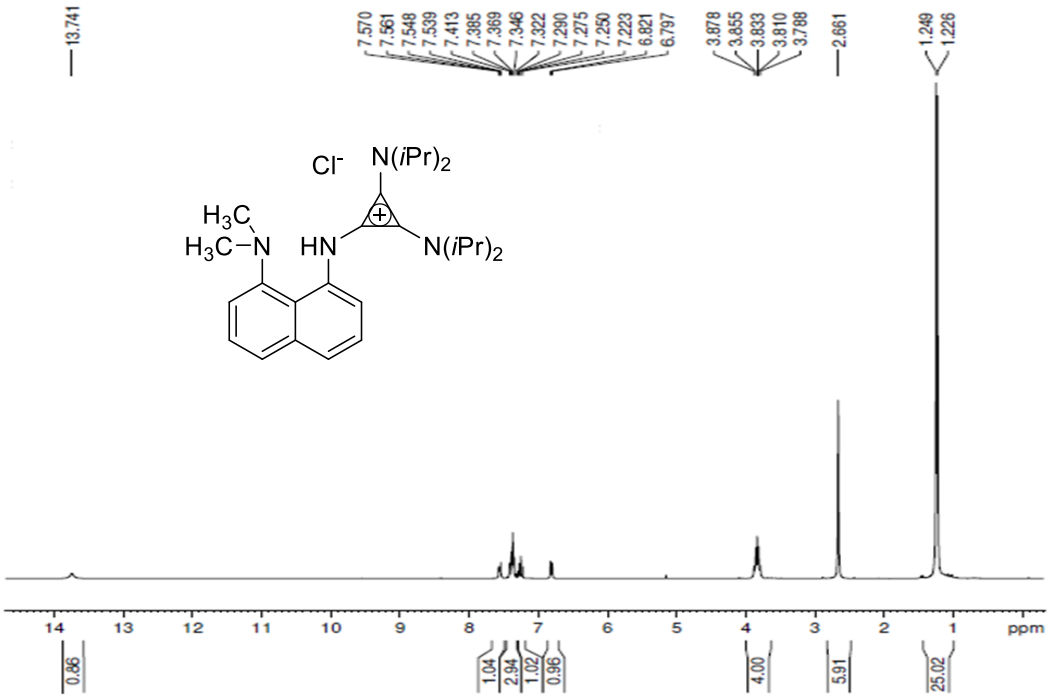

Carbon-13 NMR

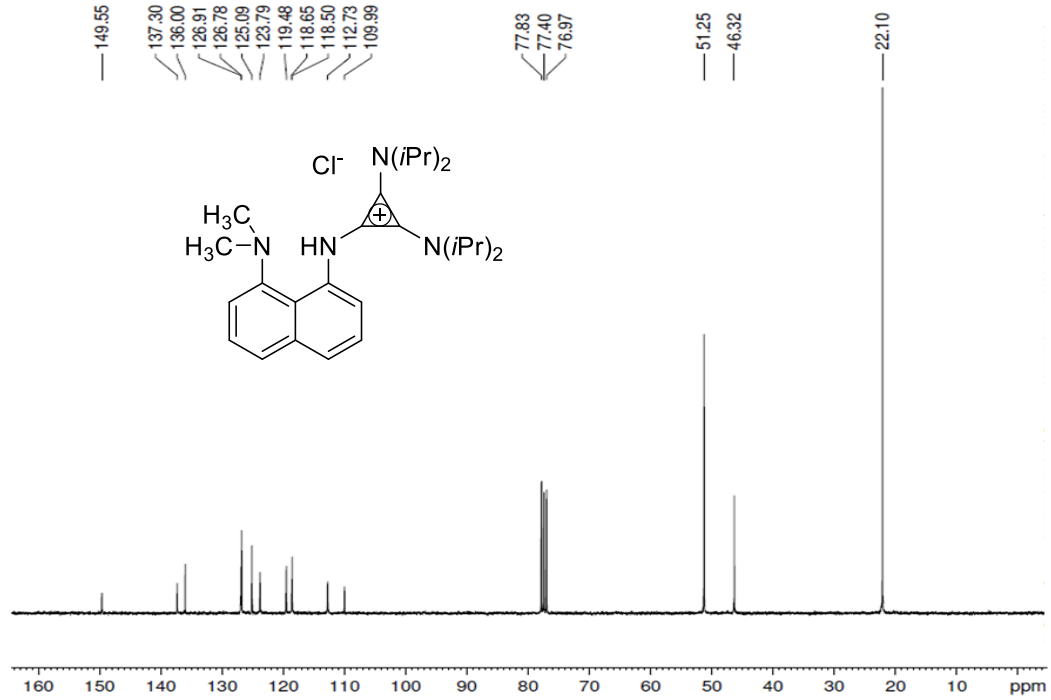

Proton NMR

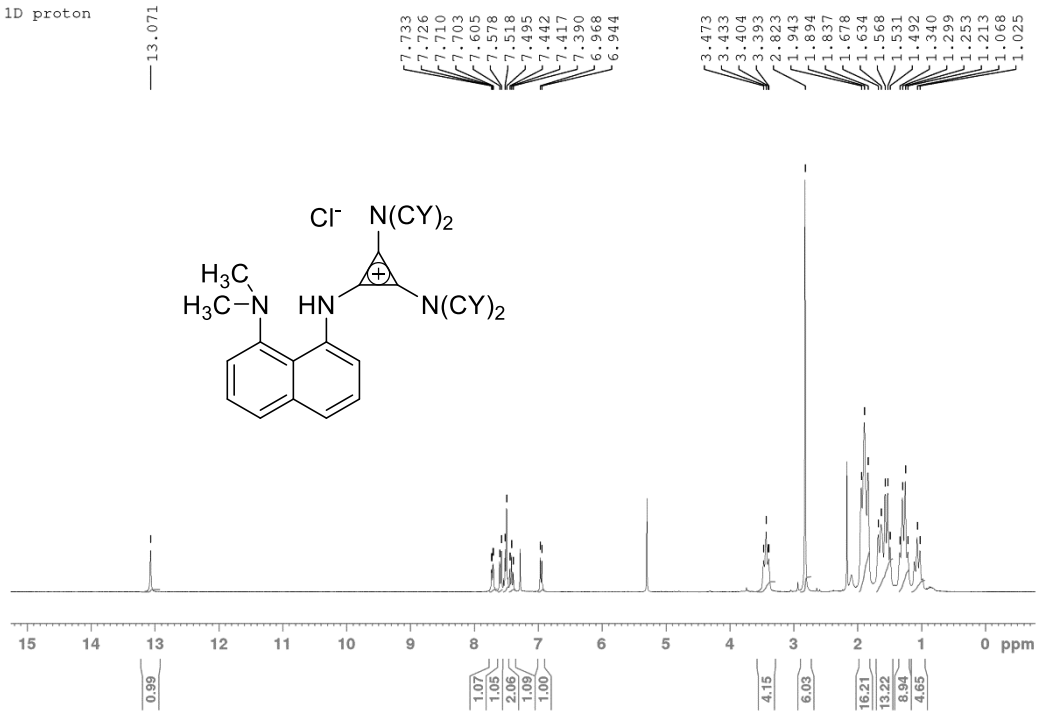

Carbon-13 NMR

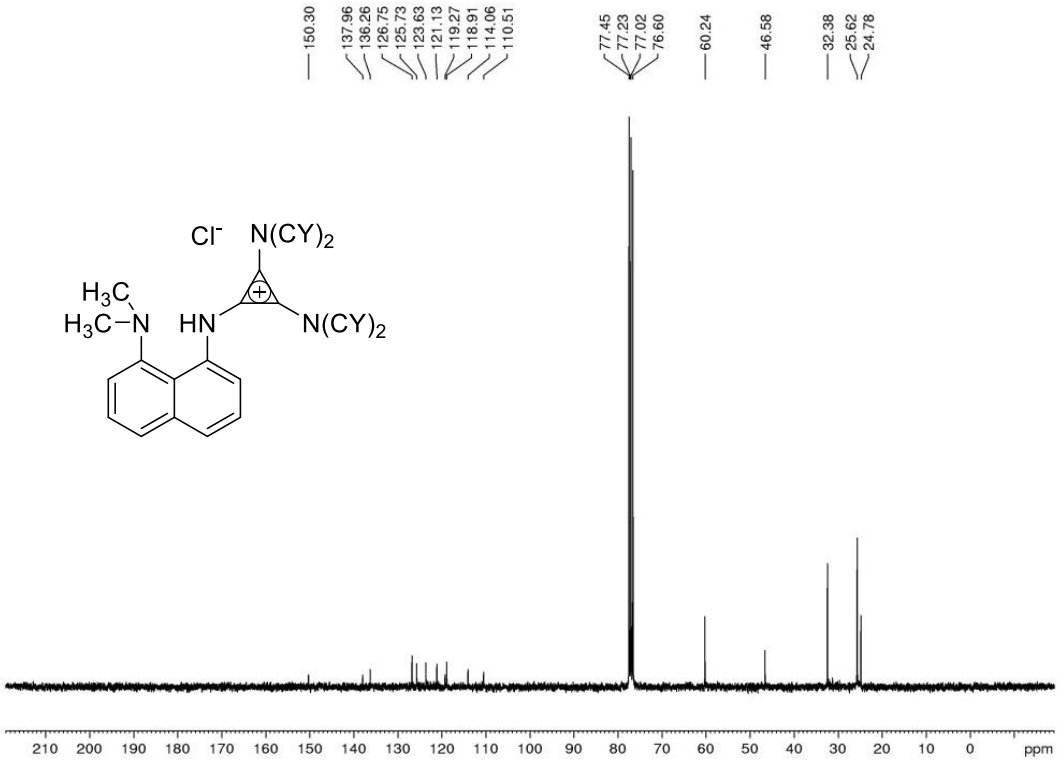

Proton NMR

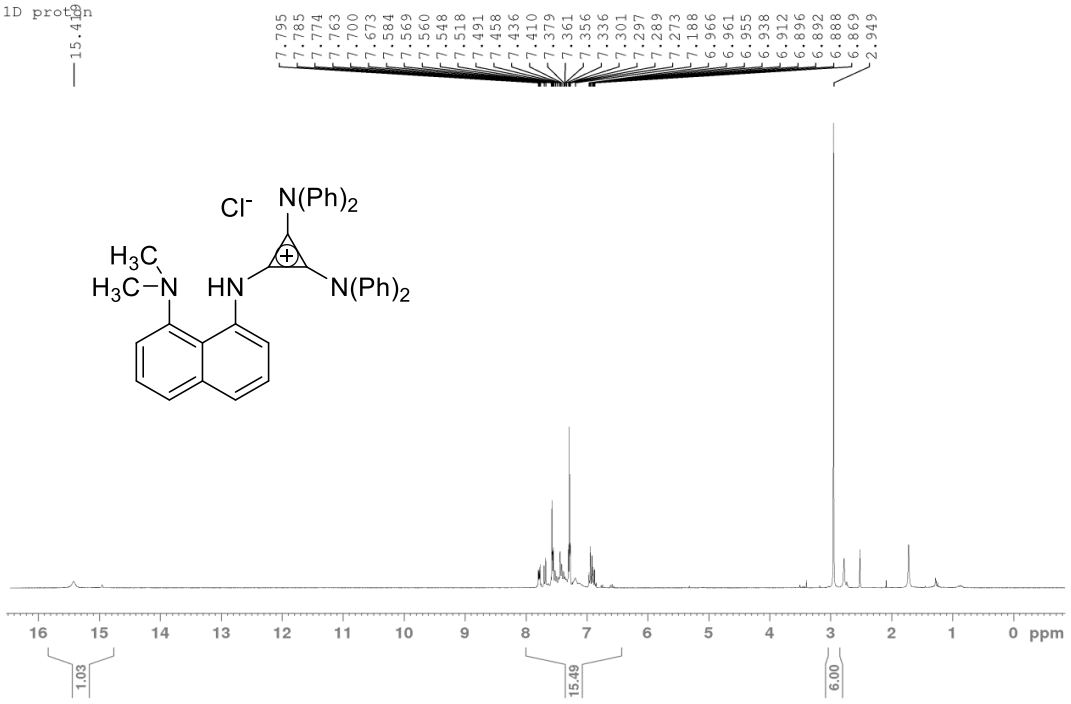

Carbon-13 NMR

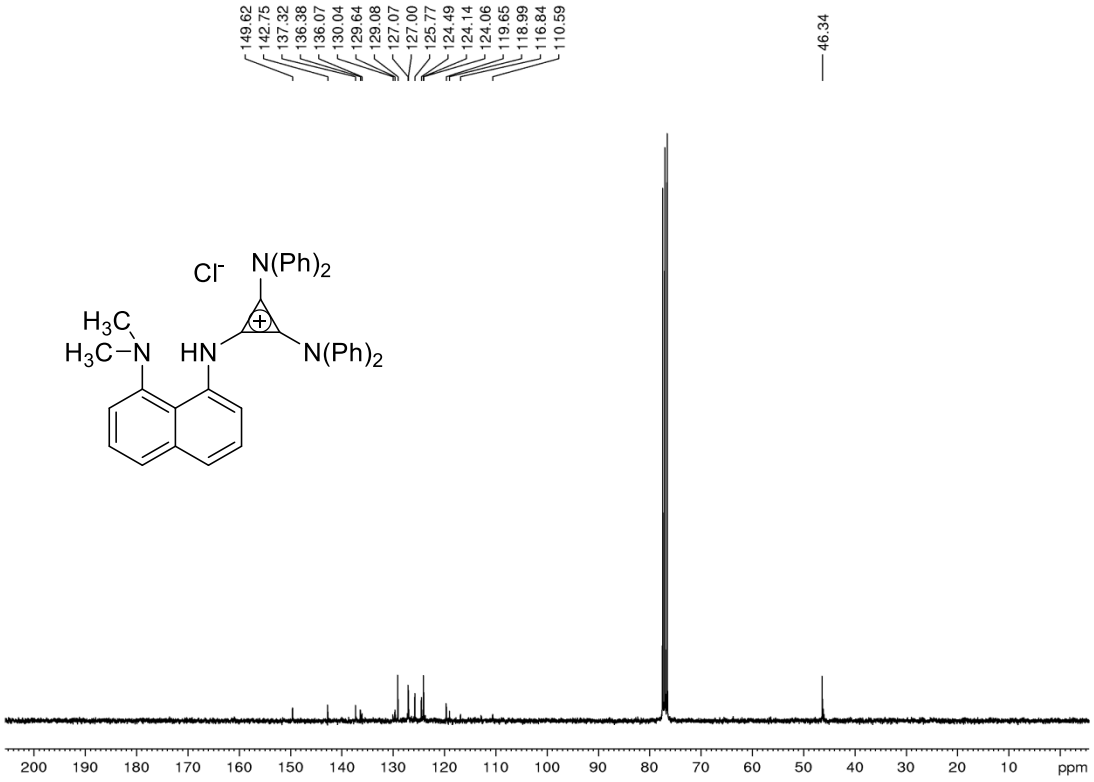

Proton NMR

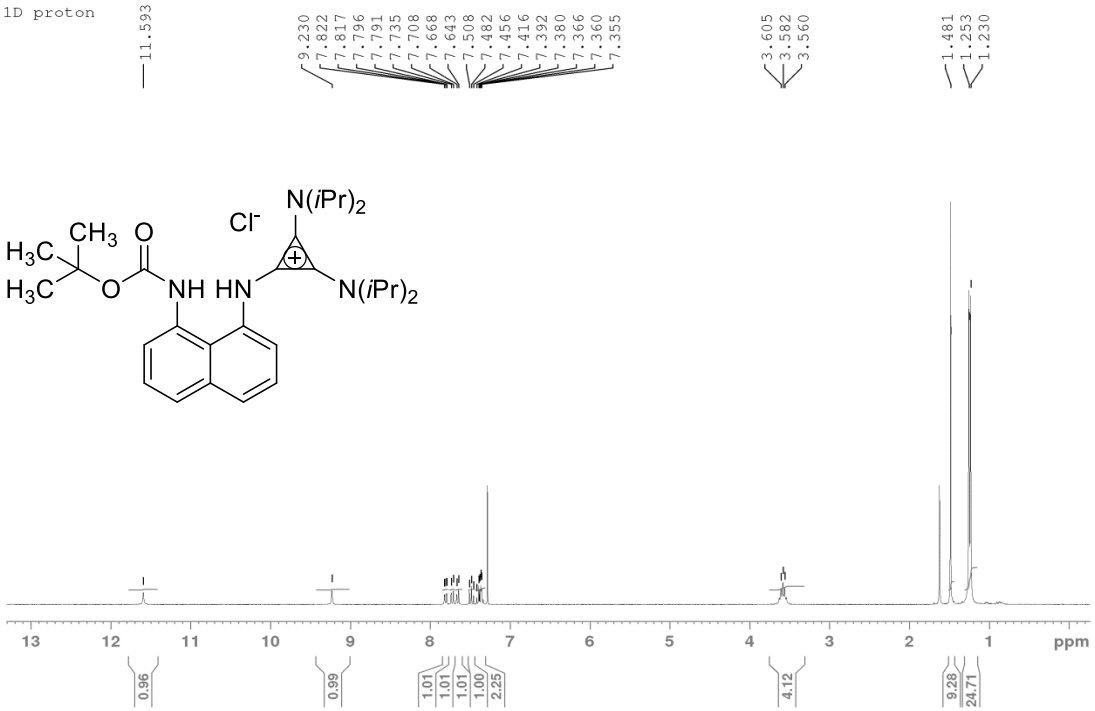

Carbon-13 NMR

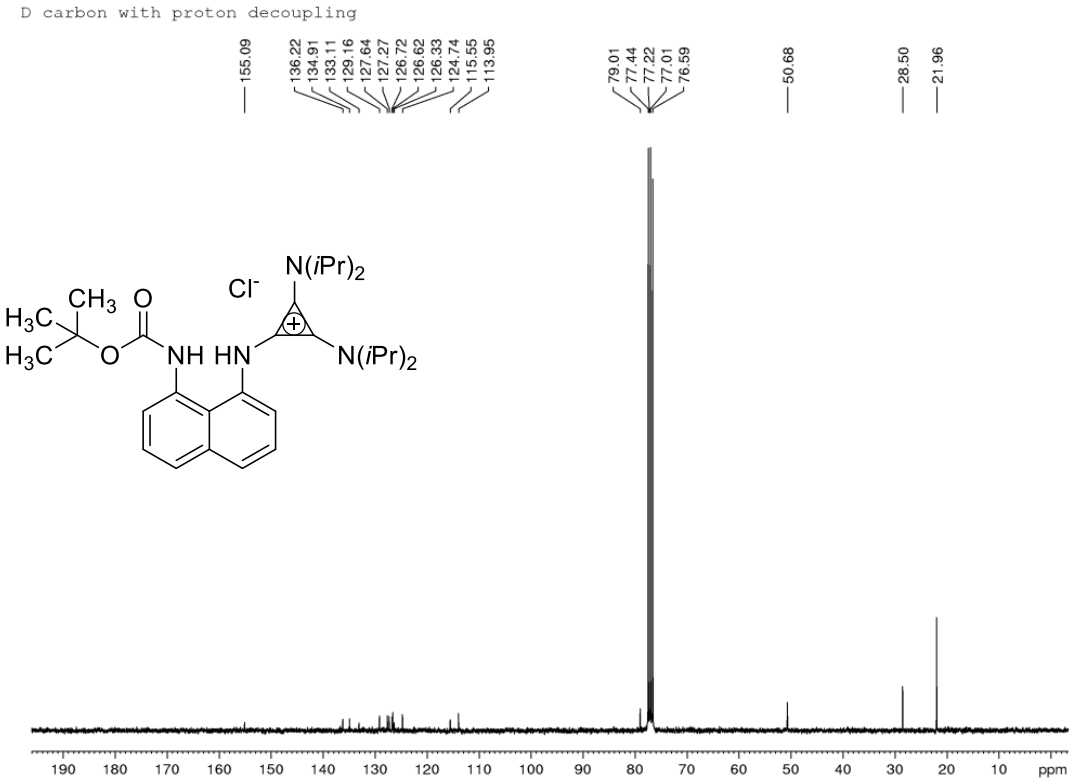

Proton NMR

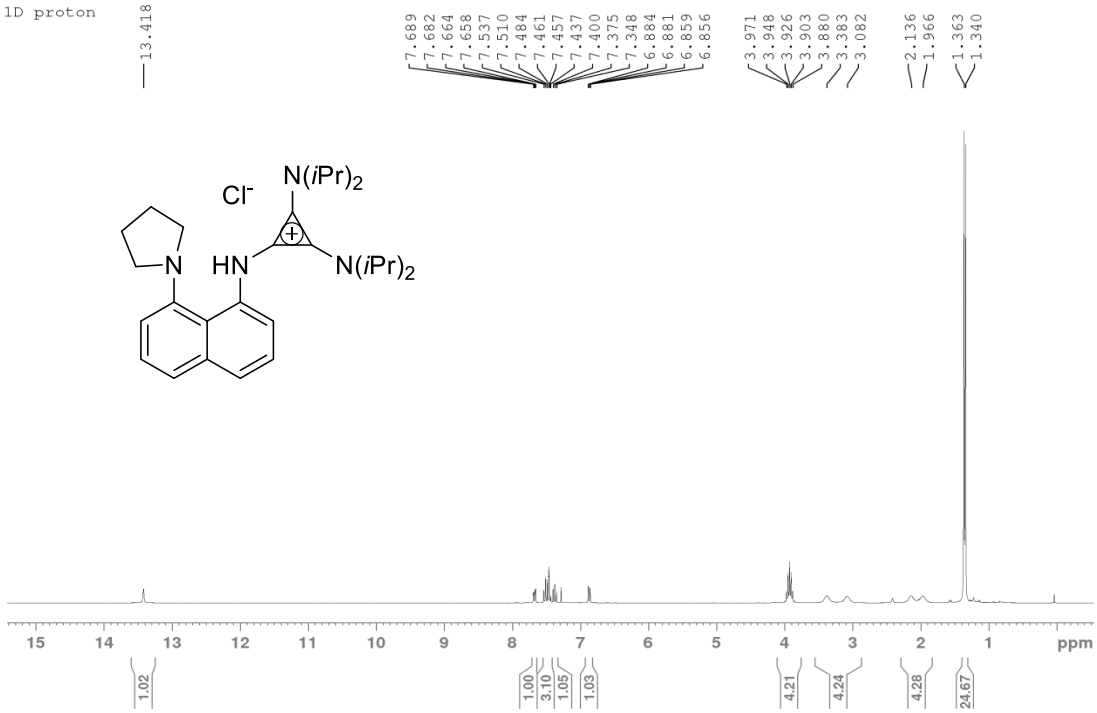

Carbon-13 NMR

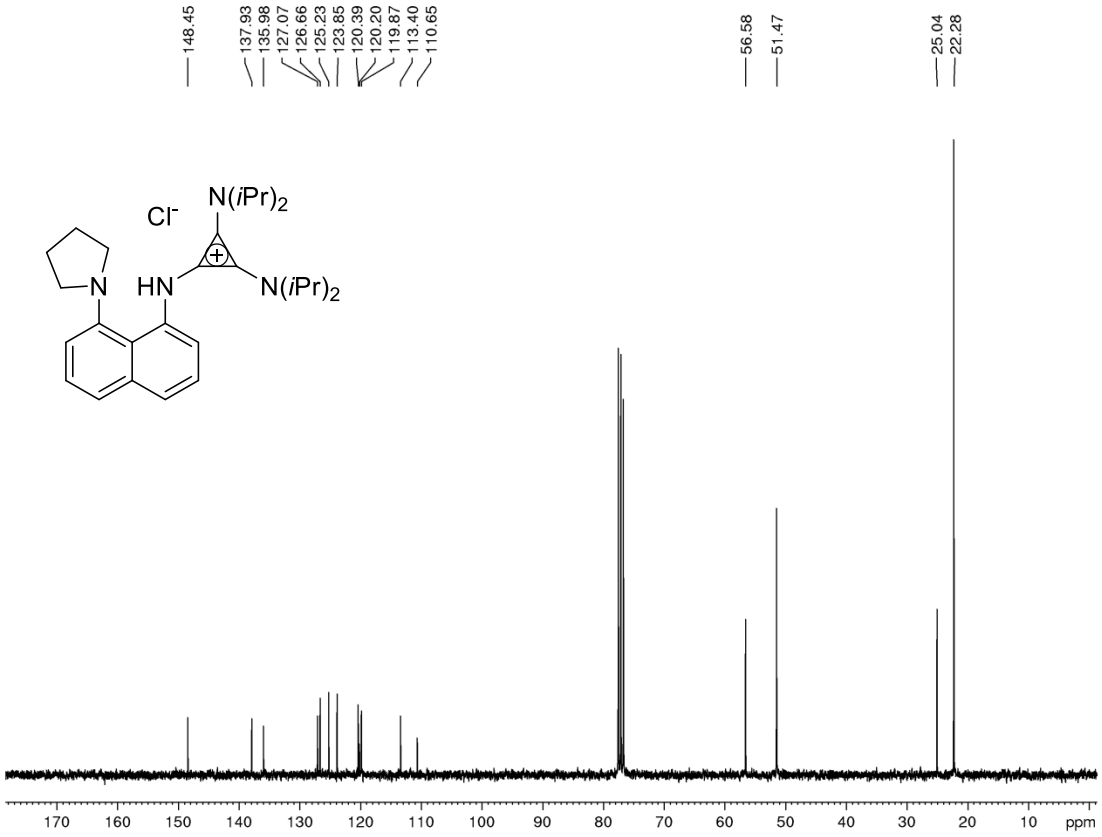

Proton NMR

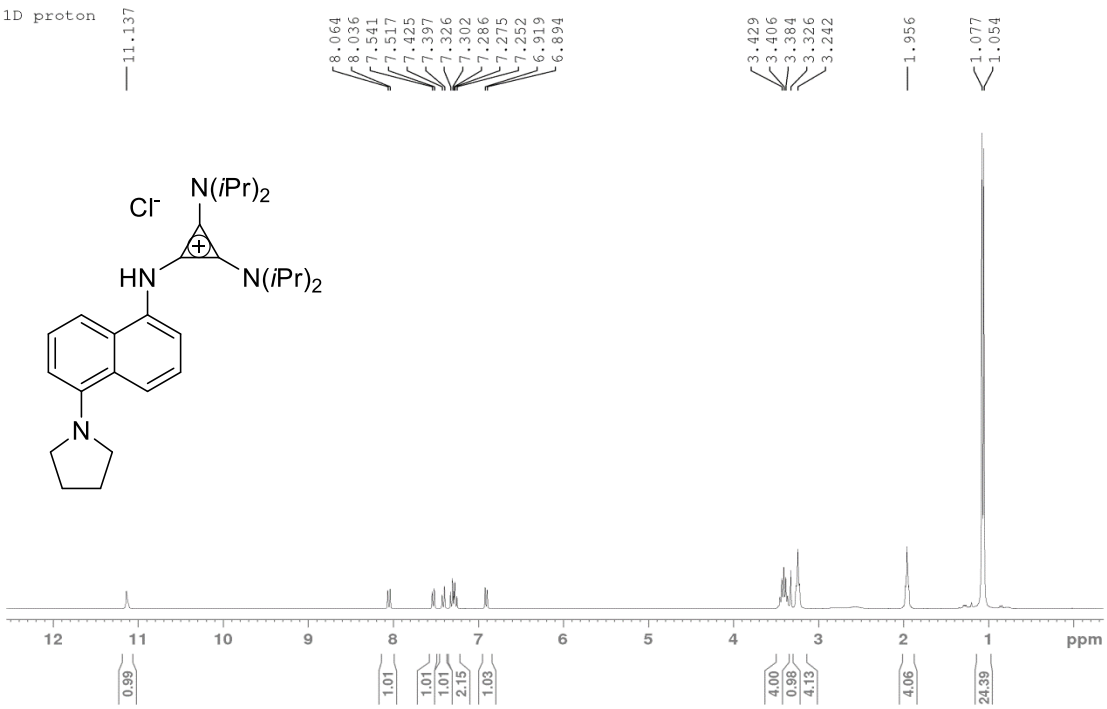

Carbon-13 NMR

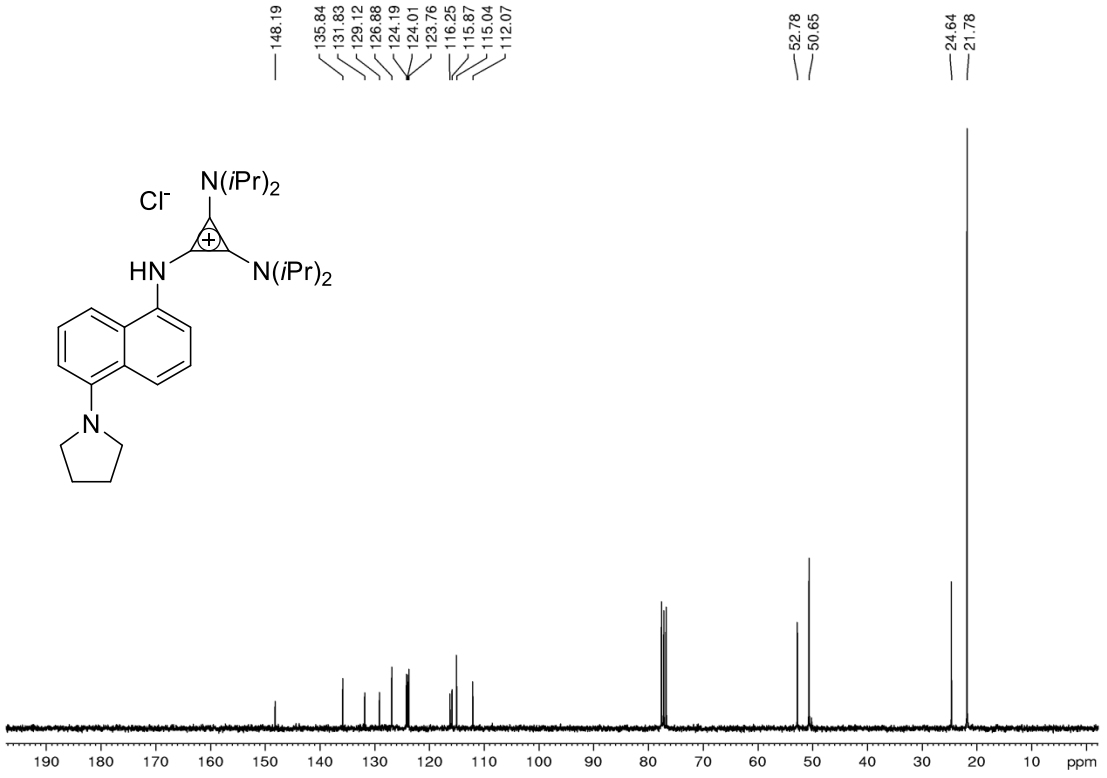

Proton NMR

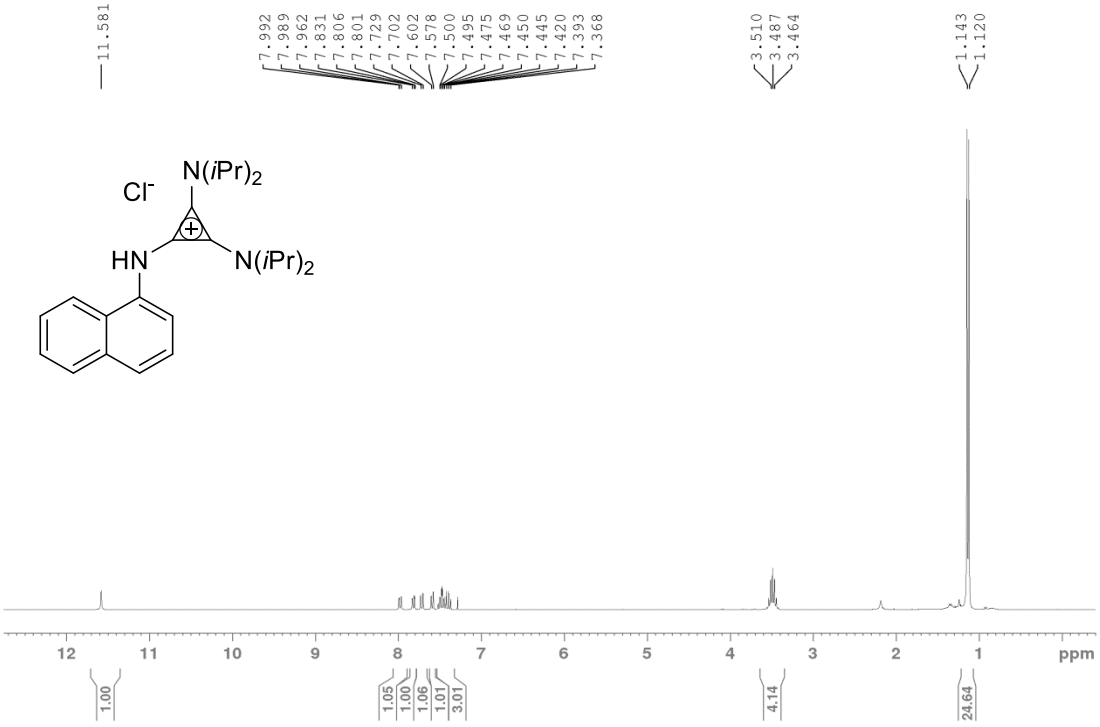

Carbon-13 NMR

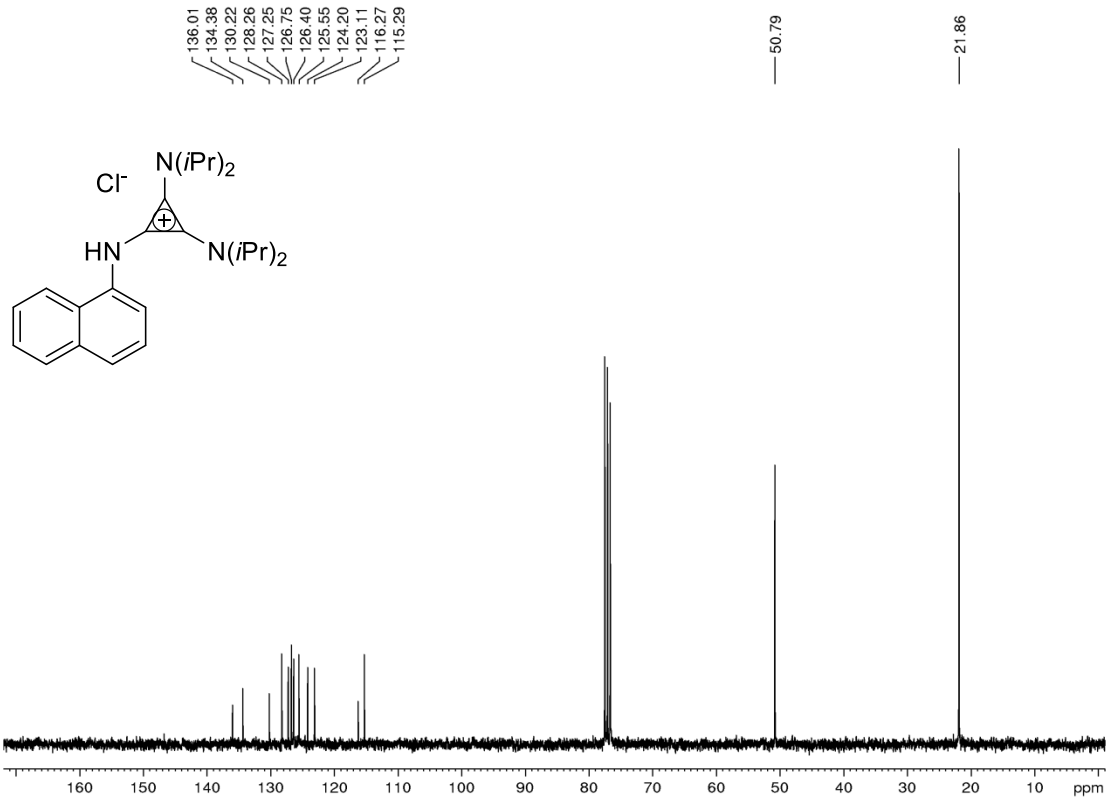

Proton NMR

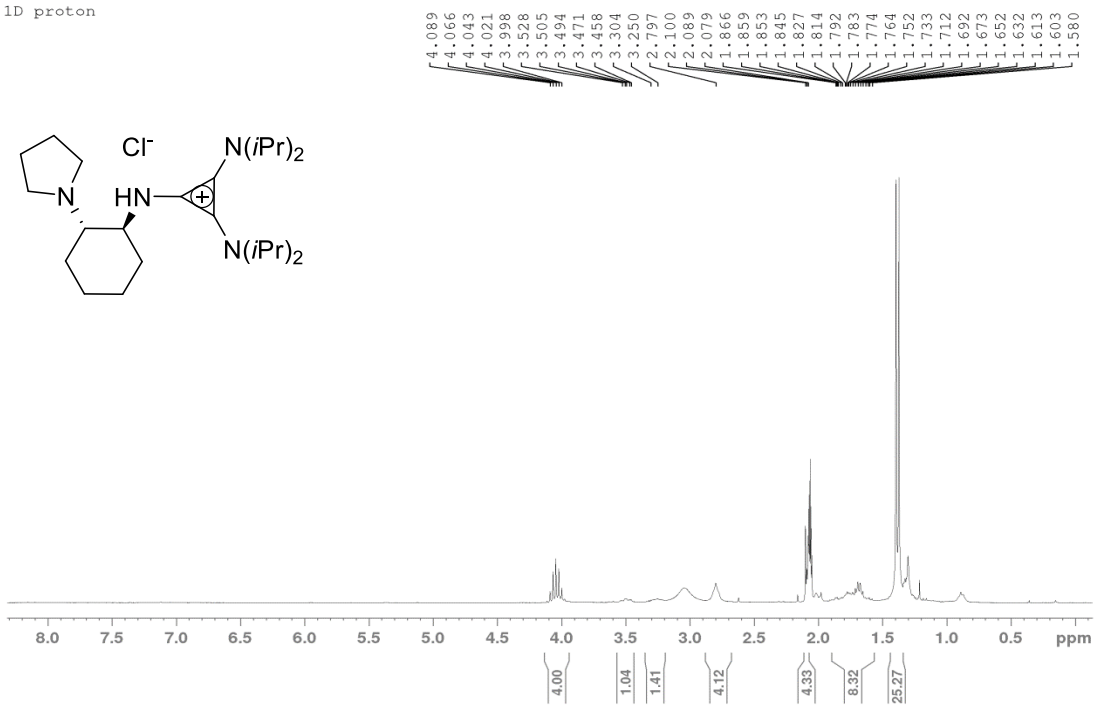

Carbon-13 NMR

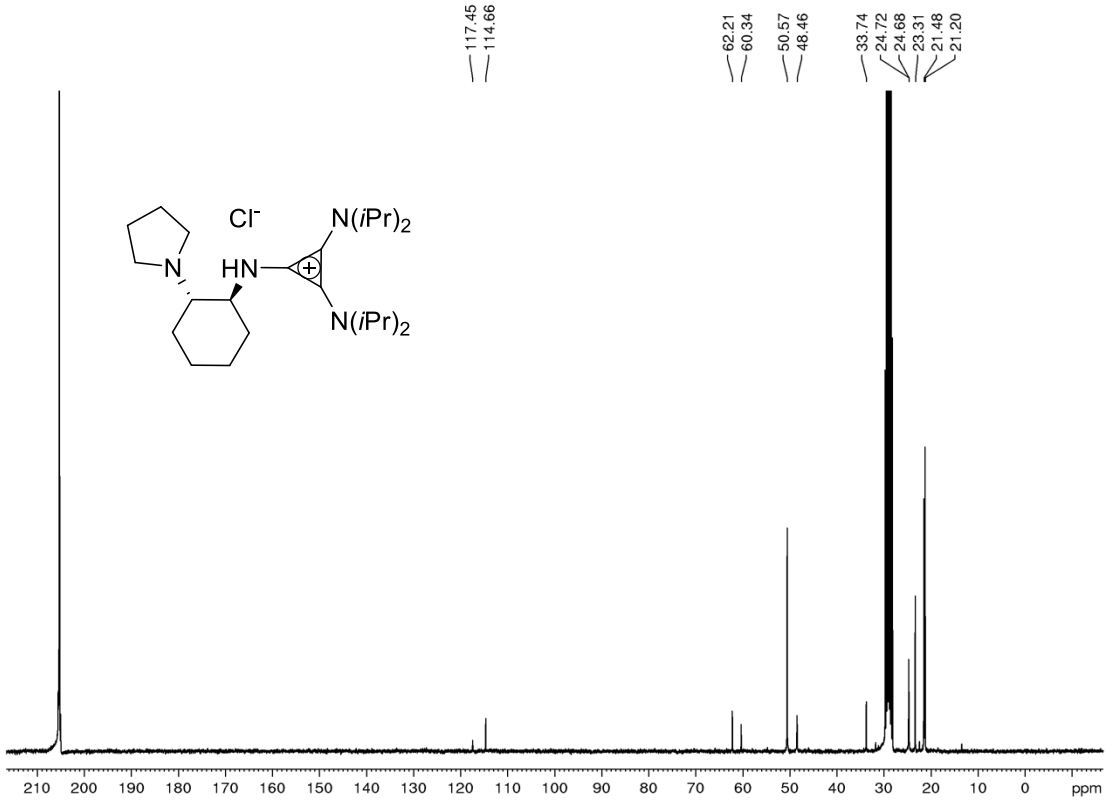

Proton NMR

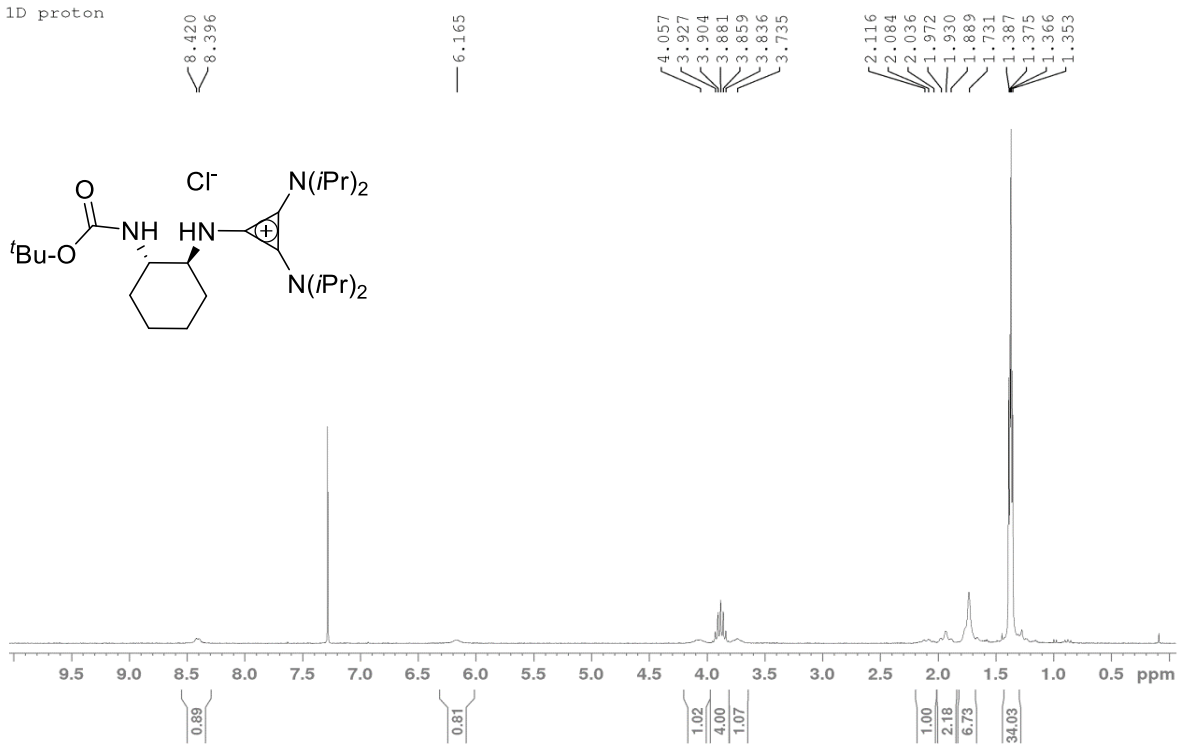

Carbon-13 NMR

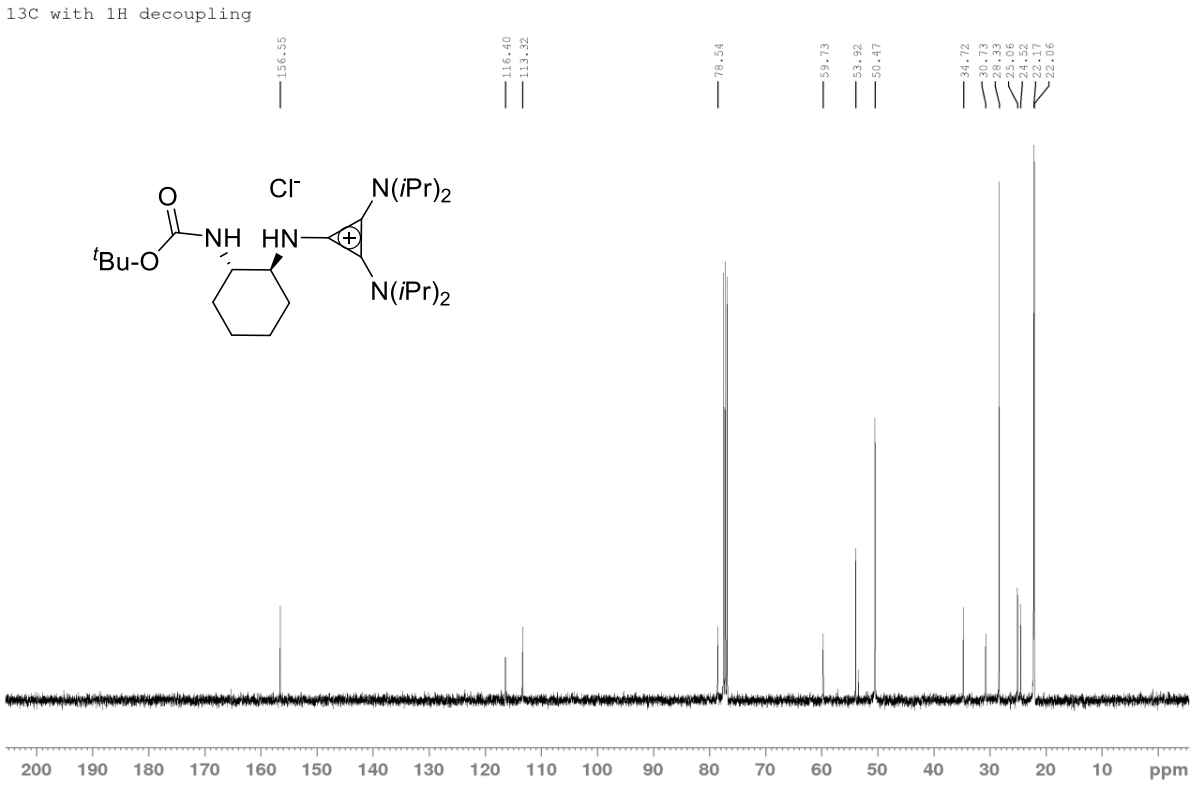

Proton NMR

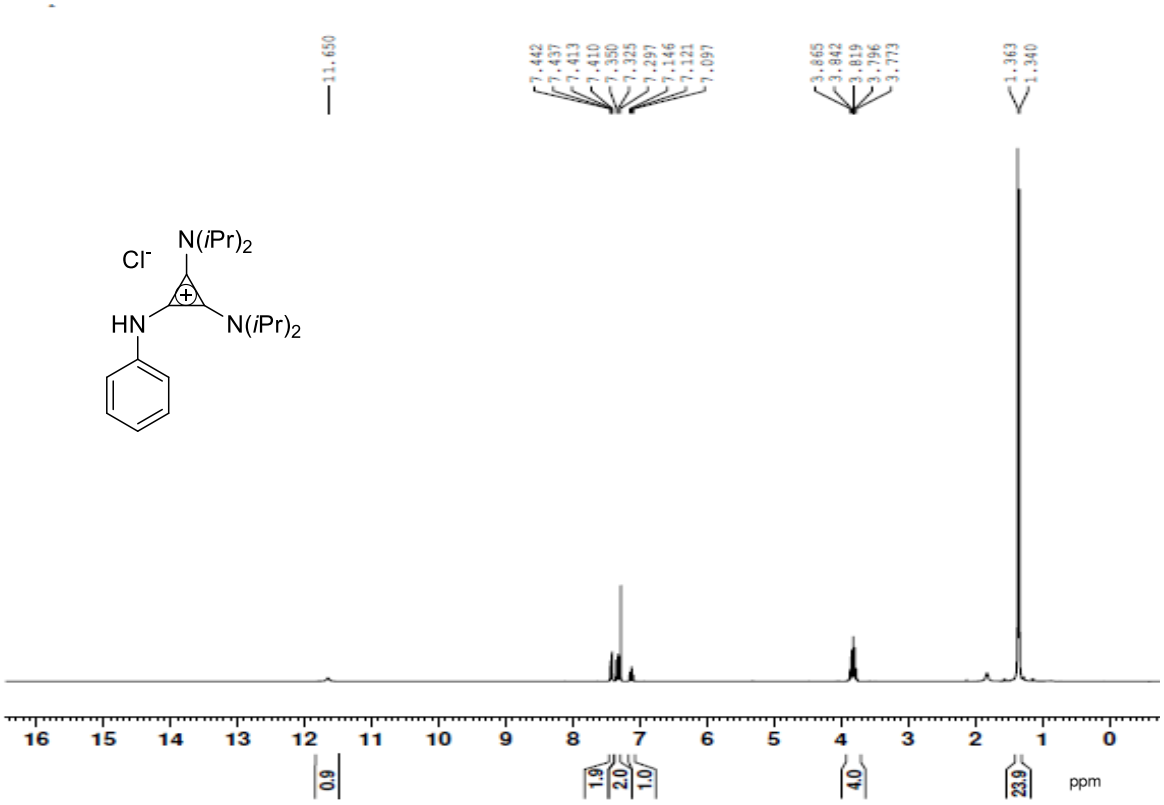

Proton NMR

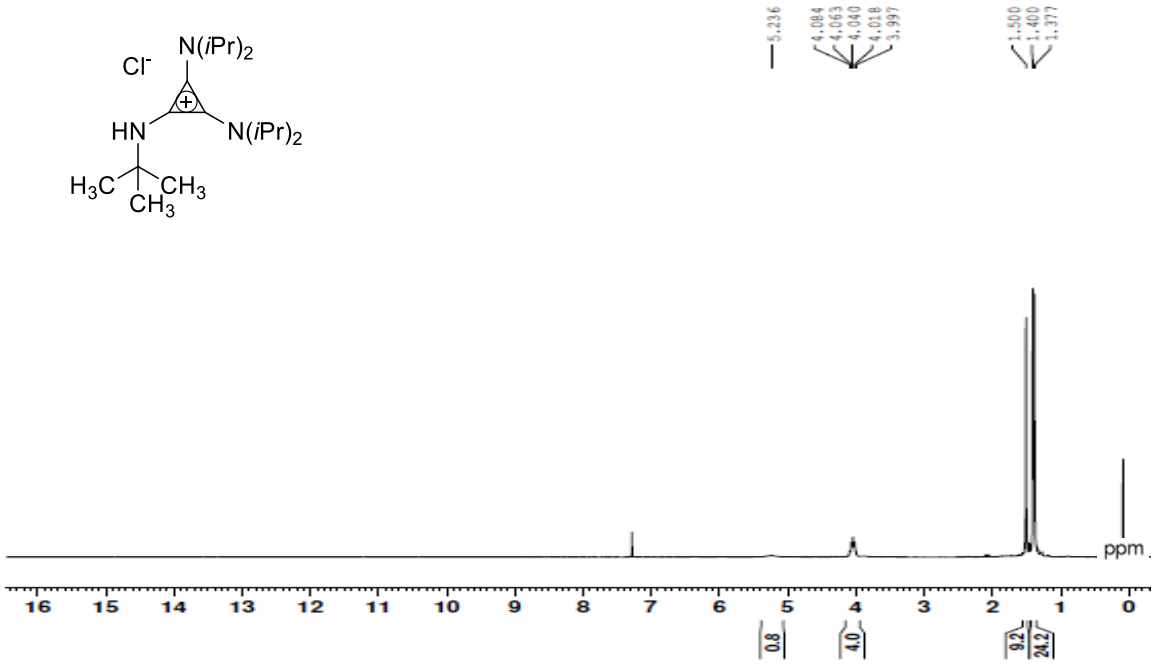

Proton NMR

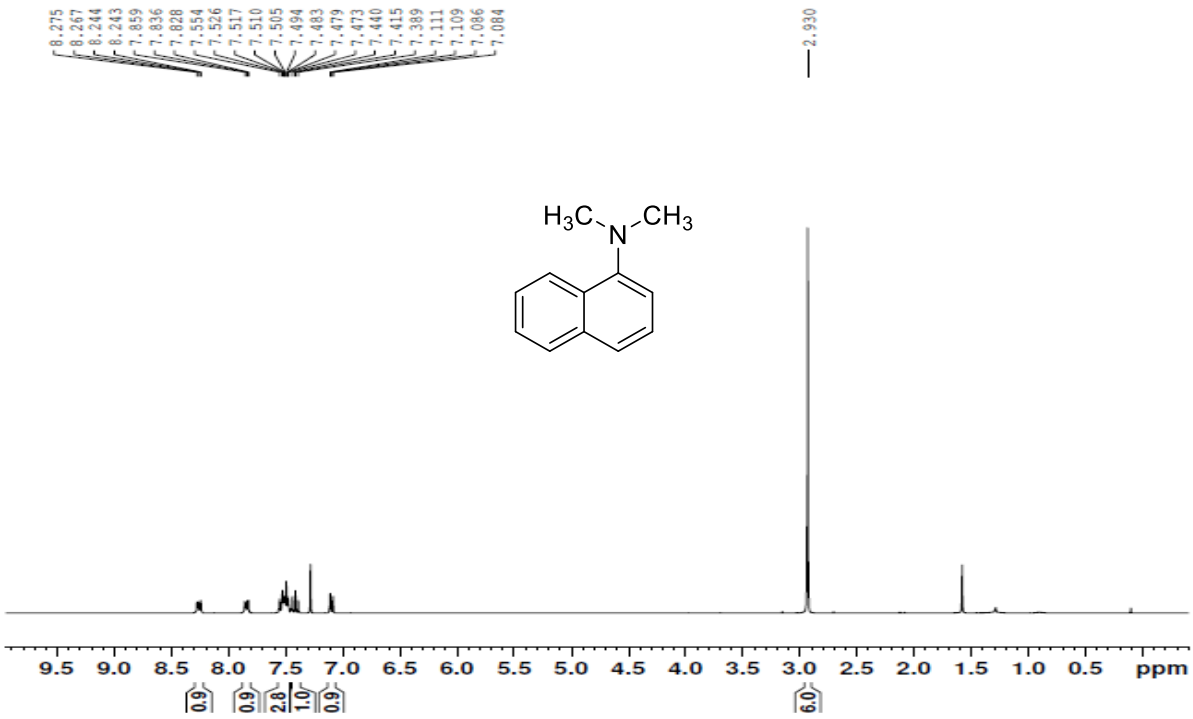

Proton NMR

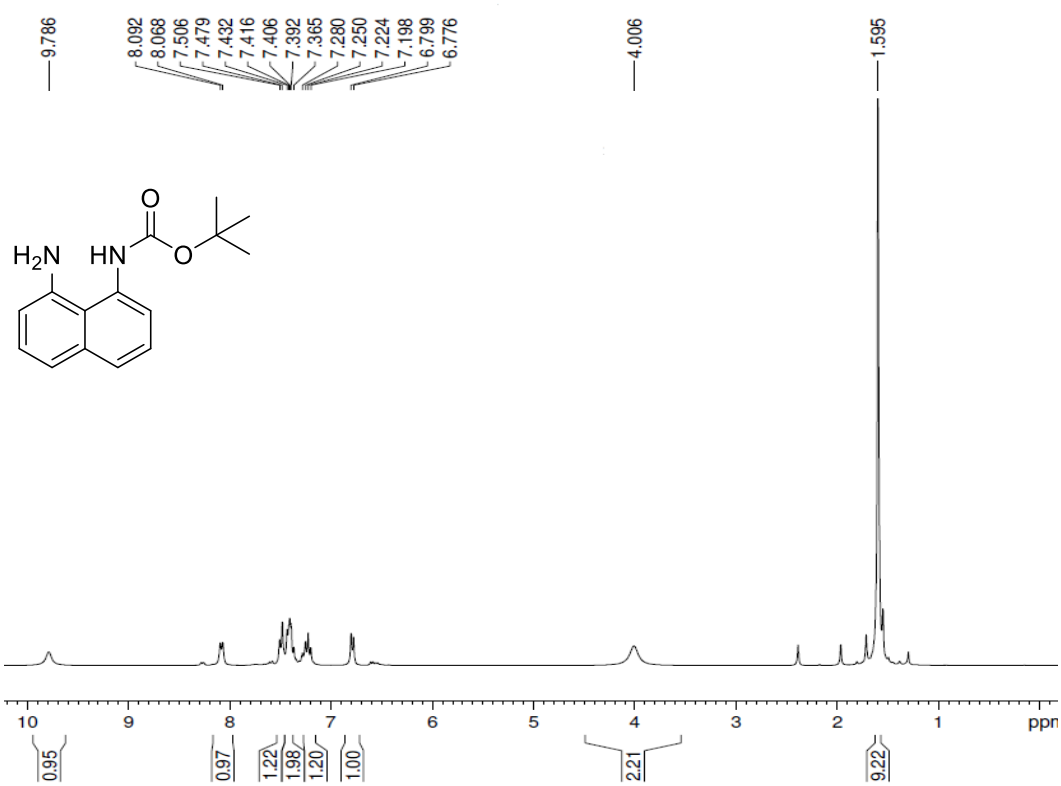

Carbon-13 NMR

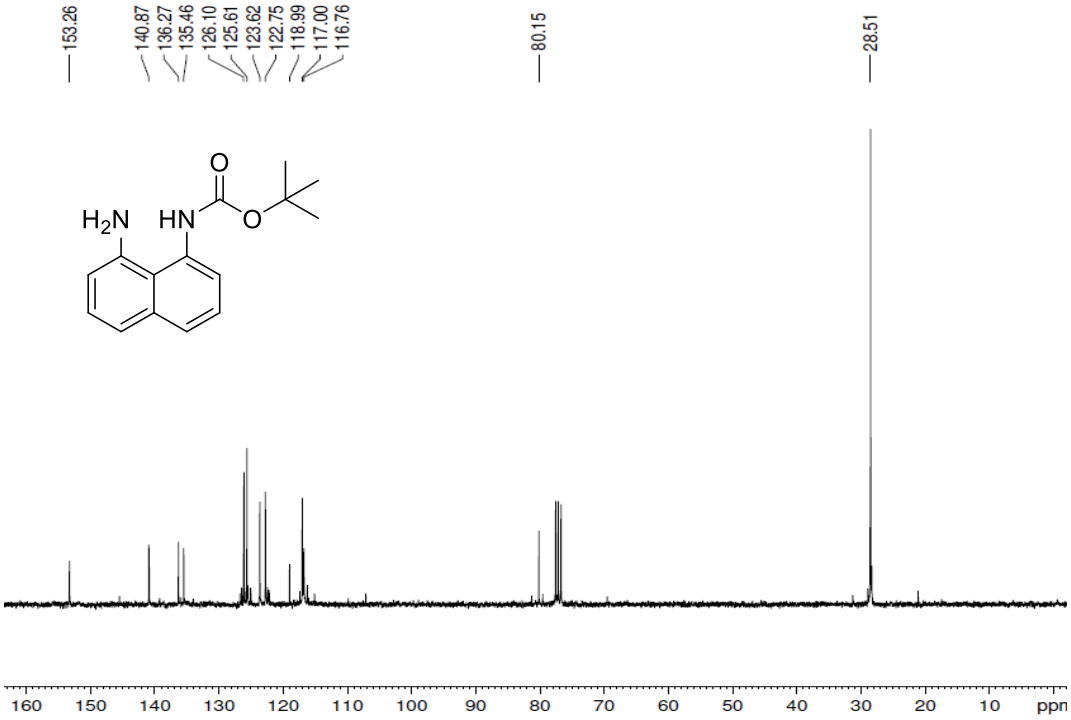

Proton NMR

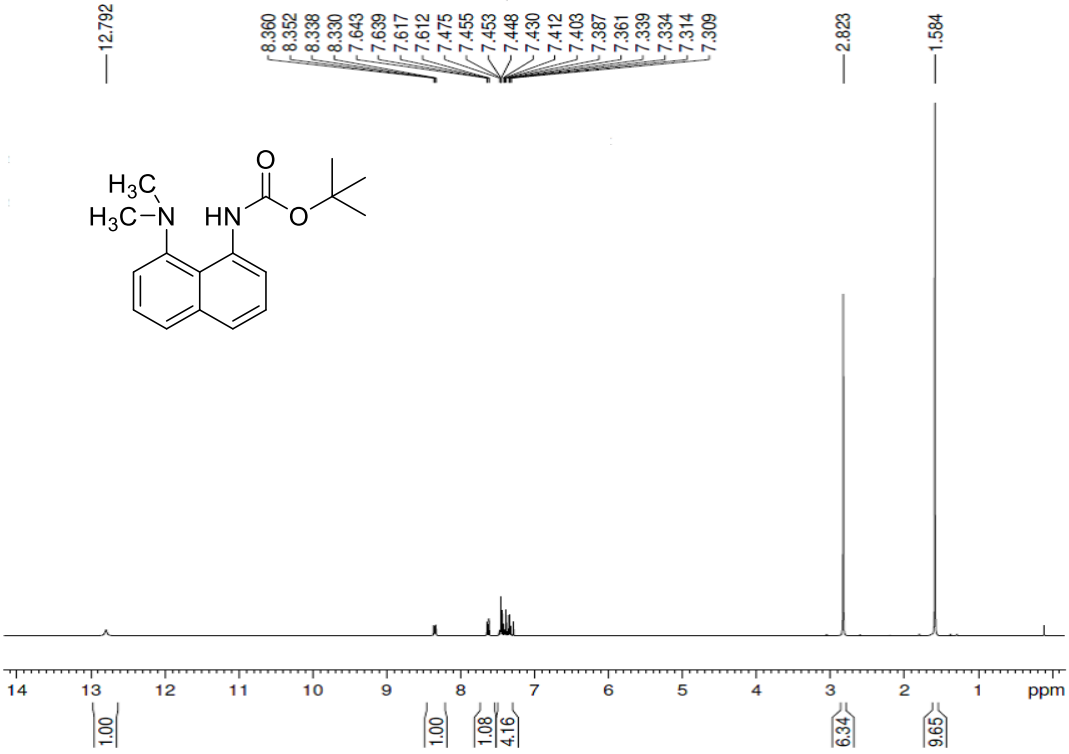

Carbon-13 NMR

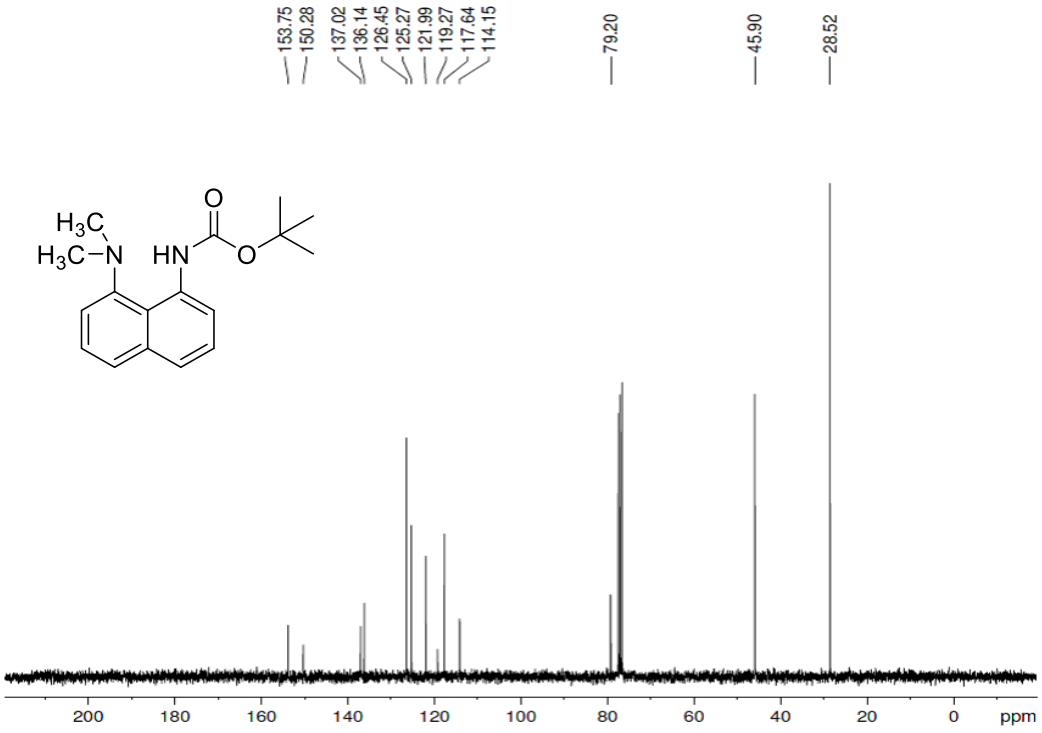

Proton NMR

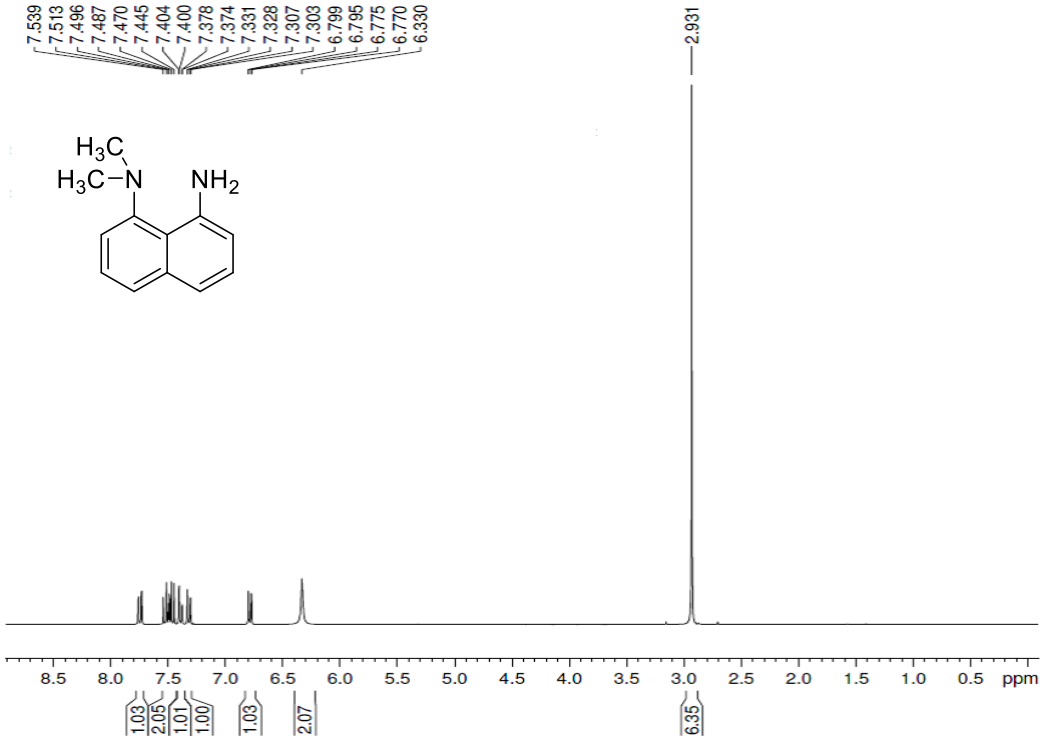

Carbon-13 NMR

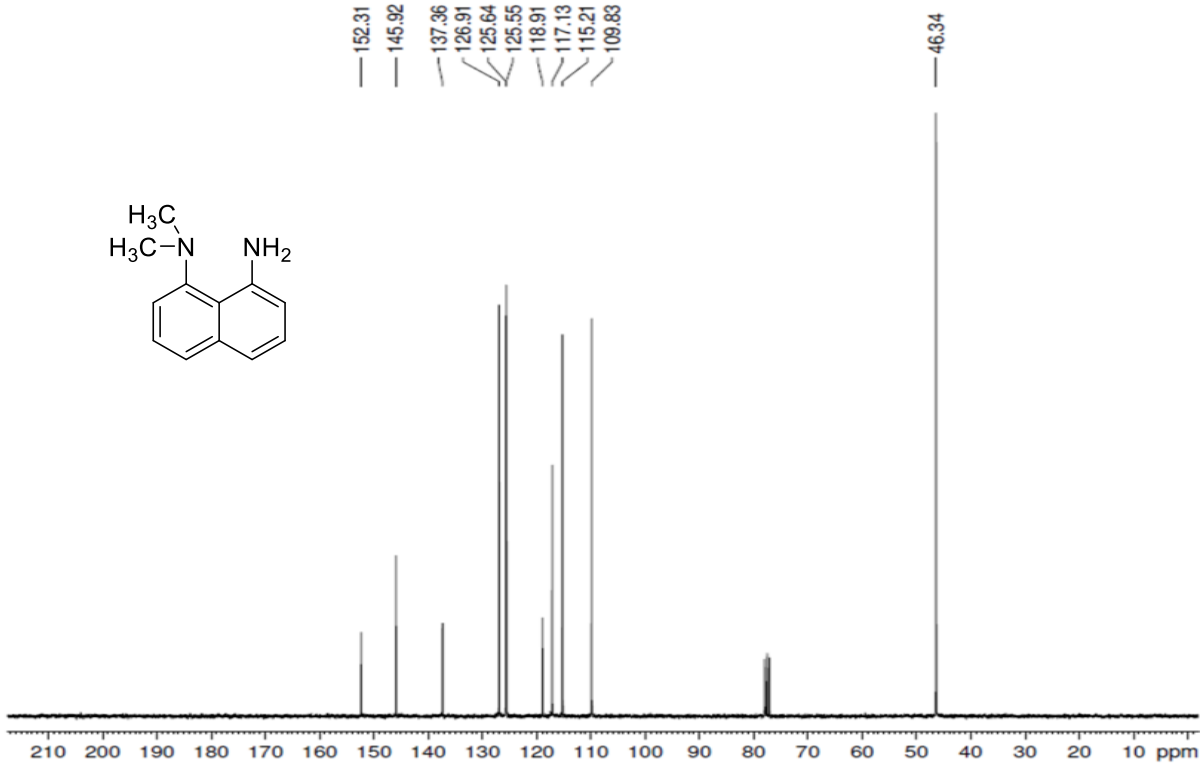

Proton NMR

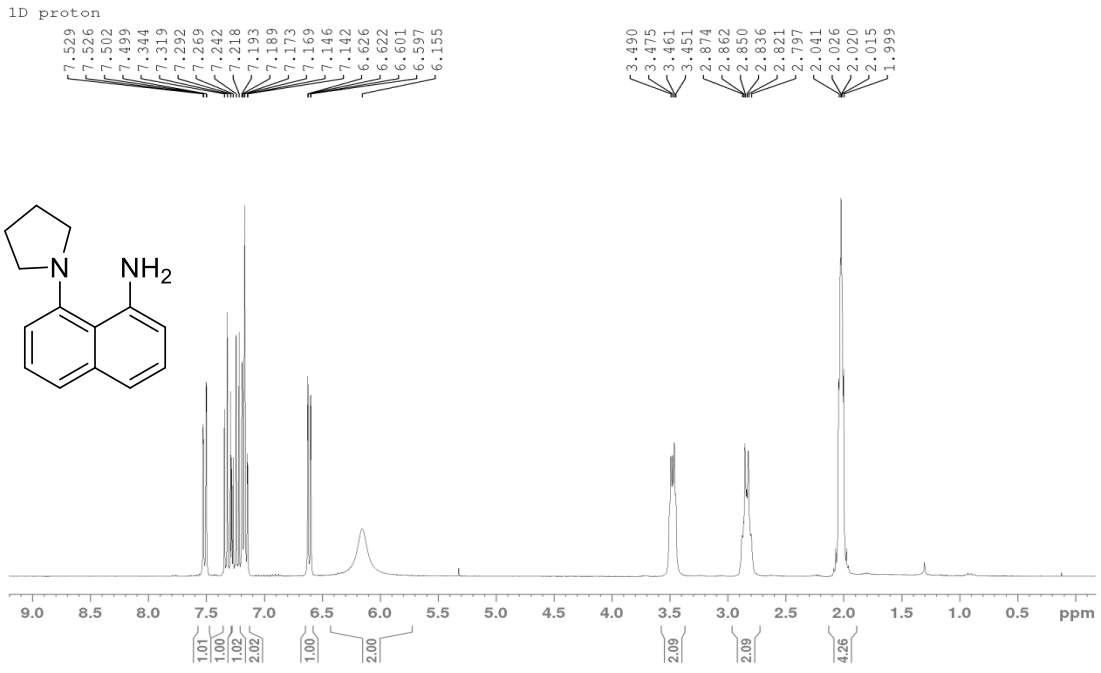

Carbon-13 NMR

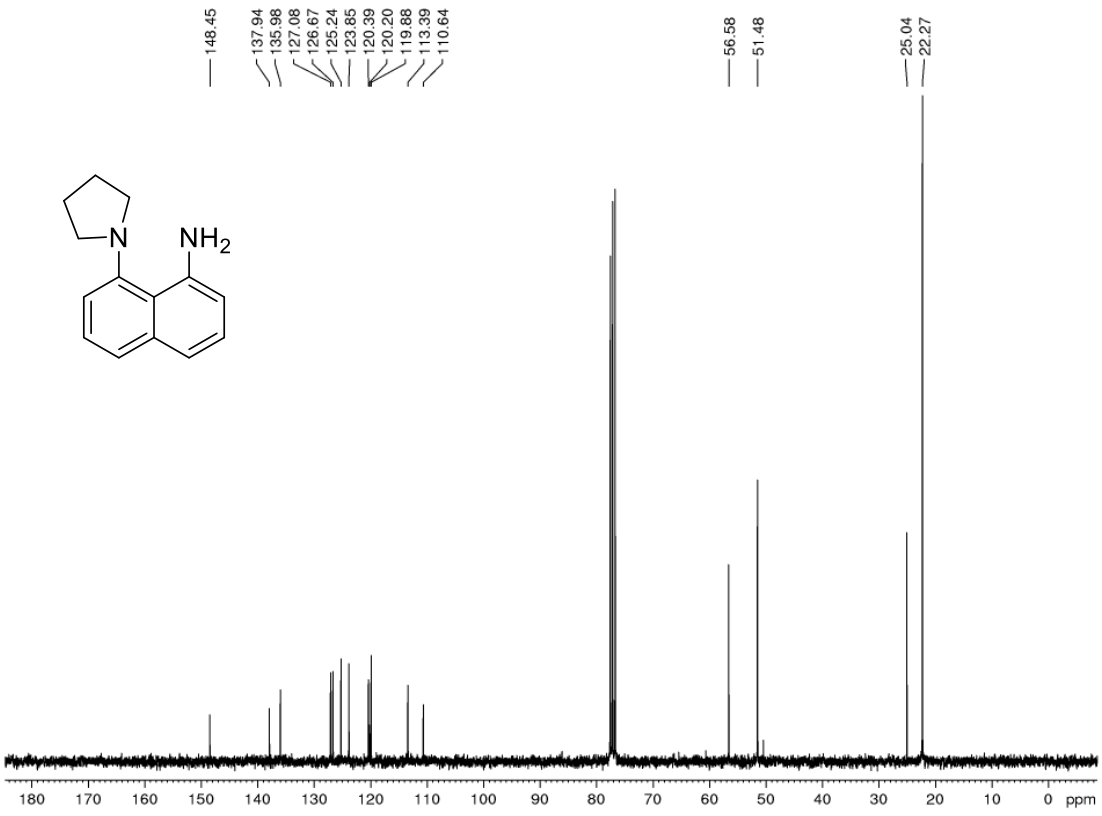

Proton NMR

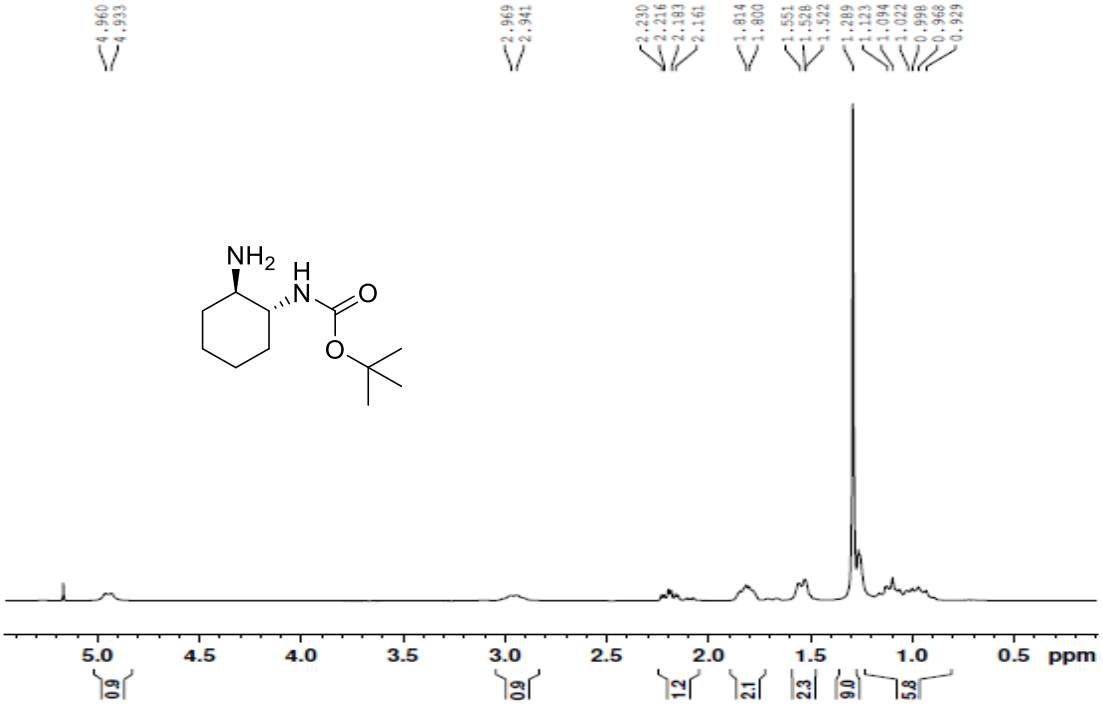

Proton NMR

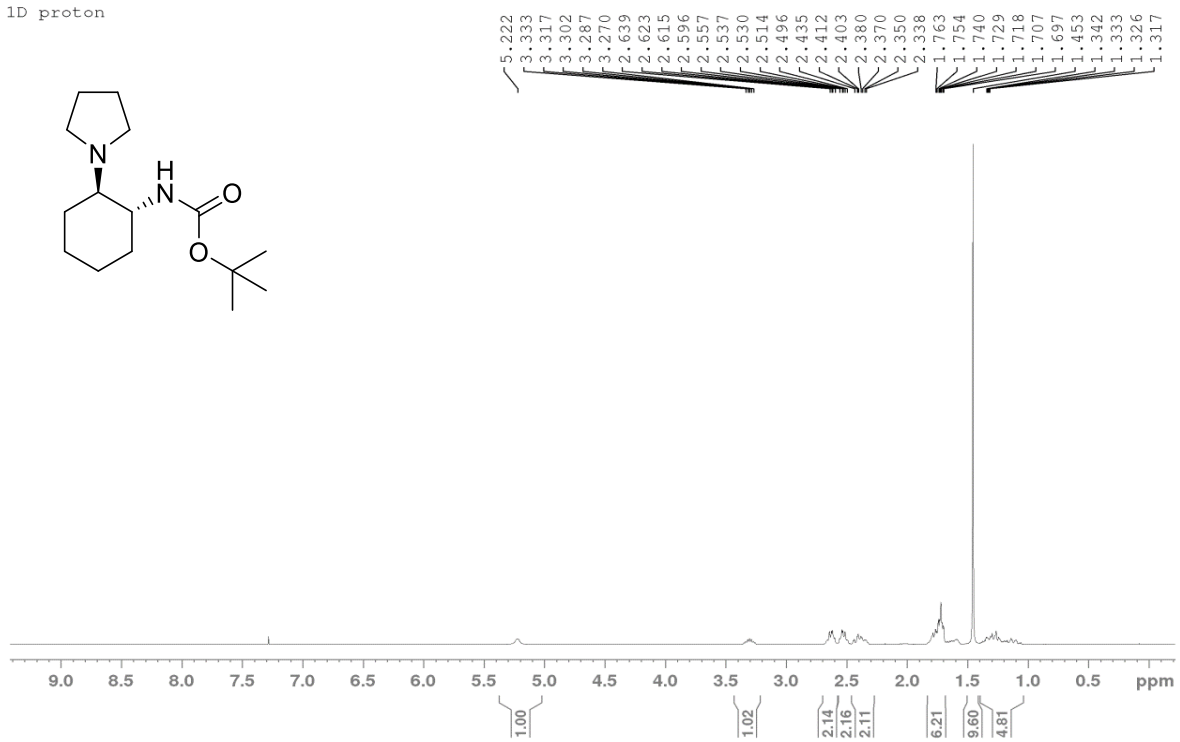

Carbon-13 NMR

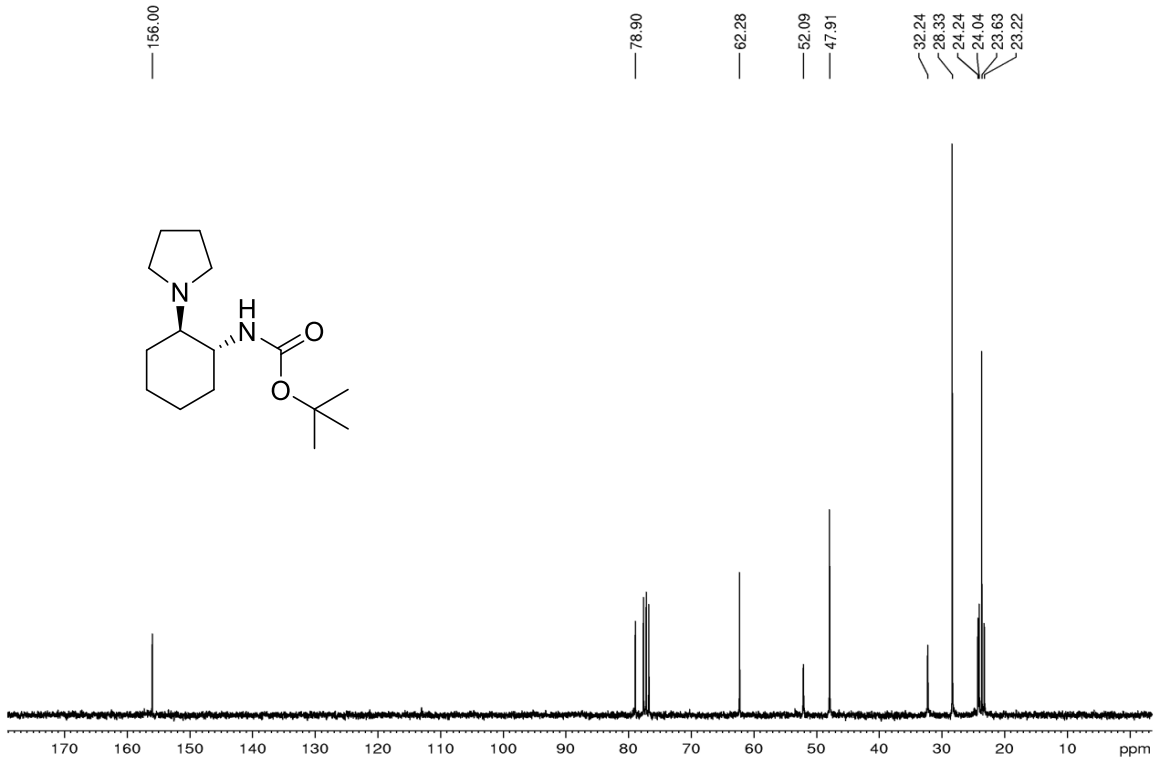

Proton NMR

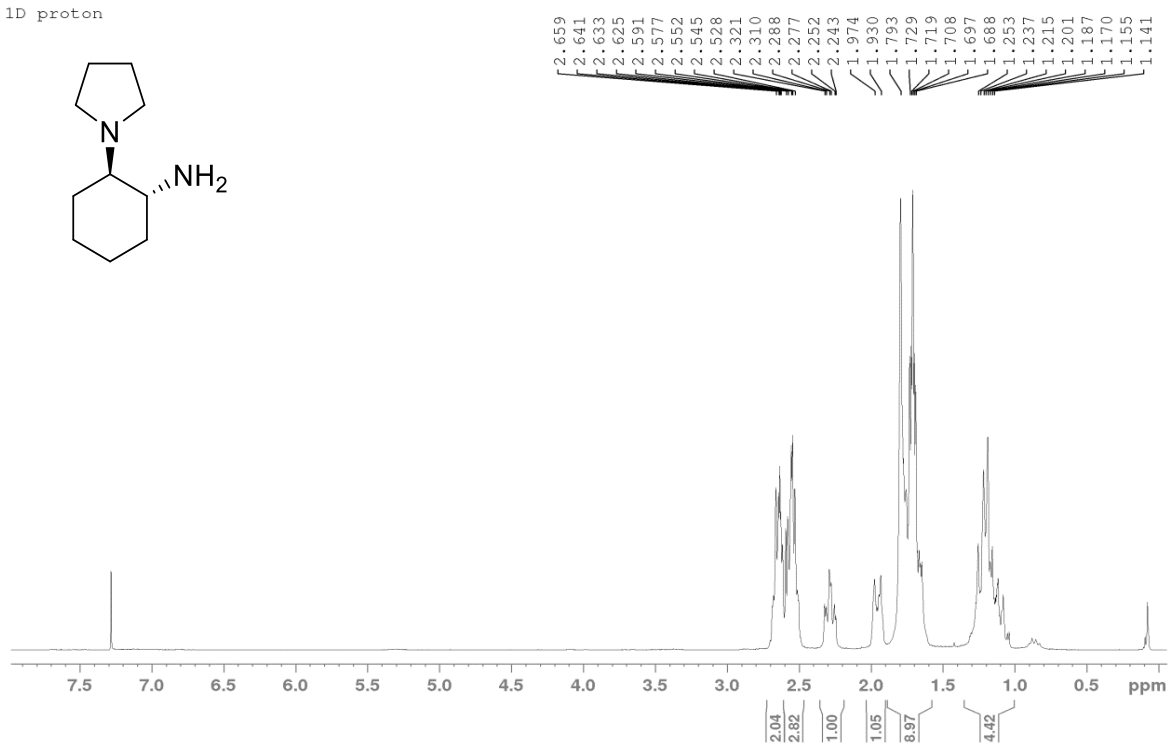

Carbon-13 NMR

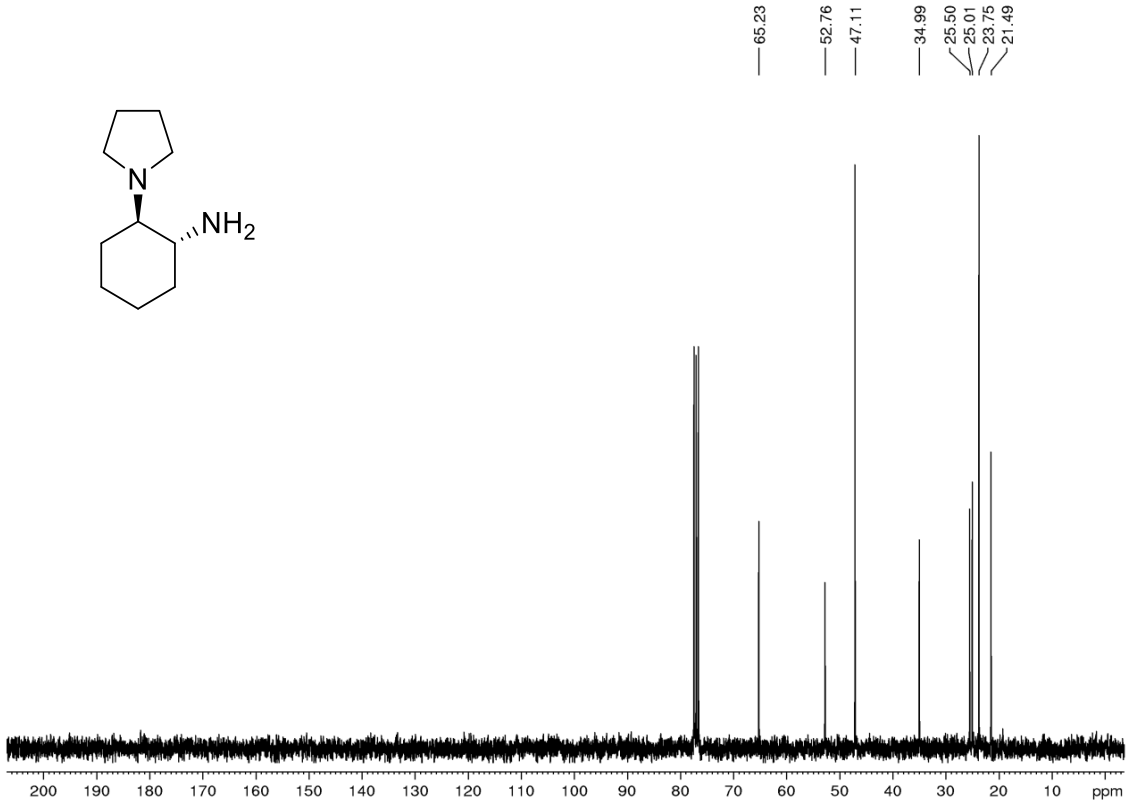

Proton NMR

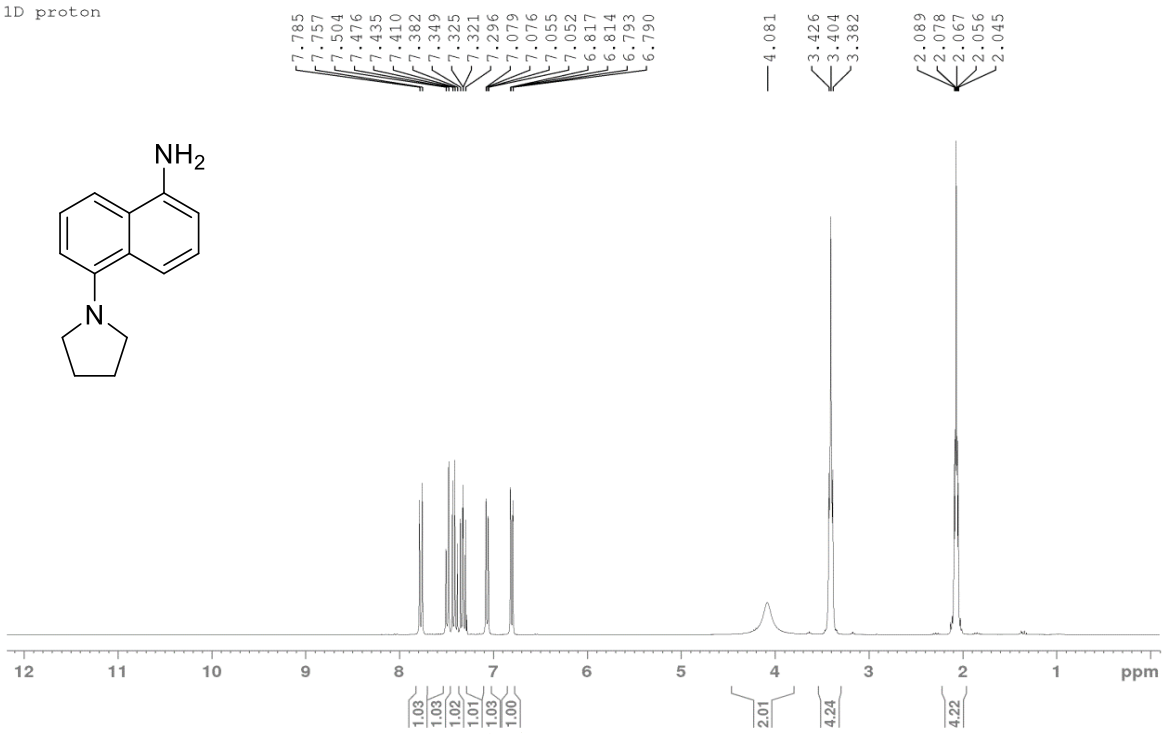

Carbon-13 NMR

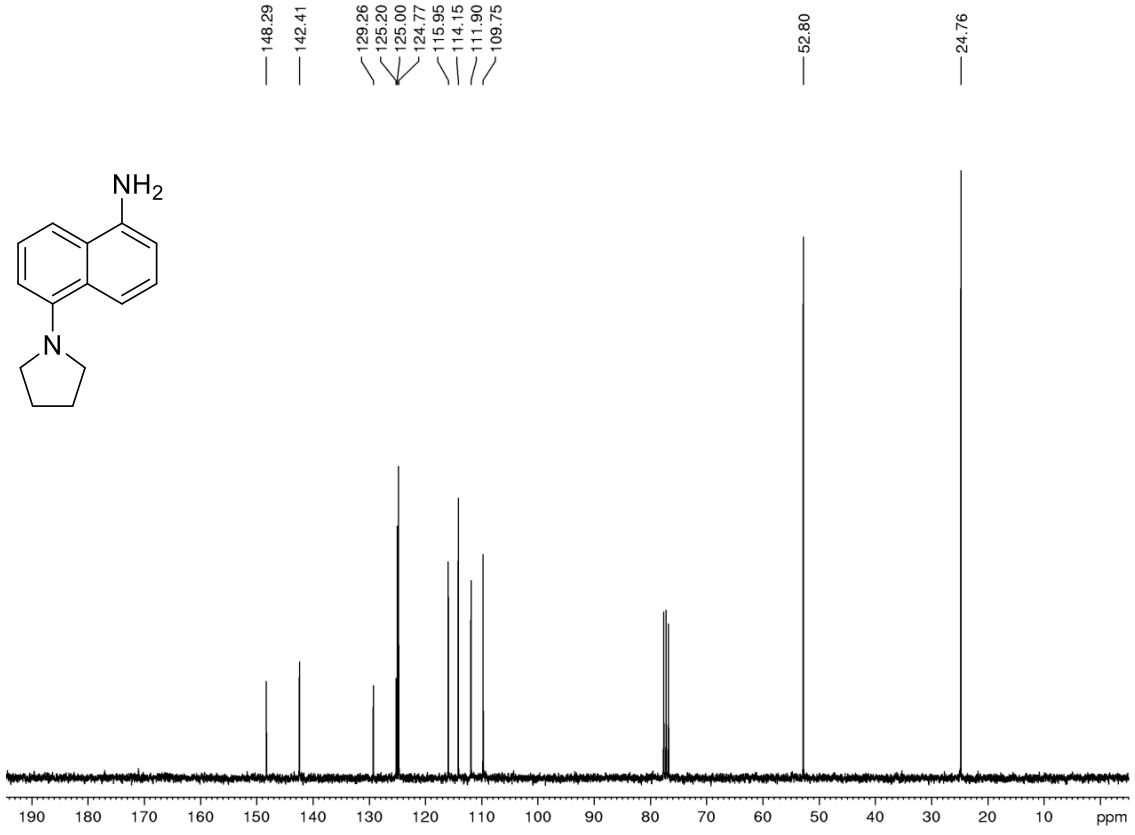

Proton NMR

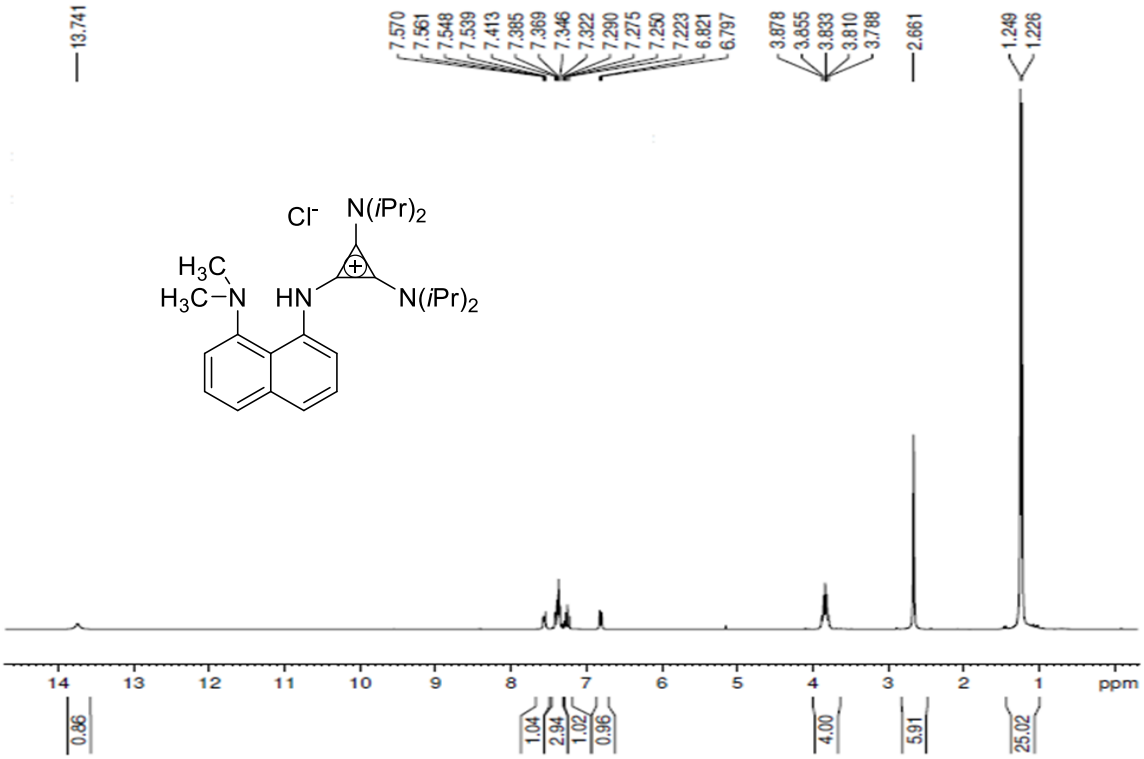

Carbon-13 NMR

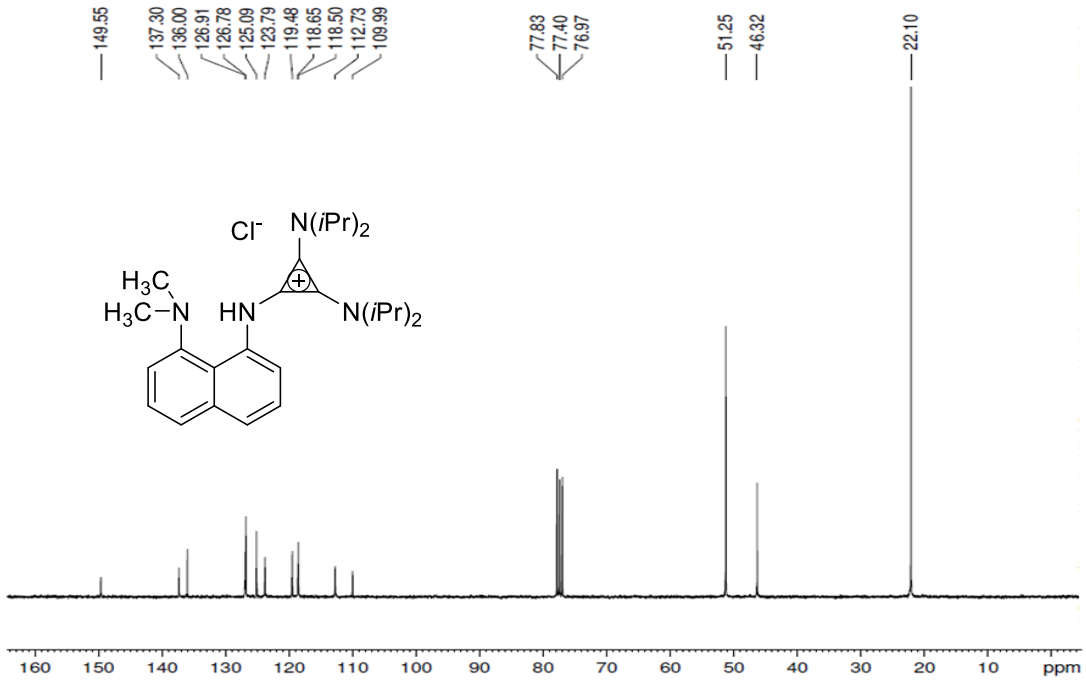

Proton NMR

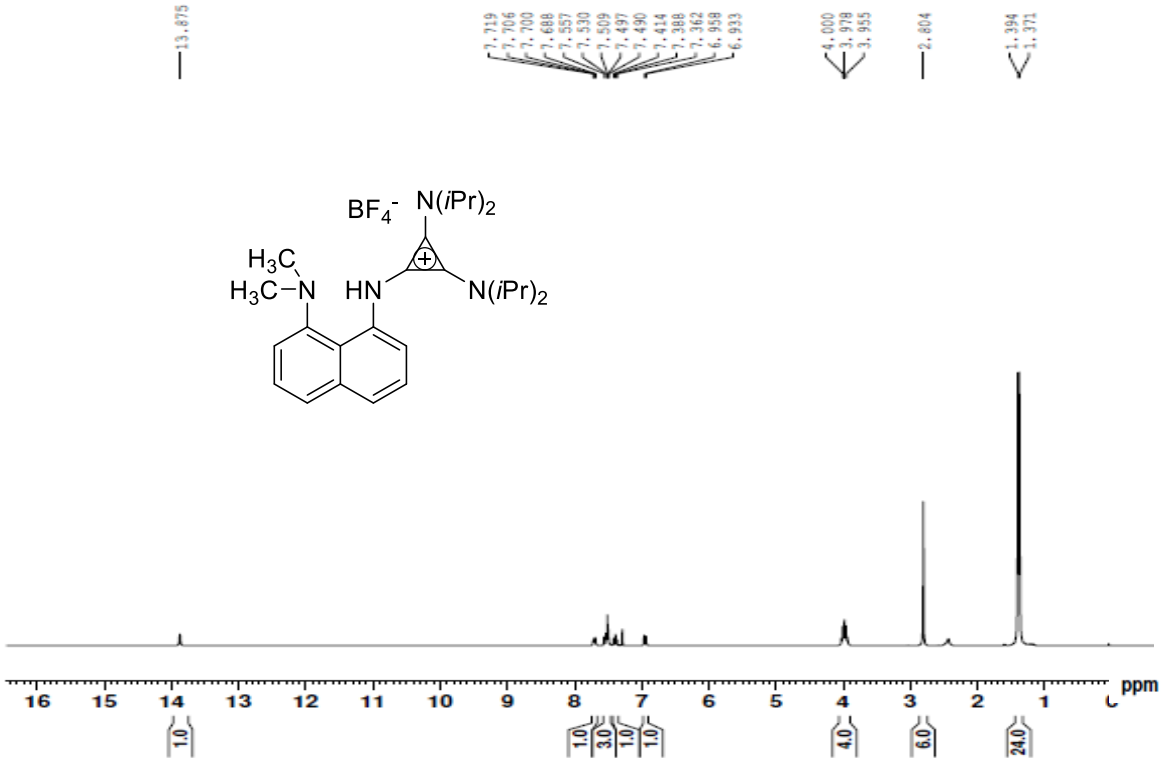

Carbon-13 NMR

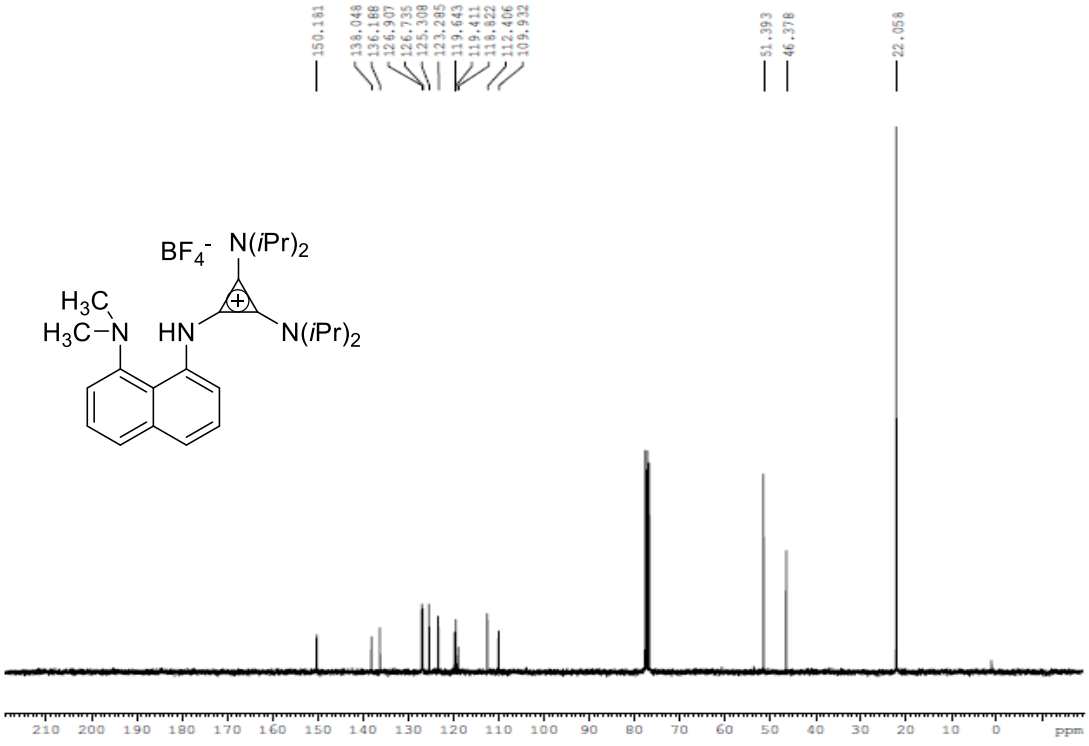

Boron-11 NMR

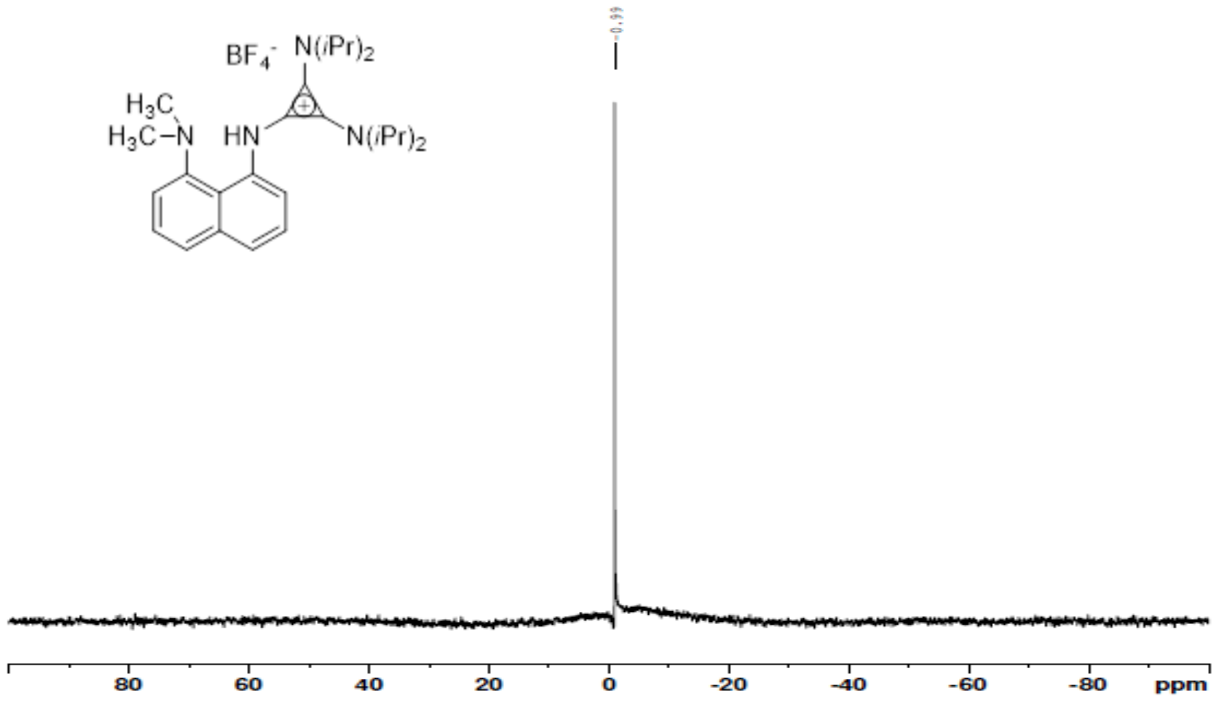

Fluorine-19 NMR

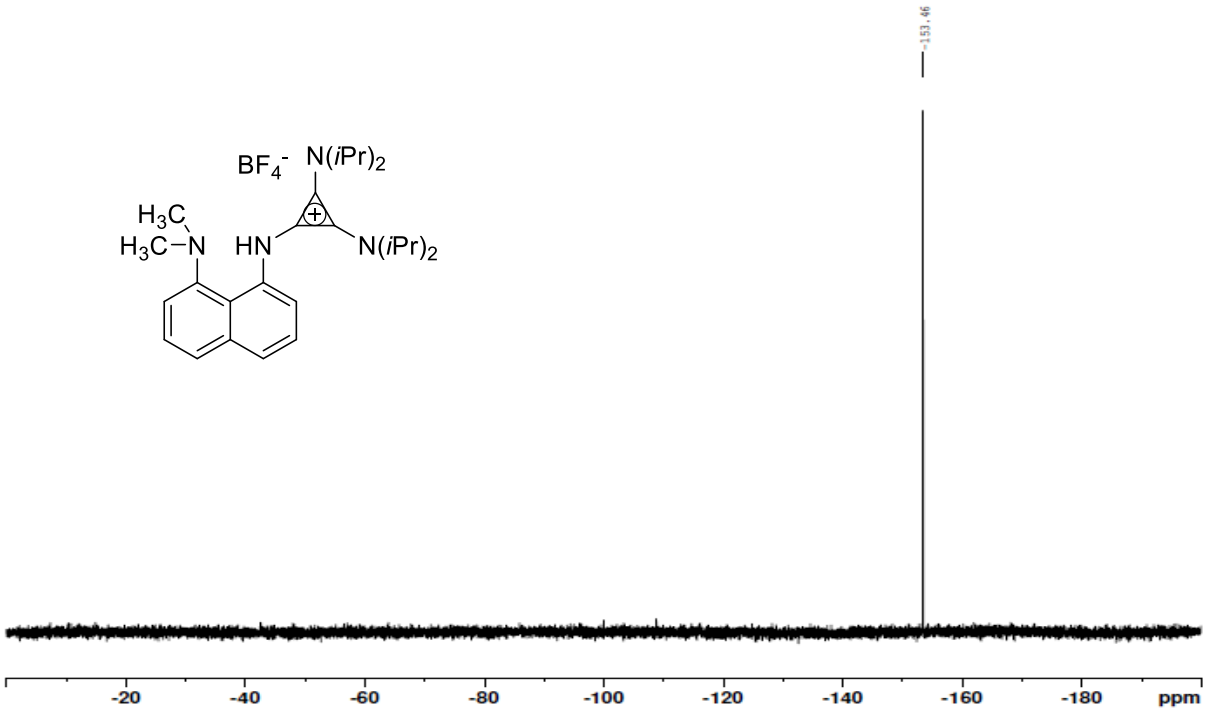

Proton NMR

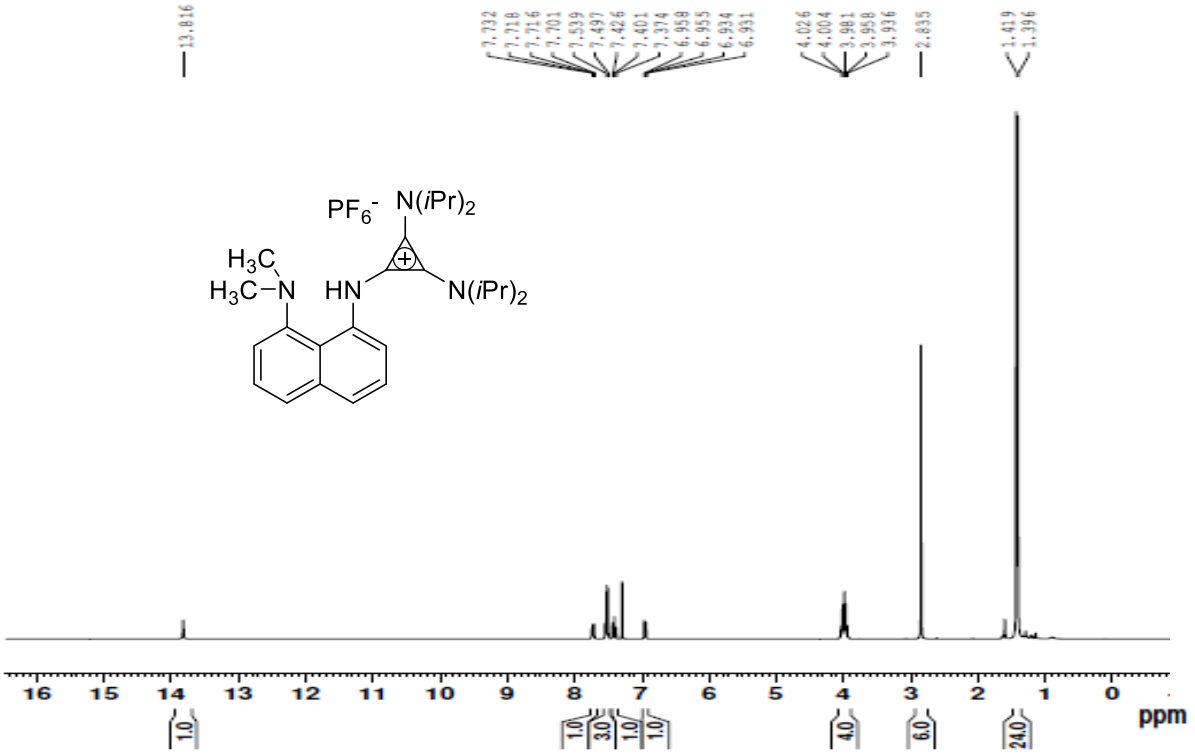

Carbon-13 NMR

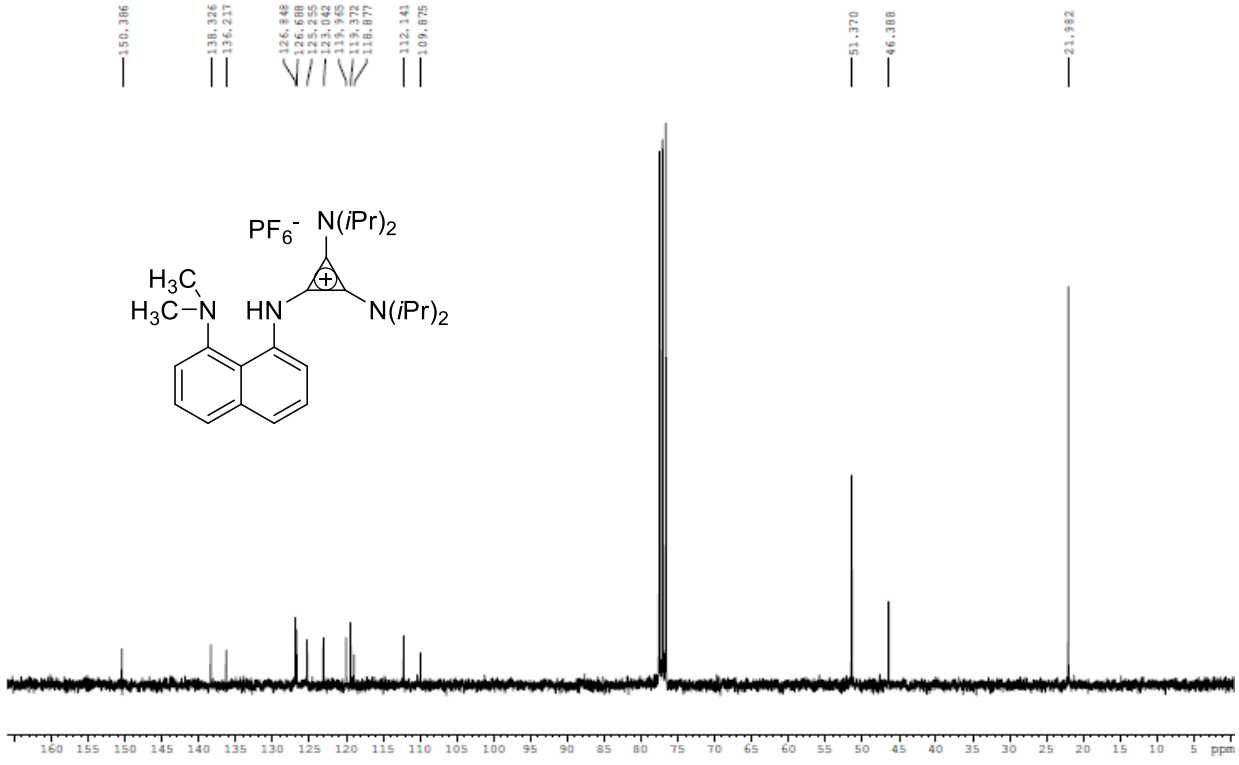

Fluorine-19 NMR

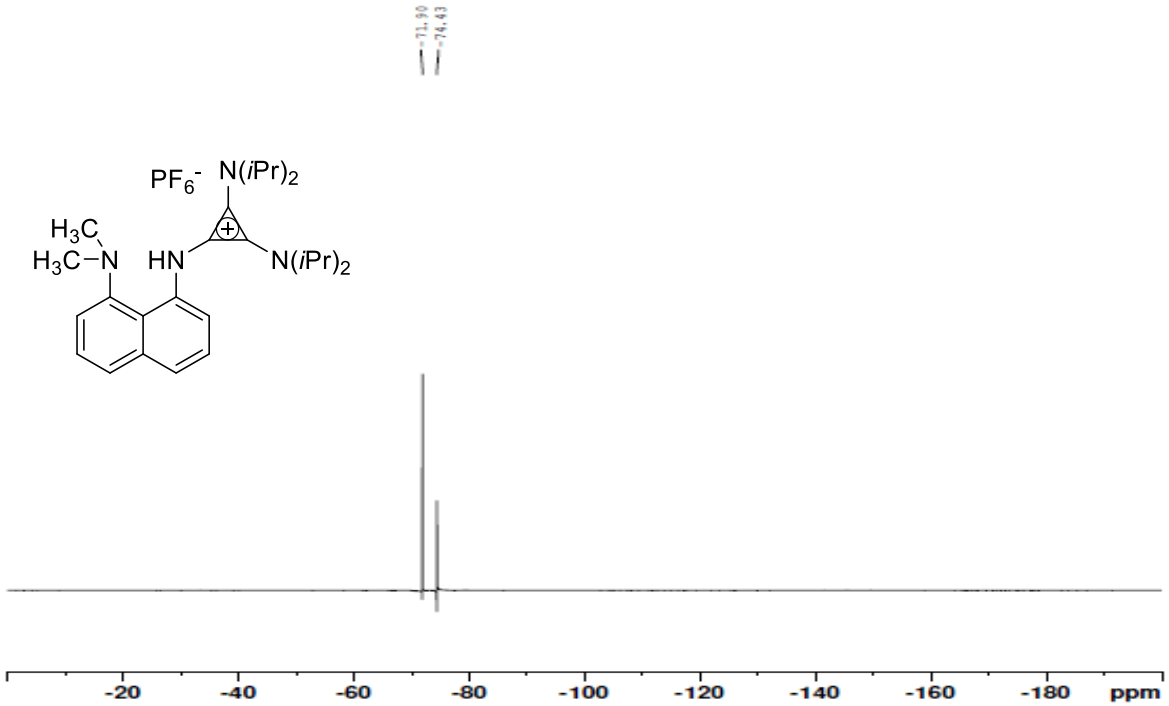

Phosphorus-31 NMR

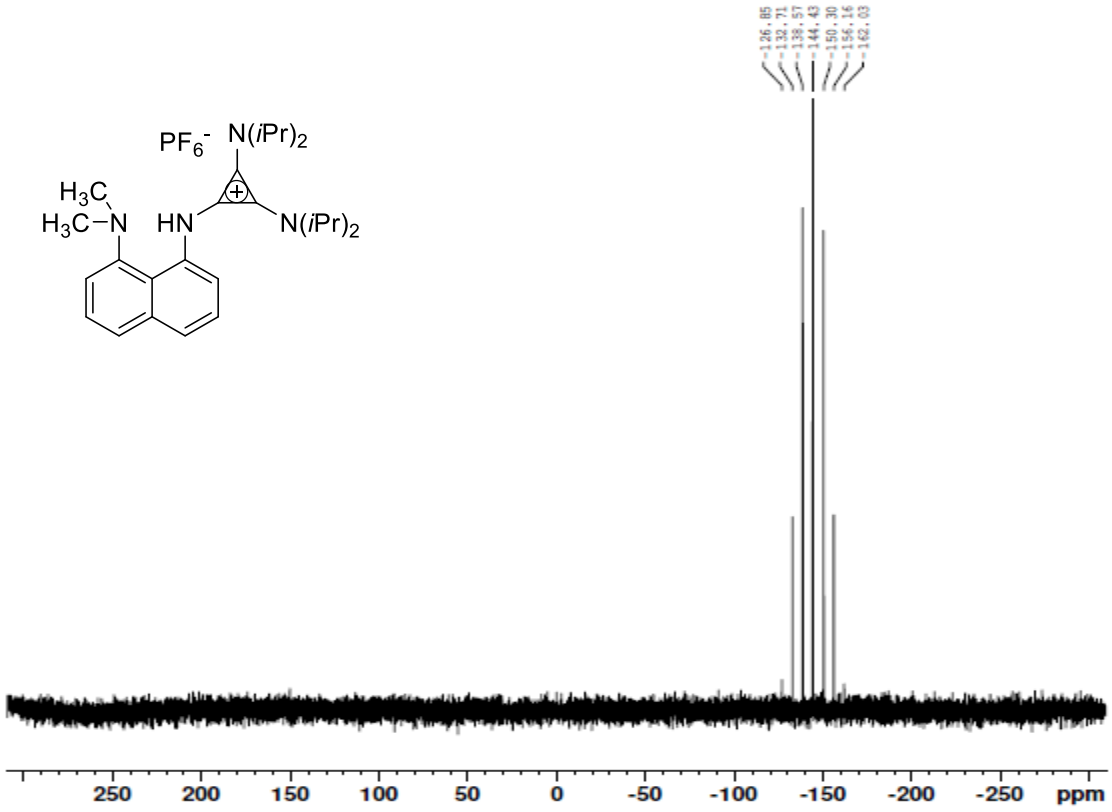

Proton NMR

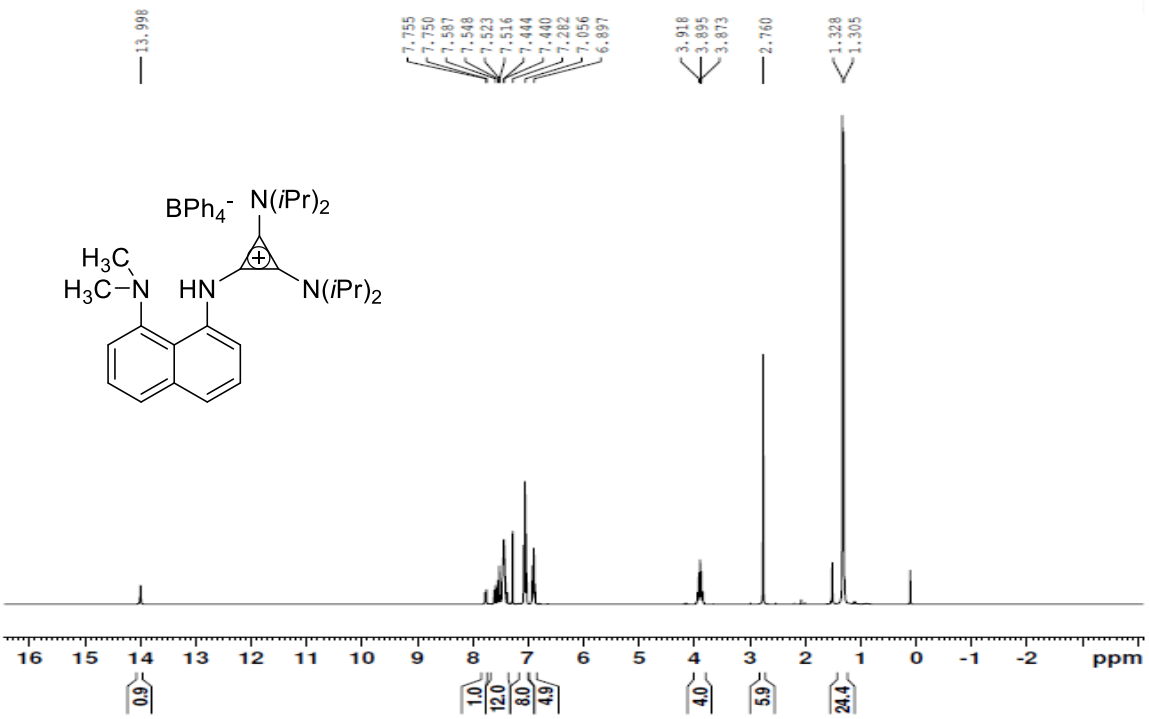

Carbon-13 NMR

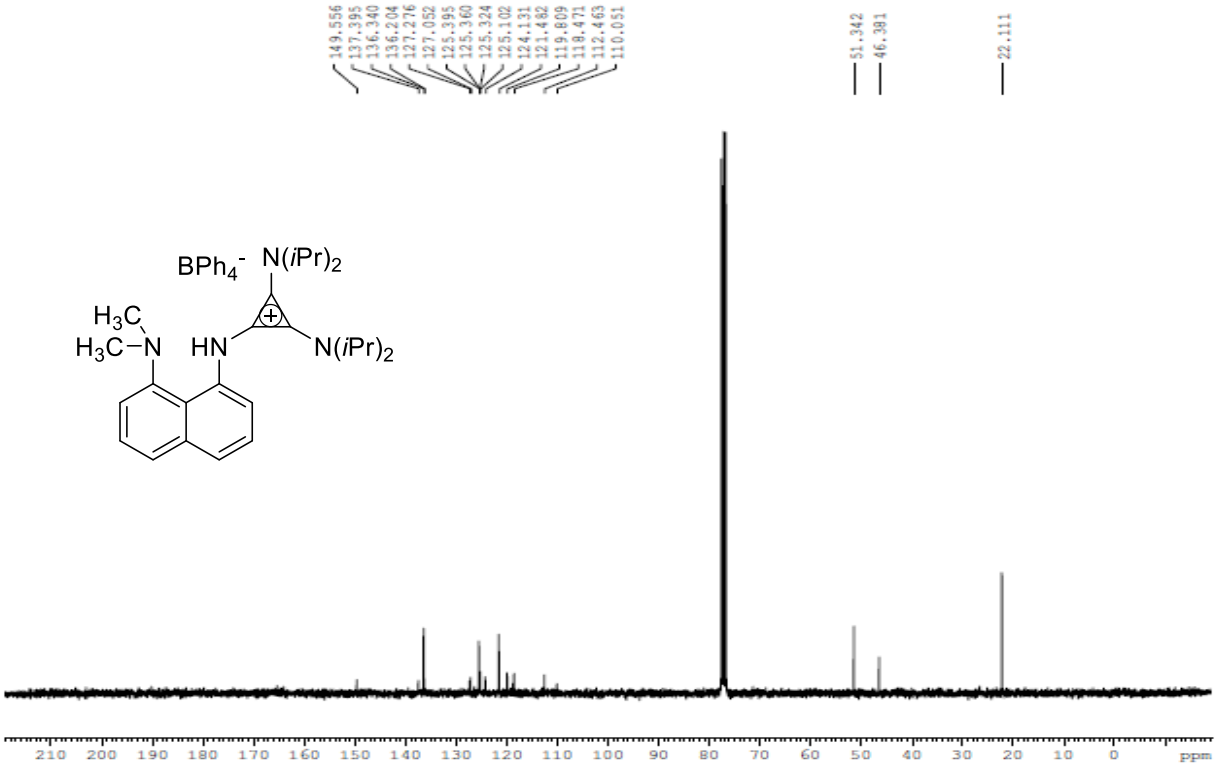

Boron-11 NMR

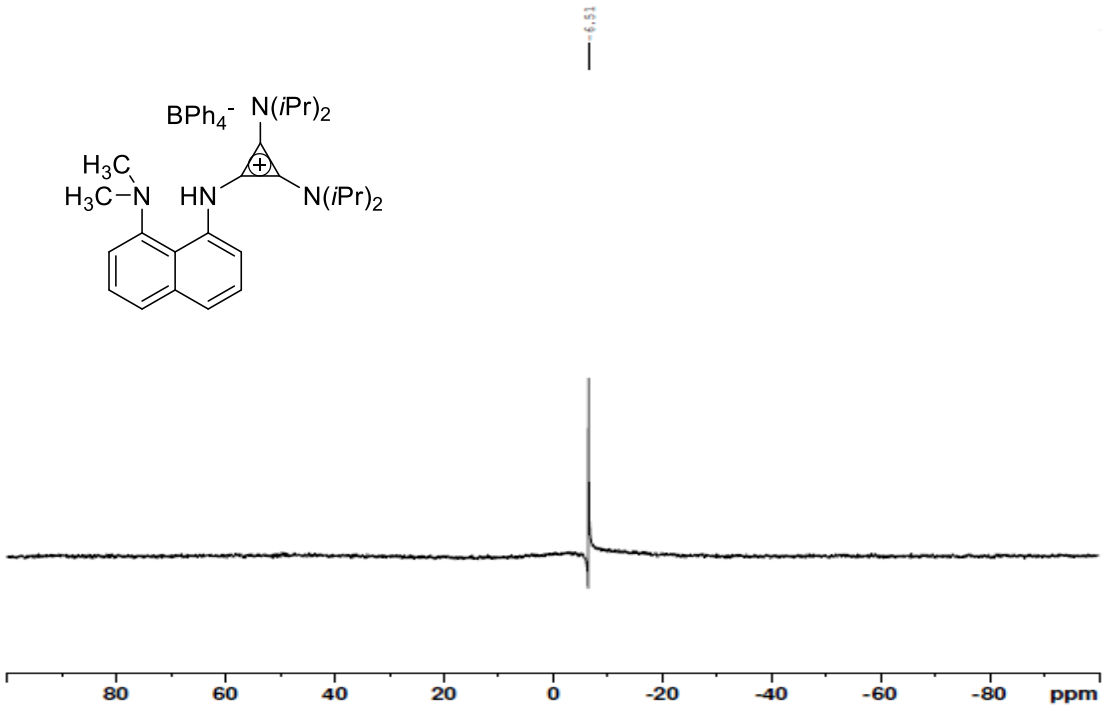

Proton NMR

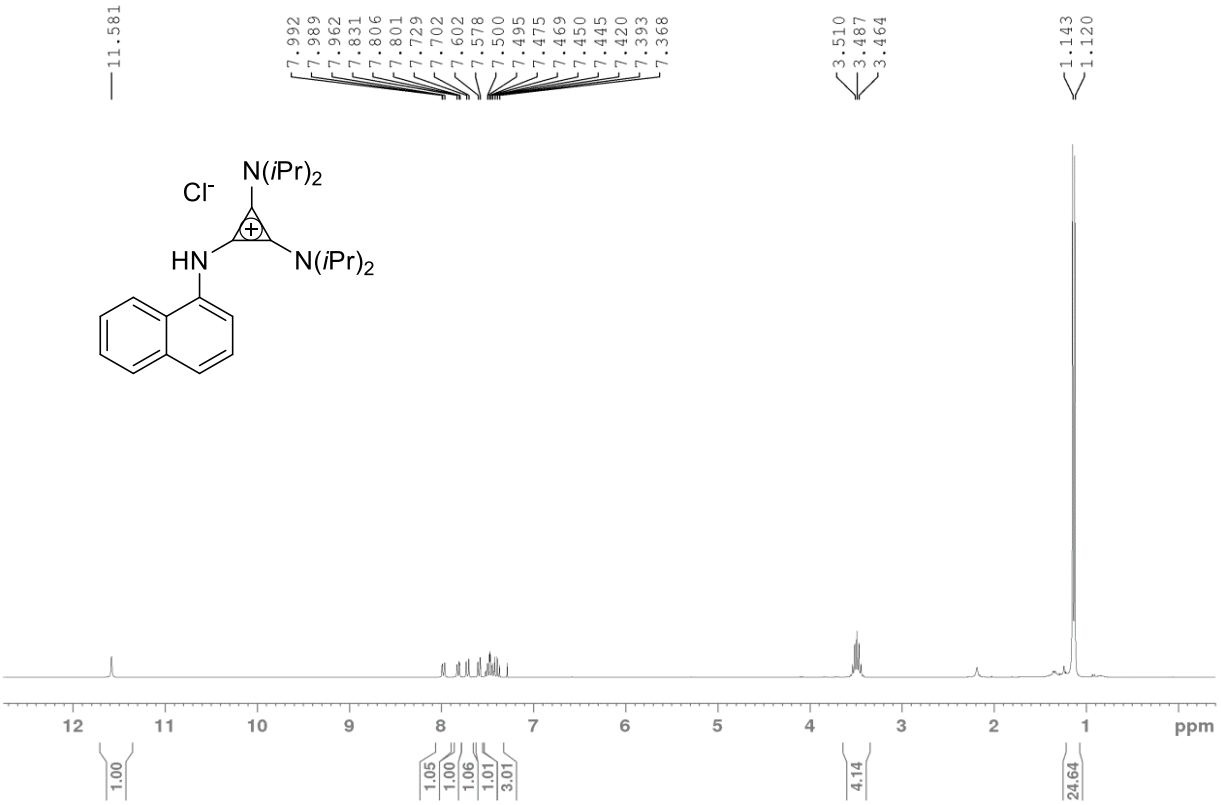

Carbon-13 NMR

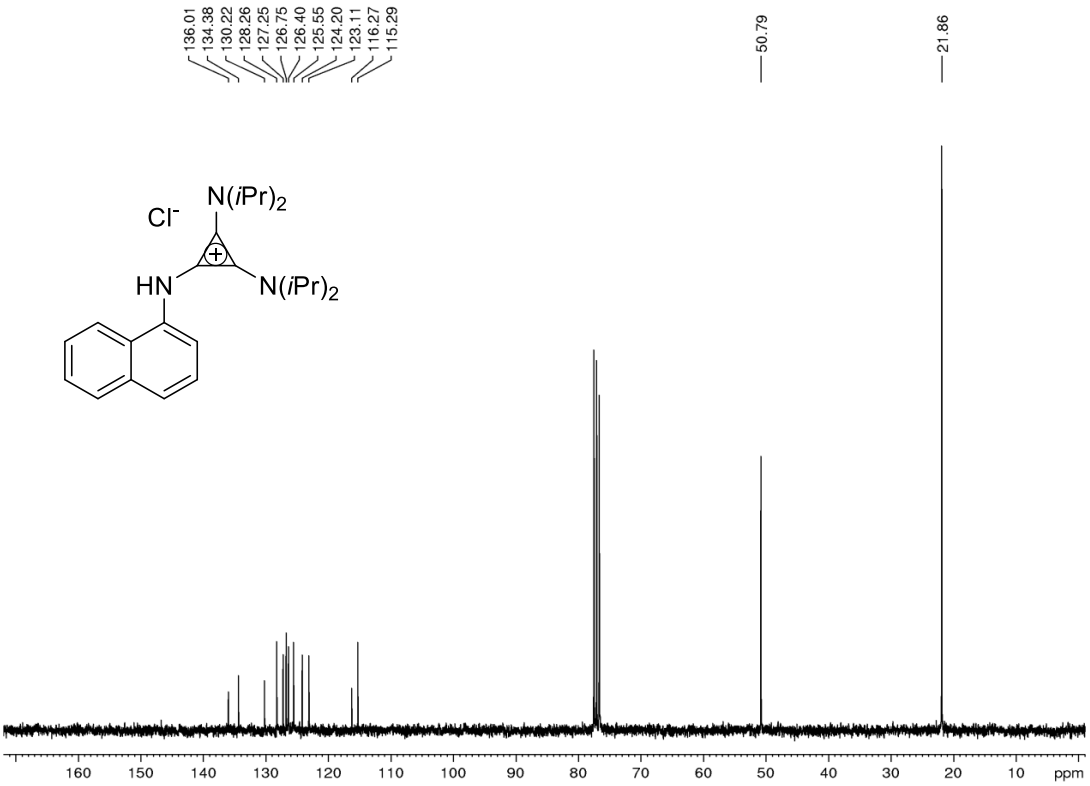

Proton NMR

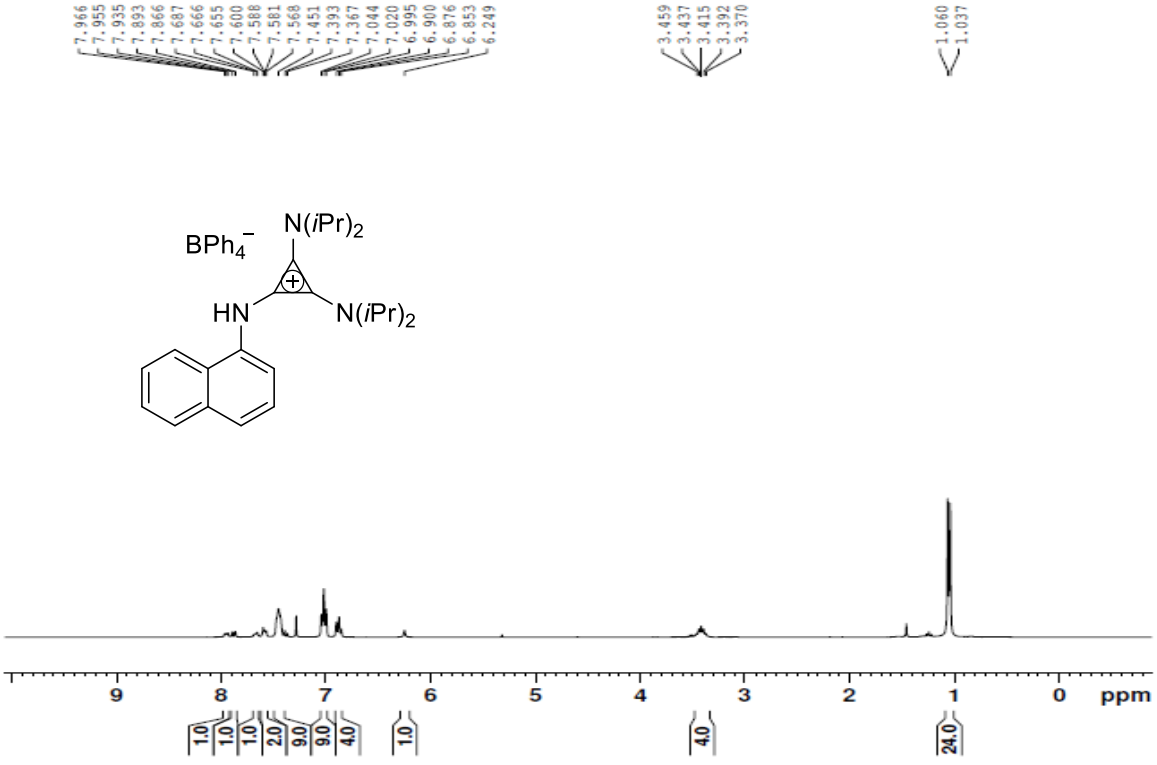

Proton NMR

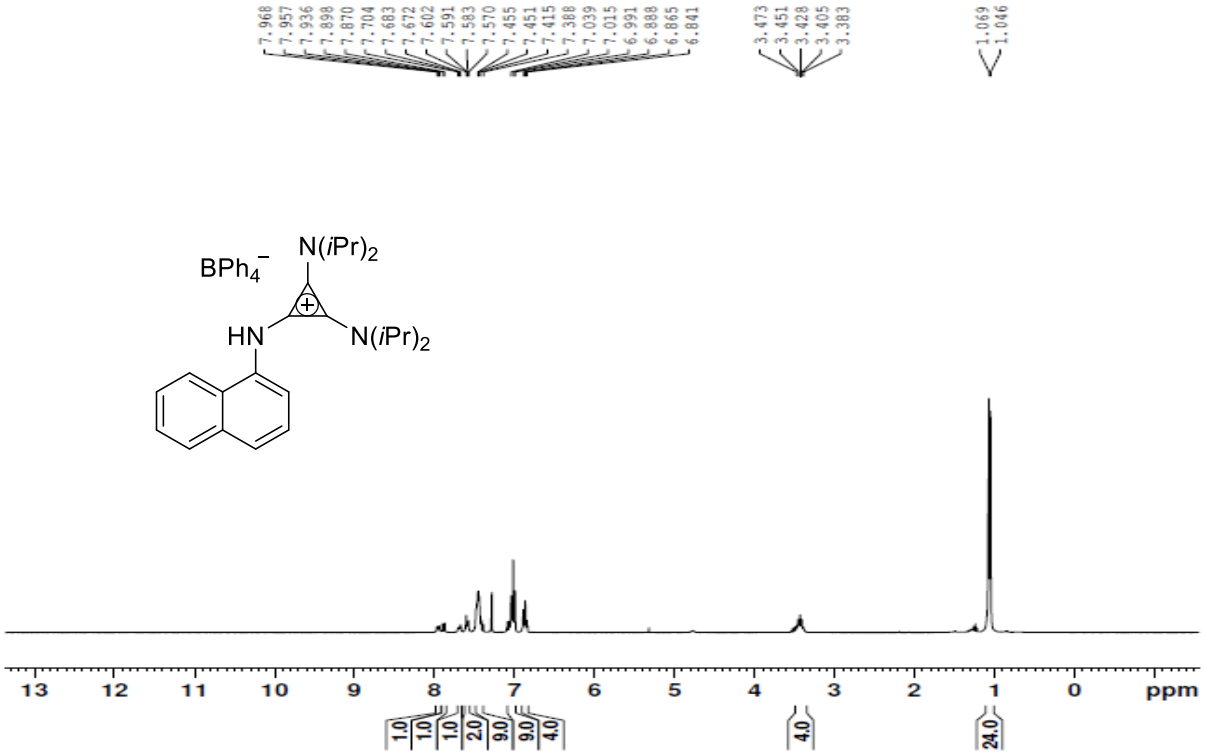

Carbon-13 NMR

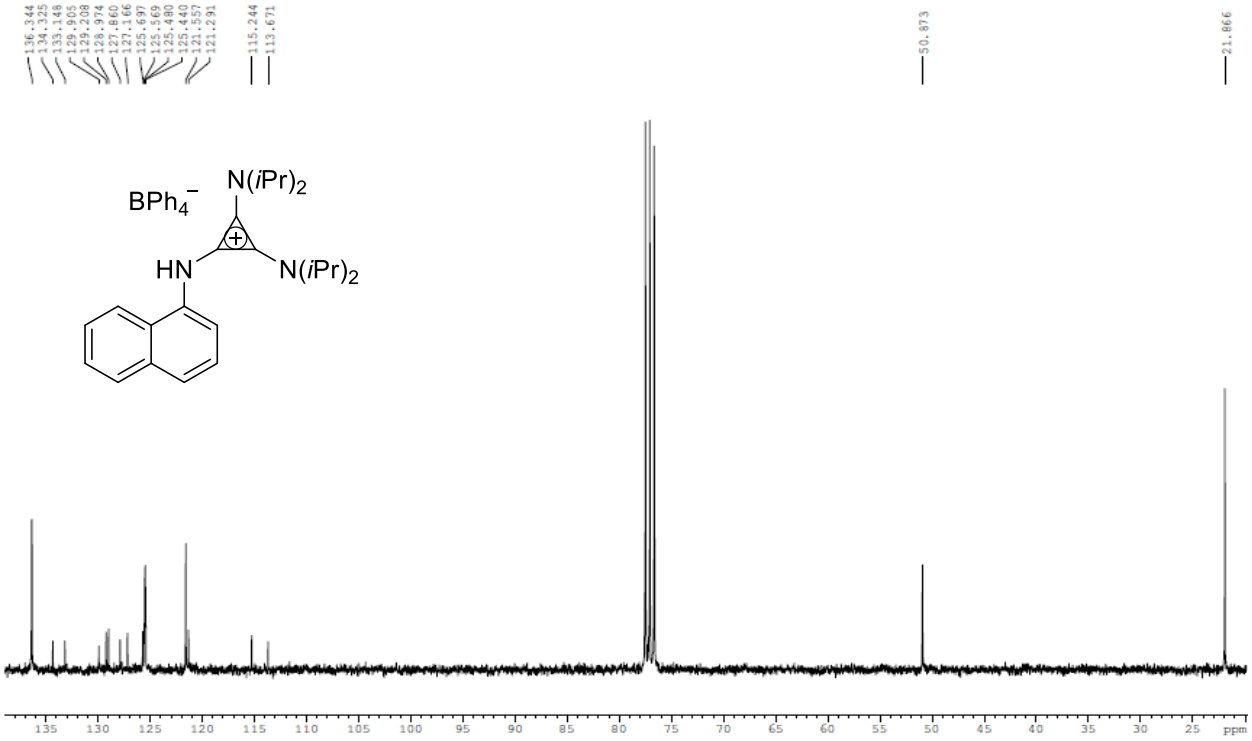

Boron-11 NMR

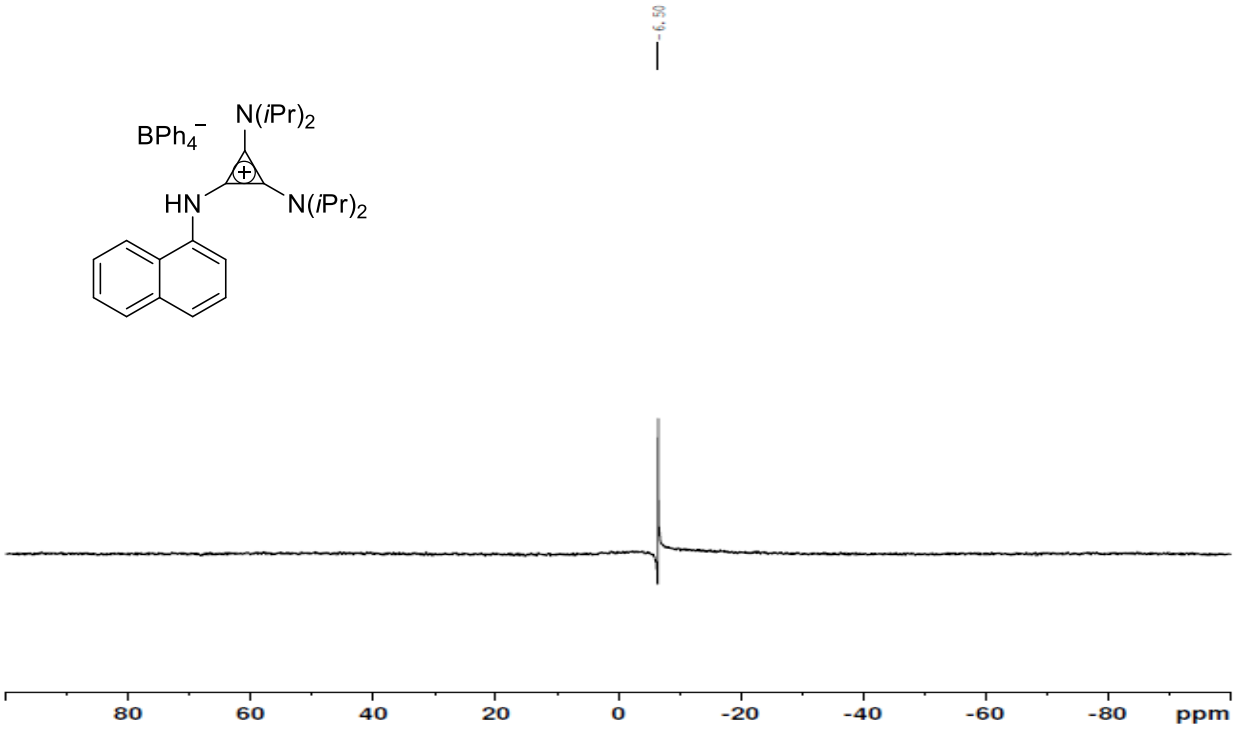

Proton NMR

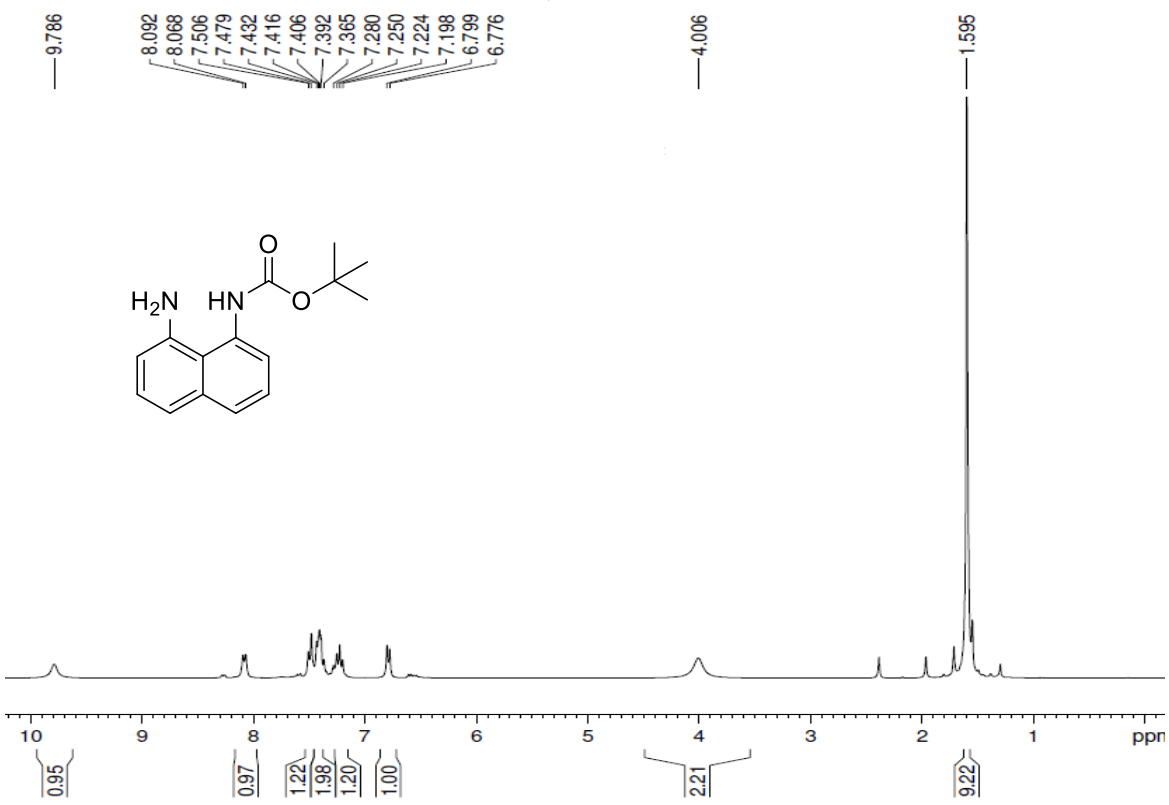

Carbon-13 NMR

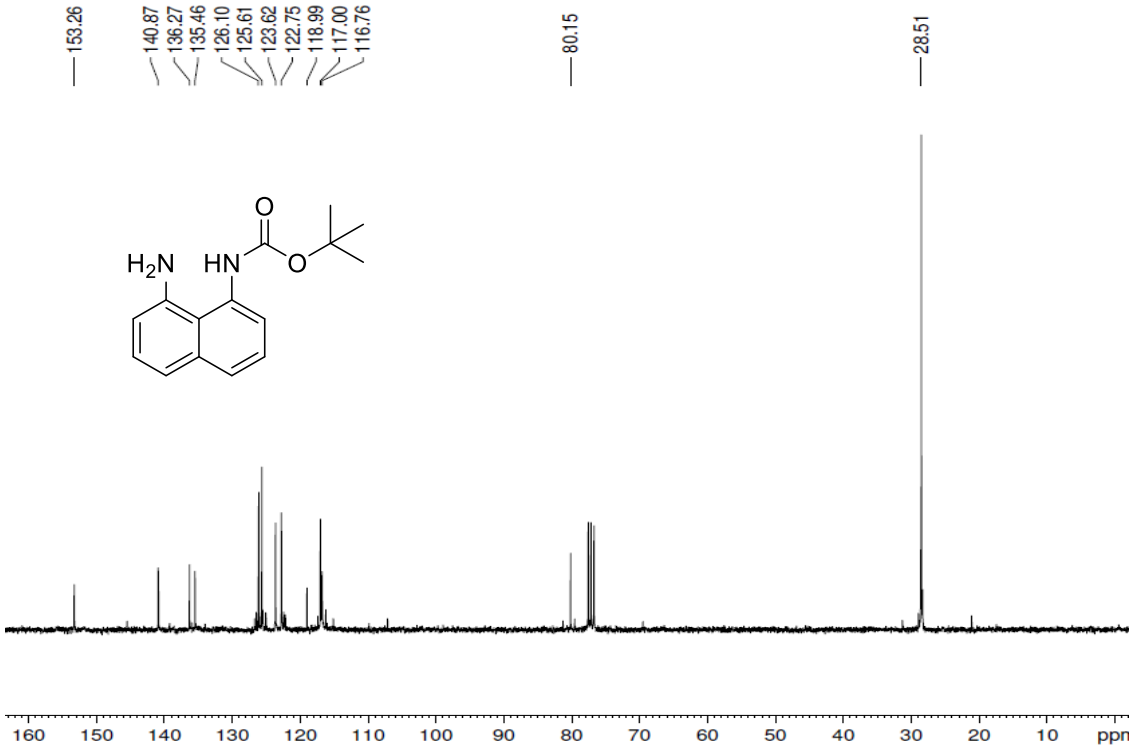

Proton NMR

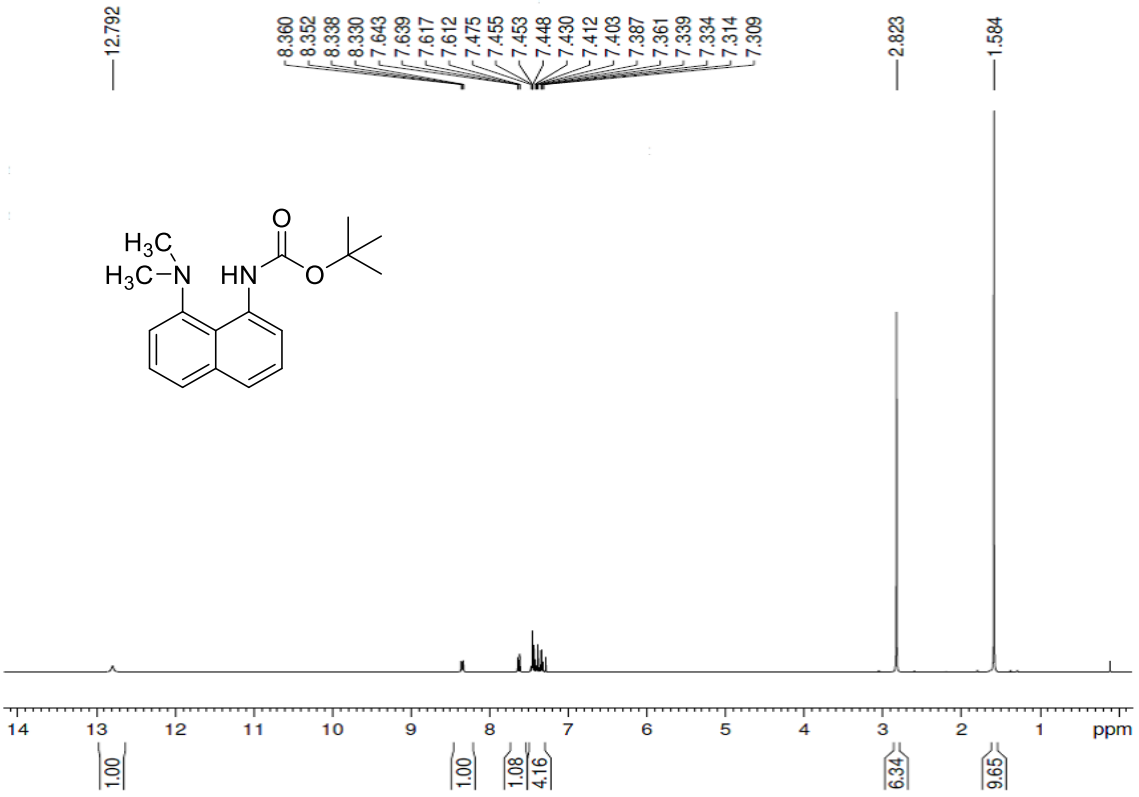

Carbon-13 NMR

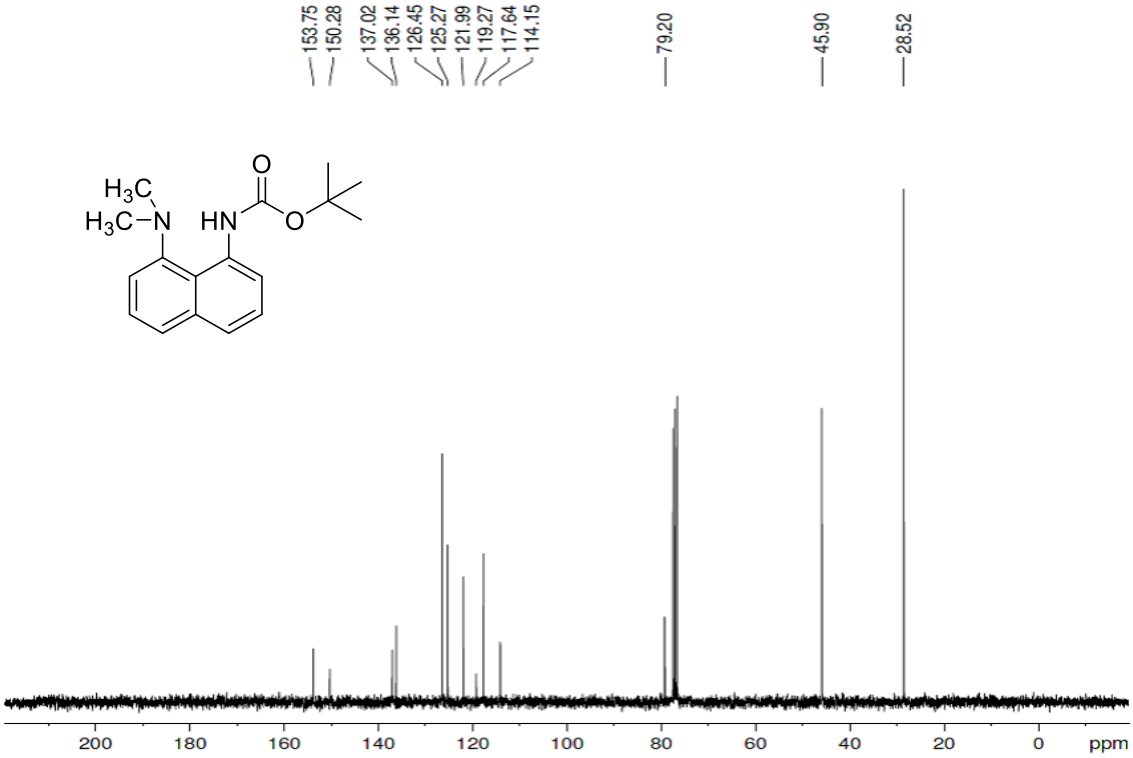

Proton NMR

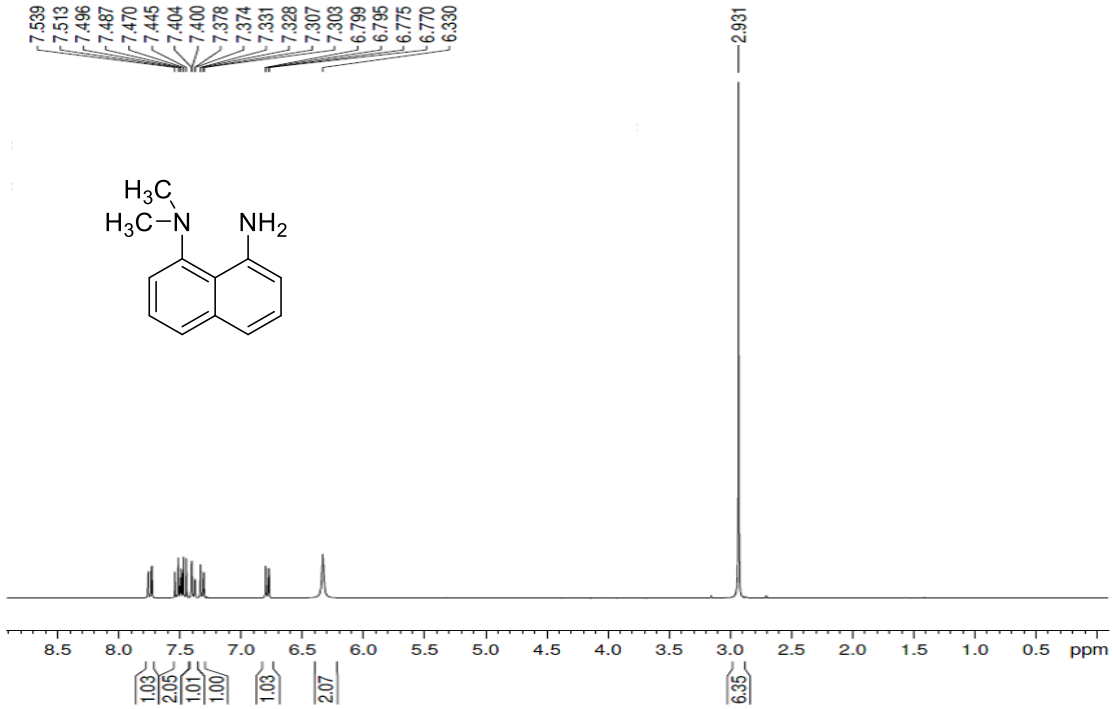

Carbon-13 NMR

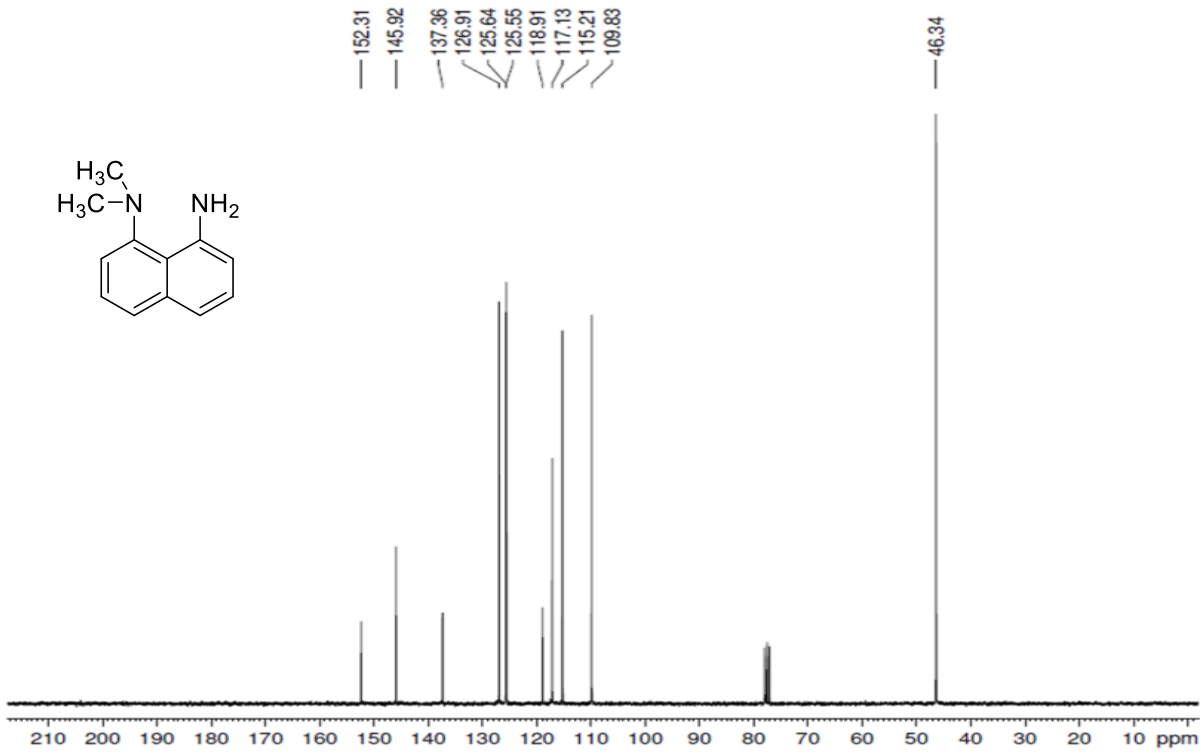

Fluorescence data of Janus Counter-Ion derivatives in dichloromethane.

Compound	λ_{max}	λ_{em}	Molar Attenuation Coefficient (ε) (M^{-1} cm^{-1})	Quantum Yield (ϕ)	Stokes Shift
12a$_{Cl}$	334 nm	465 nm	5.65 x 10^4	0.42	131 nm
12b$_{BF4}$	333 nm	467 nm	4.43 x 10^4	0.30	134 nm
12c$_{PF6}$	333 nm	465 nm	2.50 x 10^4	0.34	132 nm
12d$_{BPh4}$	333 nm	467 nm	3.32 x 10^4	0.23	134 nm

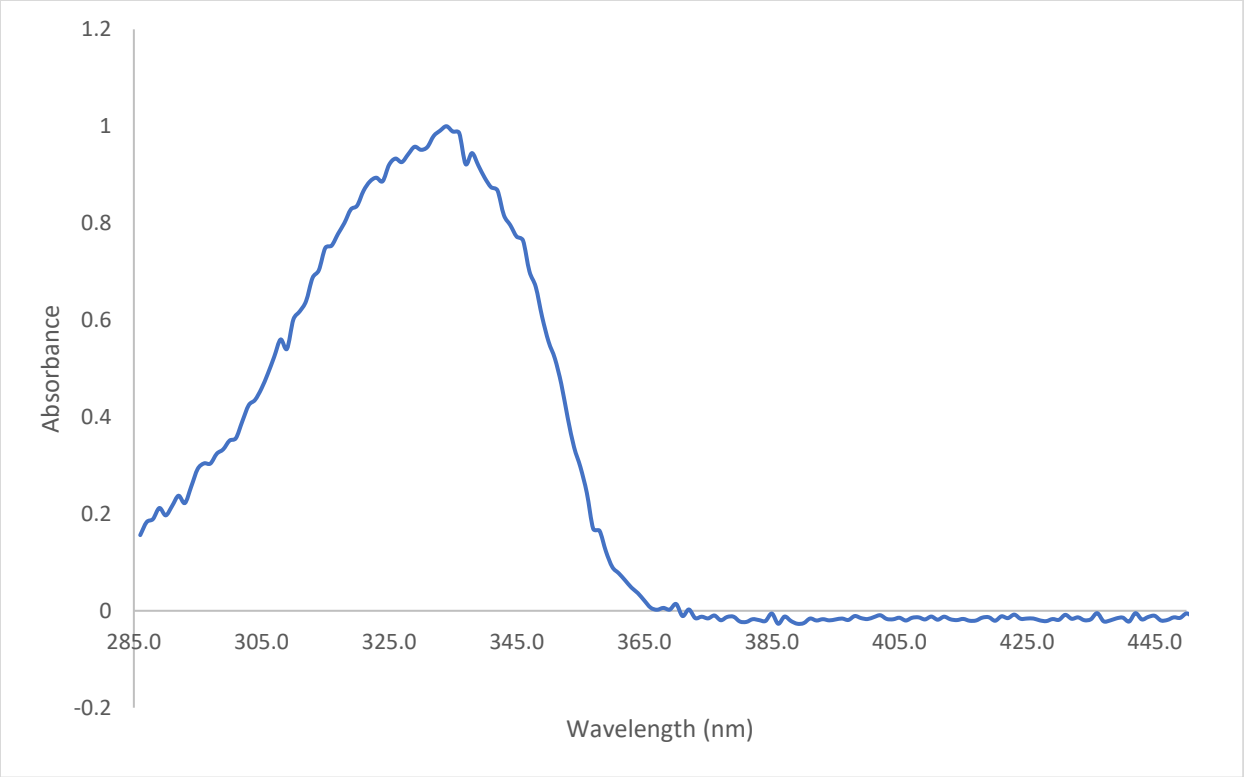

Normalized UV-Vis absorption spectra of **12a**$_{Cl}$ in DCM.

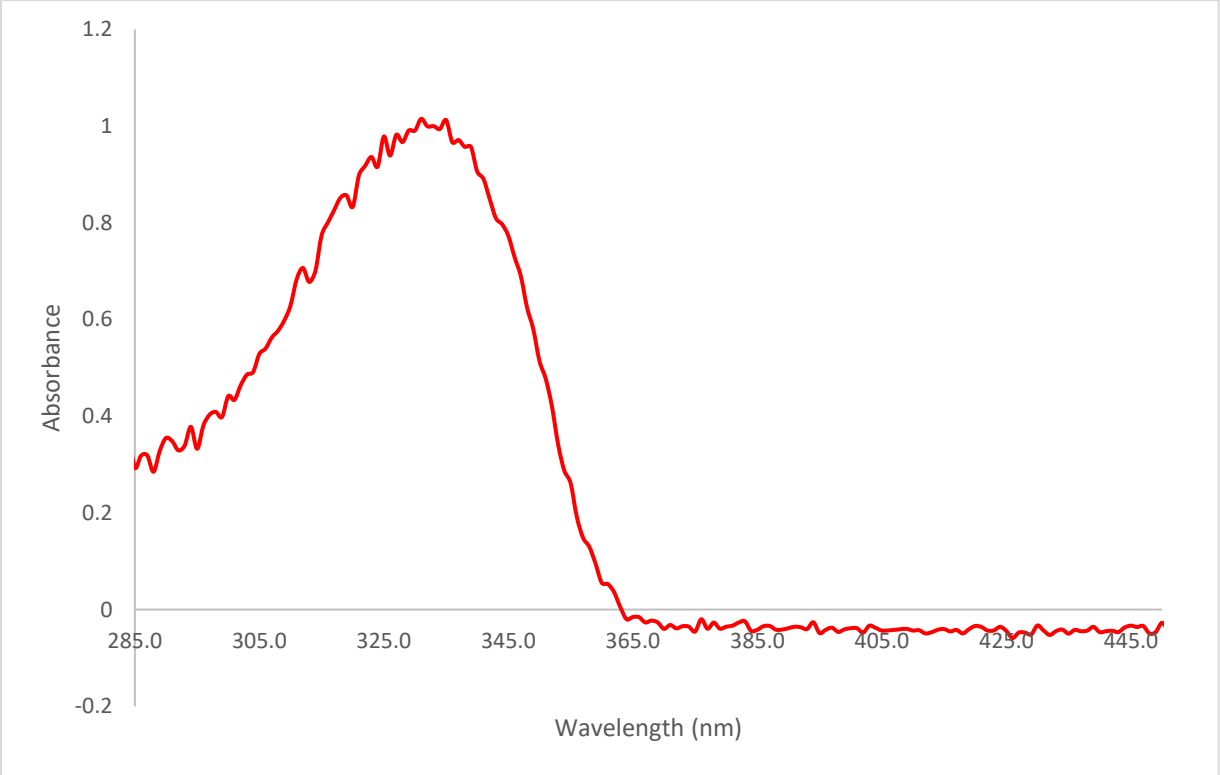

Normalized UV-Vis absorption spectra of **12b**$_{BF4}$ in DCM.

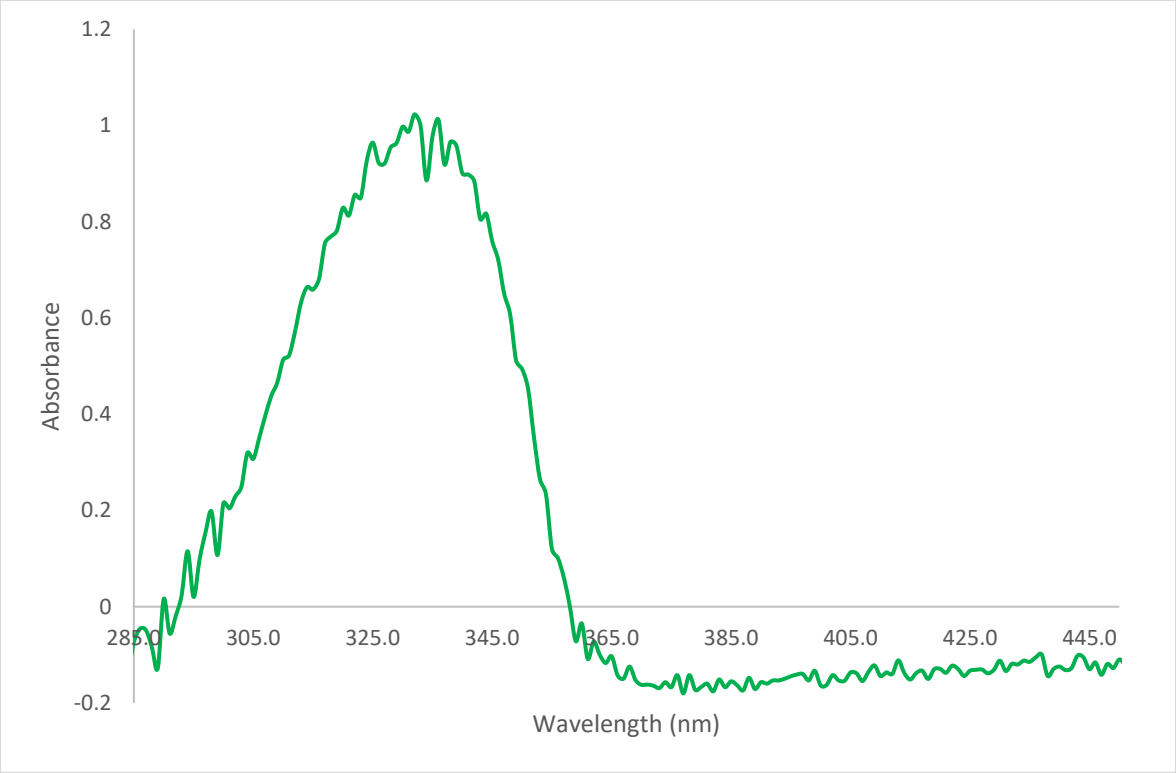

Normalized UV-Vis absorption spectra of **12c**$_{PF6}$ in DCM.

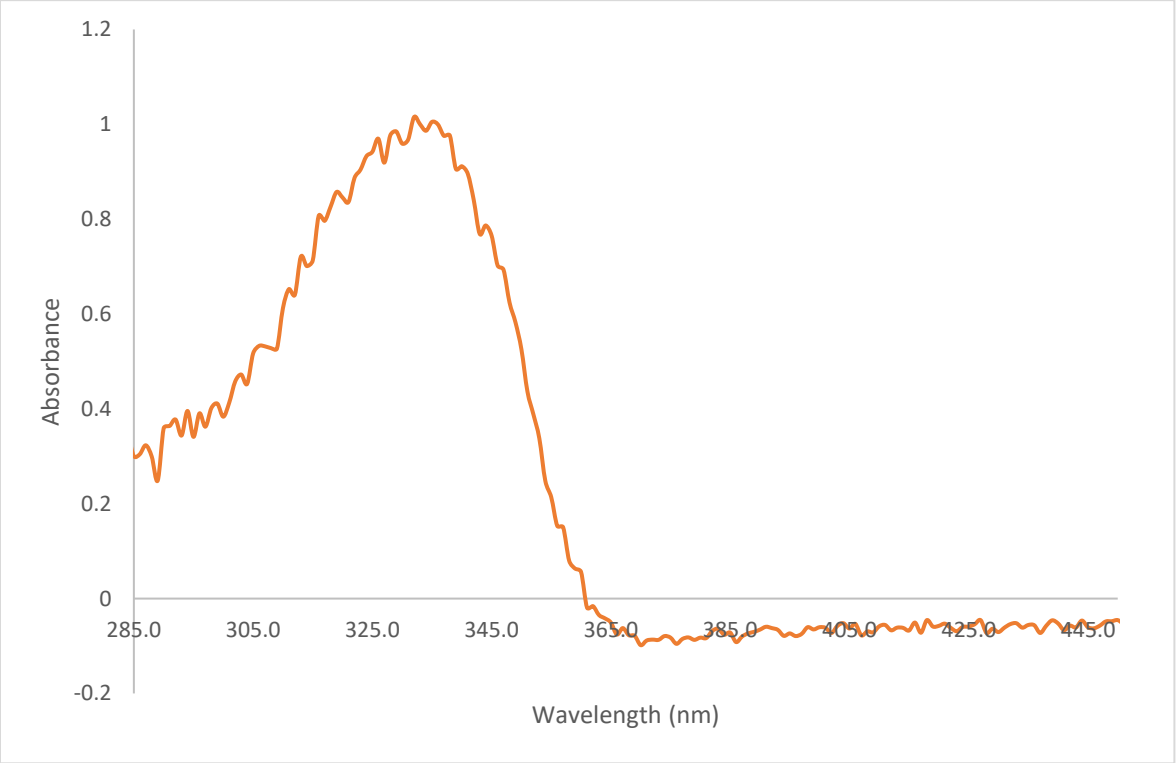

Normalized UV-Vis absorption spectra of **12d**$_{BPh4}$ in DCM.

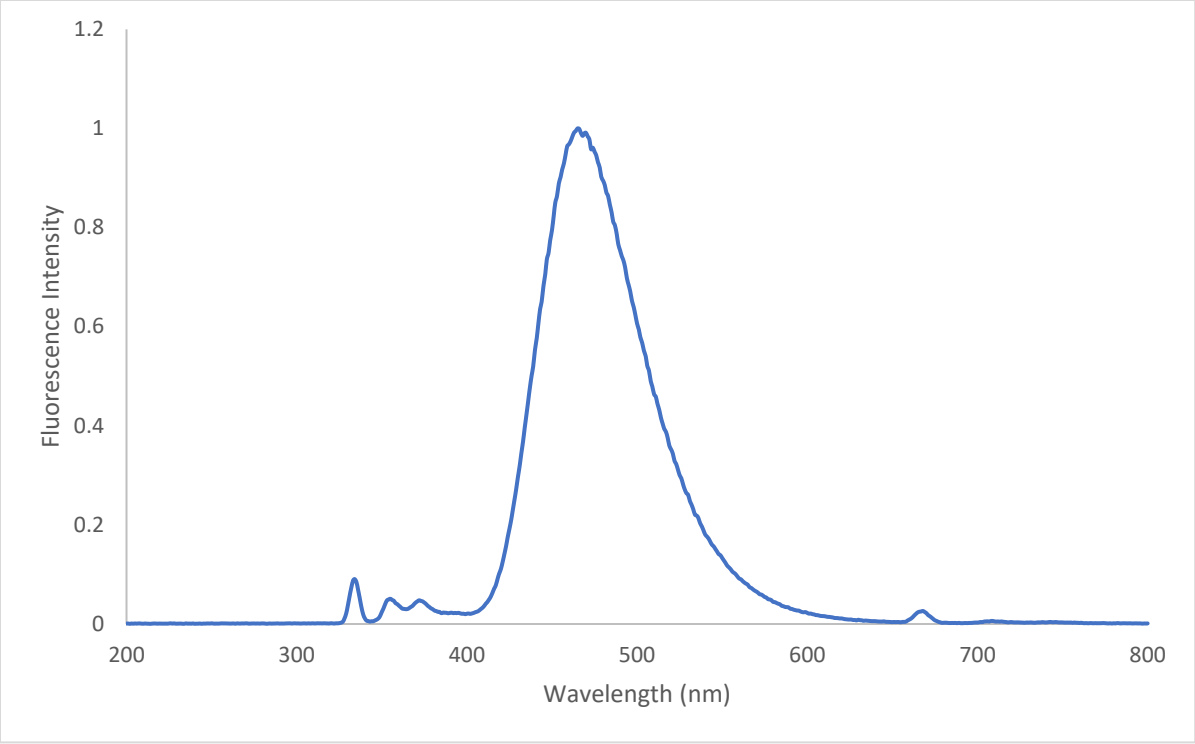

Normalized fluorescence emission spectra of **12a**$_{Cl}$ in DCM.

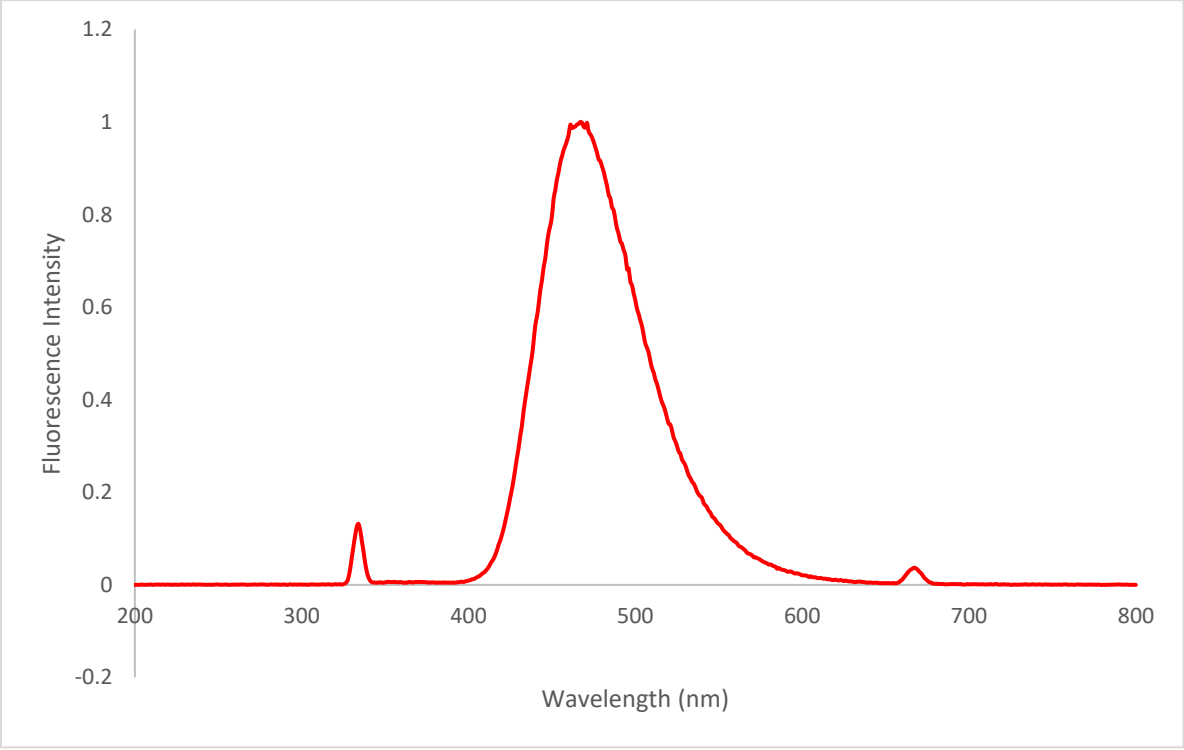

Normalized fluorescence emission spectra of **12b**$_{BF4}$ in DCM.

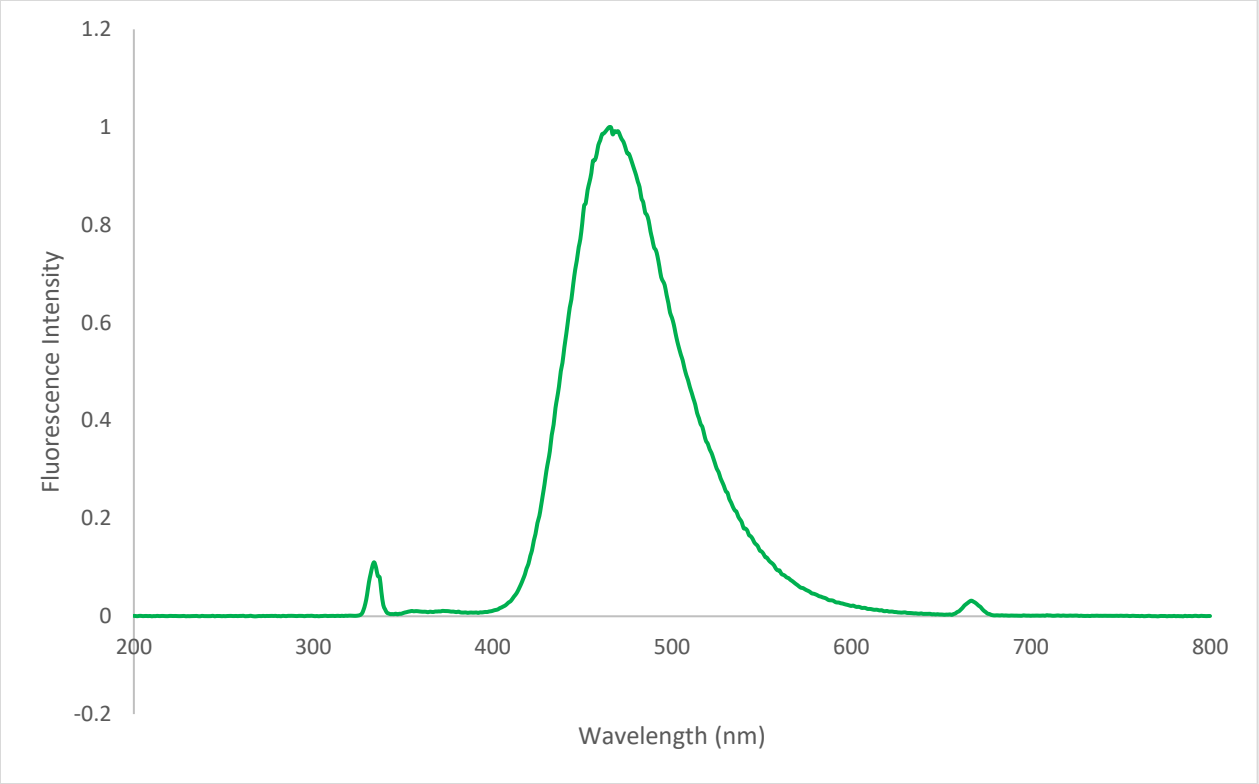

Normalized fluorescence emission spectra of **12c**$_{PF6}$ in DCM.

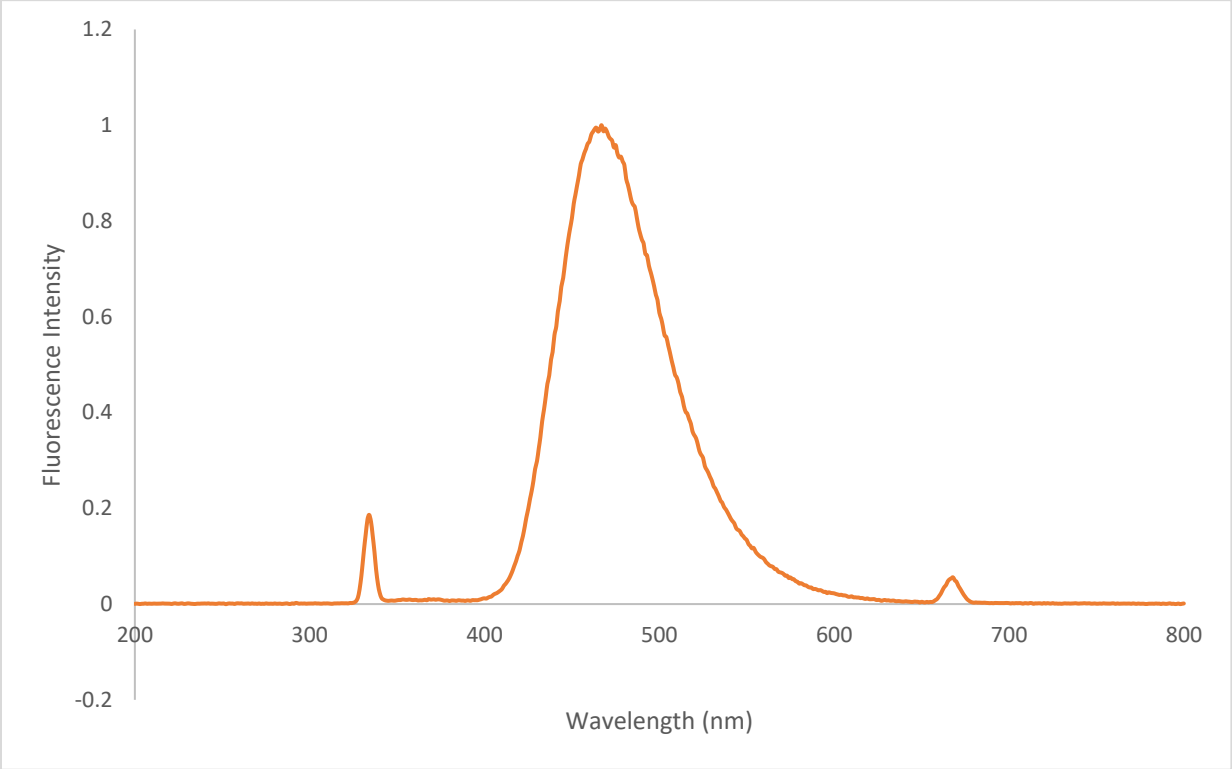

Normalized fluorescence emission spectra of **12d**$_{BPh4}$ in DCM.

Proton NMR

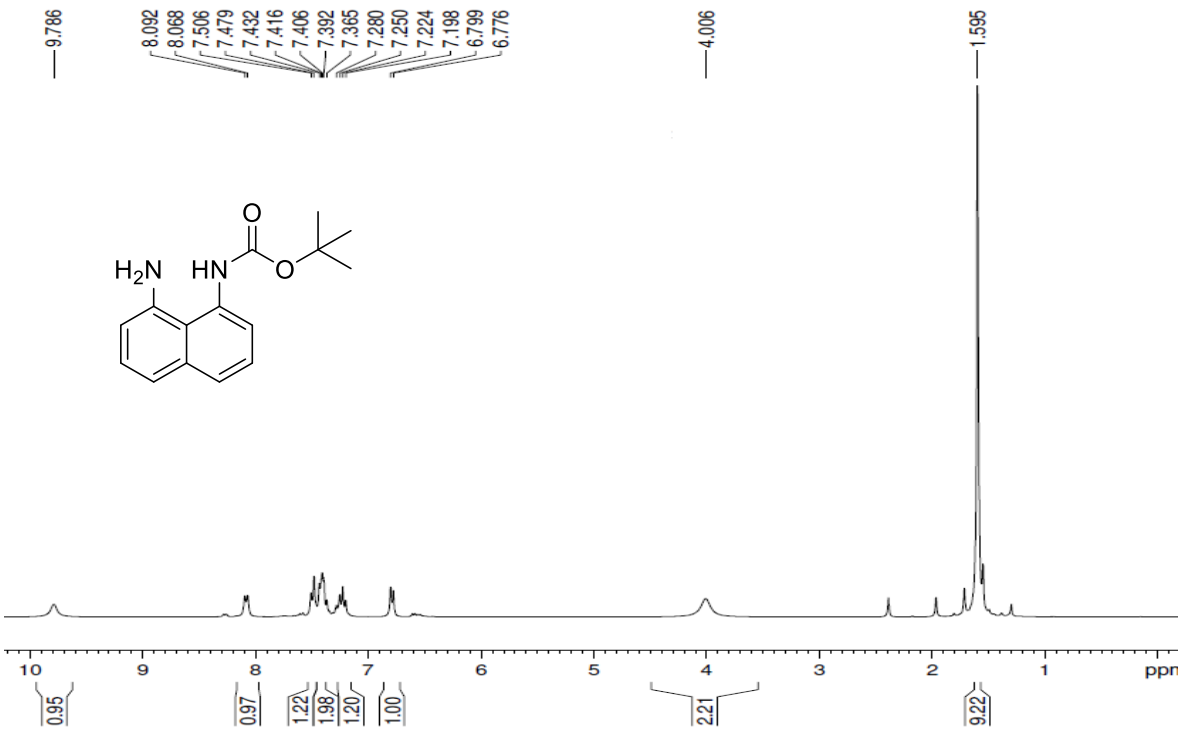

Carbon-13 NMR

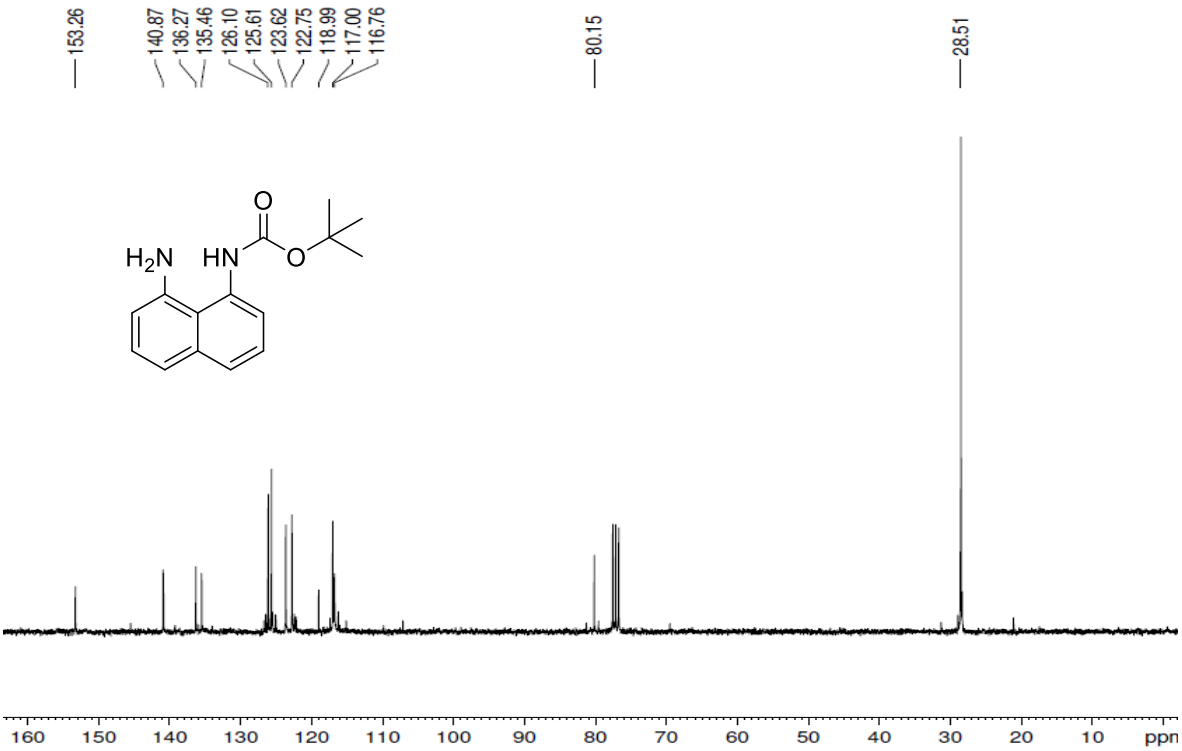

Proton NMR

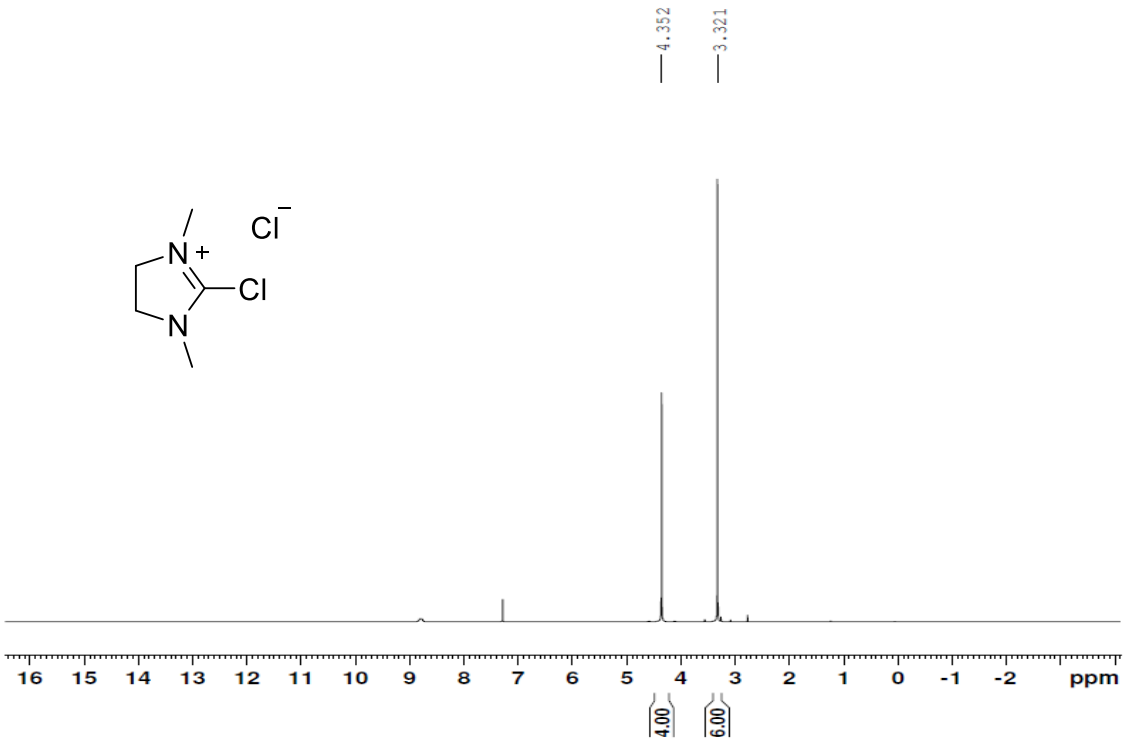

Proton NMR

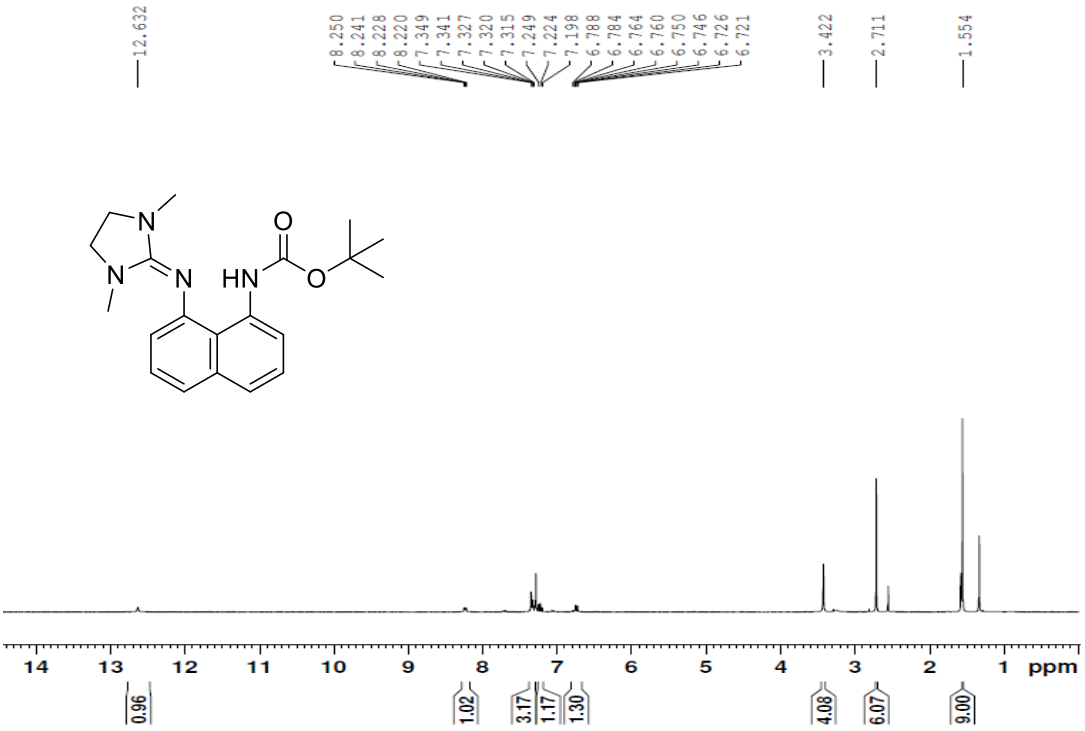

Carbon-13 NMR

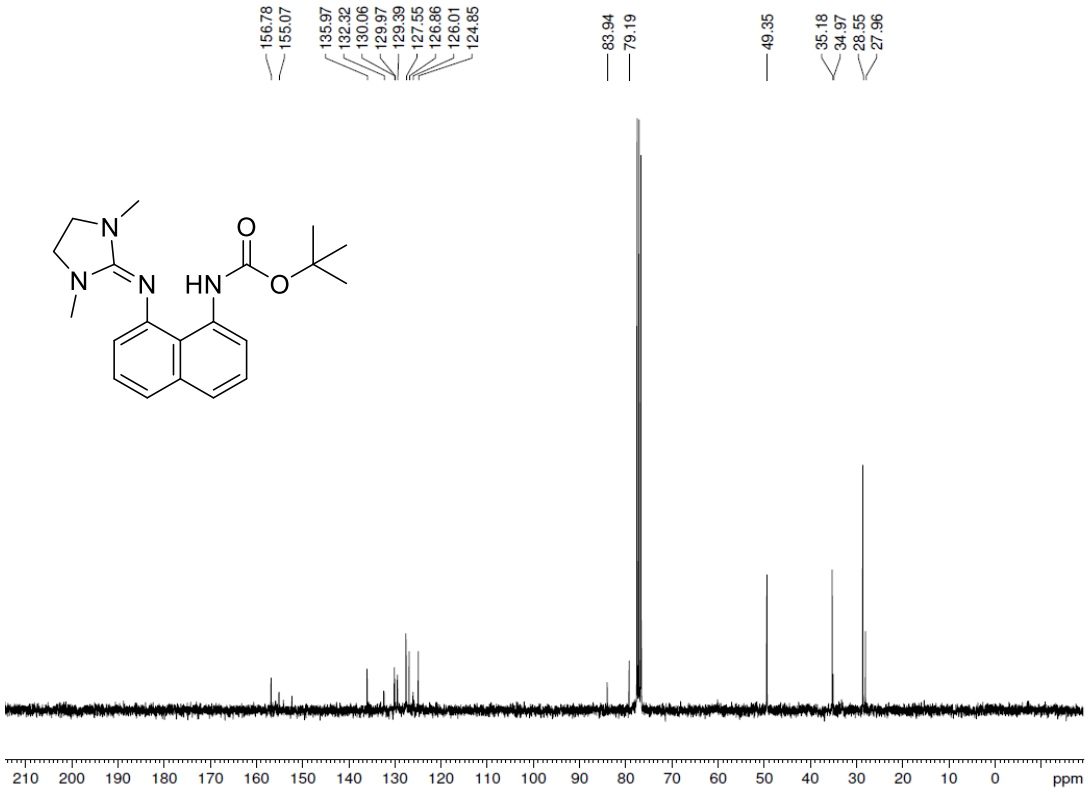

Proton NMR

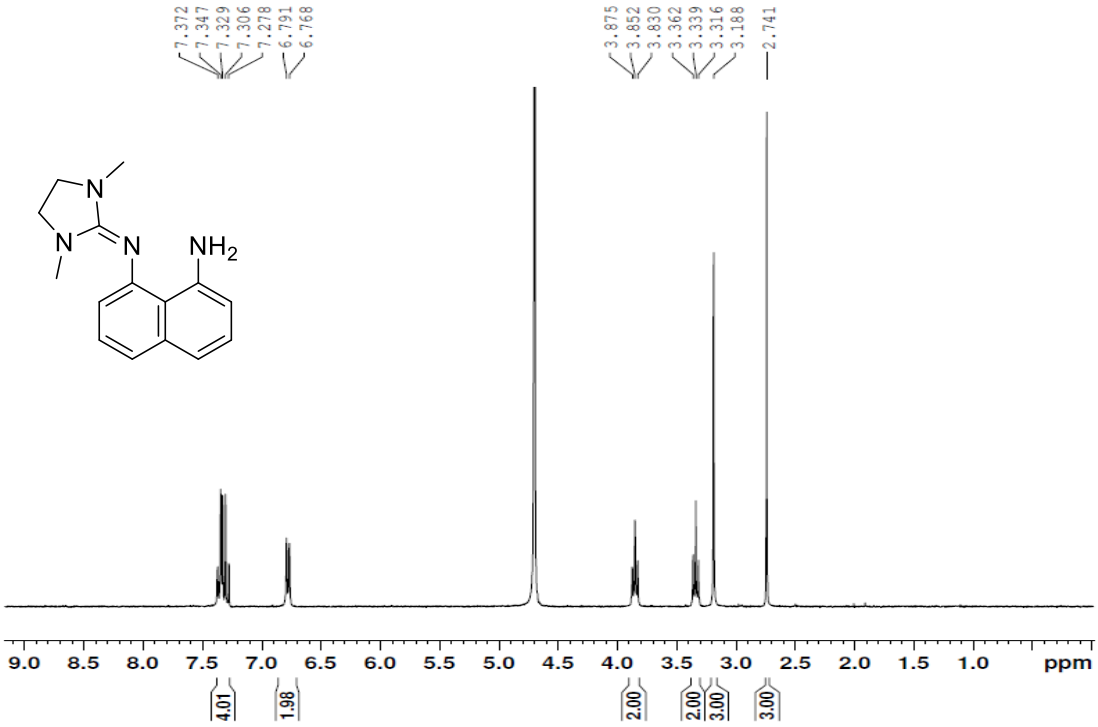

Carbon-13 NMR

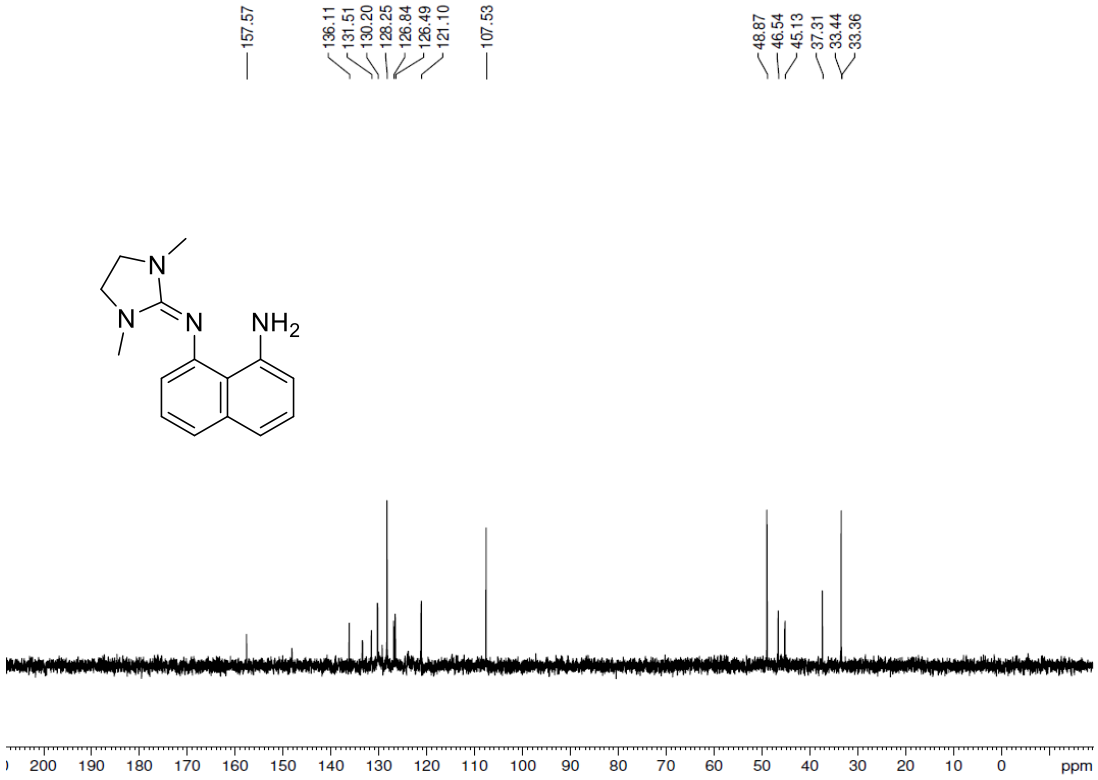

Proton NMR

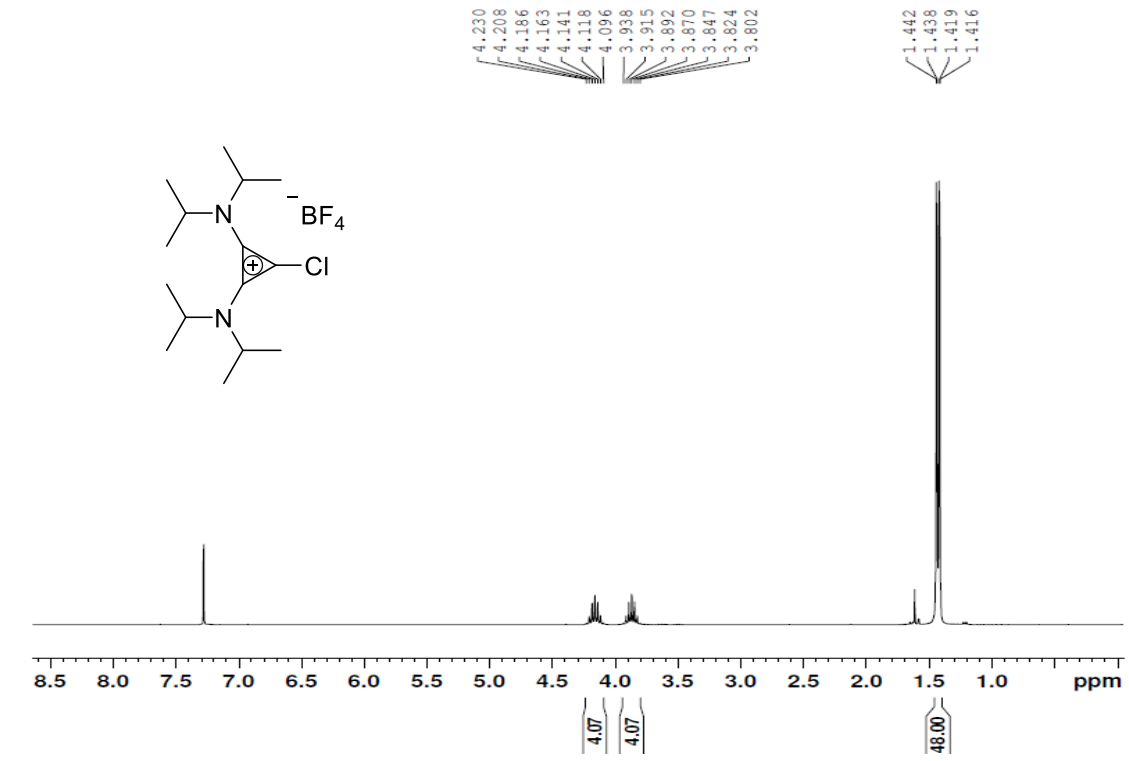

Carbon-13 NMR

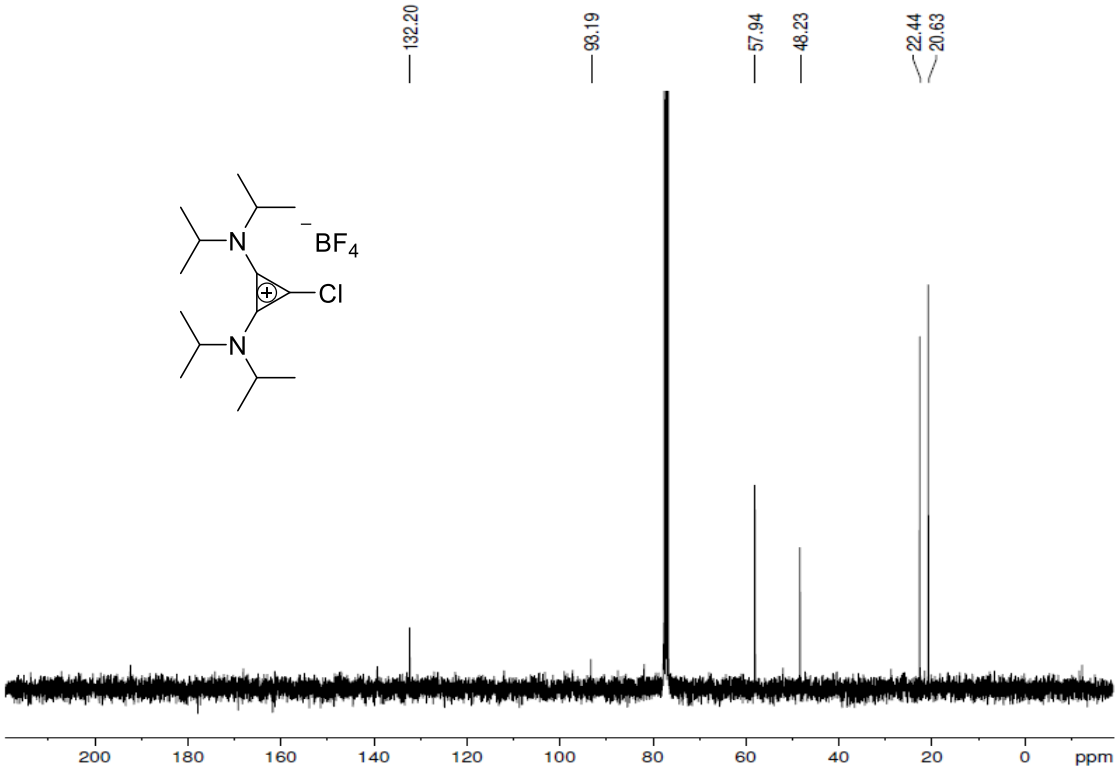

Boron-11 NMR

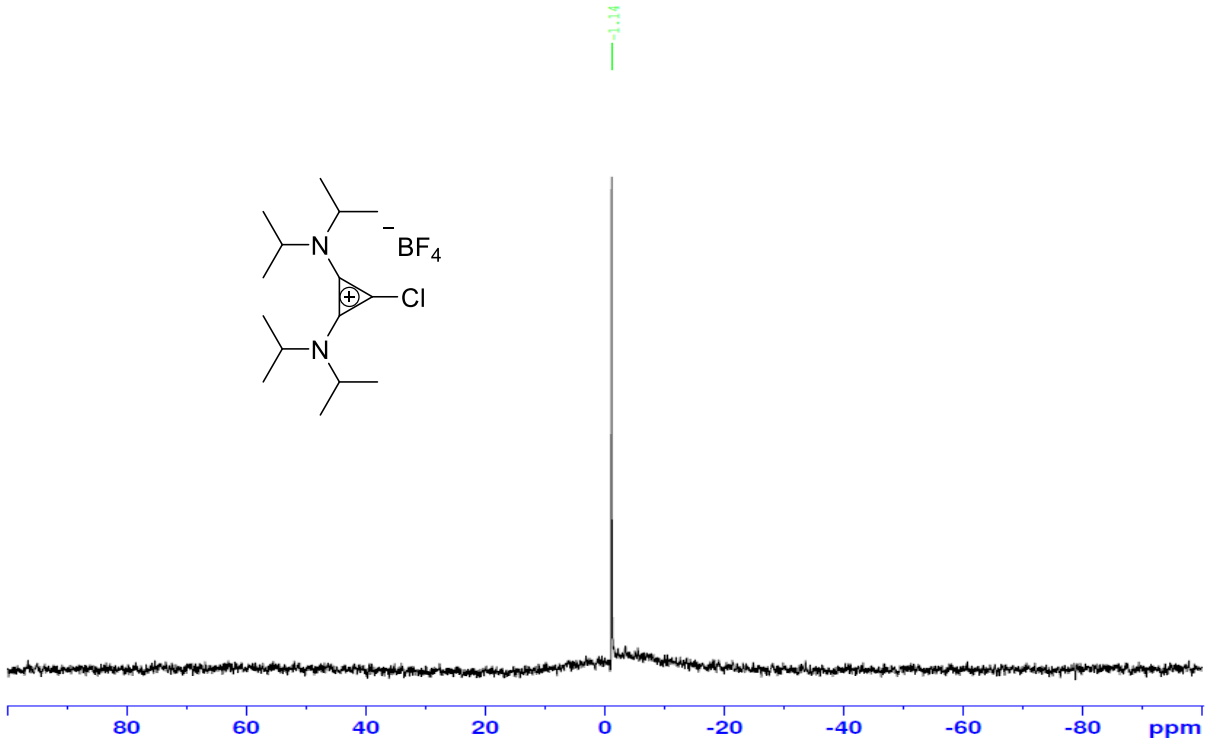

Fluorine NMR

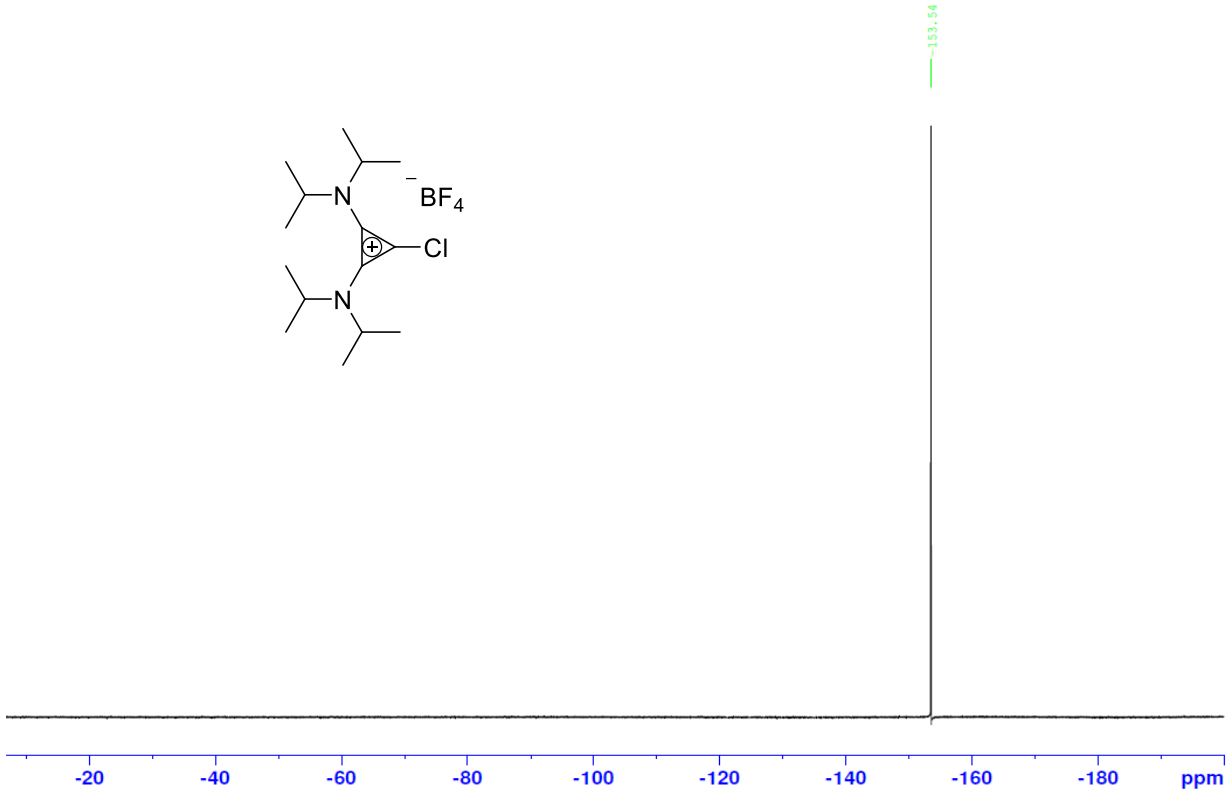

Proton NMR

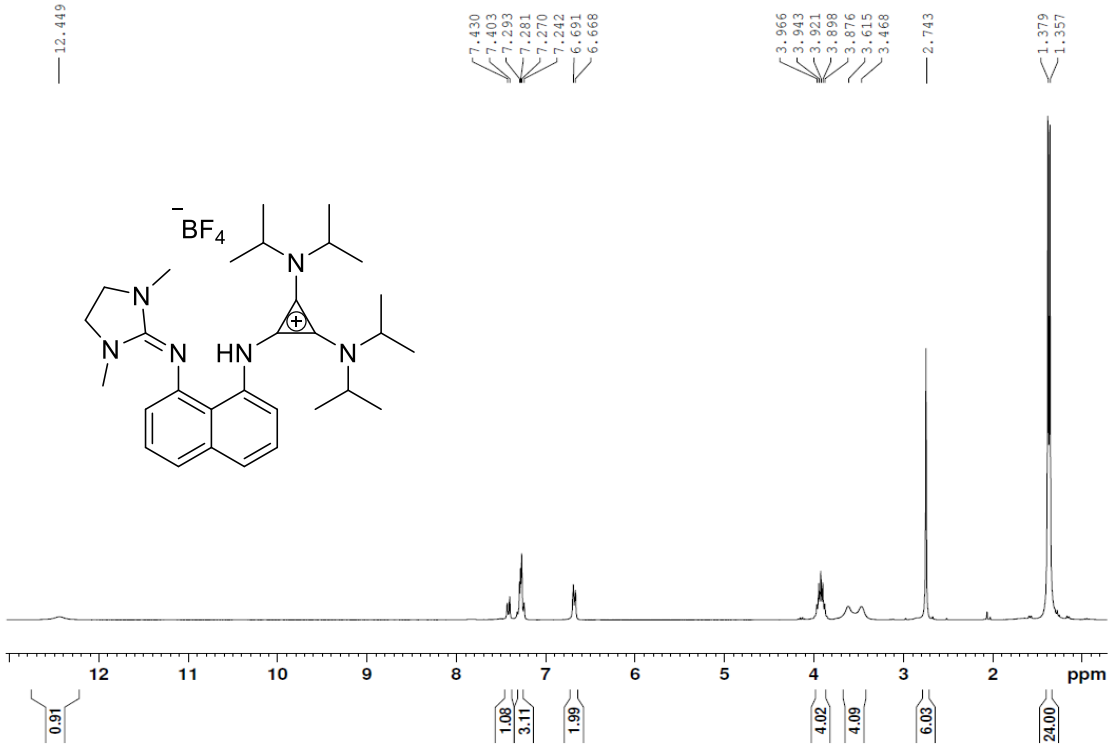

Carbon-13 NMR

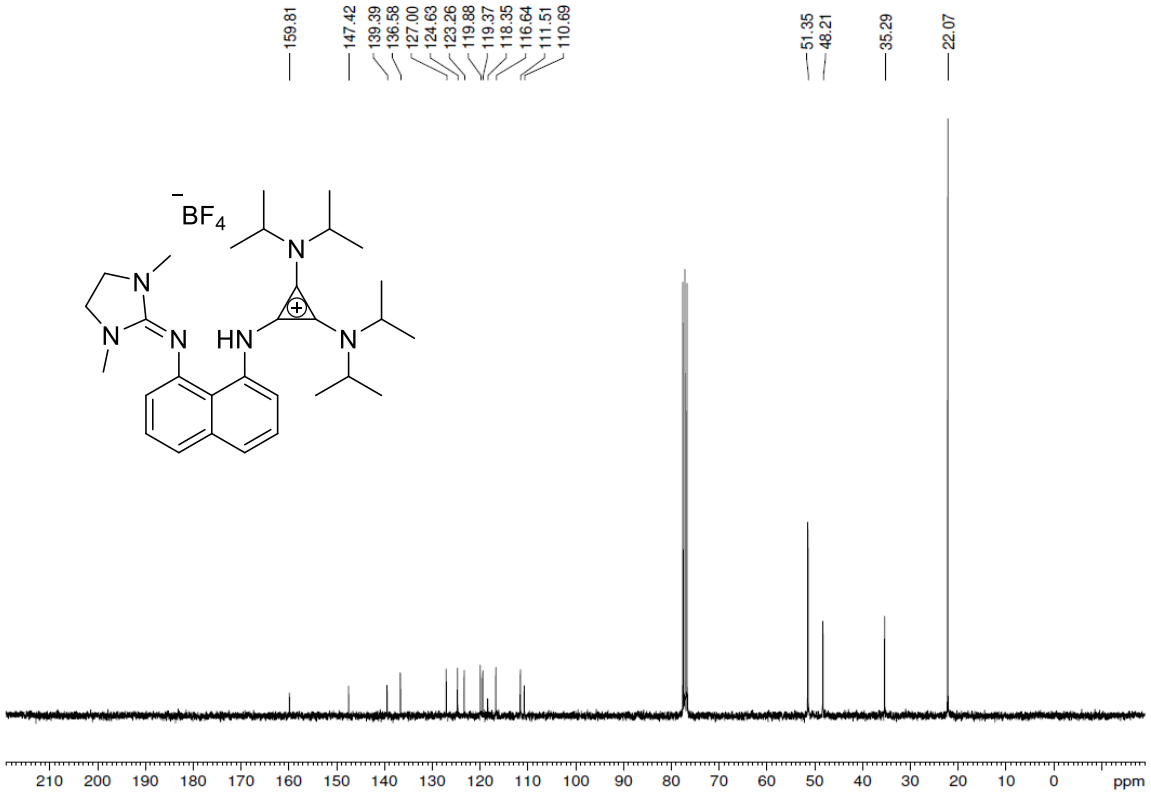

Boron NMR

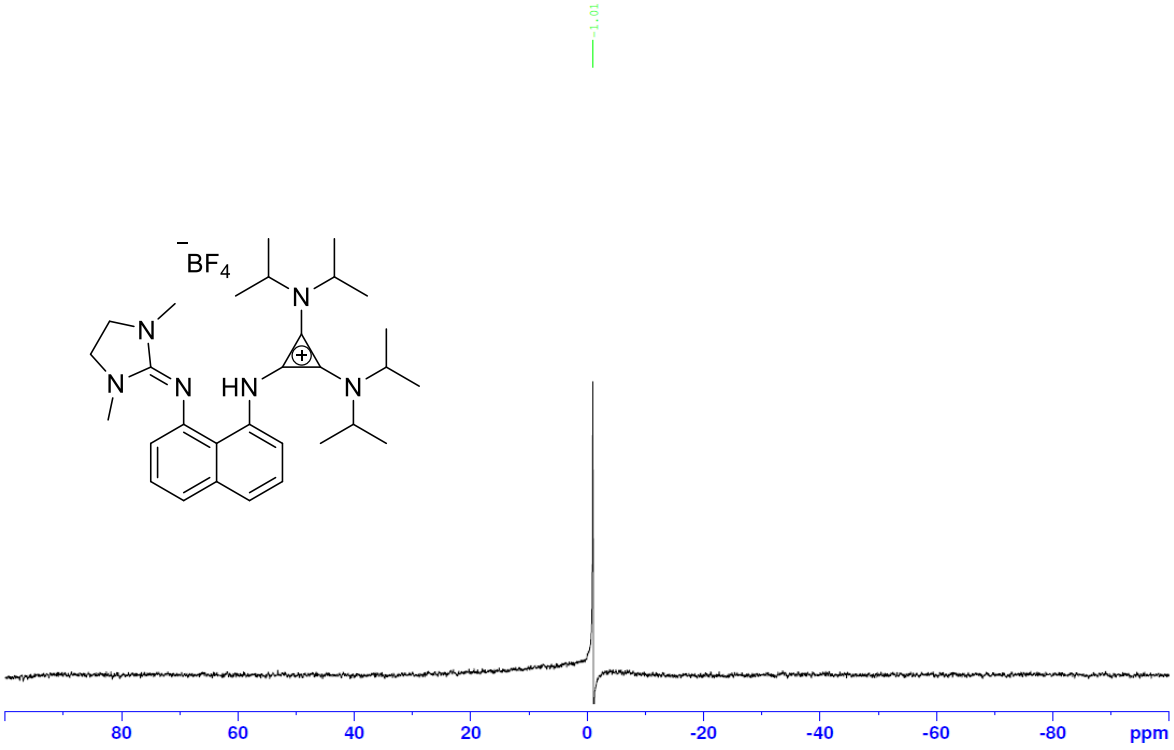

Fluorine-19 NMR

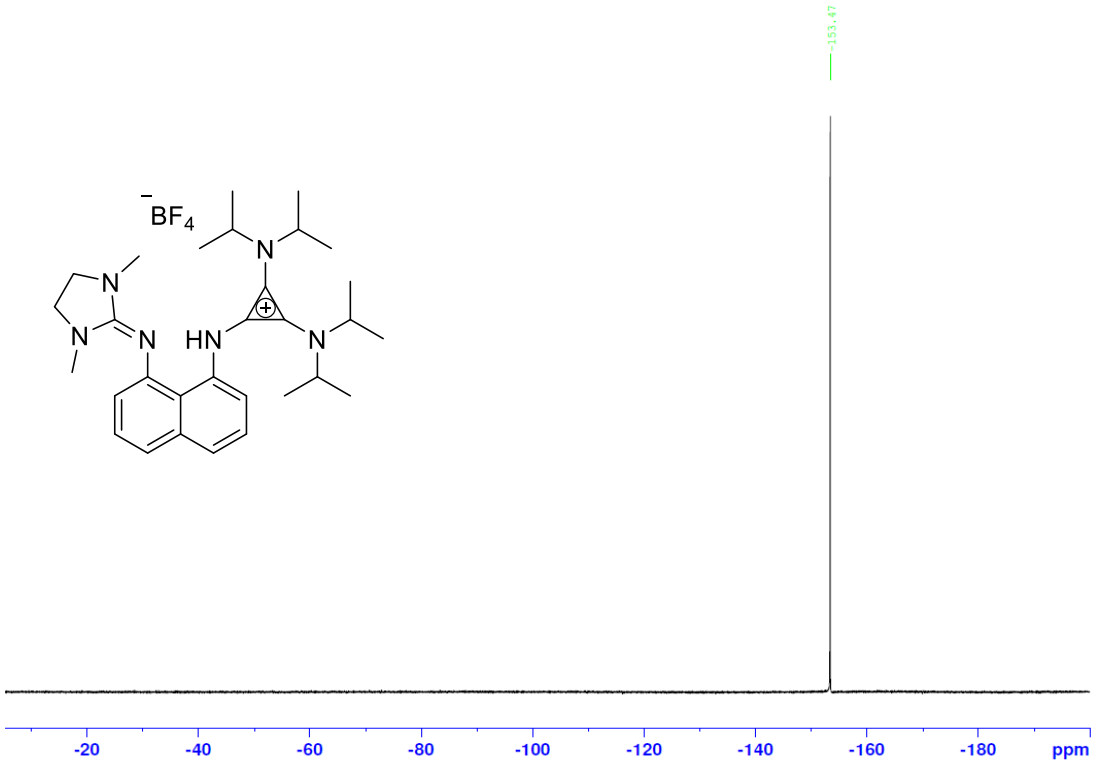

Proton NMR

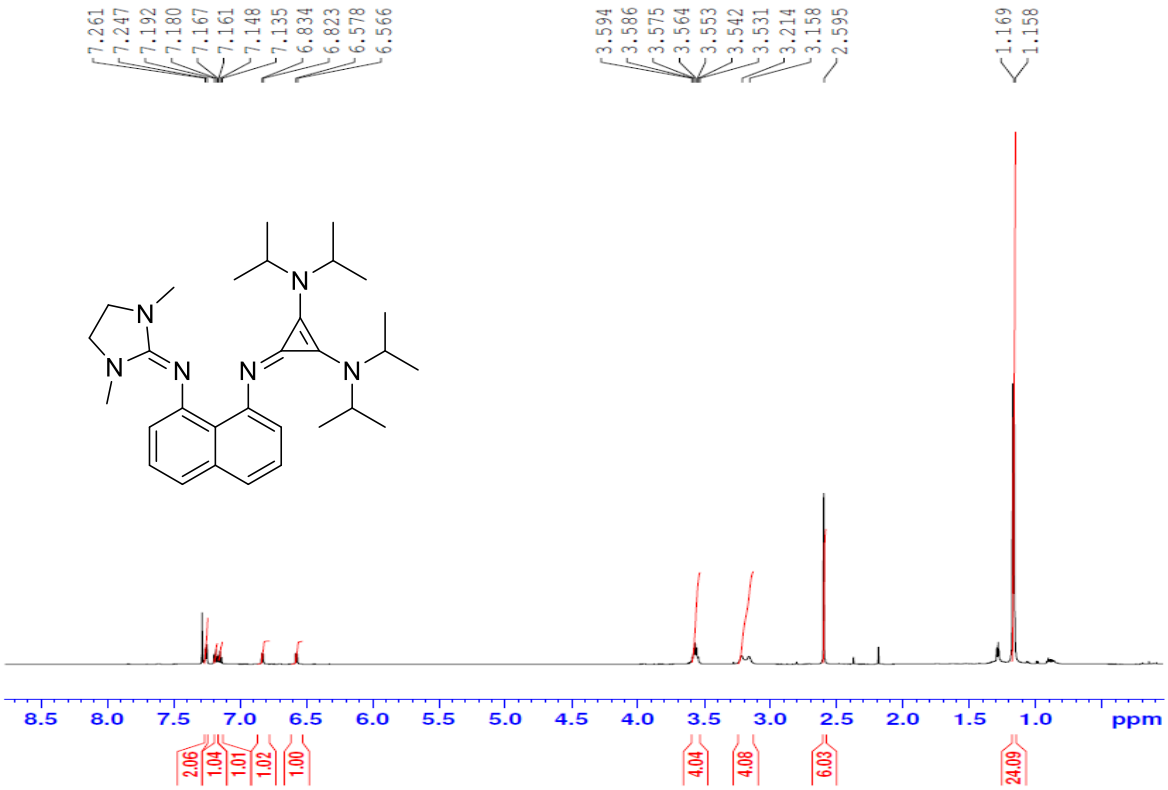

Carbon-13 NMR

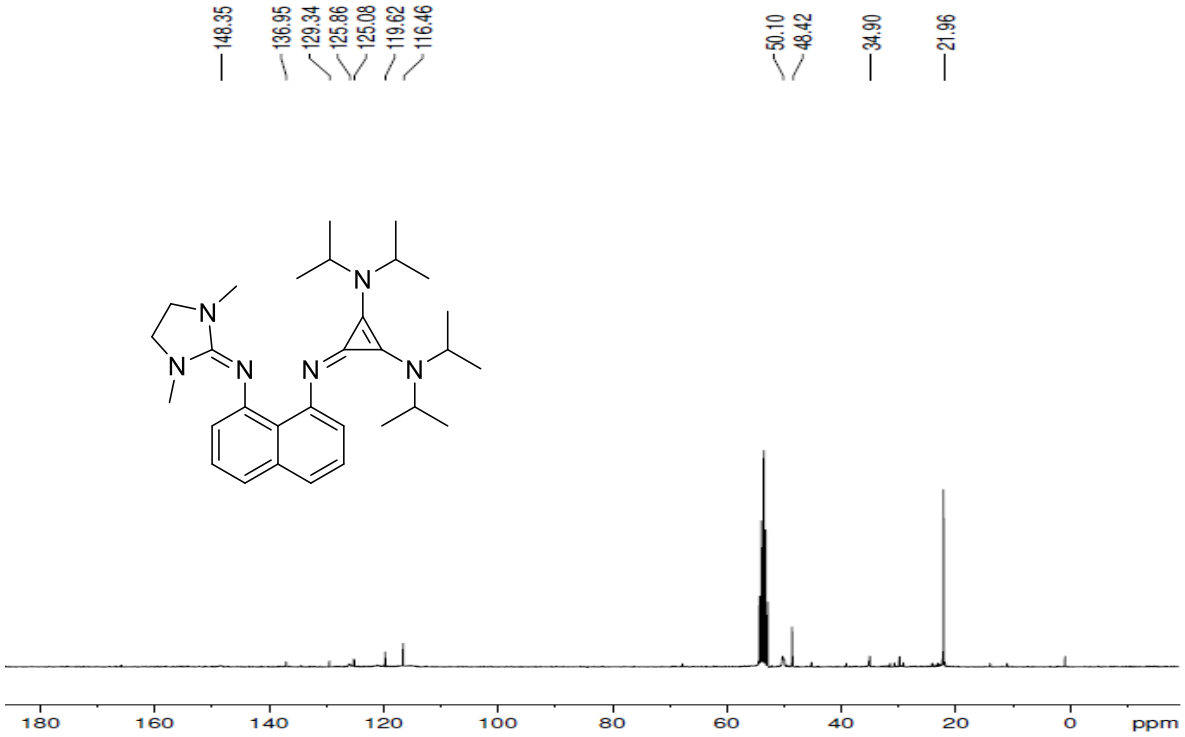

Proton NMR

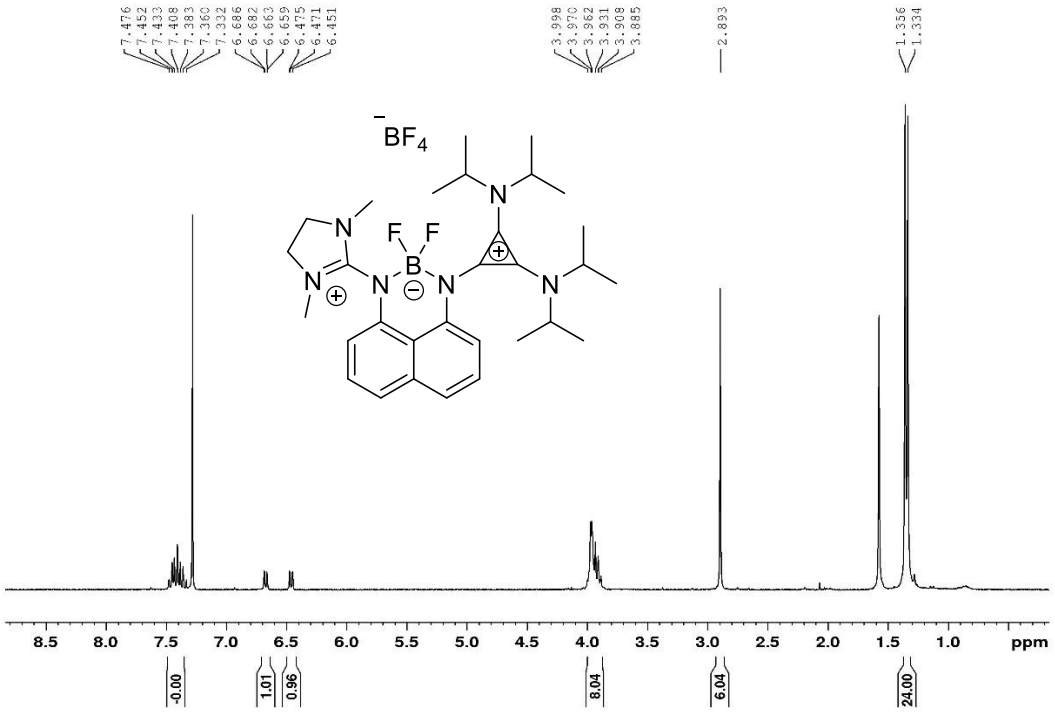

Carbon-13 NMR

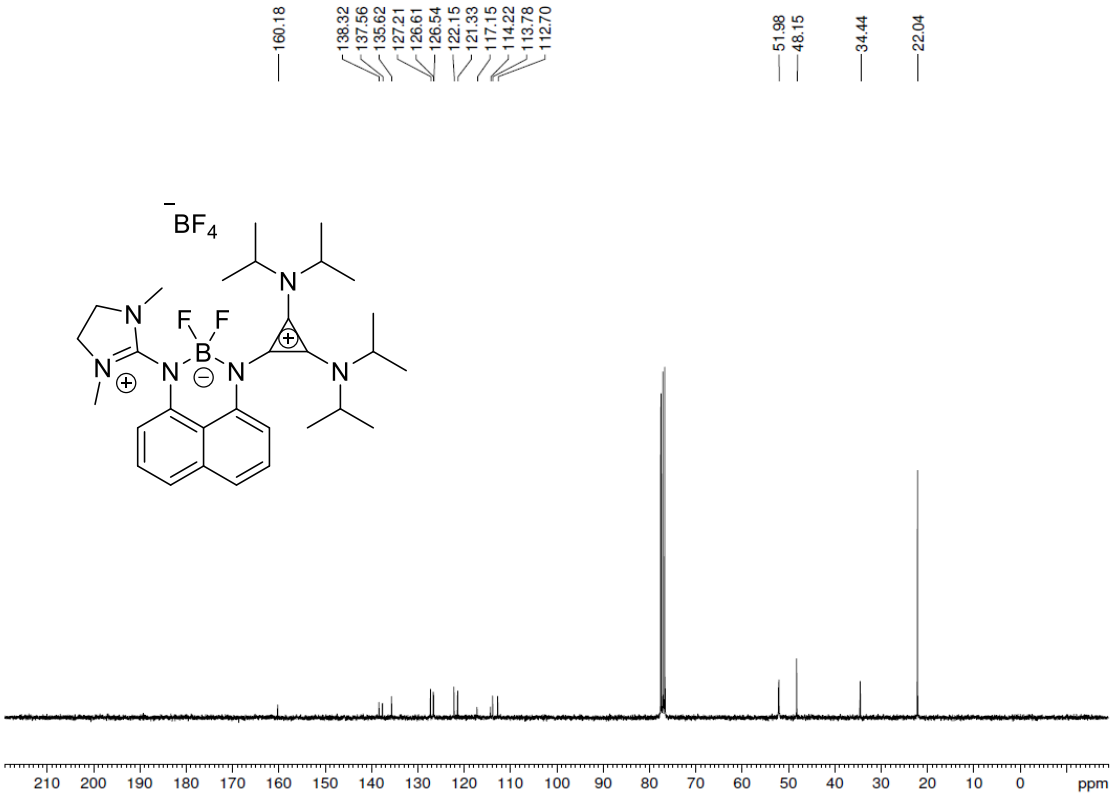

Fluorine-19 NMR

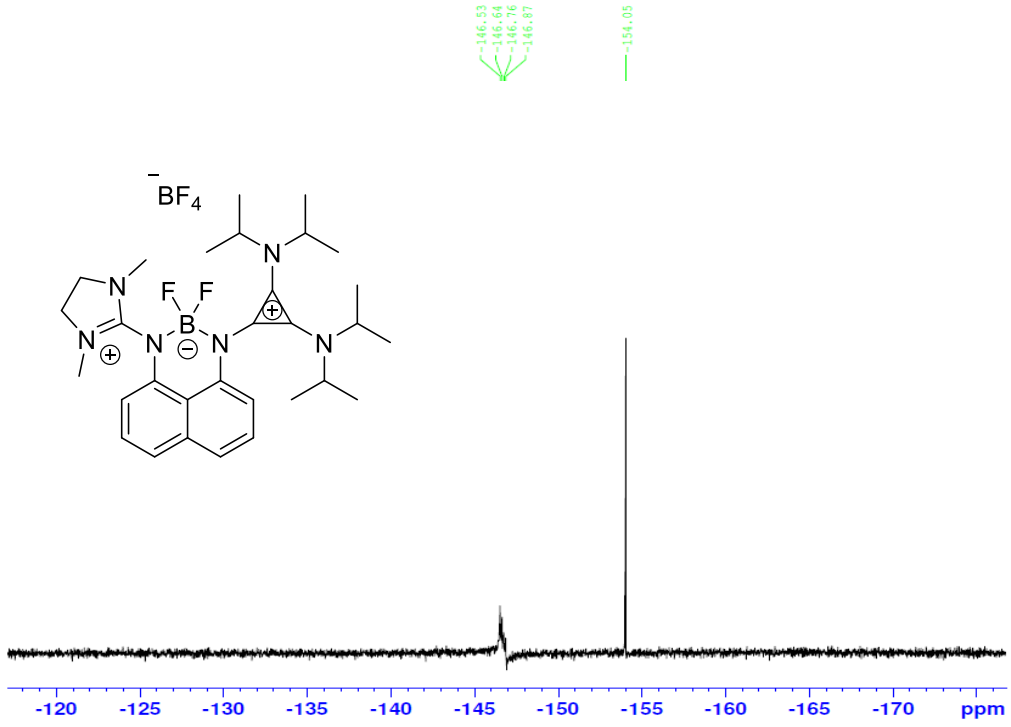

Boron NMR

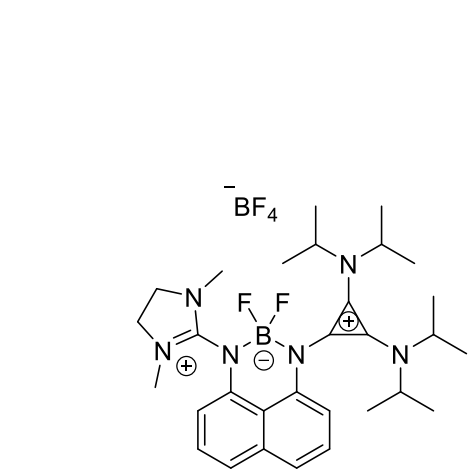

Proton NMR

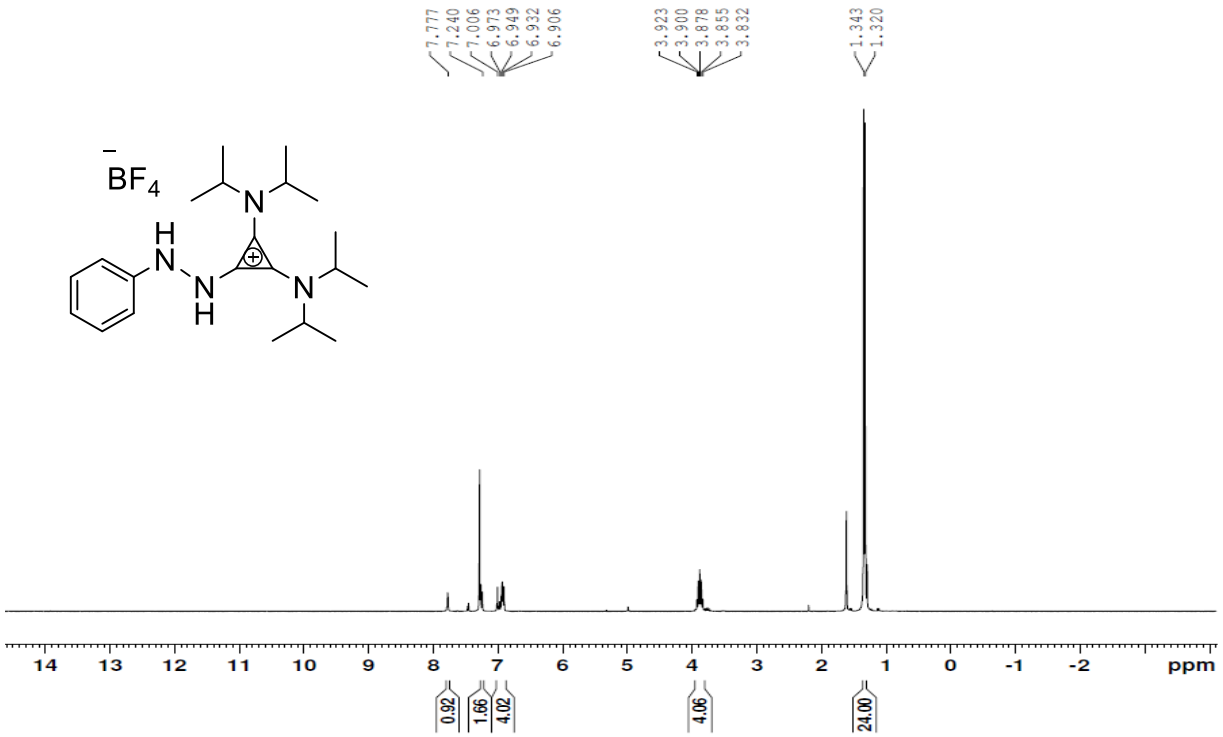

Carbon-13 NMR

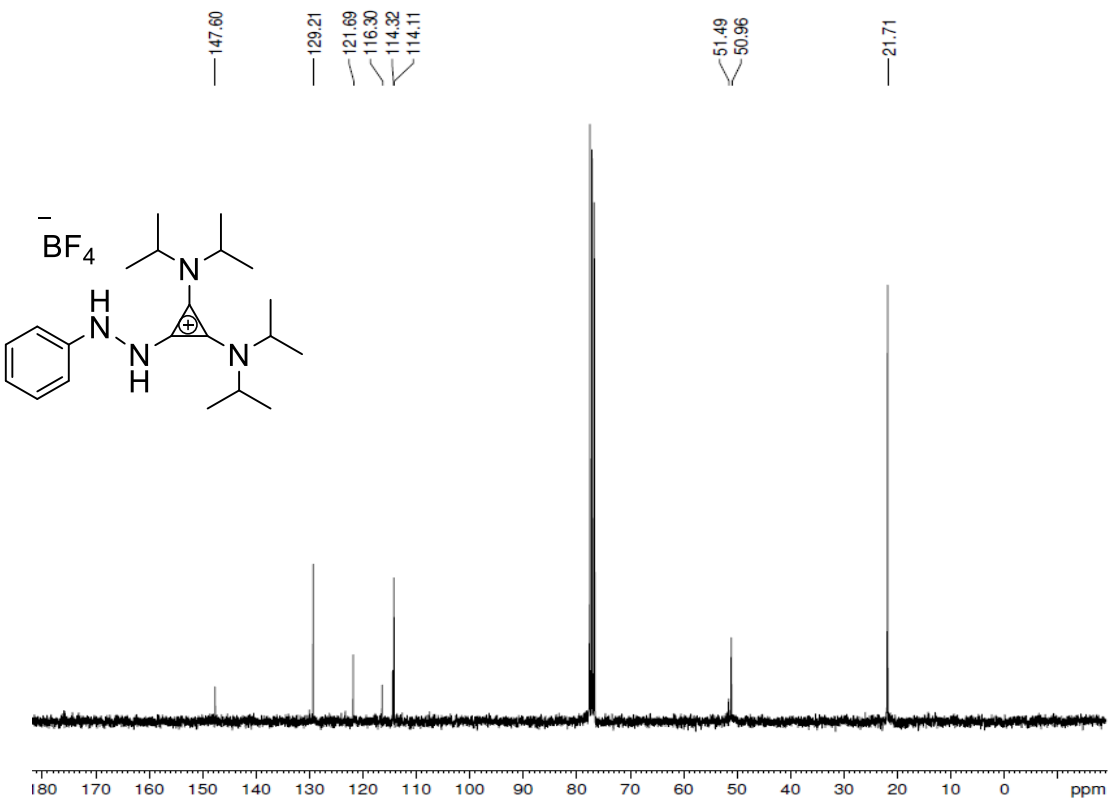

Fluorine-19 NMR

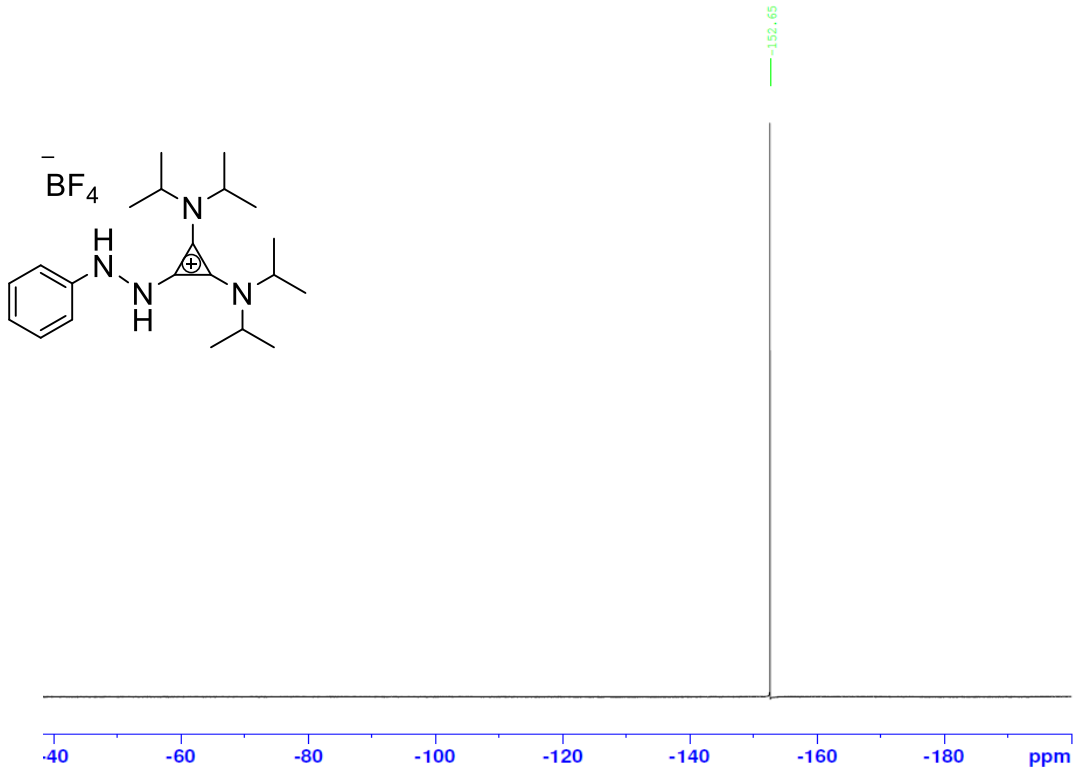

Boron-11 NMR

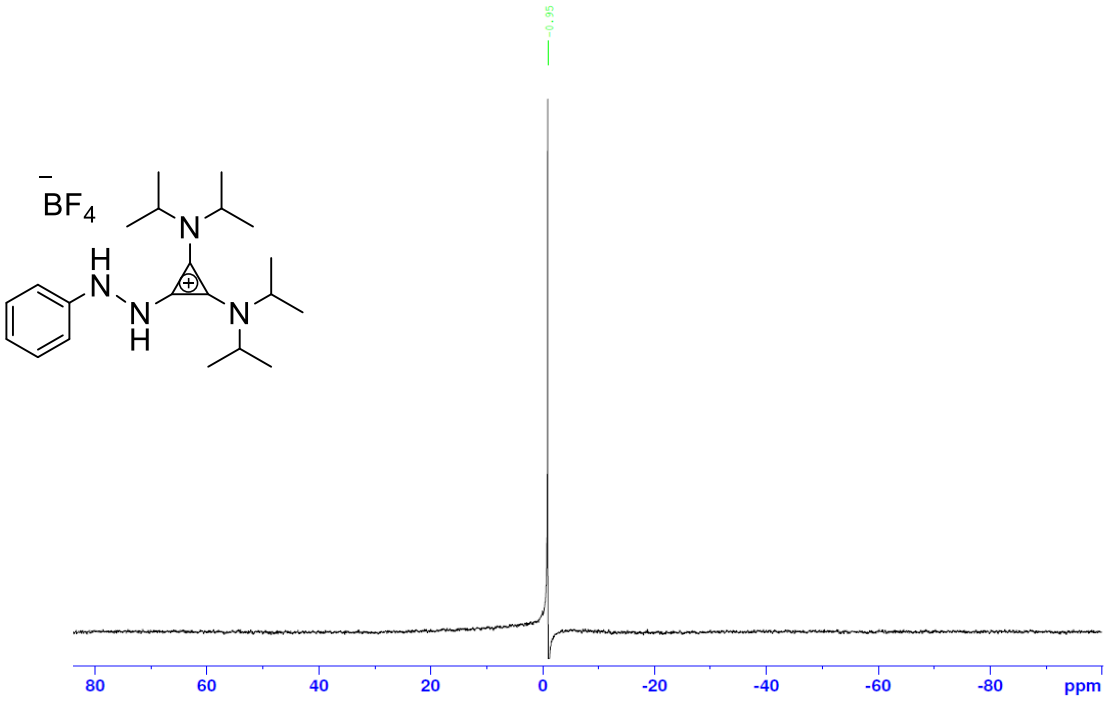

Proton NMR

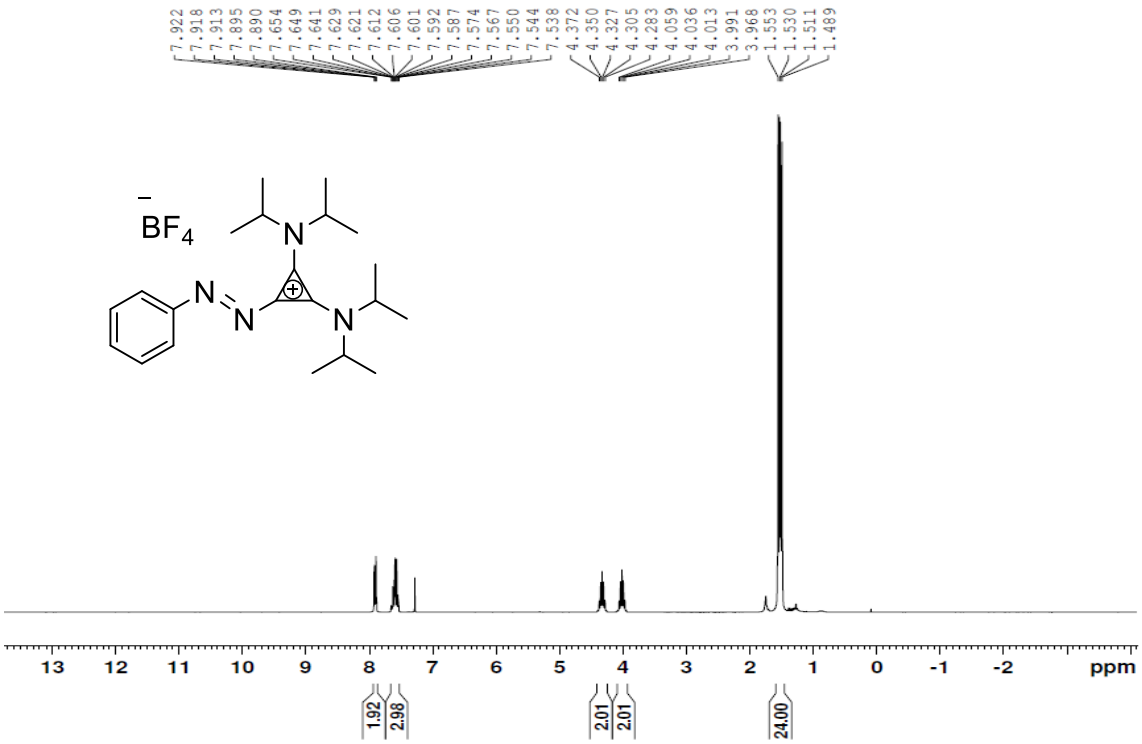

Carbon-13 NMR

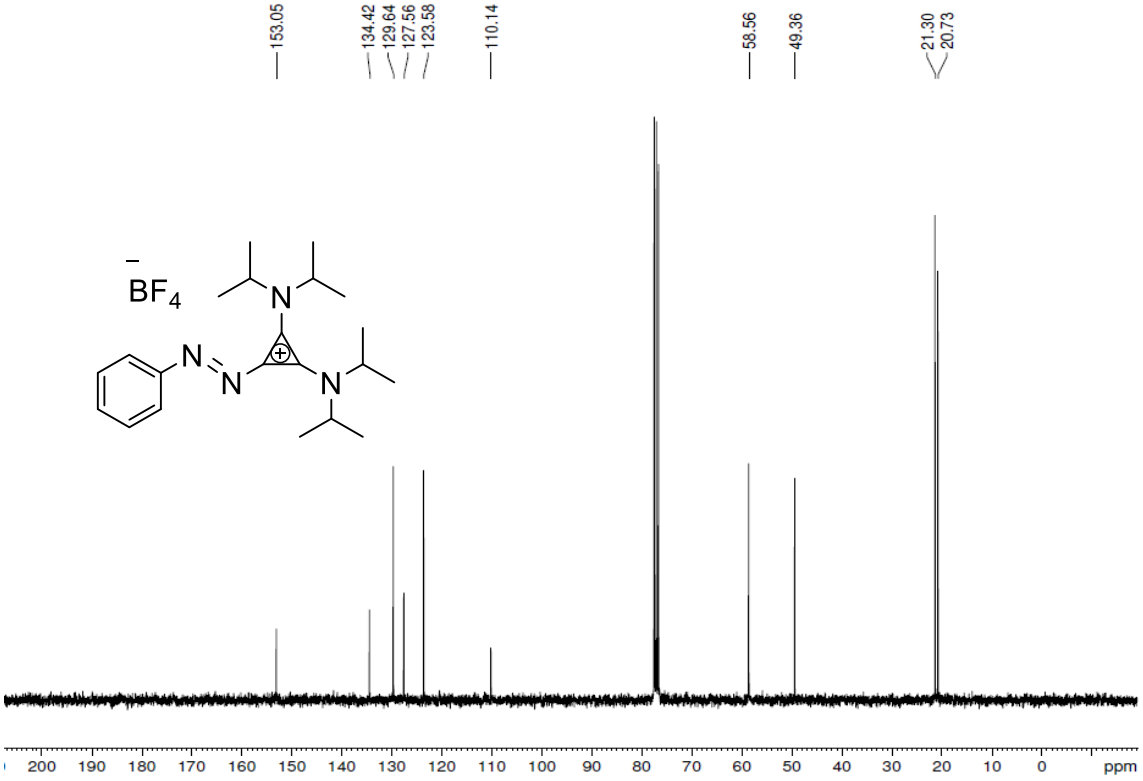

Fluorine-19 NMR

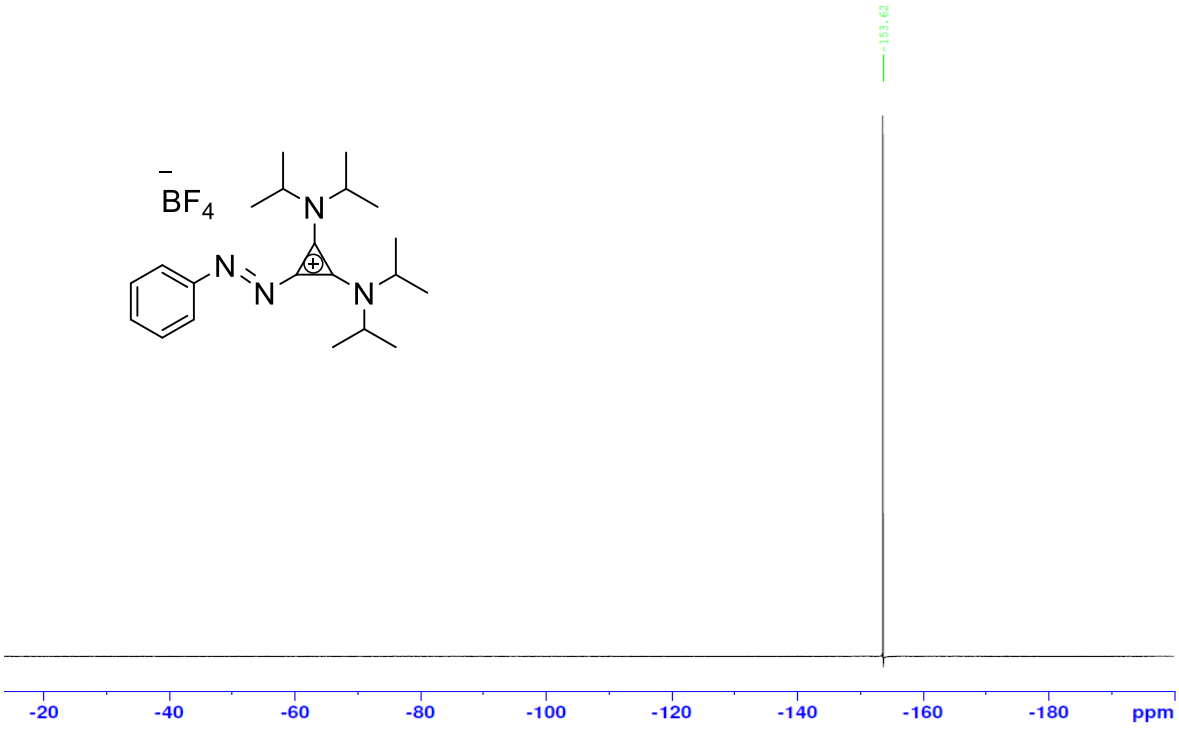

Boron-11 NMR

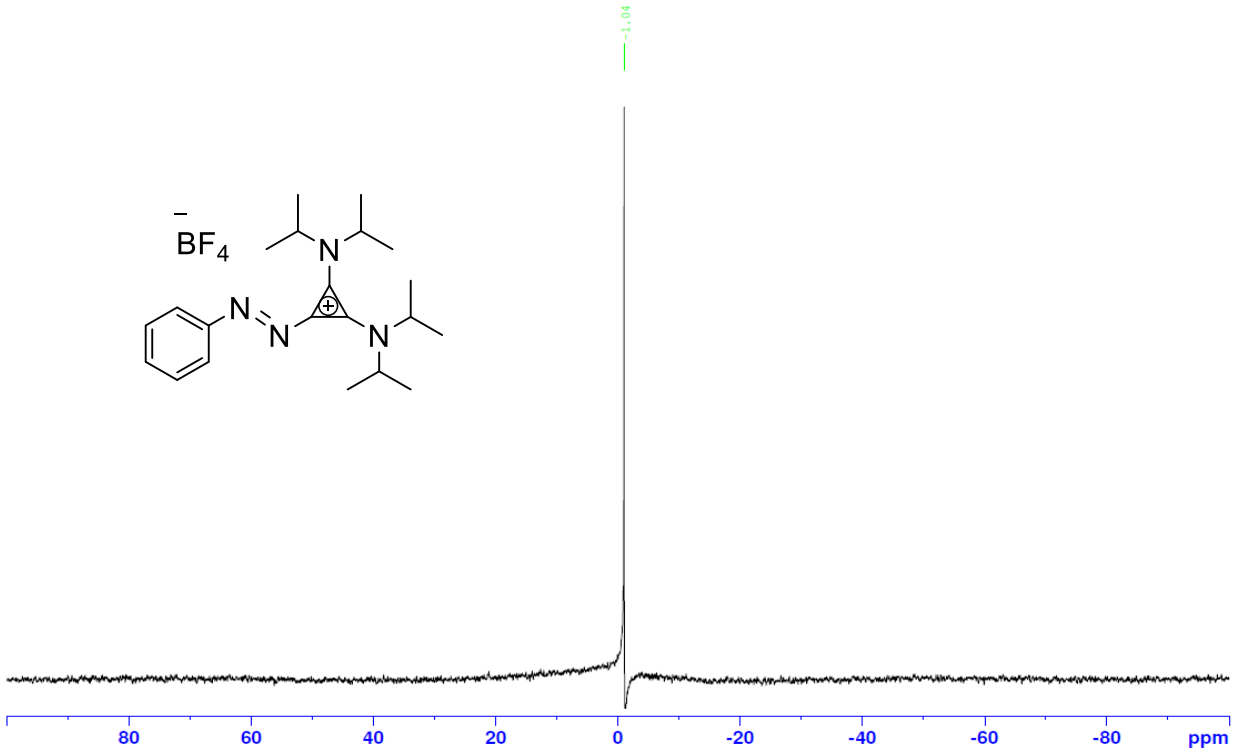

Appendix B: DFT Calculated Geometries, Thermochemical and Crystal Structure Data, and Calculated Molecular Orbitals

Janus (**12**$_{in}$) Excited State

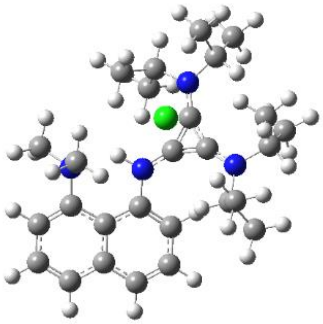

Computational model of Janus (**12**$_{in}$) excited state.

opt=calcfc freq=noraman td=singlets M062X/6-31+g(d,p) scrf=(smd,solvent=dichloromethane) geom=connectivity empiricaldispersion=gd3

Zero-point correction= 0.638315 (Hartree/Particle)

Thermal correction to Energy= 0.674425

Thermal correction to Enthalpy= 0.675369

Thermal correction to Gibbs Free Energy= 0.571323

Sum of electronic and zero-point Energies= -1731.501052

Sum of electronic and thermal Energies= -1731.464943

Sum of electronic and thermal Enthalpies= -1731.463999

Sum of electronic and thermal Free Energies= -1731.568044

N 0.90342300 -0.27637900 -0.41870300

H 1.32250100 -1.20468800 -0.05601600

N -1.91857800 2.04493700 0.04060500

N -2.43357400 -1.62956900 -0.59123200

C -0.41361900 -0.02580400 -0.39413000

C -1.49478300 0.82391300 -0.21625400

C -1.69101900 -0.55433100 -0.43171300

C 1.89492100 0.62358500 -0.69778400

C 3.25105500 0.26323500 -0.34212000

C 3.62838400 -0.96569500 0.22422200

C 4.98105800 -1.20081600 0.61213500

H 5.24944700 -2.15825600 1.04778800

C 5.93882800 -0.22395500 0.42461500

H 6.96653700 -0.40697900 0.72496800

C 5.59278500 1.00733200 -0.15988100

H 6.34371500 1.77877100 -0.30373000

C 4.26081400 1.27212400 -0.56094000

C 3.90148900 2.49708800 -1.16657300

H 4.67854700 3.24096000 -1.32120400

C 2.58292500 2.75848500 -1.62451300

H 2.36826900 3.67529700 -2.16438700

C 1.59302200 1.83809500 -1.39958500

H 0.58468800 1.98582300 -1.77493400

C 2.58113300 -2.54926000 1.75394800

C 2.81263600 -3.09175200 -0.60218000

H 2.43463400 -1.72480000 2.45497300

H 3.48971900 -3.10264700 2.02755200

H 3.76553300 -3.62341500 -0.46841700

H 2.78297300 -2.66751600 -1.60969800

N 2.64453200 -2.01704500 0.38666700

H 1.72734800 -3.22906100 1.82924100

H 1.99167800 -3.80761800 -0.49178600

C -0.93078200 3.06190500 0.47915100

C -1.21017100 3.50814900 1.91203500

C -0.88141400 4.23243700 -0.49799500

H -1.23093400 2.64431800 2.58262600

H -0.70436500 3.88942900 -1.52182900

C -3.35740000 2.38911700 0.04455200

C -3.97867600 2.10493600 -1.32052600

C -4.08154900 1.73589300 1.22075700

H -3.90847000 1.04783400 -1.59419900

C -1.75394000 -2.92704400 -0.82666200

C -0.92844100 -2.88561300 -2.10962500

C -0.92788300 -3.33317200 0.38910900

H -1.54446500 -2.58247200 -2.96149800

H -1.54829200 -3.38195600 1.28807500

C -3.90641700 -1.59269200 -0.48782600

C -4.38304000 -2.39097200 0.72177300

C -4.55411100 -2.04804400 -1.79236600

H -4.18848300 -1.45675300 -2.63734800

Cl -0.91419300 -0.32461200 2.95508000

H -0.06528800 4.90353200 -0.21347900

H -1.81133300 4.81059800 -0.48001700

H -2.15828100 4.05086300 1.98831100

H -0.41076300 4.18284300 2.23276500

H -3.47303100 2.68983900 -2.09488200

H -5.03656900 2.38198000 -1.31060300

H -3.68723500 2.10946800 2.16939600

H -5.15043900 1.96483600 1.17177900

H -3.95920100 0.64983000 1.22267900

H -5.46775800 -2.28625200 0.81992100

H 0.03446000 2.54952500 0.47282400

H -3.38267600 3.47137800 0.19490700

H -4.15940400 -0.54489400 -0.33111300

H -2.56070800 -3.65134900 -0.95882400

H -3.91174600 -2.02355500 1.63806800

H -4.15623700 -3.45664600 0.61257200

H -5.63753600 -1.91488500 -1.72024700

H -4.36183100 -3.10648200 -1.99426800

H -0.51970200 -3.87995800 -2.31244900

H -0.08670600 -2.18949500 -2.02212000

H -0.12757600 -2.61089900 0.58006600

H -0.47517700 -4.31461100 0.2170790

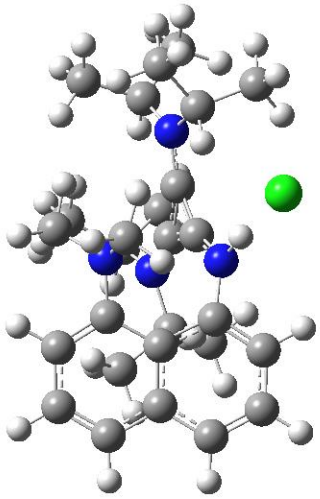

Computational model of Janus (**12$_{out}$**) excited state.

opt=calcfc freq=noraman td=singlets M062X/6-31+g(d,p) scrf=(smd,solvent=dichloromethane) geom=connectivity empiricaldispersion=gd3

Zero-point correction= 0.639011 (Hartree/Particle)

Thermal correction to Energy= 0.675055

Thermal correction to Enthalpy= 0.675999

Thermal correction to Gibbs Free Energy= 0.572820

Sum of electronic and zero-point Energies= -1731.503664

Sum of electronic and thermal Energies= -1731.467621

Sum of electronic and thermal Enthalpies= -1731.466677

Sum of electronic and thermal Free Energies= -1731.569855

N 0.44574300 1.53662000 -0.82160100

H -0.05027600 2.44306300 -0.92451000

N 0.29758200 -2.09103600 -0.71749400

N -2.77165700 0.03060200 -0.01708200

C -0.28738400 0.44017800 -0.63354400

C -0.36316900 -0.94268700 -0.58340700

C -1.49633800 -0.16235600 -0.33524500

C 1.84753600 1.53472600 -0.64604700

C 2.47580000 0.82608400 0.41403500

C 1.81454100 0.29871600 1.57750900

C 2.47844900 -0.66863600 2.42041200
H 1.93004700 -1.13402100 3.23184300
C 3.82367500 -0.90001100 2.26079100
H 4.33980500 -1.58489600 2.92697000
C 4.54025900 -0.23695100 1.24401000
H 5.60873400 -0.40712700 1.13932800
C 3.90127000 0.61334000 0.30756100
C 4.62852900 1.24229400 -0.72561700
H 5.70167600 1.08317200 -0.77767700
C 3.98803600 2.10629900 -1.64578000
H 4.57458900 2.63937000 -2.38785400
C 2.62001600 2.24866100 -1.61335000
H 2.09466900 2.87362300 -2.33071500
C -0.30130200 -0.05482900 2.79421700
C 0.26037600 2.17450700 1.98091800
H -0.22766200 -1.10607200 2.50593500
H -1.32773000 0.28656100 2.62270100
H -0.70421900 2.35877900 1.49485700
H 1.03212900 2.74779200 1.46985600
N 0.58019600 0.75548100 1.97497200
H -0.08216800 0.04920100 3.86642200
H 0.19453000 2.51510900 3.02434200
C -0.39503600 -3.38673900 -0.56615900
C -1.48843400 -3.57778600 -1.62097200
C -0.87776200 -3.55850800 0.87201600
H -1.05140500 -3.66514400 -2.61880900
H -0.02570500 -3.52731800 1.55871400
C 1.62078900 -2.04855000 -1.39180900
C 2.66462000 -2.84226600 -0.61539300
C 1.51666600 -2.51247000 -2.84301900
H 2.68369200 -2.53880700 0.43481300
C -3.64331100 -1.13808700 0.23500800
C -3.94562900 -1.34583800 1.72071200
C -4.91297700 -1.13529200 -0.61073600
H -3.03218000 -1.28072700 2.32001800
H -4.68169500 -1.01761800 -1.67320300
C -3.23045700 1.44566100 -0.04578100
C -4.10292000 1.81663800 1.14682800
C -3.88068000 1.82176300 -1.37736800
H -3.26063600 1.49137900 -2.21706300
Cl -1.03573600 4.30430900 -1.00374400
H -1.38416200 -4.52108800 0.98792700
H -1.57786100 -2.76924500 1.16220700
H -2.18958800 -2.73885700 -1.64145900
H -2.05413200 -4.49089600 -1.41263200
H 3.65173400 -2.65368600 -1.04876900
H 2.48035700 -3.92040600 -0.67055600
H 2.48294000 -2.37086400 -3.33652300
H 1.26170100 -3.57621200 -2.90187200
H 0.76294500 -1.93587000 -3.38804500
H -4.26318300 2.89892000 1.12562300
H 0.37563300 -4.14047300 -0.74624500

H 1.91346300 -0.99537400 -1.38257500

H -2.31140700 2.03578500 0.02644100

H -3.04475700 -1.98943500 -0.08973500

H -3.61769400 1.56211300 2.09401900

H -5.08333300 1.33324300 1.10842600

H -3.95889700 2.91166000 -1.43004000

H -4.88190200 1.39847700 -1.48599300

H -4.36959900 -2.34644900 1.85582800

H -4.66789200 -0.62116400 2.10272700

H -5.60496300 -0.34455200 -0.30878700

H -5.42212200 -2.09404600 -0.4726000

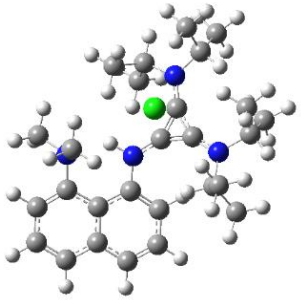

Computational model of Janus (**12$_{in}$**) ground state.

opt=calcfc freq=noraman M062X/6-31+g(d,p) scrf=(solvent=dichloromethane,smd) geom=connectivity empiricaldispersion=gd3

Zero-point correction= 0.641818 (Hartree/Particle)

Thermal correction to Energy= 0.67762

Thermal correction to Enthalpy= 0.678572

Thermal correction to Gibbs Free Energy= 0.574698

Sum of electronic and zero-point Energies= -1731.627151

Sum of electronic and thermal Energies= -1731.591341

Sum of electronic and thermal Enthalpies= -1731.590396

Sum of electronic and thermal Free Energies= -1731.694271

N 0.94518900 -0.34429400 -0.50976600

H 1.25889500 -1.29980600 -0.29227600

N -1.82842600 2.05276400 0.00155400

N -2.43234400 -1.57835700-0.75756000

C -0.36552100 -0.04742800-0.47329700

C -1.41602500 0.82185700 -0.26447000

C -1.65176900 -0.53021200-0.54656600

C 1.98117500 0.58237000 -0.67887100

C 3.32831600 0.21989800 -0.31706500

C 3.72161600 -1.05393400 0.22961500

C 5.05733100 -1.33263600 0.42723800

H 5.34959100 -2.29807000 0.82676600

C 6.06004800 -0.37680700 0.14823900

H 7.10121300 -0.62918000 0.32532100

C 5.71308200 0.86236000 -0.31960900

H 6.46951900 1.61554700 -0.52206500

C 4.35192000 1.18648500 -0.57265400

C 4.02734200 2.46278000 -1.10774400

H 4.82853500 3.17888300 -1.26561700

C 2.73316400 2.76277200 -1.44629800

H 2.48350700 3.72524100 -1.88351500

C 1.71502500 1.80686100 -1.25849500

H 0.70639600 2.02255000 -1.59589200

C 2.20242800 -1.75375000 1.94363200

C 3.09549500 -3.41554100 0.44179500

H 1.85313300 -0.72148200 2.02366000

H 2.98287900 -1.92521800 2.70084100

H 3.81357600 -3.74982300 1.20529500

H 3.52382900 -3.58169400 -0.54932300

N 2.71442100 -2.01323300 0.58942400

H 1.35935400 -2.42182200 2.14354200

H 2.19280900 -4.02520500 0.54386300

C -0.87111200 3.02962800 0.57136400

C -1.27569100 3.43673500 1.98583100

C -0.70344100 4.23776500 -0.34619300

H -1.39498500 2.55130100 2.61735200

H -0.44770900 3.93602400 -1.36644100

C -3.26392300 2.40083700 -0.06396400

C -3.81916700 2.09667200 -1.45383100

C -4.05160000 1.76486500 1.08515800

H -3.76196200 1.03226300 -1.70184000

C -1.79561900 -2.87782900-1.07019300

C -0.95003700 -2.78380400-2.33710200

C -0.99901700 -3.40855100 0.11900900

H -1.53777700 -2.38631000-3.17032900

H -1.62862700 -3.50123200 1.00820500

C -3.89213100 -1.52030200-0.54544700

C -4.30903400 -2.37960000 0.64488700

C -4.64520800 -1.87898000-1.82377300

H -4.32444800 -1.24710900-2.65786200

Cl -1.56157900 -0.41768800 2.96514400

H 0.09732400 4.87886100 0.03612000

H -1.61898300 4.83824500 -0.38622100

H -2.20879800 4.01017600 1.98842200

H -0.49330600 4.07220100 2.41226000

H -3.25933500 2.65065100 -2.21401800

H -4.86940600 2.39719600 -1.50836600

H -3.85567200 2.28784800 2.02497800

H -5.12645200 1.81254600 0.88223800

H -3.76085700 0.72269800 1.24225400

H -5.37998200 -2.25081800 0.83050400

H 0.08101900 2.49651000 0.63749100

H -3.29445000 3.48689800 0.06092400

H -4.10951000 -0.48003100-0.30440600

H -2.62525500 -3.56257900-1.26339700

H -3.75855800 -2.08275800 1.54337600

H -4.12801000 -3.44275400 0.45215500

H -5.71749600 -1.72601200-1.66783700

H -4.49685700 -2.92709900-2.10339600

H -0.58741200 -3.77866800-2.61224200

H -0.07621600 -2.13999600-2.18757100

H -0.16840800 -2.73908200 0.36876700

H -0.58203100 -4.39141700-0.121900

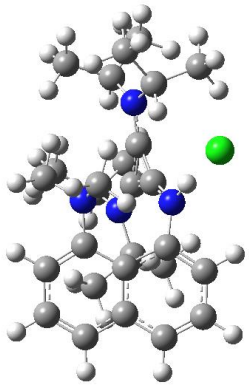

Computational model of Janus (**12**$_{out}$) ground state.

opt=calcfc freq=noraman M062X/6-31+g(d,p) scrf=(solvent=dichloromethane,smd) geom=connectivity empiricaldispersion=gd3

Zero-point correction= 0.642838 (Hartree/Particle)
Thermal correction to Energy= 0.678333
Thermal correction to Enthalpy= 0.679277
Thermal correction to Gibbs Free Energy= 0.576485
Sum of electronic and zero-point Energies= -1731.624828
Sum of electronic and thermal Energies= -1731.589333
Sum of electronic and thermal Enthalpies= -1731.588389
Sum of electronic and thermal Free Energies= -1731.691181

N -2.77165700 0.03060200 -0.01708200

N 0.44574300 1.53662000 -0.82160100

H -0.05027600 2.44306300 -0.92451000

N 0.29758200 -2.09103600 -0.71749400

C-0.28738400 0.44017800 -0.63354400

C -0.36316900 -0.94268700-0.58340700

C -1.49633800-0.16235600 -0.33524500

C 1.84753600 1.53472600 -0.64604700

C 2.47580000 0.82608400 0.41403500

C 1.81454100 0.29871600 1.57750900

C 2.47844900 -0.66863600 2.42041200

H 1.93004700 -1.13402100 3.23184300

C 3.82367500 -0.90001100 2.26079100

H 4.33980500 -1.58489600 2.92697000

C 4.54025900 -0.23695100 1.24401000

H 5.60873400 -0.40712700 1.13932800

C 3.90127000 0.61334000 0.30756100

C 4.62852900 1.24229400 -0.72561700

H 5.70167600 1.08317200 -0.77767700

C 3.98803600 2.10629900 -1.64578000

H 4.57458900 2.63937000 -2.38785400

C 2.62001600 2.24866100 -1.61335000

H 2.09466900 2.87362300 -2.33071500

C -0.30130200 -0.05482900 2.79421700

C 0.26037600 2.17450700 1.98091800

H -0.22766200 -1.10607200 2.50593500

H -1.32773000 0.28656100 2.62270100

H -0.70421900 2.35877900 1.49485700

H 1.03212900 2.74779200 1.46985600

N 0.58019600 0.75548100 1.97497200

H -0.08216800 0.04920100 3.86642200

H 0.19453000 2.51510900 3.02434200

C -0.39503600 -3.38673900-0.56615900

C -1.48843400-3.57778600-1.62097200

C -0.87776200-3.55850800 0.87201600

H -1.05140500-3.66514400 -2.61880900

H -0.02570500-3.52731800 1.55871400

C 1.62078900 -2.04855000 -1.39180900

C 2.66462000 -2.84226600 -0.61539300

C 1.51666600 -2.51247000 -2.84301900

H 2.68369200 -2.53880700 0.43481300

C -3.64331100 -1.13808700 0.23500800

C -3.94562900 -1.34583800 1.72071200

C -4.91297700 -1.13529200-0.61073600

H -3.03218000 -1.28072700 2.32001800

H -4.68169500 -1.01761800-1.67320300

C -3.23045700 1.44566100 -0.04578100

C -4.10292000 1.81663800 1.14682800

C -3.88068000 1.82176300 -1.37736800

H -3.26063600 1.49137900-2.21706300

Cl -1.035736004.30430900 -1.00374400

H -1.38416200 -4.52108800 0.98792700

H -1.57786100-2.76924500 1.16220700

H -2.18958800 -2.73885700-1.64145900

H -2.05413200 -4.49089600-1.41263200

H 3.65173400 -2.65368600 -1.04876900

H 2.48035700 -3.92040600 -0.67055600

H 2.48294000 -2.37086400 -3.33652300

H 1.26170100 -3.57621200 -2.90187200

H 0.76294500 -1.93587000 -3.3880450

H -4.26318300 2.89892000 1.12562300

H 0.37563300 -4.14047300 -0.74624500

H 1.91346300 -0.99537400 -1.38257500

H -2.31140700 2.03578500 0.02644100

H -3.04475700-1.98943500 -0.08973500

H -3.61769400 1.56211300 2.09401900

H -5.08333300 1.33324300 1.10842600

H-3.95889700 2.91166000 -1.43004000

H-4.88190200 1.39847700 -1.48599300

H -4.36959900 -2.34644900 1.85582800

H -4.66789200-0.62116400 2.10272700

H -5.60496300-0.34455200-0.30878700

H -5.42212200-2.09404600-0.4726000

Janus $[Cl]^-$ (**12a**$_{Cl}$)

NBO donor-acceptor interaction energies.

Donor	Acceptor	Energy (kcal/mol)
N_{11} (LP)	$C_8 – C_9$ (BD*)	2.23
N_{11} (LP)	$C_8 – C_7$ (BD*)	5.46
N_{11} (LP)	C_8 – C7 (BD*)	11.70

Janus $[BF_4]^-$ (**12b**$_{BF4}$)

NBO donor-acceptor interaction energies.

Donor	Acceptor	Energy (kcal/mol)
N_{11} (LP)	$N_{14} – H_{29}$ (BD*)	22.68
N_{11} (LP)	$C_8 – C_9$ (BD*)	3.04
N_{11} (LP)	$C_8 – C_7$ (BD*)	6.82
N_{11} (LP)	C_8 – C7 (BD*)	0.68

Janus $[PF_6]^-$ (**12c**$_{PF6}$)

NBO donor-acceptor interaction energies.

Donor	Acceptor	Energy (kcal/mol)

N_{11} (LP)	$N_{14} – H_{29}$ (BD*)	11.21
N_{11} (LP)	$C_8 – C_9$ (BD*)	2.44
N_{11} (LP)	$C_8 – C_7$ (BD*)	6.01
N_{11} (LP)	C_8 – C7 (BD*)	5.80

Janus $[B(Ph)_4]^-$ (**12d**$_{BPh4}$)

12d$_{BPh4}$ NBO donor-acceptor interaction energies.

Donor	Acceptor	Energy (kcal/mol)
N_{11} (LP)	H_{29} (LP*)	40.01
N_{11} (LP)	$C_8 – C_9$ (BD*)	2.90
N_{11} (LP)	$C_8 – C_7$ (BD*)	0.62
N_{11} (LP)	C_8 – C7 (BD*)	4.55

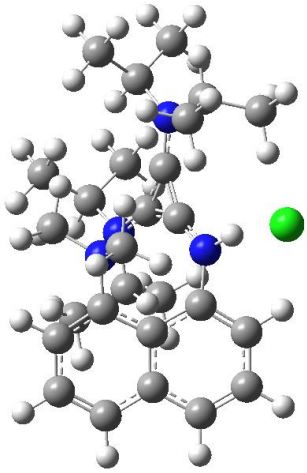

Computed Structure of Janus $[Cl]^-$ (**12a**$_{Cl}$).

opt=calcfc freq b3lyp/6-31g(d,p) scrf=(iefpcm,solvent=dichloromethane) pop=(nbo,savenbo) geom=connectivity empiricaldispersion=gd3

Zero-point correction= 0.641032 (Hartree/Particle)

Thermal correction to Energy= 0.676716

Thermal correction to Enthalpy= 0.677660

Thermal correction to Gibbs Free Energy= 0.574592

Sum of electronic and zero-point Energies= -1732.274793

Sum of electronic and thermal Energies= -1732.239109

Sum of electronic and thermal Enthalpies= -1732.238165

Sum of electronic and thermal Free Energies= -1732.341233

Cl	-0.05331100	4.52889100	-0.70293200	C	3.80382600	1.65223300	-2.07855200
N	0.43398200	1.47077500	-0.57089500	H	4.24477100	2.11441500	-2.95597700
H	0.10699300	2.45865900	-0.60968800	C	2.43586300	1.84048300	-1.80402100
N	-3.01086800	0.37377300	-0.00554300	H	1.81440200	2.41954400	-2.47830500
N	-0.25311200	-2.12370800	-0.64809000	C	0.18444900	-0.56159600	2.90213100
N	0.85474600	0.36505300	2.00111000	H	-0.86926500	-0.27216900	2.97307800
C	-0.43914900	0.47504800	-0.45780700	H	0.23258000	-1.57377400	2.49379000
C	-1.74078100	0.04504200	-0.25432800	H	0.59652100	-0.57297700	3.92554300
C	-0.72599600	-0.88048900	-0.49988400	C	0.78220100	1.75033600	2.47662900
C	1.83994100	1.26983900	-0.69336700	H	-0.26003100	2.00844600	2.67736800
C	2.61515100	0.51805800	0.25778300	H	1.36187000	1.89296900	3.40368400
C	2.13341800	-0.01036700	1.51639700	H	1.15893400	2.43925400	1.71992200
C	2.94392700	-0.86881200	2.24442400	C	-4.03582500	-0.66200400	0.24708400
H	2.58387900	-1.26847000	3.18507700	H	-3.52079300	-1.61466800	0.13970600
C	4.24833100	-1.20381800	1.82365500	C	-4.55947200	-0.58117500	1.68593300
H	4.84486200	-1.88168800	2.42677300	H	-5.25323800	-1.40578200	1.87484600
C	4.77138900	-0.63380900	0.69059000	H	-3.73402600	-0.65107100	2.40072300
H	5.79089300	-0.84299000	0.38028700	H	-5.09620200	0.35426700	1.87073900
C	3.98348800	0.24244300	-0.10482200	C	-5.15604500	-0.62080000	-0.79805500
C	4.55086200	0.83531100	-1.26392900	H	-5.84642100	-1.45281000	-0.63089800
H	5.59245900	0.62894500	-1.49287900	H	-5.73387200	0.30635300	-0.74019800

H	-4.74680400	-0.70767200	-1.80865400	H	0.57634100	-1.96173700	-3.23816900
C	-3.39927200	1.80870400	0.04660900	C	1.93622800	-3.26736600	-0.29374800
H	-4.46769200	1.79766000	0.27199700	H	2.98318500	-3.25060800	-0.60908100
C	-2.68635200	2.55123500	1.17906400	H	1.89677000	-2.97075800	0.75598000
H	-3.11294200	3.55237200	1.28869000	H	1.57728800	-4.29717200	-0.38819900
H	-2.80369200	2.01643700	2.12624400	C	-1.15120900	-3.30087000	-0.59441300
H	-1.62423000	2.68242300	0.96502000	H	-0.51218700	-4.15400800	-0.83062900
C	-3.21031000	2.47837700	-1.31776300	C	-2.23664300	-3.24539100	-1.67807600
H	-3.59891400	3.50017100	-1.28620000	H	-2.89335900	-4.11666800	-1.60106600
H	-2.15258700	2.54866500	-1.58431300	H	-2.85511800	-2.34941500	-1.60036200
H	-3.74188800	1.92391300	-2.09634500	H	-1.78026200	-3.24326700	-2.67114800
C	1.13313300	-2.29476800	-1.16091200	C	-1.67348100	-3.51740200	0.83103000
H	1.59609800	-1.31320500	-1.07034800	H	-2.35819400	-4.36966600	0.86217700
C	1.13758100	-2.68734600	-2.64247100	H	-0.83907800	-3.71697200	1.50898500
H	2.16698100	-2.71443900	-3.01238200	H	-2.20434800	-2.64211700	1.21317300
H	0.70184100	-3.67936900	-2.80028900				

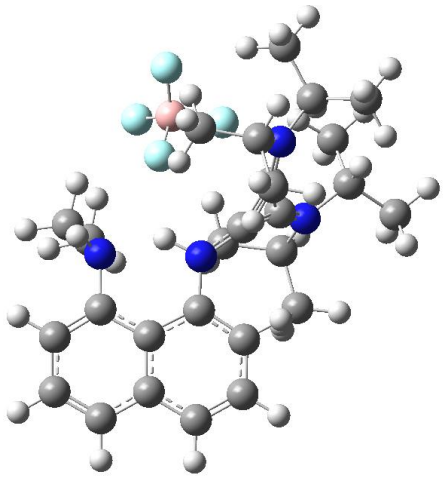

Computed Structure of Janus $[BF_4]^-$ (**12b**$_{BF4}$).

opt=calcfc freq b3lyp/6-31g(d,p) scrf=(iefpcm,solvent=dichloromethane) pop=(nbo,savenbo) geom=connectivity empiricaldispersion=gd3 ----------

---

Zero-point correction= 0.656769 (Hartree/Particle)

Thermal correction to Energy= 0.695906

Thermal correction to Enthalpy= 0.696850

Thermal correction to Gibbs Free Energy= 0.585972

Sum of electronic and zero-point Energies= -1696.508324

Sum of electronic and thermal Energies= -1696.469187

Sum of electronic and thermal Enthalpies= -1696.468242

Sum of electronic and thermal Free Energies= -1696.579121

B	-1.49235400	-2.01594400	-1.80603700	C	-1.38226400	-2.92731800	1.81334300
F	-2.34438400	-3.10105000	-1.54030900	H	-1.95126300	-3.30048100	0.96088900
F	-2.21110500	-0.80291300	-1.66100900	H	-1.25024900	-3.73005000	2.54586200
F	-0.97631300	-2.09832400	-3.10434100	H	-0.40102900	-2.62996100	1.43934600
F	-0.42062500	-2.03289200	-0.87926000	C	-3.90693600	-0.53447300	1.09951100
N	-1.57317500	2.21981600	-0.57060000	H	-3.88382000	0.11384200	0.22362600
N	-2.48268500	-0.70296500	1.48800600	C	-4.69701200	0.14771700	2.21968000
N	1.04028700	-0.12256000	0.73280800	H	-4.72571100	-0.47531500	3.11961900
H	1.25075200	-0.99455200	0.19844500	H	-5.72907800	0.32111900	1.90033300
N	2.53994100	-1.76966600	-0.69851200	H	-4.24996200	1.11075000	2.48560400
C	-1.55770700	0.06681300	0.94979900	C	-4.53071100	-1.85888400	0.65019000
C	-1.20219800	1.18570600	0.16578900	H	-3.94397600	-2.30351800	-0.15448200
C	-0.23511600	0.34319800	0.68290700	H	-5.54438100	-1.66476800	0.28623400
C	-2.08667300	-1.74224000	2.47900600	H	-4.61118600	-2.57416000	1.47467600
H	-3.02818000	-2.08803800	2.91270600	C	-3.00329400	2.62742600	-0.58246800
C	-1.24680800	-1.12637000	3.60219200	H	-3.43773100	2.15903000	0.30420100
H	-0.27868800	-0.78210700	3.22490900	C	-3.72689000	2.09538700	-1.82550100
H	-1.05521600	-1.87829700	4.37317700	H	-3.38025200	2.60139200	-2.73226700
H	-1.76480000	-0.28018300	4.06295200	H	-4.80151500	2.28106800	-1.73498800

H	-3.55361900	1.02404200	-1.94418700
C	-3.14860100	4.14249700	-0.41737100
H	-2.64228600	4.48930600	0.48754000
H	-4.20942500	4.39814100	-0.34132100
H	-2.73990400	4.68477700	-1.27528300
C	-0.64348500	2.77497200	-1.59708300
H	-1.29547800	3.25267800	-2.33278600
C	0.28404100	3.84013200	-1.00669500
H	-0.28405400	4.63483600	-0.51657400
H	0.88696400	4.28747200	-1.80327500
H	0.96541400	3.39616800	-0.27659600
C	0.12578100	1.65482900	-2.30503300
H	0.88755100	1.22769600	-1.64787600
H	0.63608500	2.06058300	-3.18313500
H	-0.54726700	0.85205600	-2.61548900
C	2.16068500	0.69774700	0.90045200
C	2.04815300	1.91648500	1.55385500
H	1.07070400	2.24063500	1.89697600
C	3.18198000	2.71021500	1.81925700
H	3.05334200	3.66133400	2.32713500
C	4.43722100	2.27148200	1.47040200
H	5.31809600	2.86433100	1.69734300
C	4.60284700	1.02100100	0.81499500
C	3.45622800	0.21787900	0.48113000
C	3.67858800	-1.01190000	-0.22543700
C	4.96409700	-1.43082300	-0.51064300
H	5.10928500	-2.36058400	-1.05125600
C	6.08459500	-0.65650800	-0.14172900
H	7.08362300	-1.00983900	-0.37861600
C	5.90393100	0.55095800	0.48999100
H	6.75818600	1.16660200	0.75738700
C	2.30579200	-1.55191800	-2.13665900
H	2.29710500	-0.47829800	-2.33874200
H	1.33386400	-1.96235700	-2.41119100
H	3.09647500	-2.01002500	-2.75162600
C	2.53203200	-3.19270400	-0.34591200
H	3.28655900	-3.78300900	-0.88856700
H	1.54011400	-3.58468500	-0.58314700
H	2.70832100	-3.30150900	0.72715300

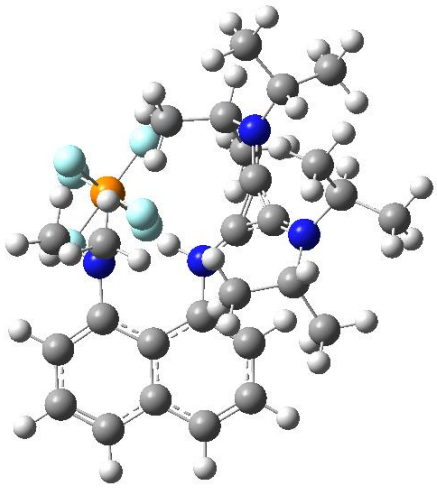

Computed Structure of Janus $[PF_6]^-$ (**12c**$_{PF6}$).

opt=calcfc freq b3lyp/6-31g(d,p) scrf=(iefpcm,solvent=dichloromethane) pop=(nbo,savenbo) geom=connectivity empiricaldispersion=gd3

Zero-point correction= 0.661603 (Hartree/Particle)

Thermal correction to Energy= 0.702960

Thermal correction to Enthalpy= 0.703905

Thermal correction to Gibbs Free Energy= 0.588234

Sum of electronic and zero-point Energies= -2212.625904

Sum of electronic and thermal Energies= -2212.584546

Sum of electronic and thermal Enthalpies= -2212.583602

Sum of electronic and thermal Free Energies= -2212.699273

P	4.04772700	-1.63868300	-0.56799600	F	4.74950000	-0.19653300	-0.23584300
F	2.56537200	-0.92406400	-0.49513100	F	5.51676600	-2.34640500	-0.63111200
F	3.95042800	-1.96987900	1.03399700	N	-3.90724300	0.34271500	-0.15196300
F	3.33604900	-3.08416700	-0.88964600	N	-1.66809400	-2.60082900	0.09057000
F	4.11412300	-1.31426000	-2.16561600	N	-0.15034900	0.64742200	-0.34591300

H	0.66963400	0.30739100	0.16996200	H	-1.68022800	-4.99326500	1.57277700
N	1.52285300	1.21702500	1.67060000	H	-3.39876800	-4.88741700	1.96373300
C	-1.85676500	-1.29915100	-0.06290500	H	-2.28468700	-3.62763600	2.53187800
C	-2.67232400	-0.16235400	-0.15373000	C	-5.04136100	-0.62283100	-0.13430900
C	-1.29077300	-0.04799700	-0.24593100	H	-4.63868800	-1.54149000	-0.56816700
C	-0.29641000	-3.15349900	-0.11958500	C	-5.50671800	-0.91058800	1.29891800
H	-0.42299700	-4.23853800	-0.09533200	H	-4.67155300	-1.23256300	1.92839400
C	0.23575700	-2.77539100	-1.50441200	H	-6.26218500	-1.70178800	1.29571800
H	-0.47504100	-3.07570000	-2.27997800	H	-5.95445500	-0.02388300	1.75767100
H	1.19213800	-3.27048500	-1.67292400	C	-6.19104000	-0.17310600	-1.03971000
H	0.42216000	-1.70264700	-1.58478600	H	-6.66911200	0.74030100	-0.67483900
C	0.63332000	-2.75256300	1.02950100	H	-6.95319300	-0.95702900	-1.06128800
H	1.64147400	-3.12335300	0.84602700	H	-5.84222800	-0.00350200	-2.06138100
H	0.26169000	-3.14605800	1.97981600	C	-4.17958700	1.77124500	0.18350900
H	0.71405200	-1.66677200	1.11343800	H	-5.15606700	1.75405900	0.67508200
C	-2.79661100	-3.50308600	0.42151200	C	-4.29153600	2.65050600	-1.06563900
H	-3.64326700	-2.84742600	0.62781600	H	-3.32788900	2.73199000	-1.56983600
C	-3.15331500	-4.39687000	-0.77045400	H	-4.60630400	3.65818100	-0.77655700
H	-3.38254700	-3.79269100	-1.65313500	H	-5.02262300	2.25290200	-1.77212900
H	-4.02786300	-5.00832700	-0.52993200	C	-3.17435500	2.32885200	1.19419900
H	-2.33111400	-5.07378900	-1.02173300	H	-3.08485400	1.67243800	2.06457700
C	-2.51540900	-4.29885100	1.70024400	H	-3.51599800	3.30919200	1.53667100

H	-2.18706300	2.46701900	0.74773500	C	2.63676000	4.75946000	1.09701400
C	-0.06673400	2.00594200	-0.72566300	H	3.34753100	5.45271800	1.53632500
C	-0.80036000	2.43398500	-1.81673700	C	1.83381100	5.15227800	0.05511400
H	-1.40848400	1.71269500	-2.35261600	H	1.89719100	6.15940300	-0.34630500
C	-0.73415000	3.77107900	-2.25582800	C	2.75808000	0.64209600	2.20911400
H	-1.33243300	4.08420800	-3.10544300	H	3.56016700	0.75700100	1.48364600
C	0.11160100	4.65480500	-1.62977100	H	2.60654900	-0.42777800	2.35698700
H	0.19334000	5.68093800	-1.97538200	H	3.05602800	1.08995300	3.17057300
C	0.91658100	4.24115700	-0.53392700	C	0.41831800	1.12329900	2.63681100
C	0.82035100	2.89635300	-0.02922400	H	0.62612600	1.69544400	3.55466200
C	1.63915700	2.53152200	1.09946200	H	0.26431500	0.07369500	2.90635200
C	2.52906300	3.45318000	1.62101200	H	-0.50329500	1.50636900	2.19522700
H	3.15222500	3.17307900	2.46222100				

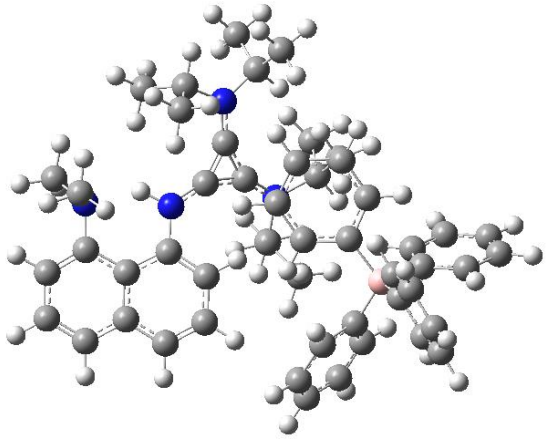

Computed Structure of Janus $[BPh_4]^-$ (**1d$_{BPh4}$**).

opt=calcfc freq b3lyp/6-31g(d,p) scrf=(iefpcm,solvent=dichloromethane) pop=(nbo,savenbo) geom=connectivity empiricaldispersion=gd3

Zero-point correction= 1.009708 (Hartree/Particle)

Thermal correction to Energy= 1.065098

Thermal correction to Enthalpy= 1.066042

Thermal correction to Gibbs Free Energy= 0.917834

Sum of electronic and zero-point Energies= -2223.225309

Sum of electronic and thermal Energies= -2223.169919

Sum of electronic and thermal Enthalpies= -2223.168975

Sum of electronic and thermal Free Energies= -2223.317183

B	-3.88592200	-0.45258300	-0.42745700
C	-2.59839800	0.33897600	-1.10172600
C	-1.29790900	-0.18691900	-1.21775300
H	-1.09802600	-1.18071100	-0.82869700
C	-0.25125300	0.51025600	-1.83416100
H	0.73484600	0.05575100	-1.90359200
C	-0.47456500	1.77811600	-2.37159200
H	0.32652800	2.32049300	-2.86407500
C	-1.75275700	2.33651200	-2.27508700
H	-1.94506500	3.32551700	-2.68567000
C	-2.77953800	1.62963800	-1.64670800
H	-3.76176100	2.09089200	-1.57107300
C	-4.63506800	0.62821400	0.57150400
C	-3.89361100	1.27109200	1.58681200
H	-2.84345600	1.01889900	1.69533100
C	-4.44760100	2.21615600	2.45065200
H	-3.83056300	2.67988000	3.21819300
C	-5.79493500	2.57100800	2.32473400
H	-6.23728800	3.30919900	2.98900700
C	-6.55940600	1.96288500	1.32825000
H	-7.60773600	2.23024500	1.21084400
C	-5.98451900	1.01271000	0.47444900
H	-6.60653000	0.56064100	-0.29336800
C	-4.91947500	-0.97352700	-1.60597400
C	-4.82004400	-0.64575000	-2.96997500
H	-4.00784400	-0.00354400	-3.30020800
C	-5.72750100	-1.11961500	-3.92579900
H	-5.60600400	-0.84203400	-4.97108800
C	-6.78383300	-1.94736600	-3.54420500
H	-7.49149200	-2.31782200	-4.28172500
C	-6.91426900	-2.29626700	-2.19565900

H	-7.72924800	-2.94352200	-1.87788900	H	1.10718300	6.11212800	-1.24884200
C	-5.99548000	-1.82029200	-1.25958800	H	0.71739600	4.47489400	-1.81411800
H	-6.10789000	-2.11460500	-0.21774600	C	3.45641200	5.49283700	0.11194300
C	-3.39780900	-1.79984500	0.39767700	H	3.98036900	5.05869100	0.96825500
C	-2.87885400	-2.90442000	-0.31432300	H	3.03301200	6.45420600	0.41639600
H	-2.82262900	-2.84201700	-1.39908100	H	4.18615900	5.68819800	-0.67962100
C	-2.44502100	-4.07383100	0.31210500	C	3.88190300	3.04568700	-1.73873100
H	-2.04608500	-4.89325900	-0.28204000	H	3.98097400	4.03028700	-2.20048100
C	-2.52723600	-4.19476200	1.70402000	C	3.43965100	2.06375600	-2.82797100
H	-2.19539000	-5.10311500	2.20055300	H	3.28909400	1.05524600	-2.43374600
C	-3.05475200	-3.13286000	2.43984400	H	4.20806100	2.00745400	-3.60427700
H	-3.14010100	-3.21157900	3.52176300	H	2.50729600	2.39287300	-3.29204800
C	-3.48008400	-1.96669000	1.79221000	C	5.23346100	2.67633900	-1.11577300
H	-3.88763900	-1.16113600	2.39599400	H	5.55103900	3.43191100	-0.39320500
N	0.82708000	1.45162700	1.98110600	H	5.99733200	2.59728300	-1.89467700
N	2.84044000	3.21276500	-0.68767900	H	5.18473700	1.71527400	-0.59645700
N	3.25215200	-0.33114600	-0.18769700	C	-0.04846500	2.61485000	2.28494300
H	4.22536900	-0.28873400	-0.54984300	H	-0.79200800	2.22264400	2.98285400
N	5.61561200	-1.28622900	-0.94232100	C	0.71920900	3.73457800	2.99911000
C	1.71734700	1.48127000	0.99681200	H	1.12175300	3.38929400	3.95387100
C	2.61553200	0.78536700	0.19900800	H	0.05235900	4.58031100	3.19022500
C	2.46571900	2.14449100	0.00808400	H	1.55780900	4.09605900	2.39850600
C	2.33268500	4.56771000	-0.36420900	C	-0.80216100	3.07384900	1.03637800
H	1.64621100	4.42364900	0.46870900	H	-0.13870400	3.49961100	0.28255500
C	1.53362400	5.14665600	-1.53573800	H	-1.53493900	3.83806800	1.30931800
H	2.16367600	5.30998200	-2.41555200	H	-1.32859300	2.24058700	0.57166300

C	0.75657800	0.23749500	2.84570400
H	1.51778600	-0.43720600	2.45005100
C	1.12923000	0.56481500	4.29540500
H	2.11152600	1.04194600	4.35296600
H	1.16011700	-0.36196400	4.87586200
H	0.39123500	1.22223600	4.76499400
C	-0.60206700	-0.45605400	2.73988300
H	-1.39010300	0.10837200	3.24671300
H	-0.55386100	-1.44059300	3.21274000
H	-0.90877000	-0.59685100	1.70228000
C	2.85262200	-1.64604100	0.11372500
C	1.52959700	-1.92698200	0.40343800
H	0.79298300	-1.13936800	0.31790800
C	1.12812700	-3.21765300	0.80139400
H	0.08285200	-3.39900400	1.02954100
C	2.05739500	-4.22615700	0.89708600
H	1.76596700	-5.21950700	1.22480400
C	3.41594000	-3.99450900	0.54768200
C	3.83900900	-2.69375900	0.09990200
C	5.20234200	-2.53371000	-0.32151900
C	6.09087900	-3.58593400	-0.20799100
H	7.11695800	-3.45832400	-0.53484900
C	5.68139100	-4.84047900	0.29292400
H	6.40406100	-5.64669200	0.37122800
C	4.36811300	-5.04459400	0.64113600
H	4.03468900	-6.01612200	0.99418000
C	5.51051500	-1.36394900	-2.41269300
H	6.21981800	-2.08908800	-2.83752100
H	5.71217600	-0.37763700	-2.84009600
H	4.49680100	-1.66372600	-2.68913700
C	6.92941800	-0.78829600	-0.51323600
H	6.96974200	-0.76500900	0.57755300
H	7.05884600	0.22882000	-0.89253900
H	7.76705000	-1.39458500	-0.8865800

	12b$_{BF4}$	**12c**$_{PF6}$	**12d**$_{BPh4}$	**59**
Chemical formula	$C_{27}H_{41}BF_4N_4$	$C_{27}H_{41}F_6N_4P$	$C_{27}H_{41}N_4 \cdot C_{24}H_{20}B$	$C_{30}H_{45}BF_4N_6$
M_r	508.45	566.61	740.84	576.53
Crystal system, space group	Triclinic, P1	Monoclinic, $P2_1$	Monoclinic, $P2_1/n$	Orthorhombic, $Pca2_1$
Temperature (K)	170	293	150	150
a, *b*, *c* (Å)	8.130 (8), 9.346 (9), 10.352 (9)	12.2767 (4), 10.1490 (3), 12.2607 (4)	13.7195 (17), 9.6147 (14), 33.008 (4)	16.9153 (8), 14.2572 (7), 12.9568 (6)
α, β, γ (°)	81.76 (4), 69.85 (4), 72.09 (4)	108.7914 (11)	93.764 (6)	
V (Å^3)	702.1 (12)	1446.21 (8)	4344.6 (10)	3124.7 (3)
Z	1	2	4	4
Radiation type	Mo Kα	Mo Kα	Mo *K*α	Mo *K*α
μ (mm^{-1})	0.09	0.16	0.07	0.09
Crystal size (mm)	0.30 × 0.28 × 0.18	0.3 × 0.2 × 0.15	0.5 × 0.2 × 0.02	0.18 × 0.12 × 0.06
Absorption correction	Multi-scan Bruker *SADABS*	Multi-scan Bruker SADABS	Multi-scan Bruker *SADABS*	Multi-scan Bruker *SADABS*
T_{min}, T_{max}	0.693, 0.746	0.690, 0.750	0.539, 0.745	0.675, 0.789
No. of measured, independent and observed [$I > 2\sigma(I)$] reflections	23748, 6944, 5076	12733, 4735, 4072	36185, 7297, 5554	18484, 6823, 6096
R_{int}	0.053	0.031	0.065	0.047
$(\sin \theta/\lambda)_{max}$ (Å^{-1})	0.668	0.667	0.595	0.650
$R[F^2 > 2\sigma(F^2)]$, $wR(F^2)$, S	0.080, 0.234, 1.04	0.046, 0.113, 0.96	0.079, 0.187, 1.07	0.047, 0.116, 1.00
No. of reflections	6944	4735	7297	6823
No. of parameters	340	382	518	383
H-atom treatment	H atoms treated by a mixture of independent	H atoms treated by a mixture of independent and	H atoms treated by a mixture of independent and	H atoms treated by a mixture of independent and

	and constrained refinement	constrained refinement	constrained refinement	constrained refinement
$\Delta\rho_{max}$, $\Delta\rho_{min}$ (e Å^{-3})	0.50, −0.67	0.21, -0.24	0.32, −0.33	0.24, −0.20
Absolute structure	Refined as an inversion twin.	Flack x determined using 1587 quotients [(I+)-(I-)]/[(I+)+(I-)] (Parsons, Flack and Wagner, Acta Cryst. B69 (2013) 249-259).	-	Flack x determined using 2346 quotients [(I+)-(I-)]/[(I+)+(I-)] (Parsons, Flack and Wagner, Acta Cryst. B69 (2013) 249-259).
Absolute structure parameter	-	0.01(4)	-	0.2 (4)

	53	**58**
Chemical formula	$C_{25}H_{35}N_3Cl$	$C_{25}H_{35}N_3 \cdot C_{24}H_{20}B$
M_r	414.02	697.77
Crystal system, space group	Triclinic, P$^-$1	Monoclinic, $P2_1/n$
Temperature (K)	150	150
a, *b*, *c* (Å)	10.9494 (8), 10.9977 (8), 11.7162 (8)	11.8181 (9), 12.8717 (9), 26.802 (2)
α, β, γ (°)	90.563 (3), 103.713 (3), 119.021 (3)	95.207 (3)
V (Å^3)	1185.52 (15)	4060.3 (5)
Z	2	4
Radiation type	Mo Kα	Mo *K*α
μ (mm^{-1})	0.18	0.07
Crystal size (mm)	0.26 × 0.12 × 0.08	0.2 × 0.1 × 0.06
Absorption correction	Multi-scan Bruker *SADABS*	Multi-scan Bruker *SADABS*
T_{min}, T_{max}	0.637, 0.746	0.630, 0.742
No. of measured, independent and observed [$I > 2\sigma(I)$] reflections	35420, 5449, 4502	38079, 7205, 5147
R_{int}	0.054	0.070
$(\sin\theta/\lambda)_{max}$ (Å^{-1})	0.650	0.617
$R[F^2 > 2\sigma(F^2)]$, $wR(F^2)$, *S*	0.070, 0.137, 1.12	0.130, 0.253, 1.17
No. of reflections	5449	7205
No. of parameters	255	457

H-atom treatment	H atoms treated by a mixture of independent and constrained refinement	H-atom parameters constrained.
$\Delta\rho_{max}$, $\Delta\rho_{min}$ (e Å^{-3})	0.42, −0.29	0.81, −0.91
Absolute structure	-	Refined as an inversion twin.

Molecular Orbitals

Janus – H – DCM (**12**)

Geometry LUMO HOMO HOMO

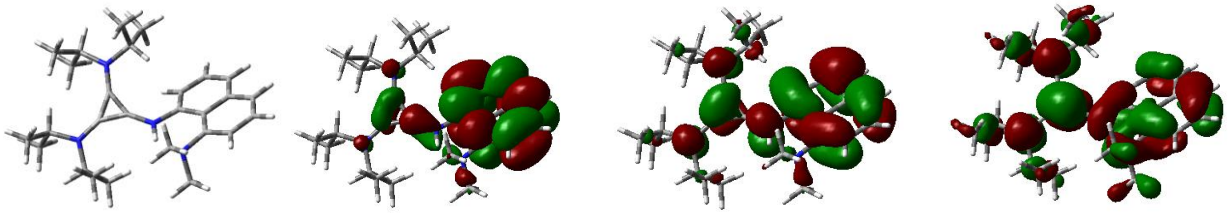

Janus – H – GAS (**12**)

Geometry LUMO HOMO HOMO

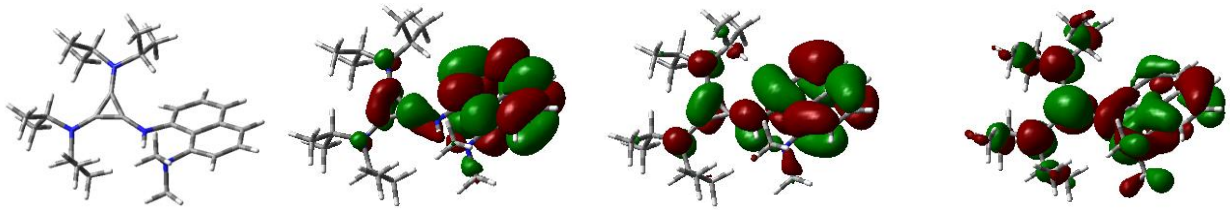

Janus – H – CY (**48**)

Geometry LUMO HOMO HO

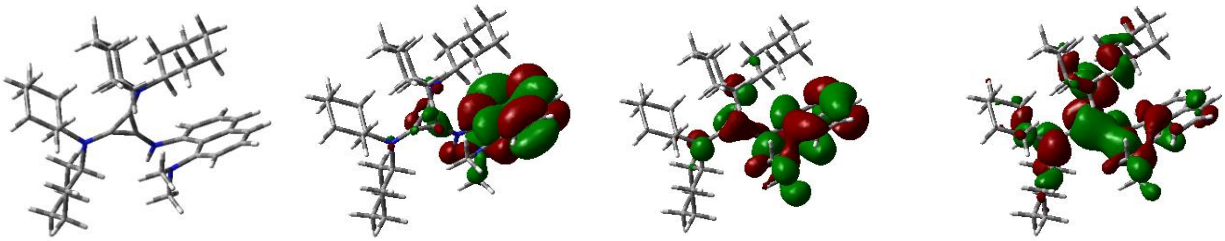

Janus – H – Ph (**49**)

Geometry LUMO HOMO HOMO

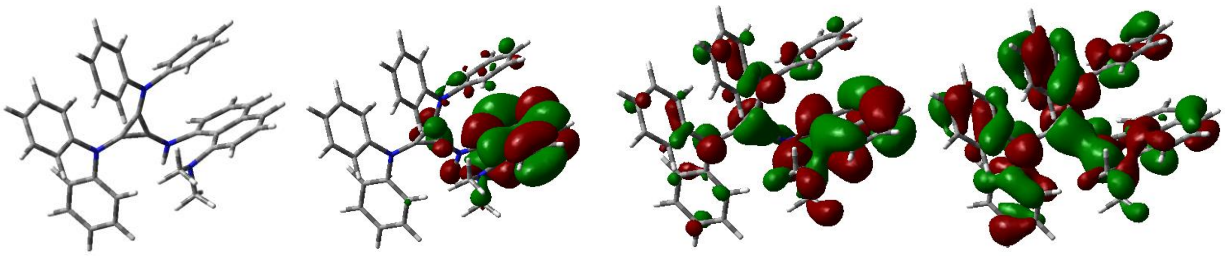

Janus – H – Boc (**50**)

Geometry LUMO HOMO HOMO

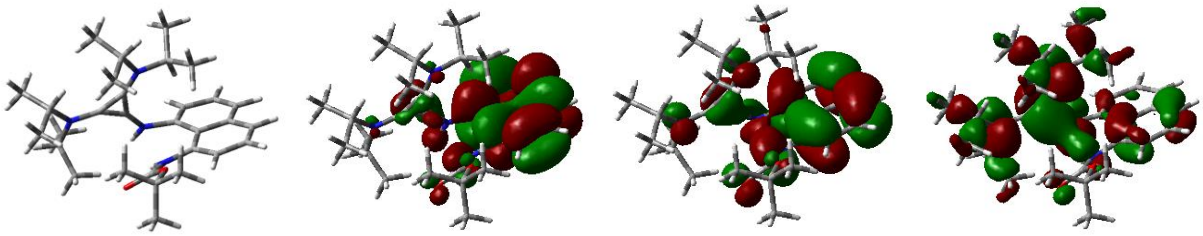

Janus – H – Pyrrolidine (**51**)

Geometry LUMO HOMO HOMO

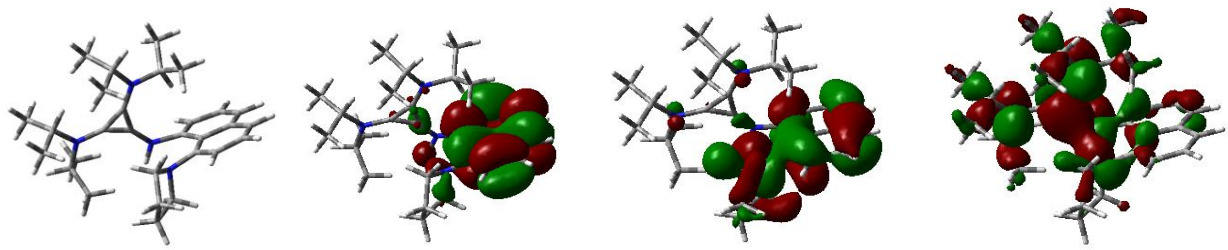

Cyc – 1 – Aminonaphthalene – H (**53**)

Geometry LUMO HOMO HOMO

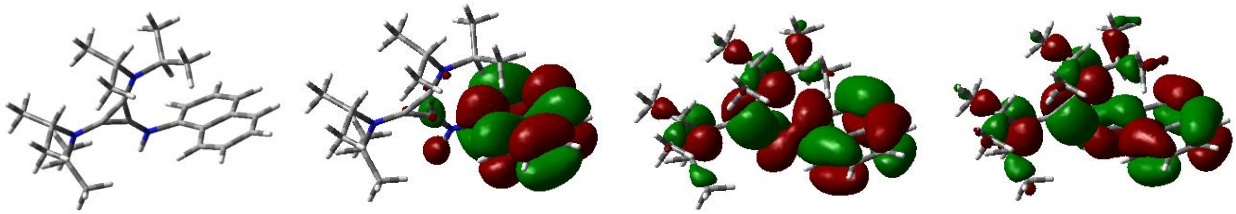

Naphthalene – Amine (**58**)

Geometry LUMO HOMO HOMO

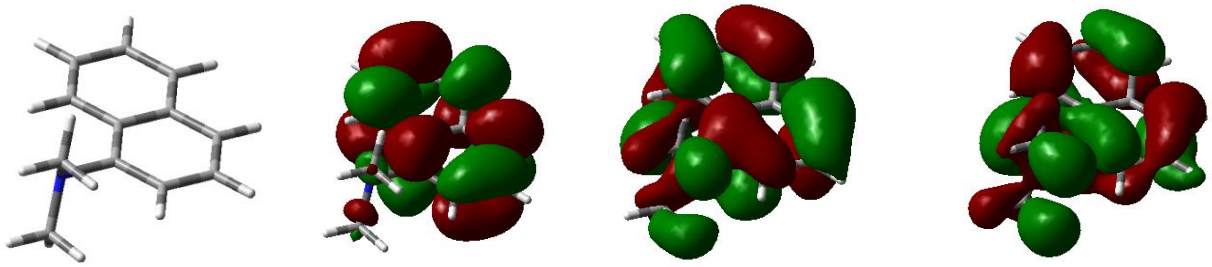

Janus – H – Para Pyrrolidine (**52**)

Geometry LUMO HOMO HOMO

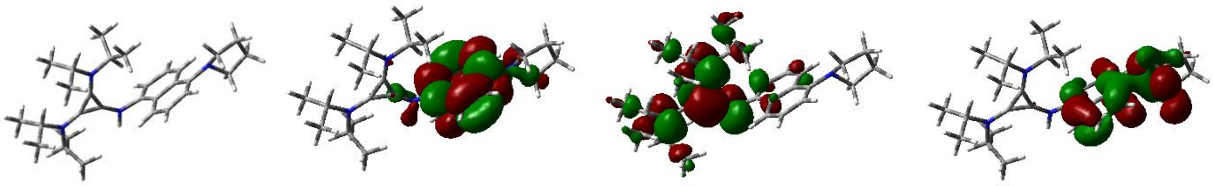

Trans – Diaminocyclohexane – Pyrrolidine – H (**54**)

Geometry LUMO HOMO HOMO

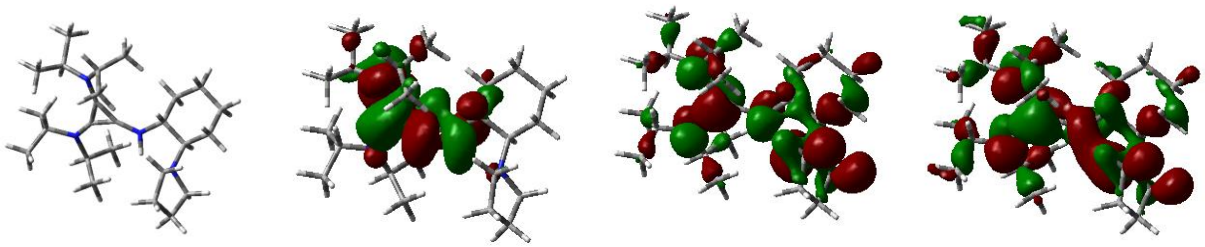

Trans – Diaminocyclohexane – Boc – H (**55**)

Geometry LUMO HOMO HOMO

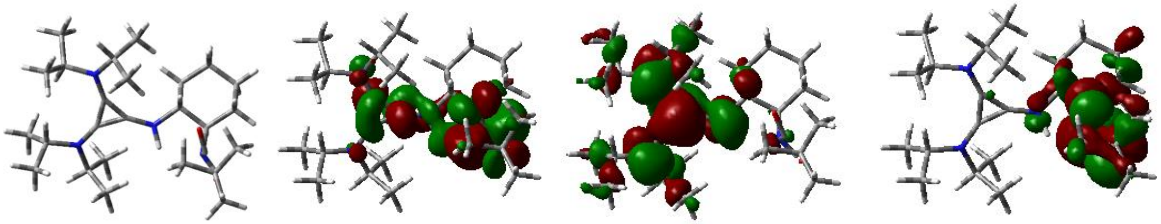

Tert – Butyl – Cyclopropenimine – H (**57**)

Geometry LUMO HOMO HOMO

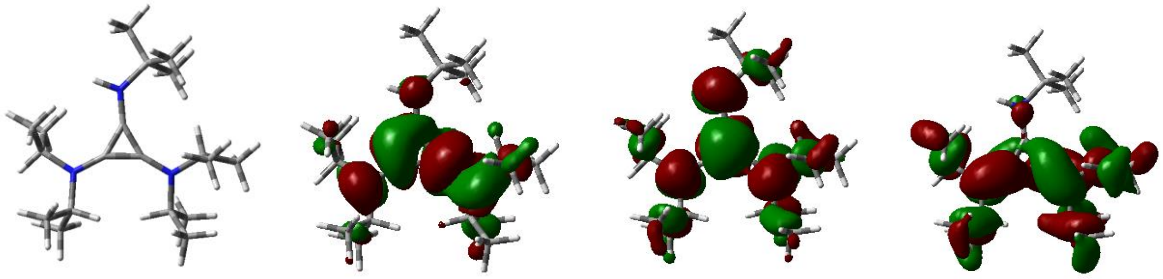

Phenyl – Cyclopropenimine – H (**56**)

Geometry LUMO HOMO HOMO

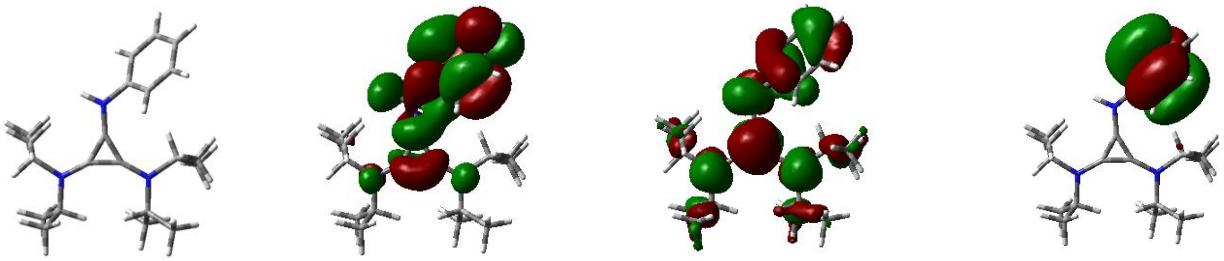

Chapter 8: References

[1] Hudson, J. The History of Chemistry, Routledge, Chapman & Hall, Inc.: New York, 1992.

[2] Brønsted, J.; Guggenheim, E. *J. Am. Chem. Soc.* **1927**, *49*, 2554.

[3] Alder, R. *Chem. Rev.* **1989**, *8*, 1215.

[4] Ishikawa, T. General Aspects of Organosuperbases. In *Superbases for Organic Synthesis: Guanidines, Amidines, Phosphazenes, and Related Organocatalysts*; Ishikawa, T. Eds.; Wiley: New York, 2009.

[5] Caubère, P. *Chem. Rev.* **1993**. *93*, 2317.

[6] Raczyńska, E.D.; Decouzon, M.; Gal, J.-F. Wozniak, M.; Kurg, R.; Carins, S.N. *Trends in Org. Chem.* **1998**, *7*, 95.

[7] Nasca, E.; Lambert, T. *J. Am. Chem. Soc.* **2015**, *137*, 10246.

[8] Alder, R. W.; Bowman, P. W.; Steele, W. R. S.; Winterman, D. R. *Chem. Commun*. **1968**, *13*, 723.

[9] Eigen, M.; *Angew. Chem., Int. Ed. Engl*. **1964**, *3*, 1.

[10] Raab, V.; Gauchenova, E.; Merkoulov, A.; Harms, K.; Sundermeyer, J.; Kovačević, B.; B. Maksić, Z.; *J. Am. Chem. Soc.* **2005**, *127*, 15738.

[11] Pozharskii, A.; Ozeryanskii, V.; Milkshiev, V.; Antonov, A.; Chernyshev, A.; Metalitsa, A.; Borodkin, G.; Fedik, N.; Dyablo, O. *J. Org. Chem*. **2016**, *81*, 5574.

[12] Haselbach, E.; Henriksson, A.; Jachimowicz, F.; Win, J. *Helv. Chim.* **1972**, *55*, 1757.

[13] Belding, L.; Dudding, T. *Chem. Eur. J.* **2014**, *20*, 1032.

[14] Belding, L.; Stoyanov, P.; Dudding, T. *J. Org. Chem.* **2016**, *81*, 6.

[15] Roberts, J. D.; Streitwieser Jr., A.; Regan, C. I. *J. Am. Chem. Soc*. **1952**, *74*, 4579.

[16] Breslow, R. *J. Am. Chem. Soc*. **1957**, *79*, 5318.

[17] J. Griffiths. *Chem. Soc. Rev*., **1972**, *1*, 481.

[18] Bandar, J.S.; Lambert, T.H. *J. Am. Chem. Soc.* **2012**, *134*, 5552.

[19] Tobey, S.; West, R.; *Tetrahedron Lett.* **1963**, 1179.

[20] Tobey, S.; West, R. *J. Am. Chem. Soc*. **1965**, *88*, 2478.

[21] Yoshida, Z.; Tawara Y. *J. Am. Chem. Soc.* **1971**, *93*, 2573.

[22] Mir, R.; Dudding, T. *J. Org. Chem*. **2017**, *82*, 709.

[23] Mirabdolbaghi, R.; Dudding, T.; Stamatatos, T. *Org. Lett.* **2014**, *16*, 2790.

[24] Smajlagic, I.; Durán, R.; Pilkington, M.; Dudding, T. *J. Org. Chem.* **2018**, *83*, 13973.

[25] Lakowicz, J. R. *Principles of Fluorescence Spectroscopy*, Kluwer, New York, 2nd edn, 1999.

[26] Turro, N. J.; Ramamurthy, V.; Scaiano, J. C. *Principles of Molecular Photochemistry: An Introduction*, University Science Books, 2008.

[27] Anslyn, E. V.; Dougherty, D. A. *Modern Physical Organic Chemistry*, University Science Books, 2006.

[28] Wu, J.; Liu, W.; Ge, J.; Zhang, H.; Wang, P. *Chem. Soc. Rev*. **2011**, *40*, 3483.

[29] Lavis, D.; Raines, R. *ACS. Chem. Biol.* **2008**, *3*, 142.

[30] Kumar, K.; Renuka, N.; Pavithra, G.; Kumar, G. *J. Chem. Pharm. Res*. **2015**, *7*, 67.

[31] Beija, M.; Afonso, C.; Martinho, *J. Chem. Soc. Rev.* **2009**, *38*, 2410.

[32] Zheng, Q.; Lavis, L. *Curr. Opin. Chem. Biol.* **2017**, *39*, 32.

[33] Treibs, A.; Kreuzer, F. *Justus Liebigs Ann. Chem*. **1968** *718*, 208.

[34] Falk, H.; Hofer, O.; Lehner, H. *Monatsh. Chem.* **1974**, *105*, 169.

[35] Ulrich, G.; Ziessel, R.; Harriman, A. *Angew. Chem. Int. Ed*. **2008**, *47*, 1184.

[36] Duke, R.; Weale, E.; Pfeffer, F.; Kruger, P.; Gunnlauggson, T. *Chem. Soc. Rev*. **2010**, *39*, 3936.

[37] Li, X.; Gao, X.; Shi, W.; Ma, H. *Chem. Rev*. **2014**, *114*, 590.

[38] Zhang, W.; Zhao, X.; Gu, W.; Cheng, T.; Wang, B.; Jiang, Y.; Shen, J. *New. J. Chem.*, **2018**, *42*, 18109

[39] Baleeva, N. S.; Khavroshechkina, A. V.; Zaitseva, E. R. *Tetrahedron Lett.* https//:doi.org/10.1016/j.tetlet.2019.150963. Just accepted.

[40] Astumian, R. *Chem. Sci.* **2017**, *8*, 840.

[41] Conyard, J.; Cnossen, A.; Browne, W.; Feringa, B.; Meech, S. *J. Am. Chem. Soc*. **2014**, *136*, 9692.

[42] Abendroth, J.; Bushuyev, O.; Weiss, P.; Barrett, C. *ACS Nano.* **2015,** *98*, 7746.

[43] Hunger, K. *Industrial Dyes: Chemistry, Properties, Application*, Wiley-VCH: Weinheim, **2003**.

[44] Bafana, A.; Devi, S. S.; Chakrabarti, T. *Environ. Rev*. **2011**, *19*, 350.

[45] Kumar, S. G. *Azo Functional Polymers: Functional Group Approach in Macromolecular Design*, Technocomic Publishing Company, Inc. Lancaster, Pennsylvania, **1992**.

[46] Xia, J.; Matyjaszewski, K. *Macromolecules*. **1997**, *30*, 7692.

[47] Merino, E.; Ribagorda, M. *Beilstein J. Org. Chem.* **2018**, *8*, 1071.

[48] Merino, E. *Chem. Soc. Rev*. **2011**, *40*, 3835.

[49] Hagarty, A. F. in *The Chemistry of Diazonium and Diazo Group*, Wiley, New York, 1978, Part 2, 545.

[50] Ullrich, R.; Grewer, T. *Thermochim. Acta*. **1993**, *225*, 201.

[51] Haghbeen, K.; Tan, E. *J. Org. Chem.* **1998**, *63*, 4503.

[52] Svele, I.; Zollinger, H. *Top. Curr. Chem*. **1983**, *112*, 1.

[53] Wawzonek, S.; McIntyre, T. *J. Electrochem. Soc.* **1972**, *119*, 1350.

[54] Karunakaran, C.; Palanisamy, P. *J. Mol. Catal. A: Chem*. **2001**, *172*, 9.

[55] Noureldin, N.; Bellegarde, J. *Synthesis.* **1999**, *1*, 939.

[56] Wang, C.; Wang, X.; Wang, Y. *Indian J. Chem.* **1999**, *38*, 964.

[57] Li, J.; Liu, P.; Wang, Y. *J. Chem. Research (S).* **2003**, 109.

[58] Kumar, S.; Patil, S. *J. Phys. Chem.* **2015**, *119*, 19297.

[59] Lee, D.; Kim, B.; Lee, C.; Im, Y.; Yook, K.; Hwang, S.; Lee, J. *ACS Appl. Mater. Interfaces.* **2015**, *7*, 9625.

[60] Siraj, N.; Hasan, F.; Das, S.; Kiruri, L. W.; Steege Gall, K. E.; Baker, G. A.; Warner, I. M. *J. Phys. Chem.* **2014**, *118*, 2312.

[61] Yang, Y.; Wang, X.; Cui, Q.; Cao, Q.; Li, L. *ACS Appl. Mater. Interfaces.* **2016**, *8*, 7440.

[62] Sun, Z.; Li, Y.; Chen, L.; Jing, X.; Xie, Z. *Cryst. Growth Des.* **2015**, *15*, 542.

[63] Singh, A.; Raj, T.; Aree, T.; Singh, N. *Inorg. Chem.* **2013**, *52*, 13830.

[64] Harada, T.; Sano, K.; Sato, K.; Watanabe, R.; Yu, Z.; Hanaoka, H.; Nakajima, T.; Choyke, P.L.; Ptaszek, M.; Kobayashi, H. *Bioconjugate Chem.* **2014**, *25*, 362.

[65] Zhang, J.; Chen, W.; Kalytchuk, S.; Li, K.F.; Chen, R.; Adachi, C.; Chen, Z.; Rogach, A.L.; Zhu, G.; Yu, P.K.; Zhang, W. *ACS Appl. Mater. Interfaces.* **2016**, *8*, 11355.

[66] Xu, J.; Zhang, B.; Jansen, M.; Goerigk, L.; Wong, W.; Ritchie, C. *Angew. Chem. Int. Ed.* **2017**, *56*, 13882.

[67] Sekar, R. B.; Periasamy, A. *J. Cell. Biol.* **2003**, *160*, 629.

[68] Daly, B.; Ling, J.; de Silva, A. P. *Chem. Soc. Rev.* **2015**, *44*, 4203.

[69] Mei, J.; Leung, N. L.; Kwok, R. T.; Lam, J. W.; Tang, B. Z. *Chem. Rev.* **2015**, *115*, 11718.

[70] Zhai, D.; Xu, W.; Zhang, L. Chang, Y. T. *Chem. Soc. Rev.* **2014**, *43*, 2402.

[71] de Silva, A. P.; Gunaratne, H. Q.; Gunnlaugsson, T.; Huxley, A. J.; McCoy, C. P.; Rademacher, J. T.; Rice, T. E. *Chem. Rev.* **1997**, *97*, 1515.

[72] Su, D.; Teoh, C. L.; Wang, Lu.; Liu, X.; Chang, Y. *Chem. Soc. Rev.* **2017**, *46*, 4833.

[73] Sameiro, M.; Congalves, T. *Chem. Rev.* **2009**, *109*, 190.

[74] Liu, X.; Savy, A.; Maurin, S.; Grimaud, L.; Darchen, F.; Quinton, D.; Labbé, E.; Buriez, O.; Delacotte, J.; Lemaître, F.; Guille-Collignon, M. *Angew. Chem. Int. Ed.* **2017**, *56*, 2366.

[75] Kim, H. M.; Cho, B. R. *Acc. Chem. Res.* **2009**, *42*, 863.

[76] Mao, G. J.; Wei, T. T.; Wang, X. X.; Huan, S. Y.; Lu, D. Q.; Zhang, J.; Zhang, X. B.; Tan, W.; Shen, G. L.; Yu, R. Q. *Anal. Chem.* **2013**, *85*, 7875.

[77] Tewaria, N.; Joshi, N.K.; Rautela R.; Gahlauta, R.; Joshi, H. C.; Pant. S. *J. Mol. Liq.* **2011,** *160*, 150.

[78] Alexiou, M. S.; Tychopoulos, V.; Ghorbanian, S.; Tyman, J. H. P.; Brown, R. G.; Brittain, P. I. *J. Chem. Soc., Perkin Trans.* **1990**, *2*, 837.

[79] Xian-En, Z.; Jin-Mao, Y.; Hong-Zhen, L.; You-Rui, S. *Chin. J. Anal. Chem.* **2007**, *35*, 938.

[80] You, J. M.; Ming, Y. F.; Shi, Y. W.; Zhao, X. E.; Suo, Y. R. *Talanta* **2005**, *68*, 448.

[81] Weber, G.; Farris, F. J. *J. Biochem.* **1979**, *18*, 3075.

[82] Liu, X.; Qiao, Q.; Tian, W.; Liu, W.; Chen, J.; Lang, M. J.; Xu, Z. *J. Am. Chem. Soc.* **2016**, *138*, 6960.

[83] Grimm, J. B.; English, B. P.; Chen, J.; Slaughter, J. P.; Zhang, Z.; Revyakin, A.; Patel, R.; Macklin, J. J.; Normanno, D.; Singer, R. H.; Lionnet, T.; Lavis, L. D. *Nat. Methods*. **2015**, *12*, 244.

[84] Song, X.; Johnson, A.; Foley, J. *J. Am. Chem. Soc*. **2008**, *130*, 17652.

[85] Niko, Y.; Hiroshige, Y.; Kawauchi, S.; Konishi, G. I. *J. Org. Chem*. **2012**, *77*, 3986.

[86] Hachiya, S.; Asai, K.; Konishi, G. I. *Tetrahedron Lett.* **2013**, *54*, 1839.

[87] Belding, L.; Dudding, T. *Chem. Eur. J.*, **2014**, *20*, 1032.

[88] Kozma, Á.; Rust, J.; Alcarazo, M. *Chem. Eur. J.*, **2015,** *21*, 10829.

[89] Mir, R.; Dudding, T. *J. Org. Chem.* **2016**, *81*, 2675.

[90] Le Sueur, R.; Guest, M.; Belding. L.; Pilkington, M.; Dudding, T. *Tetrahedron Lett*. https://doi.org/10.1016/j.tetlet.2019.07.019.

[91] Komatsu, K.; Kitagawa, T. *Chem. Rev.* **2003**, *103*, 1371.

[92] Bandar, J.; Lambert, T. *Synthesis*. **2013**, *45*, 2485.

[93] Etter, M. C. *Acc. Chem. Res.* **1990**, *23*, 120.

[94] Smajlagic, I.; Durán, R.; Pilkington, M.; Dudding, T. *J. Org. Chem.* **2018**, *83*, 13973.

[95] Bander, J.; Lambert, T. *J. Am. Chem. Soc.*, **2013**, 135, 11799.

[96] Dempsey, K.; Mir, R.; Smajlagic, I.; Dudding, T. *Tetrahedron*. **2018**, *74*, 3507.

[97] Mir, R.; Dudding, T. *J. Org. Chem.* **2017**, *82*, 709.

[98] Belding, L.; Guest, M.; Le Sueur, R.; Dudding, T. *J. Org. Chem*. **2018**, *83*, 6489.

[99] Freyer, J.; Bucks, S.; Gobieski, G.; Russell, S.; Yozwiak, C.; Sun, M.; Chen, Z.; Jiang, Y.; Bander, J.; Stockwell, B.; Lambert, T. *Angew. Chem. Int. Ed.* **2016**, *55*, 12382-12386.

[100] Jiang, Y.; Freyer, J.; Cotando, P.; Brucks, S.; Killops, K.; Bander, J.; Torsitano, C.; Balsara, C.; Lambert, T.; Campos, L. *Nat. Commun.* **2015**, *6*, 5950.

[101] Hadrich, D.; Berthold, F.; Steckhan, E.; Bönisch, H. *J. Med. Chem.*, **1999**, *42*, 3101.

[102] Zhang, J.; Chen, W.; Kalytchuk, S.; Li, K.; Chen, R.; Adachi, C.; Jiménez-Sánchez, Z.; Farfán, N.; Santillan, R. *J. Phys. Chem. C*. **2015**, *119*, 13814.

[103] Kumar, S.; Patil, S. *J. Phys. Chem. C*. **2015**, *119*, 19297.

[104] Lee, D.; Kim, B.; Lee, C.; Im, Y.; Yook, K.; Hwang, S.; Lee, J. *ACS Appl. Mater. Interfaces.* **2015**, *7*, 9625.

[105] Siraj, N.; Hasan, F.; Das, S.; Kiruri, L.; Steege Gall, K.; Baker, G.; Warner, I. *J. Phys. Chem.* **2014**, *118*, 2312.

[106] Flamigni, L.; Ventura, B.; You, C.; Hippius, C.; Würthner. F. *J. Phys. Chem. C*. **2007**, *111*, 622.

[107] Yang, Y.; Wang, X.; Cui, Q.; Cao, Q.; Li, L. *ACS Appl. Mater. Interfaces*. **2016**, *8*, 7440.

[108] Sun, Z.; Li, Y.; Chen, L.; Jing, X.; Xie, Z. *Cryst. Growth Des.* **2015**, *15*, 542.

[109] Singh, A.; Raj, T.; Aree, T.; Singh, N. *Inorg. Chem.* **2013**, *52*, 13830.

[110] Harada, T.; Sano, K.; Sato, K.; Watanabe, R.; Yu, Z.; Hanaoka, H.; Nakajima, T.; Choyke, P.; Ptaszek, M.; Kobayashi, H. *Bioconjugate Chem.* **2014**, *25*, 362.

[111] Xu, J.; Zhang, B.; Jansen, M.; Goerigk, L.; Wong, W.; Ritchie, C. *Angew. Chem., Int. Ed*. **2017**, *56*, 13882.

[112] Raab, V.; Gauchenova, E.; Merkoulov, A.; Harms, K.; Sundermeyer, J.; Kovacevic, B.; Maksic, Z. B. *J. Am. Chem. Soc.* **2005**, *127*, 15738.

[113] Le Guennic, B.; Jacquemin, D.; *Acc. Chem. Res.* **2015**, *48*, 530.

[114] Green, T. W.; Wuts, P. G. M.; *Greene's Protective Groups in Organic Chemistry,* 4th ed. **2007**, New Jersey: John Wiley and Sons.

[115] Isobe, T.; Fukuda, K.; Ishikawa, T. *J. Org. Chem*. **2000**, *65*, 7770.

[116] Shendage, D. M.; Frohlich, R.; Haufe, G. *Organic Lett.* **2004**, *6*, 3675.

[117] Green, T. W.; Wuts, P. G. M.; *Greene's Protective Groups in Organic Chemistry,* 4th ed. **2007**, New Jersey: John Wiley and Sons.

[118] March, J.; Smith, M.; *Advanced Organic Chemistry*, 6th ed. **2007**, New York: John Wiley and Sons, Chapter 8: Acids and Bases.

[119] Hansen, M.; Lerch, M.; Szymanski, w.; Feringa, B. *Angewandte.* **2016,** *55*, 1.

[120] Goeldner, E.; Givens, R. *Dynamic studies in biology: phototriggers, photoswitches and caged biomolecules*, Wiley-VCH Verlag GmbH & Co, Weinheim, **2005**.

[121] Davies, G. *Nat. Methods*. **2007**, *4*, 619.

[122] J. Griffiths. *Chem. Soc. Rev.*, **1997**, *1*, 481.

[123] Hansen, M.; Lerch, M.; Szymanski, W.; Feringa, B. *Angew. Chem.* **2016**, *55*, 1.

[124] Davies, G. *Nat. ethods.* **2007**, *4*, 619.

[125] Hammerich, m.; Schutt, C.; Stahler, C.; Lentes, P.; Rohricht, F.; Hoppner, R.; Herges R. *J. Am. Chem. Soc.* **2016**, *10*, 1021.

[126] Beharry, A. A.; Woolley, G. A. *Chem. Soc. Rev*. **2011**, *40*, 4422.

[127] Mo, F.; Dong, G.; Zhang, Y.; Wang, J. *Org. Biomol. Chem.* **2013,** *11*, 1582.

[128] Mir, R.; Dudding, T. *J. Org. Chem.* **2018**, *83*, 4383.

[129] Du, H.; Fuh, R. C. A.; Li, J.; Corkan, L. A.; Lindsey, J. S. *Photochem. Photobiol.* **1998**, *68*, 141.

[130] Brouwer, A. M. *Pure Appl. Chem.* **2011**, *83*, 2213.

[131] Frisch, M. J.; Trucks, G. W.; Schlegel, H. B.; Scuseria, G. E.; Robb, M. A.; Cheeseman, J. R.; Scalmani, G.; Barone, V.; Mennucci, B.; Petersson, G. A.; Nakatsuji, H.; Caricato, M.; Li, X.; Hratchian, H. P.; Izmaylov, A. F.; Bloino, J.; Zhang, G.; Sonnenberg, J. L.; Hada, M.; Ehara, M.; Toyota, K.; Fukuda, R.; Hasegawa, J.; Ishida, M.; Nakajima, T.; Honda, Y.; Kitao, O.; Nakai, H.; Vreven, T.; Montgomery, J. A.; Peralta, Jr., J. E.; Ogliaro, F.; Bearpark, M.; Heyd, J. J.; Brothers, E.; Kudin, K. N.; Staroverov, V. N.; Kobayashi, R.; Normand, J.; Raghavachari, K.; Rendell, A.; Burant, J. C.; Iyengar, S. S.; Tomasi, J.; Cossi, M.; Rega, N.; Millam, J. M.; Klene, M.; Knox, J.e.; Cross, J. B.; Bakken, V.; Adamo, C.; Jaramillo, J.; Gomperts, R.; Stratmann, R. E.; Yazyev, O.; Austin, A. J.; Cammi, A. R.; Pomelli, C.; Ochterski, J. W.; Martin, R. L.; Morokuma, K.; Zakrzewski, V. G.; Voth, G. A.; Salvador, P.; Dannenberg, J. J.; Dapprich, S.; Daniels, A. D.; Farkas, Ö.; Foresman, J. B.; Ortiz, J. V.; Cioslowski, J.; Fox, D. J.Gaussian 09, Revision C.02; Gaussian, Inc.: Wallingford, CT, **2009**.

[132] Ganem, B. *Acc. Chem. Res.* **2009**, *42*, 463.

[133] Tomasi, J.; Mennucci, B.; Cances, E. *J. Mol. Struct.* **1999**, *464*, 211.

[134] (a) Szemik-Hojniak, A.; Zwier, J. M.; Buma, W. J.; Bursi, R.; van der Waals, J. H. *J. Am. Chem. Soc.* **1998**, *120*, 4840-4844. (b) Szemik-Hojniak, A.; Rettig, W.; Deperasińska, I. *Chem. Phys. Lett.* **2001**, *343*, 404.

[135] *Schrodinger Materials Science Suite 2014-2*; Schrödinger, LLC, New York, NY, 2014.

[136] Lee, D. W.; Ha, H. J. *Synth. Commun.* **2007**, *37*, 737.

[137] Kozma, Á.; Gopakumar, G.; Farès, C.; Thiel, W.; Alcarazo, M. *Chem. Eur. J.* **2013**, *19*, 3542.

[138] Bandar, J. S.; Lambert, T. H. *J. Am. Chem. Soc.* **2012**, *134*, 5552.

[139] Shohji, N.; Kawaji, T.; Okamoto, S. *Org. lett.* **2011**, *13*, 2626.

[140] Sauer, M.; Yeung, C.; Chong, J. H.; Patrick, B.; MacLachlan, M. J. *J. Org. Chem.* **2006**, *71*, 775.

[142] Isobe, T.; Fukuda, K.; Ishikawa, T. *J. Org. Chem.* **2000**, *65*, 7770.